EXPLORATION OF PAVEMENT OXIDATION MODEL APPLICATIONS AND FIELD VALIDATION

A Dissertation

by

YUANCHEN CUI

Submitted to the Office of Graduate and Professional Studies of
Texas A&M University
in partial fulfillment of the requirements for the degree of

DOCTOR OF PHILOSOPHY

Chair of Committee,	Charles J. Glover
Committee Members,	Amy Epps Martin
	Mark T. Holtzapple
	Benjamin A. Wilhite
Head of Department,	M. Nazmul Karim

August 2014

Major Subject: Chemical Engineering

ABSTRACT

Asphalt paved road is one of the building blocks of the modem world. Flexibility is one of its major advantages；however, this flexibility suffers from asphalt oxidation since the first day of pavement service life. Several elements of binder oxidation have been investigated, such as oxidation kinetics, asphalt hardening in response to oxidation, pavement design, and environmental conditions. Based on understandings on those elements, pavement oxidation models have been developed to predict the oxidation rates in pavements in specific locations. This prediction contributes greatly to reducing the pavement life cost and elongating pavement service life. However, experimental methods to determine required model inputs, values of those oxidation elements, seriously limit the model application. This work focuses on understanding the elements of asphalt oxidation and on exploring applications of the pavement oxidation model.

This dissertation presents a detailed investigation of pavement oxidation, two new test methods to obtain the model inputs, and a study on dynamic diffusion-reaction balance. First, a detailed investigation on pavement oxidation was reported to give some general conclusions about asphalt oxidation rates vary largely in different climate zones, and pavement design defines thickness of the asphalt film and thus controls aging. Secondly, new methods to obtain the model inputs were proposed: (1) Aging tests on laboratory made asphalt concretes have been proven as new information sources on asphalt concretes aging to replace sampling field cores. This method makes a pavement oxidation prediction before construction a reality; (2) Aging on recovered asphalt binders have been proven as

new information sources on asphalt kinetics and hardening properties. This method solves the problem that original binders are not available in many cases. With the data obtained from these aging tests, long term oxidation predictions for the pavements were made using the pavement oxidation model and validated their accuracies by field data, including one complicated case, a layer-by-layer prediction on a seal coat treated pavement. To better understand the asphalt aging process, the last topic in this dissertation was to study a dynamic balance between oxygen diffusion and oxidation reaction using the pavement oxidation model.

ACKNOWLEDGEMENTS

I would like to thank my committee chair, Dr. Charles Glover, and my committee members, Dr. Amy Epps Martin, Dr. Mark Holtzapple and Dr. Benjamin Wilhite, for their guidance and support throughout the course of this research.

Thanks also go to my colleagues, Nikornpon Prapaitrakul, Rongbin Han, Xin Jin, Guanlan Liu, Avery Rose, Jim Lawrence, Padigala Meghana and Arif Chowdhury. Without them, this work would not be possible.

Finally, thanks to my parents and grandparents for their encouragement and endless love.

TABLE OF CONTENTS

Page

LIST OF FIGURES

Page

LIST OF TABLES

CHAPTER I

INTRODUCTION

Roads are arteries of modern society. In the United States only, there are more than 2 million miles of paved roads. This nationwide network provides a rapid and reliable transportation method inside the country and beyond its border.

With the fact that over 94 percent of the paved roads in the United States are surfaced with asphalt concrete, this precisely engineered product has become the most regularly used material in road construction (NAPA 2014). The asphalt concrete is composed of about 95 percent stone, sand and gravel by weight, and about 5 percent asphalt. The asphalt acts as glue to hold the aggregates together and gives flexibility to the asphalt concrete. With this flexibility, the concrete is able to take high stress from traffic loading, even when loads exceed the maximum anticipated for the pavement.

Since the first day of the pavement service life, an irreversible reaction between the asphalt and the oxygen has started damaging the asphalt binder, the asphalt concrete, and consequently the pavement performance and durability. As oxidation occurs, asphalt hardens and loses its adhesive capability (between asphalt and aggregate) and cohesive capability (inside asphalt). Also the asphalt concrete becomes too brittle to release the stress build-up in the materials. Finally, micro cracks propagate in concrete, and the pavement failure starts.

To better build and maintain the pavements, asphalt oxidation has become an essential subject of study. Several separate but related facets have been explored.

Asphalt Oxidation in Pavements

Tracking oxidation in pavements is critical but rather difficult. Without intensive studies of pavements under a large number of actual field conditions over many years, the answer to what actually happened in the pavements cannot be found. Only a well-organized cooperation, among government organizations, construction companies and asphalt scientists, could support such a complex project. A number of field data have been reported and only a few conclusions were widely accepted, but the massive load required in those works makes those results precious (Halstead 1963, Martin et al. 1990b, Woo, Chowdhury, and Glover 2008, Hagos, Molenaar, and Van de Ven 2009).

First, the importance of a binder's stiffness to the pavement durability is both clear and well accepted (Clark 1958, Doyle 1958, Kandhal and Wenger 1975, Kandhal 1977, Kandhal and Koehler 1984). Previous research indicates that a value of the 15 ℃ ductility at 1 cm/min in a range of 2 to 3 cm corresponds to a critical level of cracking in pavements (Kandhal 1977). Mechanistic Empirical Pavement Design Guide formalized this conclusion into its pavement performance calculations.

Second, asphalt oxidation causes binder stiffness to increase, but its impact on pavement performance and durability was seriously underestimated for a long time. In spite of concern about substandard pavement condition, the first systematic study in the United States has not executed until AASHTO Road Test in 1958 to 1960. That test was a massive experiment but only in a limited region in Ottawa, Illinois. It is not surprising that asphalt oxidation did not show much influence on pavement performance under the cold climate as well as in such a short period (3 years). A long-term field test, which

systematically covers a wider range of climate, construction, maintenance, and loading conditions, was essential. After a study on the pavements in Georgia, one conclusion was made by Coons and Wright (1968) that binder oxidation could only be found in the top 1.5 in (38.1 mm) of the pavement. But two decades later, a contradicting conclusion was reported by Glover et al. (2005) and Al-Azri et al. (2006), based on the studies on Texas pavements. Strong evidence proves that asphalt aging occurs even 6 in below the surface in hot climate regions after a long period of time and it tremendously affects the pavement performance.

Asphalt Oxidation Kinetics and Hardening

A quantitative analysis on asphalt oxidation becomes an important issue after confirming its influence on the pavement performance. Basic oxidation chemistry has been extensively explored in laboratory experiments (Lee and Huang 1973, Lau et al. 1992, Jemison et al. 1992, Mill et al. 1992, Petersen et al. 1993, Branthaver et al. 1993, Petersen and Harnsberger 1998). In those reports, it is generally accepted that both a formation of carbonyl compounds and an increase in binder stiffness result from binder oxidation.

Efforts were made to precisely describe the formation rate of carbonyl compounds (Lee and Huang 1973, Petersen 1975, Petersen et al. 1993). This rate is determined by the nature of the asphalt and varies from one asphalt to another. However, a common ground was found. For each asphalt, oxidation occurs rapidly in an initial period, named as fast-rate period, and this fast rate continues over time until a constant-rate period is reached. The form of the constant rate was proposed first by Lau et al. (1992). In 2011, an advanced model was proposed, which covers both non-linear fast-rate period and linear constant-

rate period (Jin et al. 2011). This model assumes that both periods could be described in Arrhenius. The total carbonyl formation with time is described as follows:

$$CA = CA_0 + M(1 - e^{-k_f t}) + k_c t$$

$$k_f = A_f P^{\alpha} e^{-E_{af}/RT} = A_f' e^{-E_{af}/RT}$$

$$k_c = A_c P^{\alpha} e^{-E_{ac}/RT} = A_c' e^{-E_{ac}/RT}$$

where $M = (CA_0 - CA_{tank})$, CA_{tank} is the carbonyl area value of the unaged asphalt, CA_0 is the intercept of the constant-rate line, k_f and k_c are two reaction constants that are temperature dependent. A_f , A_c , A_f', A_c' are pre-exponential factors, and E_{af}, E_{ac} are activation energies, subscript *c* or *f* indicates this parameter belongs to constant-rate period or fast-rate period. Those parameters in Arrhenius expression are temperature independent and are following universal correlations (Jin et al. 2011).

The reaction rate describes the chemical changes in asphalt, and to predict the binder performance, asphalt stiffness increases with chemical changes also are essential (Knotnerus 1972, Anderson et al. 1994, Herrington 1998). Generally, more carbonyl compounds created in binders lead to higher binder stiffness (Roberts et al. 1996). Dynamic shear rheometer function (DSR Function) is used to present the binder stiffness. This index combines both elastic and viscous properties measured at a relative mid-range test conditions (frequency and/or temperature). A linear relationship was reported between natural logarithm of DSR Function and carbonyl area. This slope is termed the DSR Function hardening susceptibility (DSR Function HS) (Ruan, Davison, and Glover 2003,

Woo et al. 2007, Al-Azri et al. 2006, Juristyarini, Davison, and Glover 2011). For either fast-rate period or constant-rate period, the DSR Function HS keeps constant for a certain asphalt (Jin et al. 2011). Thus the DSR Function hardening rate could be expressed as the oxidative reaction rate (r_{CA}) multiplied by the DSR Function hardening susceptibility:

$$r_{\text{DSR Function}} = \partial \ln(\text{DSR Function}) / \partial t = (\text{DSR Function HS}) \cdot (\partial \text{CA} / \partial t)$$

Oxygen Diffusion in Asphalt Binder

Besides the oxidation kinetics and hardening, another key question is how quickly oxygen can transport in asphalt binder. To react with the asphalt, oxygen molecules have to penetrate into the asphalt film and diffuse through the film. An early attempt to measure the oxygen diffusivity in the asphalt was made by Lunsford (1994) by using basic transport and reaction equations. Although the experimental results appeared that the asphalt film in the experiment was too thin to establish any diffusion dependence needed for accurate measurements, this work proposed the experimental methods that would make measurements on the oxygen diffusivity in asphalt for the first time. In 2013, an improved work was conducted by Han (2011). Same fundamental transport and reaction equations were used on various binder films. By comparing the oxidation rates at the binder surface and at a solid-binder interface at the asphalt film depth, calculation results gave an oxygen diffusivity (D_{O_2}) ranging from 10^{-10} to 10^{-11} m^2/s. A clear decrease of oxygen diffusivity over absolute temperature with increases in limiting viscosity (η_0^*) was given. The data show a power law dependence as following:

$$\frac{D_{O_2}}{T} = 5.21 \times 10^{-12} \left(\eta_0^*\right)^{-0.55}$$

Pavement Oxidation Model

Several pavement oxidation models have been developed to predict aging in the pavements (Dickinson 1984, Lunsford 1994, Prapaitrakul et al. 2009, Han 2011). Important concepts have been concluded in those models, including air void, asphalt content, pavement temperatures, oxygen diffusion, oxidation kinetics and asphalt hardening. Among those concepts, air void and asphalt content are determined in asphalt concrete design. Those two factors define the thickness of the asphalt film. In this film, oxygen diffuses and reacts with asphalt. Oxidation kinetics and hardening are directly related to the nature of the asphalt and vary from one asphalt to another. Oxygen diffusion is determined by the asphalt concrete design, oxygen diffusivity and pavement temperature. However, the model could only give an oxidation range, which is not precise enough for practice application. At this time, some empirical factors are necessary.

Based on those existing models, Jin, Cui, and Glover (2013) developed an advanced asphalt oxidation model. This model introduces two new concepts, diffusion depth and field calibration factor (*fcf*). The first concept, diffusion depth, defined as the asphalt thickness in case of binder spreads equally on the surface of accessible air voids, and the value is calculated from X-ray CT images after a detailed layer-by-layer scanning on field cores. The second concept, field calibration factor, is to account for the issues not well understood, for example, the film thickness increased by fines (tiny aggregates) merged in asphalt, or decreased by absorbed binder in aggregate. To fit the *fcf*, at least two

field samples are required from the same location but aged to different levels. Therefore, to determine the diffusion depth and *fcf*, measurements on field samples are unavoidable. A prediction could only be made after X-ray CT scans on one field core as well as an oxidation analysis on at least two field cores aged to different levels to guess the *fcf* and diffusion depth.

In summary, to apply this model on a specific pavement, three elements are required: pavement design (for binder content); original binders stored during the construction (for asphalt kinetics and hardening properties); field cores collected from the pavement (for diffusion depth and *fcf*). Those prerequisites seriously limit the application of the model.

In most of the real cases, those prerequisites could not be met all. For example, a prediction before construction would provide not only the status of the pavement after many years, but also some instructive suggestions on pavement design. However, the model requires the field samples to do model calibration, which makes a prediction before construction improbable. Another example is, for a pavement already built for many years, the original binder likely is not available any more. This situation makes a prediction on a pavement without original binder difficult.

Asphalt Binder Oxidation in a Seal Coat Treated Pavement

In need of the increasing demands of pavement maintenance, seal coat treatment becomes one of the most widely used methods due to its simple structure and functionality. Its structure is essentially a single layer of asphalt covered by embedded aggregate. This thin layer of fresh asphalt has the potential of providing a better, longer-lasting pavement.

Most of the research only focuses on the instant ride quality restoring brought by the application of the seal coat, such as cracks sealing, surface raveling and waterproofing (McLeod et al. 1969, Brown 1988, O'Brien 1989, Gransberg and James 2005, Lawson and Senadheera 2009). Actually, many seal coat failures, for example, loss of aggregates, obviously relates to asphalt brittleness, which is a result of oxidation. An official standard for seal coat oxidative aging is still blank.

Asphalt Binder Aging Simulation in PAV

All the earlier studies (Mill et al. 1992, Petersen 1994) have indicated that asphalt oxidative aging is a result of a set of several oxidation reactions. Those reactions are expected to be accelerated by increasing oxygen pressure or oxygen partial pressure. Domke, Davison, and Glover (2000) studied the asphalt oxidative aging under several elevated pressures, and indicated that the oxygen diffusion process through maltenes to polar aromatic and asphaltene aggregates is believed to cause an effect of a change on oxidation kinetics. Thus, the expressions of asphalt binder oxidation given in asphalt binder kinetics and hardening section still fit the elevated pressure aging simulation, but the kinetic parameters need to be determined under elevated pressures again. Those conclusions agree exactly with the work of Huh and Robertson (1996). They reported similar results based on their observation of viscosity increase under only one fixed pressure 2.1 MPa (20.7 atm) in PAV.

Dissertation Outline

This dissertation is to explore the model applications and to validate the modeling results with field data. Research interests include investigations of pavement aging, establishment of new experimental methods, and evaluations of model predictions.

Chapter II presents a detailed investigation of pavement aging in different climate regions. Included are the measurements of binder oxidation and hardening over time. Data covers nineteen road sections all over Texas plus one section in Minnesota. Due to the complicated experimental process required on the field samples and the potential usage for future research, these field data are the most significant contribution in the dissertation.

Chapter III reports a correlation between the field aged asphalt concrete and laboratory aged asphalt concrete. Comparing to the traditional method, which is using field cores, laboratory aged sample not just saves time and work but also provides more information on pavement design. A pavement aging prediction is made based on the experimental results from laboratory aged samples, and verified by comparing to field data.

Chapter IV presents a accelerated aging test on recovered binders to determine the asphalt oxidation kinetics and asphalt hardening parameters. In many cases, there is no original binder stored during construction. This experiment is designed to solve this problem. The recovered binder, extracted from field cores, was further aged and then tested for its kinetics and hardening properties. Comparing with the test results from original binders, test results on recovered binders indicate that asphalt properties do not change during the extraction and recovery, and recovered binders could replace original binders in pavement oxidation model predictions.

In Chapter V, an asphalt aging investigation is conducted on a seal coat treated road. Multiple asphalt binders exist in one pavement and different oxidation rates are expected. This makes the case much more complicated. To evaluate the oxidation in different layers with different binders and to predict the oxidation in those layers is the objective of this chapter.

Chapter VI presents a new accelerated aging method using the Pressure Aging Vessel (PAV, ASTM D6521-08) under high temperatures, and elevated air pressure 2.1 MPa (20.7 atm) to estimate the required kinetics parameters. Due to the higher pressure, both the oxidation activation energies and pre-exponential factors are different from those determined at 1 atm. Consistent correlations exist between data at the two pressures. These correlations provide the basis for estimating reaction kinetics parameters at pavement conditions from measurements at PAV conditions. These parameters can then be used in the pavement oxidation model to compare their impacts on pavement durability at any specific pavement location.

Chapter VII presents an application of the pavement oxidation model in a study of the dynamic balance of oxygen diffusion and oxidative reaction in asphalt aging. The model simulates the aging process happens in the asphalt: oxygen molecules first penetrate into the asphalt film and then react with the asphalt molecules. In some cases, either oxygen diffusion or oxidative reaction may dominate the aging process. By using this oxidation model, a number of controlling factors are well explored without doing a huge amount of experiments.

Finally, Chapter VIII provides an executive summary of the dissertation and some recommendations for future research.

CHAPTER II

LONG-TERM FIELD AGING OF ASPHALT BINDERS

Introduction

Asphalt concrete pavements, because of their long service lives as designed, place extraordinary demands for long-term research. The aging characteristics, which are strongly affected by years of use and climate of the location, are necessary to be better understood under a long period and actual aging conditions.

The existence of the asphalt oxidation in pavements was seriously underestimated for a long period of time. In the U.S. first systematically studied road performance test, the AASHTO Road Test, massive experiments were planned but only involved one test location (Ottawa, Illinois) and lasted three years (from 1958 to 1960). Not surprisingly, asphalt oxidation did not show much influence on pavement performance in this cold climate region and in such a short period. In 1968, based on studies on 14 pavements in Georgia, Coons and Wright (1968) concluded that asphalt aging only occurs in the top 1.5 in (38.1 mm) of the pavement. But two decades later, a contradicting conclusion was made by Woo et al. (2007) based on studies on pavements in Texas. Strong evidence showed that binders can oxidize even 6 in (152.4 mm) below the pavement surface in hot climate regions after a long period of time.

In order to expand the findings and to quantitatively analyze pavement oxidation, a continuous long-term field test was essential. The wider range of climate, soil,

construction, maintenance, and loading conditions the test could systematically cover, the more solid the conclusion could be.

Objectives

Previous studies on binder oxidation in pavements provide strong evidence that the degree of the oxidation increases with time through the whole pavement depth. The objective of this work was an extensive study on the effect of the pavement design and climate on asphalt aging. Extensive data are reported in this chapter, including increases in carbonyl area and DSR Function in pavements as a function of time as well as depth below the surface.

Experimental Methods

This section describes the material, equipment and procedures followed in this research. The experimental materials were the recovered binders, extracted from the field cores. Those field cores were collected from pavements across Texas plus one pavement in Minnesota. A dynamic shear rheometer was used to measure the rheological properties of the binder. An infrared spectroscopy was used to measure the carbonyl content in the binder. Details of these methods and materials are explained in the following sections.

Material

As mentioned above, answers to how asphalt field aging occurs cannot be found without an intensive study of a large number of pavements under actual field conditions over many years.

Table 1 lists the pavement test sites and the binders used in those test sites. The locations of the sites in Texas are shown in Figure 1. The sites range from the Northern

Panhandle to the Southern Rio Grande Valley and from Odessa in the West to the Lufkin and Atlanta districts in the East. Moreover, some of the Texas pavements applied seal coat maintenance on the surface, whether seal coats might be able to retard oxidation is also of interest. The thickness of the various pavement layers ranged up to 6 in (152.4 mm) but down to as little as 2 in (50.8 mm) and the thickness of the maintenance (seal coat) layer is less than 0.2 in (5.1 mm).

Cores were also collected in Minnesota by Mn/DOT (Minnesota Department of Transportation). The MnRoad test site used to be studied in previous projects, named as MnRoad Cell 1, and results on its original binders are also available. Further information about this site is given in the following sections.

A typical coring layout is shown in Figure 2. There are four coring dates for the new field sections built in 2008 and two coring dates for the old field sections built before 2008. At each coring date, cores were taken from the shoulder (SH), where only aging had affected the asphalt concrete, and the wheel path (WP), where both traffic and aging had affected the asphalt concrete simultaneously. If part of the pavement had maintenance treatment, cores were taken from both treated sections and untreated sections. After the collection, cores were sliced into layers from top to bottom, and each layer was about 0.5 in (12.7 mm). Binders were extracted from the cores and tested to evaluate the condition of binder oxidation and hardening.

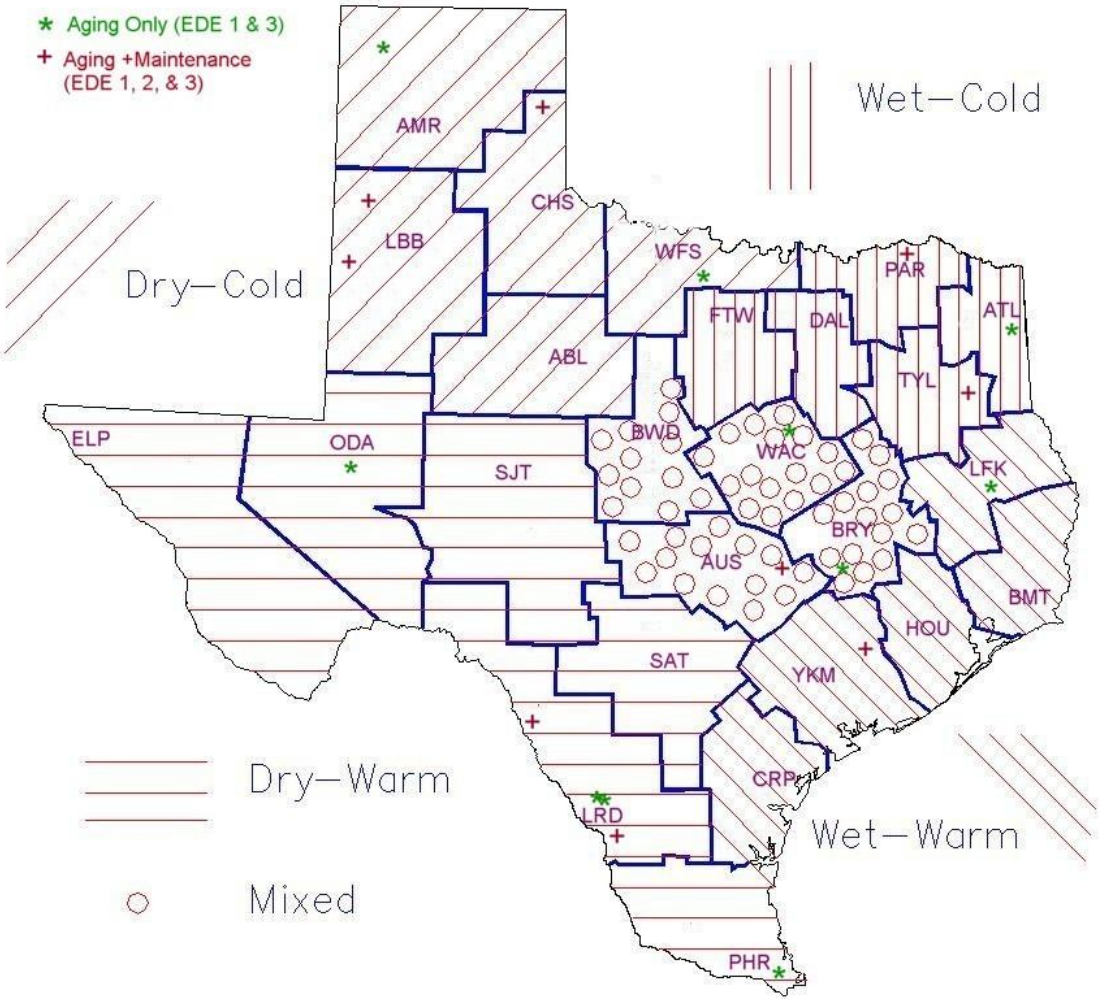

Figure 1 Field Section Locations and Texas Environmental Zones.

Table 1 Collected Cores from TxDOT Districts and MnRoad District.

Section #	Section ID	Location	Env-Zone	Construction Date	Binder Type	AC (% of mix by wt, Design)	Mix Type	Binder Supplier	Aggregate Type	Aggregate Supplier	Layer Thickness (in)
1	BRY	US 290	M	2002	PG 64-22	4.4	Type C	Eagle	Limestone	Colorado Materials LS, and Eagleman Field Sand	2.0
2	ATL	IH 20	WC	2001	PG 76-22 (SBS)	5.1	12.5 mm Sp	Wright Asphalt	Sandstone	SS from Meridian (MM), Sawyer; Fines from Ark Granite Donnafill, Little Rock	2.5
3	WAC	IH 35	M	2002	PG 70-22 (SBS)	5.3	19 mm Sp	Fina, Port Aurther	Igneous (grantie?) / LS	Hanson (OK): Granite, Young/Maddox: Limestone	3.5
4	WFS	SH 59	DC	7/5/2007	PG 70-22	4.8	Type D	SEM materials, Saginaw	Limestone	Hanson, Bridgeport	2.0
5	LRD	IH 35 Layer #3	DW	Fall 2007	PG 76-22(SBS)	4.4	25 mm SFHMA C	Valero, Corpus	Traprock/River Gravel	TR: Vulcan Mat.; RG: Galo Pit; Dry Scrn: MM	6.0
6	LRD	IH 35 Layer #5	DW	Fall 2007	PG 70-22 (SBS)	5.9	12.5 mm Sp	Valero, Corpus	River Gravel	RG: Galo Pit, Dry Scrn: MM	2.0

Table 1 Continued.

Section #	Section ID	Location	Env-Zone	Construction Date	Binder Type	AC (% of mix by wt, Design)	Mix Type	Binder Supplier	Aggregate Type	Aggregate Supplier	Layer Thickness (in)
7	LFK	US 69	WW	Summer 2003	PG 70-22	4.3	Type C	Marlin	River Gravel	Hanson Perchhill and Hanson Little River	2.0
8	LRD	FM 649	DW	2006 (March)	PG 76-22	4.9	Type C	Valero, Corpus	Limestone	Martin Marietta	2.0
9	LRD	US 277	DW	2008 (April/May)	PG 70-22	4.2	Type C	Valero, Corpus	Limestone with TR Screening	LS from South Tx Aggr (sabinal), TR Scrn Vulcan Knippa	3.0
10	TYL	US 259	WC	2007 (Feb)	PG 70-22	4.3	Type C	Lion Oil, Arkansas	Sandstone / Limestone	SS: Capitol Agg at Brwonlee; LS: Hanson Perch Hill	2.0
11	LBB	US 82	DC	2008 (July)	PG 76-22	6.2	CMHB-F	Alon, Big Spring	Limestone	Kiewet (Higginbotham) and Price Const. Cllements Scrn	3.0
12	CHS	US 83	DC	2008 (June)	PG 70-28	5.3	Type D	SEM materials, Saginaw	Granite	Martin Marietta, Snyder, OK: Tx Lime from Cleburne	2.0
13	YKM	SH 36	WW	2006 (July)	PG 64-22	4.9	Type D	Martin Asphalt	Limestone	Colorado Materials LS, and Sand Supply Field Sand	2.0
14	ATL	US 259	WC	2005 (Oct-Nov)	PG 76-22	5.6	Type D	Lion Oil, Arkansas	River Gravel	Hanson Little River; and Day Pit Field Sand	2.0

Table 1 Continued.

Section #	Section ID	Location	Env-Zone	Construction Date	Binder Type	AC (% of mix by wt, Design)	Mix Type	Binder Supplier	Aggregate Type	Aggregate Supplier	Layer Thickness (in)
15	PAR	SH 24	WC	2009 (July)	PG 64-22	6.0	Type D	Lion Oil, Arkansas	Sandstone		2.0
16	ODA	FM 1936	DW	2002	PG 70-22 (SBS)	7.3	CMHB_F	Alon	Rhyolite	Rhy: Hoban with Jones Scrn	3.0
17	PHR	FM 2994	DW	2002	PG 70-22 (SBS)	5.5	Type D	Eagle Asphalt	River Gravel	Fordyce, Shower Quarry	3.0
18	AMR	US 54	DC	1998 (Sept.)	PG 70-28		Type D		River Gravel		2.0
19	BRY	SH 6	M	2000 (June)							2.0?
20	MnRoad	Cell 1	MN	1992	AC 120-150		Marshall 75 blow				5.9

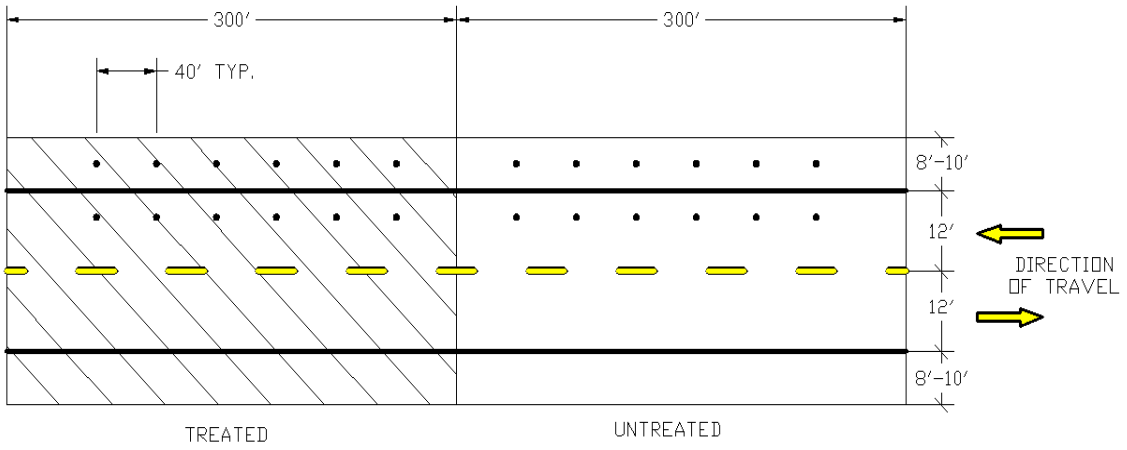

Figure 2 A Typical Coring Layout with Maintenance Treatment.

Test Methods

Pavement Core Properties

A number of field core properties were tested, including the bulk and maximum specific gravities and the total and accessible air void contents. Standard method ASTM D 6752-03 is used to determine the bulk specific gravity of compacted specimens. Standard method ASTM D 6857-03 is used to determine the maximum specific gravity of compacted specimens (Cooley et al. 2002, Buchanan and White 2005). The measurements are given by the following equations:

$$G_{bm} = \frac{DA}{SeA - SeW - \frac{BA}{B_{sg}}}$$

$$AAV = \frac{SeA - SeW - \frac{BA}{B_{sg}} - (DA - SaW)}{SeA - SeW - \frac{BA}{B_{sg}}}$$

$$G_{mm} = \frac{DA}{SeA_{broken} - (SaW_{broken} + BW) - \frac{BA}{B_{sg}}}$$

$$TAV = 1 - \frac{G_{bm}}{G_{mm}}$$

where, G_{bm} = Bulk specific gravity

G_{mm} = Maximum specific gravity

AAV = Accessible air voids

TAV = Total air voids

DA = Dry sample weight in air

BA = Bag weight in air

BW = Bag weight in water

B_{sg} = Bag specific gravity

SaW = Saturated sample weight in water

SaW_{broken} = Saturated broken sample weight in water

SeA = Sealed sample weight in air

SeA_{broken} = Sealed broken sample weight in air

SeW = Sealed sample weight in water

In method ASTM D 6857-03, to measure the total air voids, mixtures need to be broken into smaller pieces to open the trapped air voids. As a single measurement, after

determining the SeA_{broken}, the broken mixture was vacuum sealed in a flexible bag and immersed in water, the bag opened to let the water fully saturate the sample, and both sample and bag weighed underwater to obtain ($SaW_{broken} + BW$).

Extraction and Recovery

The extraction used successive washes: each wash is a blend of 85 % toluene plus 15 % ethanol. When the last wash was light brown instead of black, the binder was considered to be completely extracted from the mixture. The solution was distributed into 15 mL conical type tubes to do the centrifuge at 3100 rpm for 10 min to remove the big particles. After the centrifuge, the solution was filtered using a basket coffee filter to remove all particles.

The asphalt binder was recovered from the solvents with a Büchi, Re 111 Rotovap. The rotovap "flask" was specially designed as a straight glass tube that would mate with a 55 mm diameter ointment tin. During the recovery, nitrogen gas was introduced into the vessel to drive off any remaining solvent and to prevent asphalt reacting with oxygen. The bath temperature was kept at 100 ^{o}C to avoid hardening or softening of asphalt in the dilute solution. When no more tiny drops of the solvents could be detected visually on the condenser, the bath temperature was increased to 174 ^{o}C for an additional 50 min to ensure sufficient solvent removal. The total time of extraction and recovery was 4 to 6 hours for each sample.

Binder Content

To determine the binder content as a percent of the initial core weight, the binder was weighted after the extraction and recovery process. The measurement of the binder

content is given as follows:

$$\text{Binder Content} = \frac{\text{Binder Weight}}{\text{Mixture Weight}} \times 100\ \%$$

Dynamic Shear Rheometer (DSR)

After the solvent removal, the rheological properties of the binder were determined using a Carri-Med CSL 500 Controlled Stress Rheometer. A 2.5 cm composite parallel plate geometry was used with a 500 μm gap between the plates. The rheological properties of interest are complex viscosity (η_0^*) measured at 60 °C and 0.1 rad/s, storage modulus (G') and dynamic viscosity (η'), both at 44.7 °C and 10 rad/s. The DSR Function, calculated from the dynamic storage modulus and the dynamic viscosity (see Chapter I), could reflect the performance of the binder in pavement service (King et al. 2012).

Fourier Transform Infrared Spectrometer (FTIR)

Carbonyl Area was measured using a Nicolet 6700 Fourier Transform Infrared Spectrometer (FTIR) with an attenuated total reflection (ATR) ZnSe prism. The absorption band (from 1650 to 1820 cm^{-1}) relates directly to carbonyl content, provides a good measurement of binder oxidation (Liu et al. 1998).

Results and Discussion

In previous studies, results were obtained from test sites across Texas (Woo et al. 2007). These results provide not just clear evidence of binder aging in pavements but also strongly indicate that binder aging happens through all the depth of pavement. A general conclusion was made that binder aging is controlled by both pavement environmental conditions and binder kinetics and hardening properties. However, due to the limited

pavement aging periods in each study, some of the pavements were still in the initial jump period when the samples were collected, higher aging rates were determined probably, therefore the accuracy of the pavement aging estimation suffers. However, the massive data gathered from all over Texas provided a database for estimating an approximate aging rate for a certain binder used in the pavement in a certain region.

Oxidative Aging in Minnesota

As a further study of the effect of pavement temperature on asphalt binder aging, besides the Texas pavements aged under hot temperatures, one MnRoad test site was also brought into this study. The MnRoad site is located in Minnesota near Minneapolis-St. Paul, and the annual pavement temperature in Minnesota is much lower than in Texas. This pavement is special because it was well designed and carefully constructed for a scientific study of pavement performance. The test site incorporated within this study, was from the main line test road constructed in 1992 and used an unmodified AC 120-150 penetration grade and Superpave PG 58-28 grade binder. In one of the previous studies, the first coring date was in 2004, giving 12 years of service, but it did not mention the core was from wheel path or shoulder. In this study, two more coring occurred, once in 2008 on wheel path and again in 2010 on both wheel path and shoulder, thus giving 16 and18 years of service. In addition, in previous study, the original binder used in this pavement was tested in a number of controlled laboratory aging methods, including environmental room aging at 60 ^{o}C, stirred air flow test (SAFT) aging and modified pressure aging vessel (PAV) aging (Woo et al. 2007) . A complete comparison of data from the previous and from the new studies on the pavement cores and their binders follow.

As mentioned in the material section, the cores were sliced into layers of a half inch (12.7 mm) thickness and then each layer was tested for its binder content, total air voids and accessible air voids. Figure 3, Figure 4 and Figure 5 show the binder content for Cells 1 (Figure 3), the total air voids (Figure 4) and the accessible air voids (Figure 5). In Figure 3, the binder content is quite consistent in each of these four cores, and all of them are around 4.5 percent by weight.

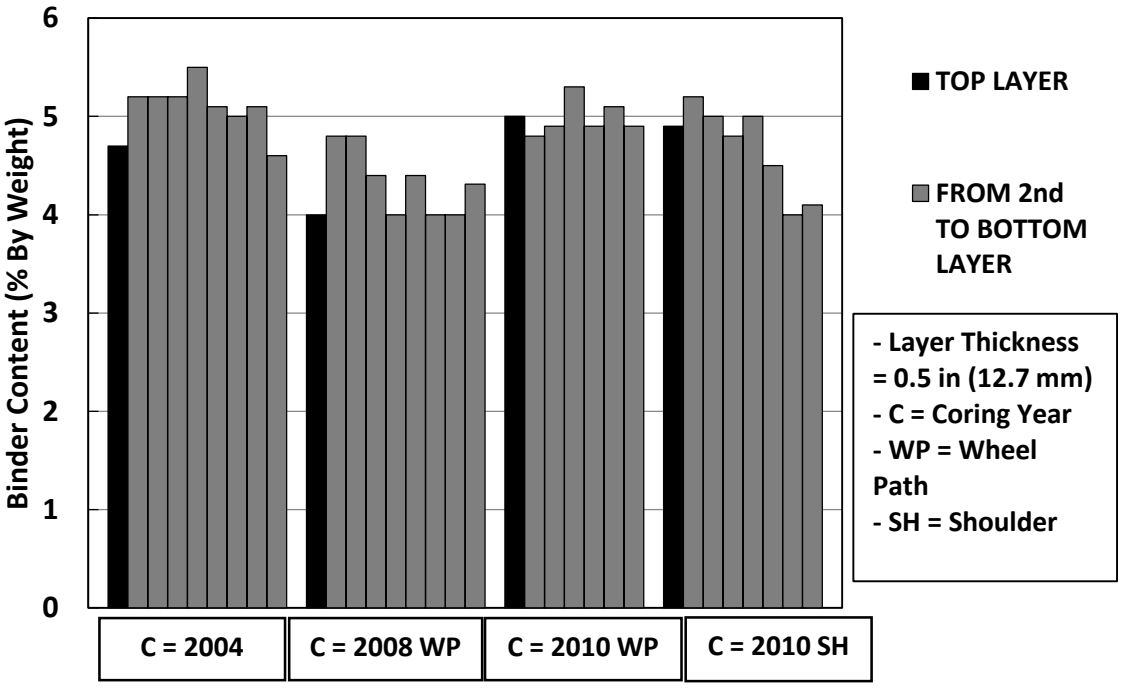

Figure 3 MnRoad Binder Content.

Figure 4 shows the total air voids in each layer of those four cores as determined by the Corelok® method. Note that there is variability of the total air voids in each core so that the range is from 5 to 13 percent. It should also be noted that the top and bottom layers

have much higher total air voids than the middle layers. Therefore, the total air voids shows a C-shaped distribution in each core. Moreover, except the top layer, the total air voids increase with the pavement depth for the cores collected in 2004, 2008 (wheel path), 2010 (wheel path). One exception is the core of 2010 shoulder, the distribution of the total air voids of the middle layers is quite consistent within itself, at approximately 7 percent. This could be easily explained as much less compaction on the pavement shoulder in construction than the wheel path.

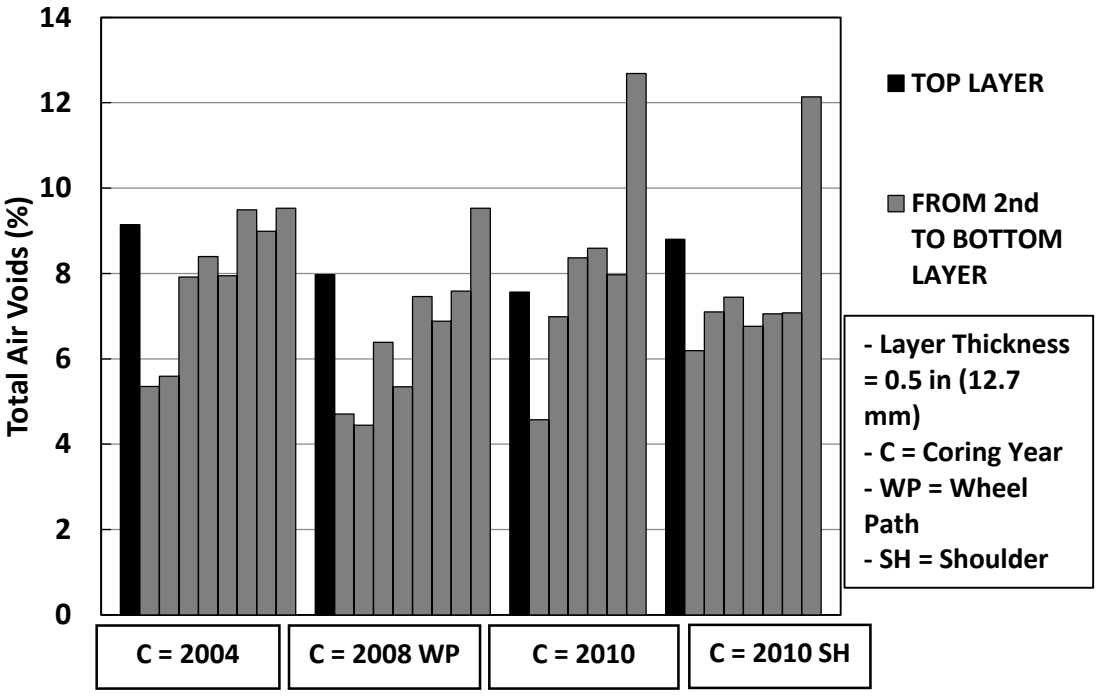

Figure 4 MnRoad Total Air Voids.

The accessible air voids determined by the Corelok® methods are shown in Figure 5. The accessible air voids are controlled by asphalt-aggregate ratio coupled with the compaction during construction. The core of 2004 has a very low accessible air voids compared with other cores collected later from the same road. The value is even below 1 percent for the layers in top half of the core (0 to 3 in and 0 to 76.2 mm from the pavement surface). As the depth goes down to the bottom, the accessible air voids increase to 5 percent. Relative high accessible air void percentages are found in the core of 2008. It may due to the cracking happened in those 4 years. The cracks connect the trapped air voids and open those enclosed spaces to the air channels in the core thus creating more accessible air voids. In the cores collected in 2010, the accessible air voids seem to stay at the same level as in 2008. Comparing the wheel path and the shoulder cores collected in the same year, obviously, the shoulder appears to have higher accessible air voids in the top and middle layers, which is due to less compaction.

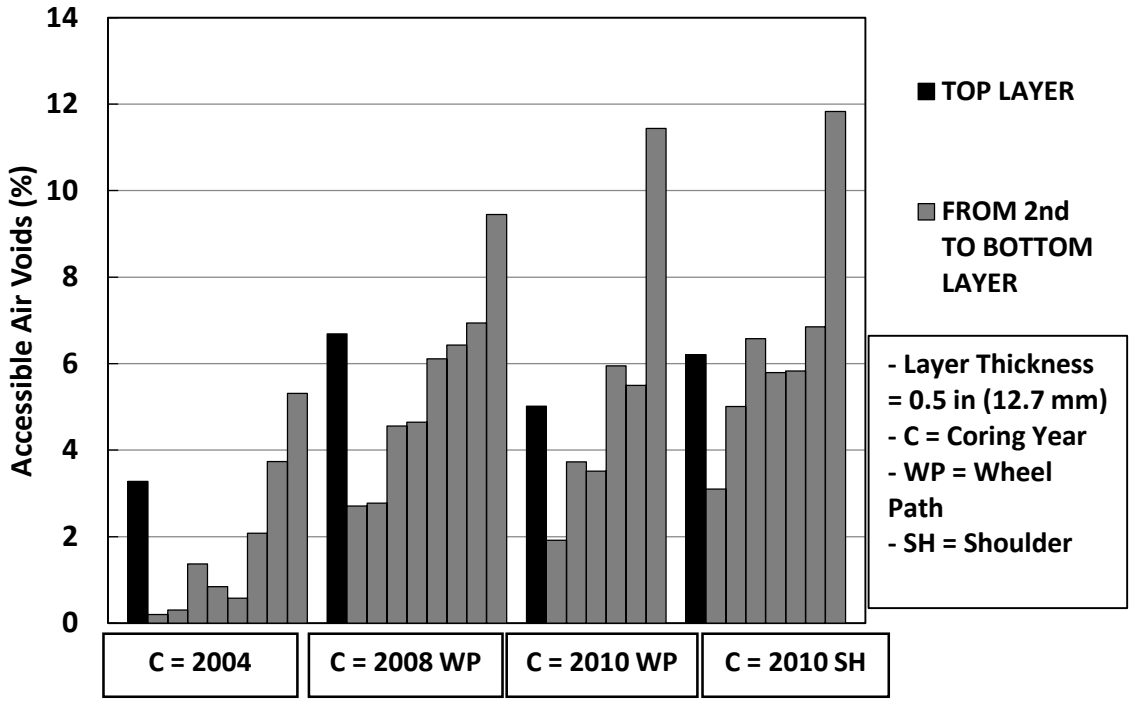

Figure 5 MnRoad Accessible Air Voids.

Figure 6 through Figure 10 show the test results of the recovered binder from the four cores. The recovered binder was tested for its carbonyl area and the rheology properties (limiting viscosity and DSR Function) to evaluate its level of oxidation. Due to the lack of the carbonyl content and limiting viscosity data of the core collected in 2004, only DSR Function properties are shown and plotted in Figure 6 to 9 on DSR Function map. The DSR Function map is a plot of binder's elastic modulus versus the ratio of its viscosity to elastic modulus. A binder appears at the lower right corner on the map first, and as the binder hardens, it moves to the upper left.

On these figures, to better understand the recovered binder properties, the properties of original binder aged in laboratory, which were reported by Woo et al. (2007), are shown in the graph. The laboratory aging methods included SAFT, a modified Pressure Aging Vessel test (PAV* 16 hours and 32 hours) and Environmental Room (ER 3, 6, 9, 12 months). Note that the unaged binder lies far away from the others, to keep the graph clear, only its coordinates are given. The SAFT aging, which simulates the aging in the hot mix plant, is near the lower right corner. The PAV* 16 hours aging is in the center of the graph, and PAV* 32 hours aging is near the 10-cm ductility dashed line. The ER 3 months aging is close to the PAV* 32 hours aging. With the extension of aging time, the ER aging statues move toward the upper left corner. The most aged sample, ER 12 months aging is close to the ductility equals 3-cm dashed line. These dashed ductility lines are plotted from the correlation reported by Ruan, Davison, and Glover (2003).

The data for all the layers in each core are shown in Figure 6 to 9. One conclusion in previous studies is that all the recovered binders from the same core fall along the same path (Walubita et al. 2006). Actually, this conclusion could be extended to be true of the same binder, whether it is unaged, aged in laboratory, or aged in pavement. In those figures, although those aging conditions vary significantly, the SAFT, PAV* aging and ER aging binders follow the same path as the binders recovered from the cores. And in each graph, the levels of aging through the top layers to the middle layers and then to the bottom layers follows a similar trend. For the top layers (the 1st layer to the 4th or 5th layer), the binder deeper in the pavement is less aged. This observation partially agrees with the conclusion of Coons and Wright (1968) as noted in the introduction. However, the data from the lower

layers surprisingly move in the opposite direction. That is, the binder from progressively greater depths (the 4th or 5th layer to the bottom layer), is progressively more aged. Note that, contradicting the work by Coons and Wright, the binder that was recovered from the very bottom layer, which is nearly 5 in deep into the pavement, is aged as much as the binder at the surface of the pavement (Figures 6, 7, 8) or even more (Figure 9).

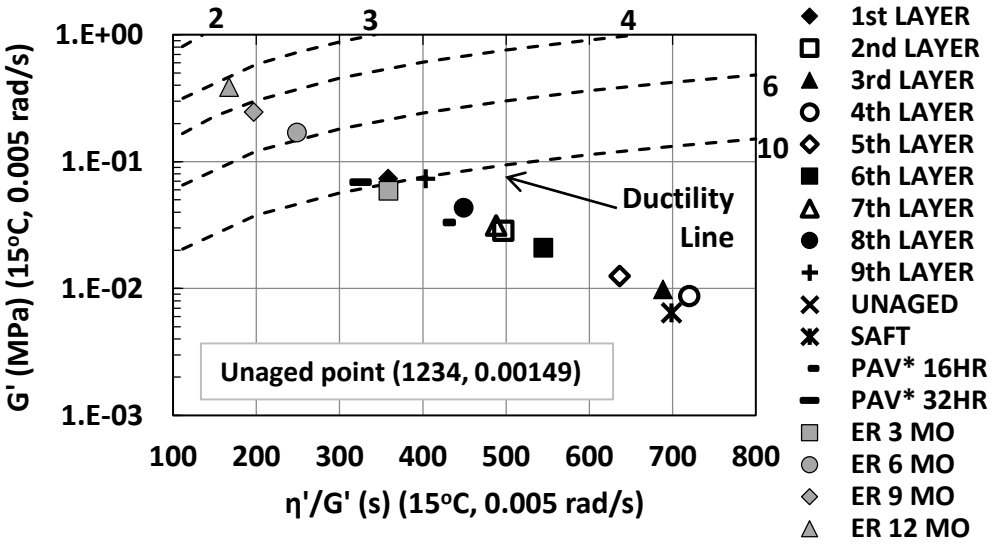

Figure 6 MnRoad Aging Comparison of the Core Collected in 2004.

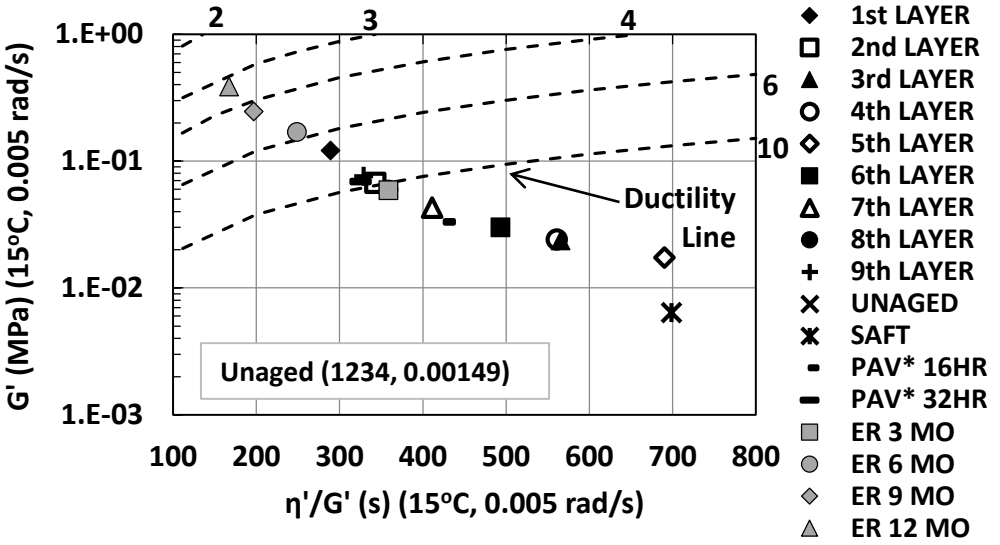

Figure 7 MnRoad Aging Comparison of the Core Collected from Wheel Path in 2008.

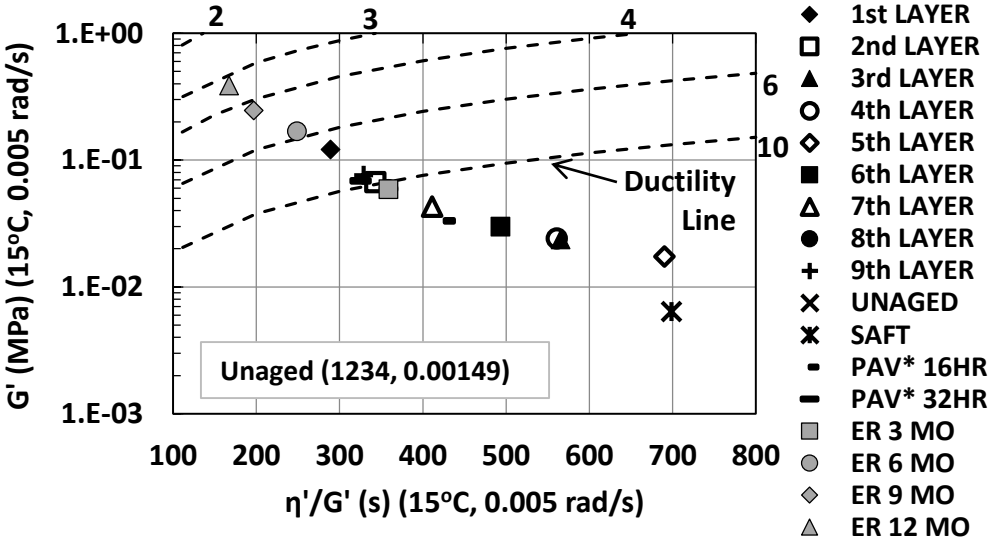

Figure 8 MnRoad Aging Comparison of the Core Collected from Wheel Path in 2010.

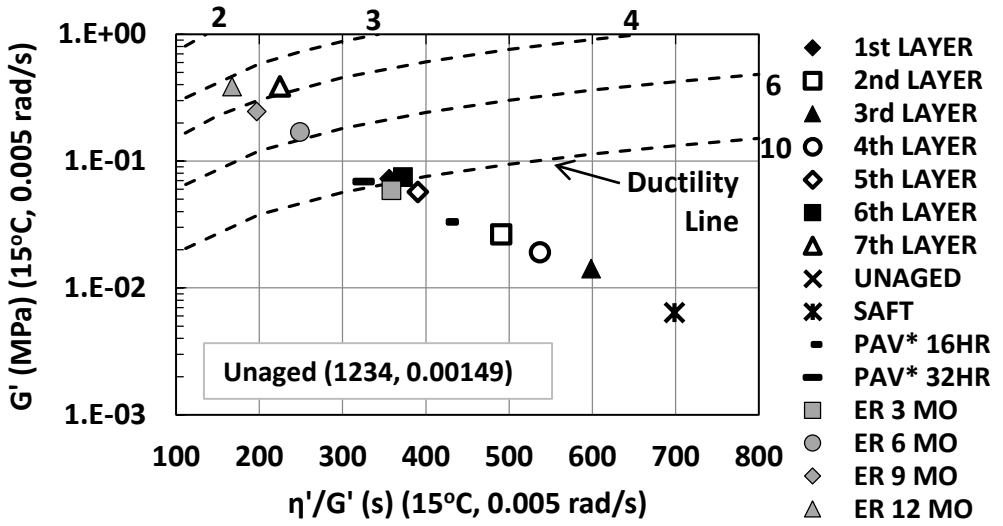

Figure 9 MnRoad Aging Comparison of the Core Collected from Shoulder in 2010.

Figure 10, which covers all the data from the MnRoad cores shown in Figure 6 to 9, is in view of asphalt aging with time. It is noted that all the recovered binders from different cores followed the same path on the DSR Function map. To find the binder DSR data increasing over time is not easy in Figure 10 due to sample variation, however, a general conclusion could be found by observing the sample point distributions in the DSR map. For example, if only six data points from the recovered binder are counted in the lower right corner (not including SAFT aging), three of the six points are from the core collected in 2004. Again, if only six data points from the recovered binder are counted in the upper left corner (not including ER aging), five of the six points are from the cores collected in 2010 (both wheel path and shoulder). Thus, Figure 10 strongly supports the fact that binder in pavement ages with time.

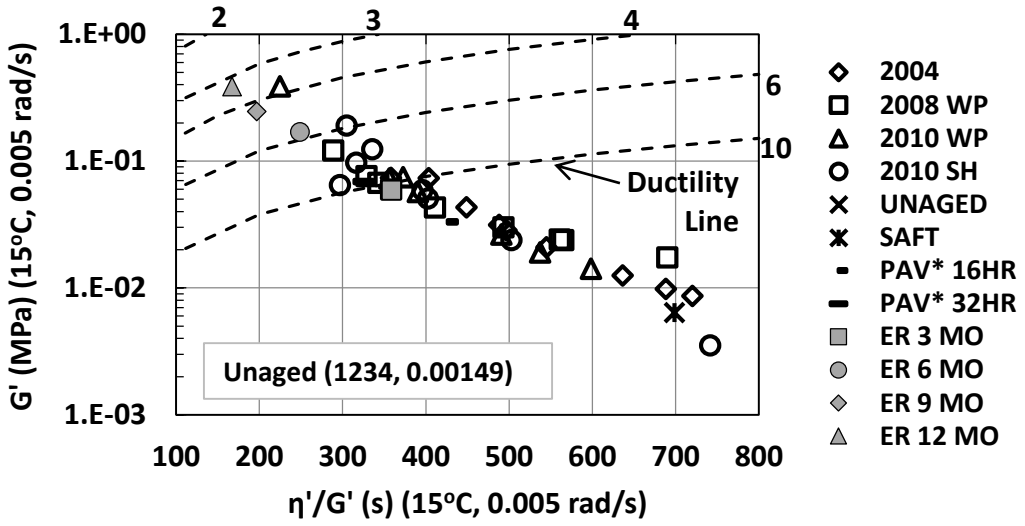

Figure 10 MnRoad Aging Comparison of the Cores Collected in Different Years.

In an effort to quantify the relationship between binder aging and air voids, Figure 11 shows data for the four cores, where accessible air voids appear to affect binder aging rates. The DSR Function is shown layer-by-layer as well as the air voids of those layers. In each core, it is clear that the lower the accessible air voids, the lower the level of binder hardening (lower DSR Function). Coupled with the data of air voids, the reason for the phenomenon that heavier aging in the top and bottom layer than middle layers is quite clear. The amount of aging is reduced by the progressively lower accessible air voids from the pavement surface to the center, and then that increasing accessible air voids towards the bottom enhance the aging. It should be noted that each of these comparisons is only within one pavement core. A comparison between two different cores may consider two variables, accessible air voids and aging time, thus that general correlation between the air voids and aging is not always true in such a comparison. For example, the 4th layer of 2010

shoulder core has the lowest DSR Function value of all the 33 layers, but has a related high accessible air void (the 7th highest) and longest aging time. Nonetheless, Figure 11 strongly supports that the variables of the air voids significantly affect the aging rates of the binders under different depth.

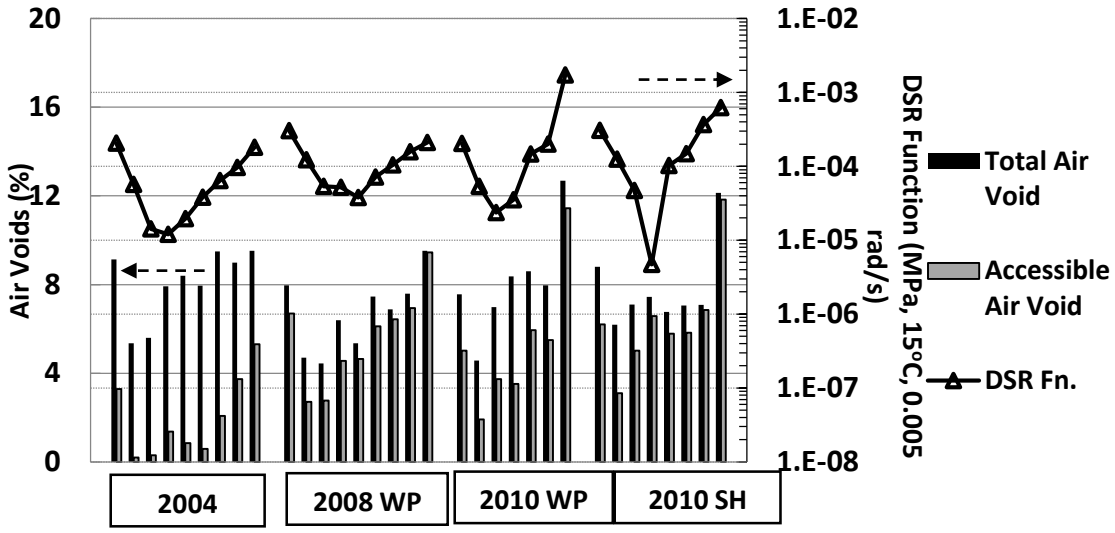

Figure 11 Binder Hardening Related to Local Pavement Accessible Air Voids.

Oxidative Aging in Texas Pavements

During the course of this study, field cores were collected from over 19 pavement sites in 14 TxDOT districts in four years, from 2008 to 2012. The cores were first sliced into half inch thickness layers from top to bottom, then measured each layer's total and accessible air voids. After that, asphalt binder was extracted and recovered. The measurements including binder content, DSR and FTIR, were made on these recovered binders. These first-hand information on pavement aging covers every climate regions in

Texas (see Figure 1), together with comparable data for the pavement in Minnesota, comprise a database of significance for the scientists and engineers to estimate the pavement aging rates in two very different regions. The results are reported in various appendices attached in the end of the dissertation and the following discussion is only made on the DSR Function values.

Figure 12 and 13 summarize the hardening of various binders in all 20 pavement sites, both in Texas and in Minnesota. The average DSR Function values of the cores (weight averaged from each layer) collected from the wheel path versus the corresponding pavement ages is given in Figure 12. The same analysis on the cores collected from the shoulder is given in Figure 13.

In Figure 12 and Figure 13, there appears to be a lot of scatter and disorganization to the data. However, when considered in detail, for each pavement, the results are, in fact, quite consistent. In Figure 12, as expected that the hardening rate of the MnRoad pavements is much less than the rates of pavements in Texas due to the vast difference in climate. Binder ages from a low aging level in the pavement, and the DSR Function value increases over time, indicating the binders turn stiffer with service year. According to the aging model proposed in the previous study (Liu et al. 1996), after two or three years of fast-rate aging in Texas (the number may increase in Minnesota), the binder aging eventually reaches a constant annual rate and in principle can increase indefinitely throughout the pavement life. There are exceptions, however, BRY US 290 shows a sharp decreasing trend in Figure 12. This exception will be discussed as follows.

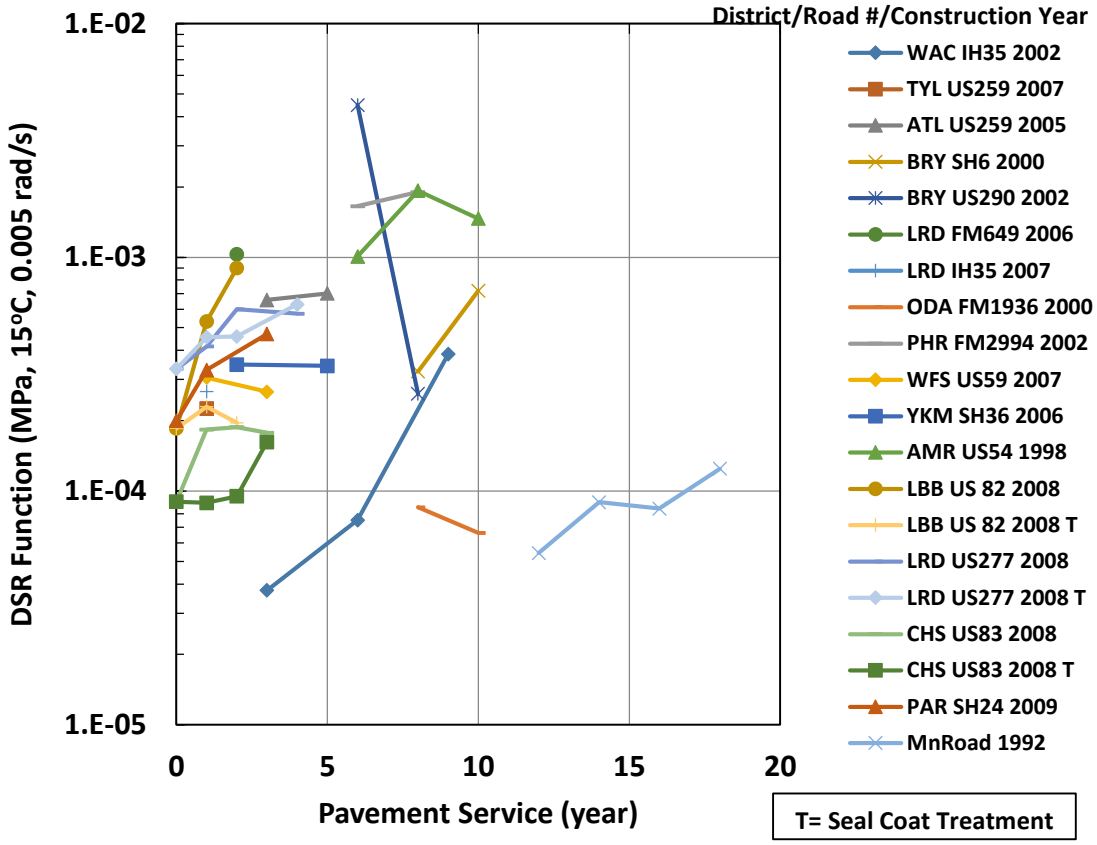

Figure 12 DSR Function Hardening with Pavement Service Time in Texas and MnRoad Pavement (Wheel Path).

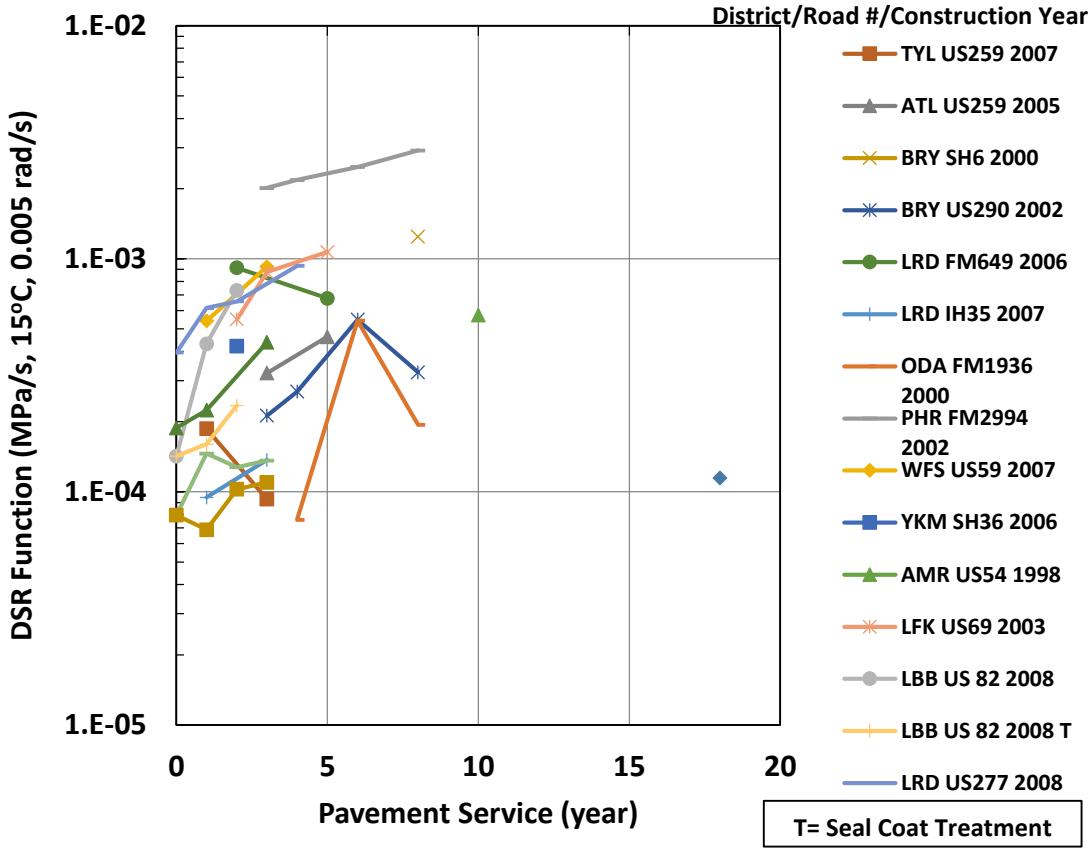

Figure 13 DSR Function Hardening with Pavement Service Time in Texas and MnRoad Pavement (Shoulder).

Figure 14 shows a comparison of the average air voids of the field cores collected from BRY US 290. The values are averaged from layers in those field cores. Shoulder in 2005 and 2006 have 3 layers each (0.5 in per layer) and the data were reported in Woo et al. (2007). Wheel path in 2008 has 5 layers (0.5 in per layer) and shoulder in 2008 has 4 layers. Wheel path in 2010 and shoulder in 2010 have been measured as a whole piece. It is surprising that the core of wheel path in 2008 has both total air voids and accessible air voids (Corelok method) significantly higher than the other cores. The average total air

void content for the core of wheel path in 2008 is 16.4±4.3 %, and the average accessible air void content is 16.3±4.3 %. However, the average total air void content for the other five cores including another wheel path (2010) and four shoulders (2005, 2006, 2008 and 2010) is only 10.3±1.2 %, and the average accessible air void content is only 7.7±1.5 %. Generally, high accessible air voids result a much accelerated effect on binder hardening. Thus, it is not difficult to understand that the heavy aging in this core is an exception due to its extremely high air voids. This kind of exception should be avoid in the future studies by expanding the sample numbers.

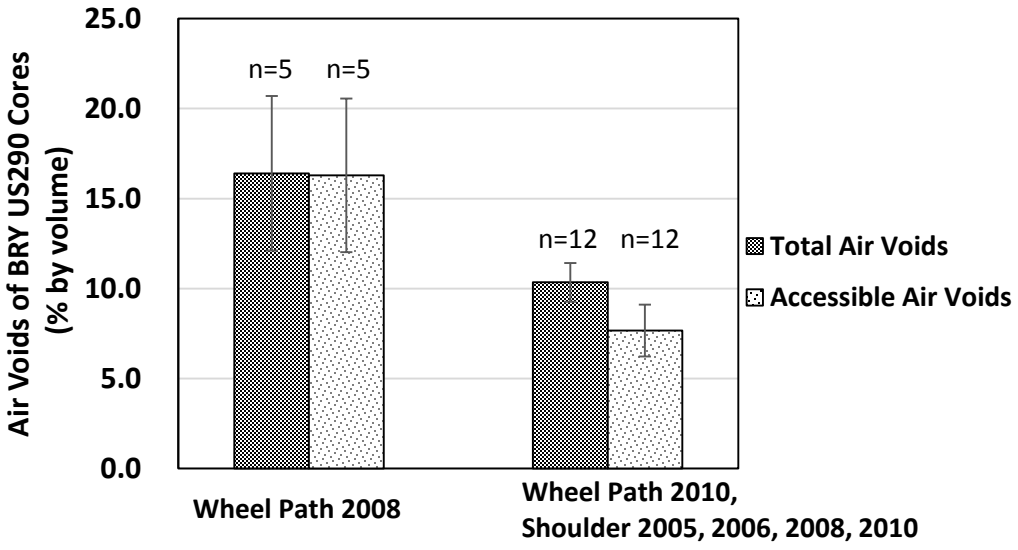

Figure 14 Air Voids of BRY US 290 Cores (Mean ± 95 % Confidence Interval).

For most of the pavements, the field cores were obtained twice or more times during the research periods. A general observation is that the cores collected in the later years are noticeably more aged than the cores collected earlier. Either the time between

coring is relatively too short or the exceptions caused by the uncontrolled variables (like high air voids in BRY US 290 wheel path in 2008), may weaken this simple conclusion. But, there is no doubt that the binder progressively hardens in the pavement over time.

Another observation relates to the possible effectiveness of the seal coat in slowing oxidation in the underlying pavement layers that are beyond seal coat penetration. After making a paired *t*-test comparison of CA values (see Table A11, Table A12, Table A13, Table A14 and Table A21 in Appendix A), the treated and untreated cores in US 82, US 83 and US 277 were paired with each other, by corresponding layer (but excluding the seal coat and the first pavement layer) and by corresponding coring year. This procedure gave five comparisons, WP and SH for each of three pavements, US 82, US 83 and US 277, except that SH for US 277 was not treated so no comparison was possible. For the US 82 data, which would be further discussed in Chapter V, and for both WP and SH treated layers, the CA values for treated cores were uniformly less than for untreated, including both 2009 and 2010 cores ($p<0.005$). Also the WP comparison for US 83 gave $p<0.05$. The consistency of this result in these cores appears to be a compelling result, supporting the notion that seal coats may retard oxidation in pavements for a time. However, such comparisons were not observed for US 83 SH or for US 277 WP. Perhaps it is due to three factors: inconsistency that can occur in pavement analyses, or that achieving an effective seal is problematic or, that oxidation remains available from the edges and below the pavement in spite of an effective seal.

Figure 15 to Figure 19 show the DSR Function hardening characteristics of all the recovered binders in this study. As mentioned above, the cores were sliced into layers and

detailed studies were conducted on the binders extracted from each layer. As oxidation occurs, both CA and DSR Function increase with time, so a binder moves from the vicinity of the lower left corner in the direction of the upper right corner. The slope of this linear correlation between natural logarithm of DSR Function and CA is called DSR Function hardening susceptibility and the *y*-intercept of the line is DSR Function hardening intercept. Every binder has its own hardening characteristics but they are not unique. In most of the cases, measurement of this DSR Function-CA correlation is able to identify binders. For example, in Figure 15, binders from LBB US 82 and MnRoad are significantly different anqualty because the MnRoad binder is selected to be a softer binder, to acccrmodate colder temperatures; the HS values of two binders show no significant differences.

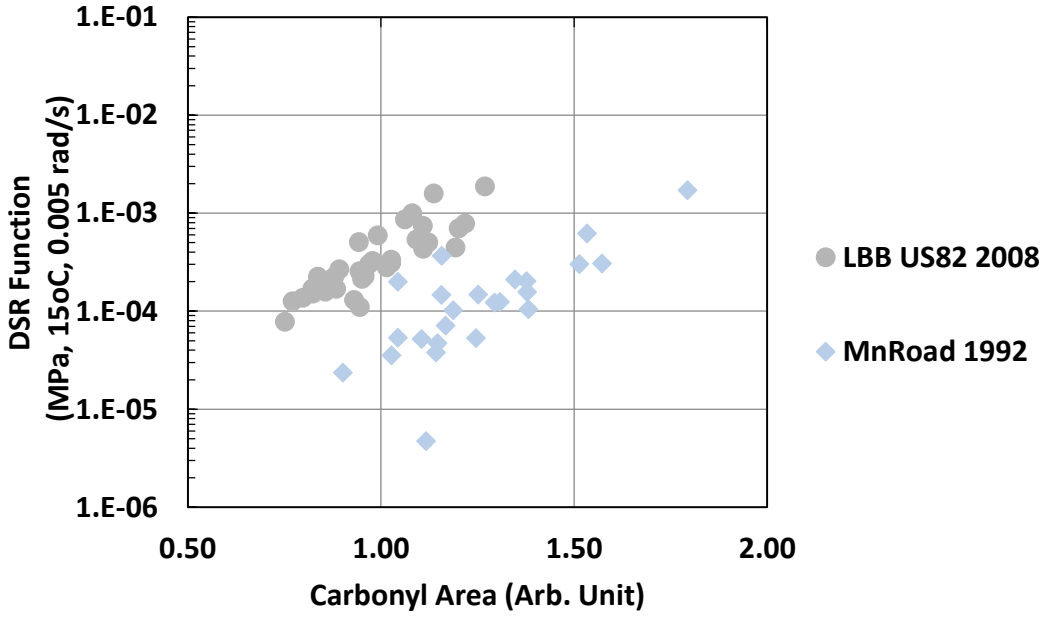

Figure 15 DSR Function versus Carbonyl Area of Recovered Binders (1).

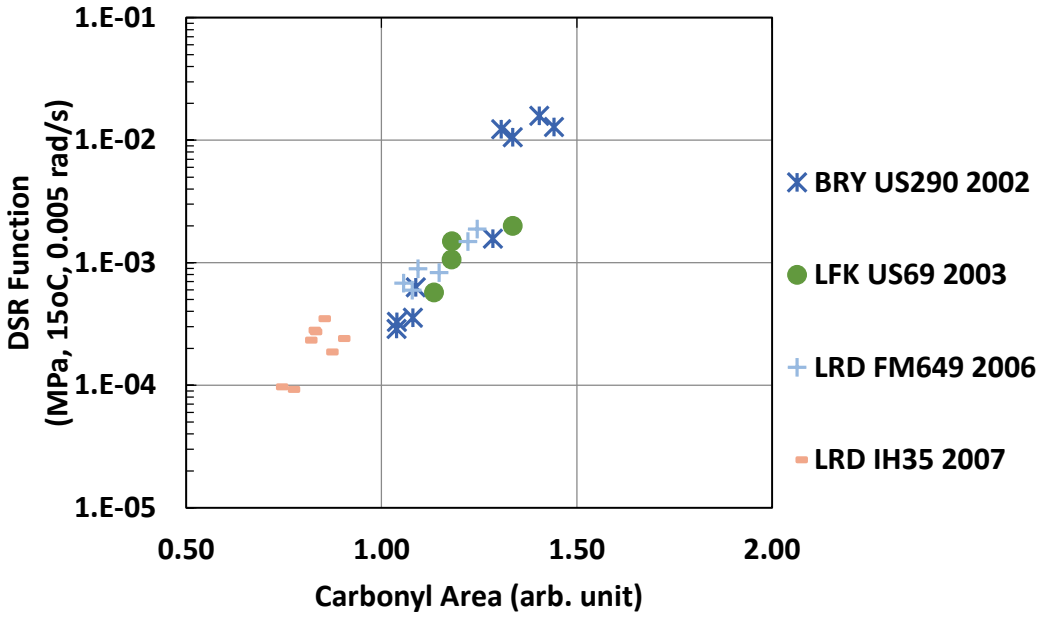

Figure 16 DSR Function versus Carbonyl Area of Recovered Binders (2).

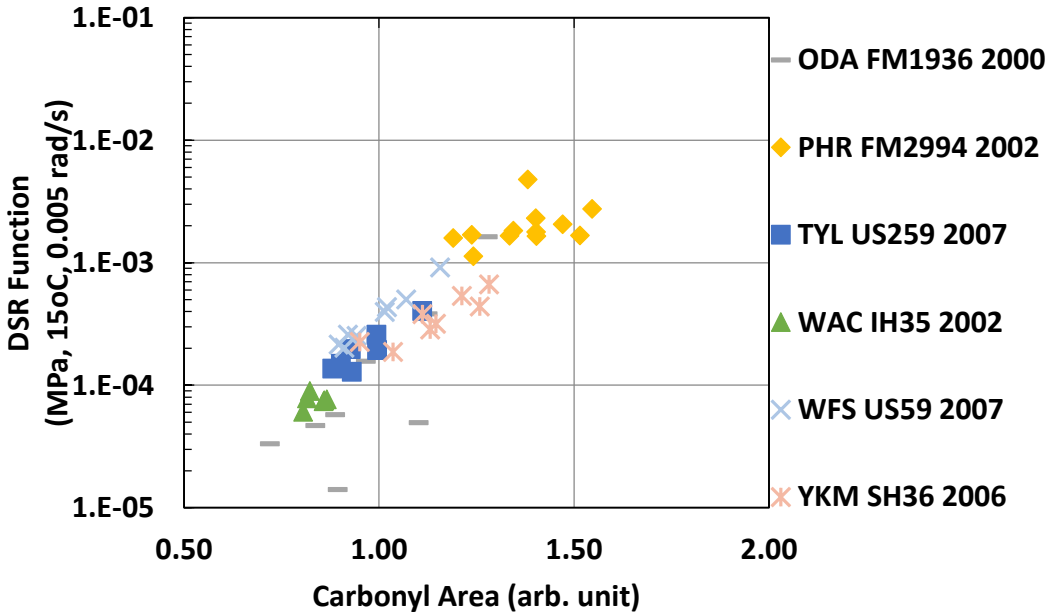

Figure 17 DSR Function versus Carbonyl Area of Recovered Binders (3).

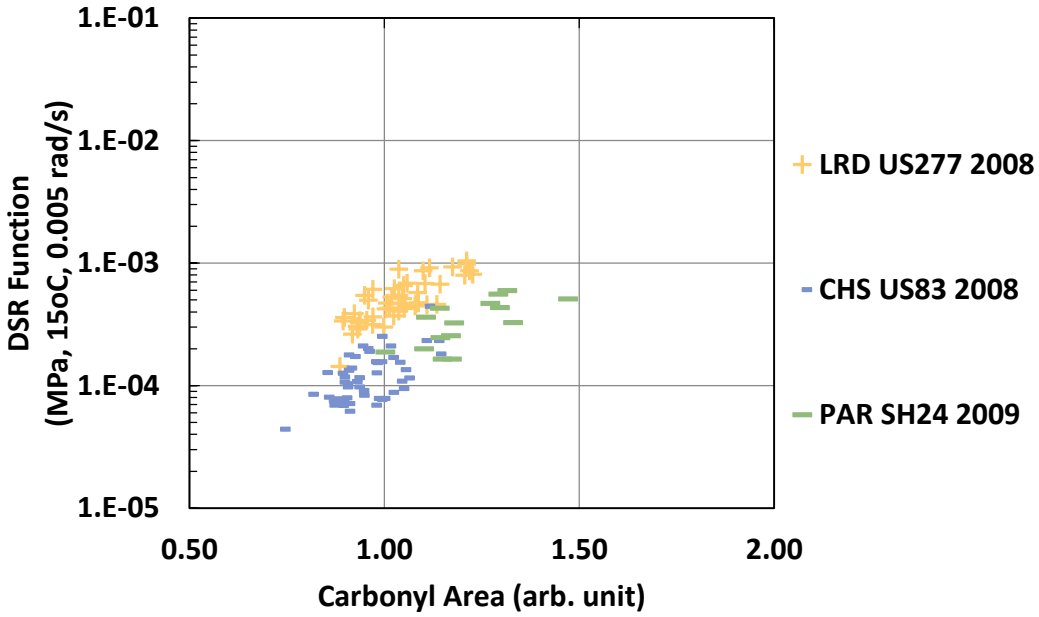

Figure 18 DSR Function versus Carbonyl Area of Recovered Binders (4).

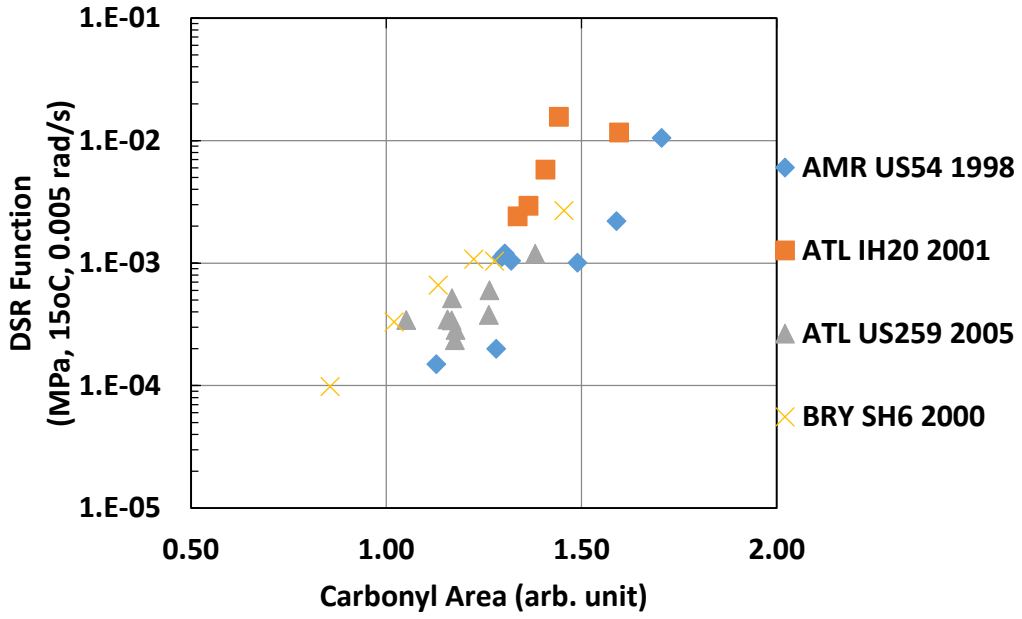

Figure 19 DSR Function versus Carbonyl Area of Recovered Binders (5).

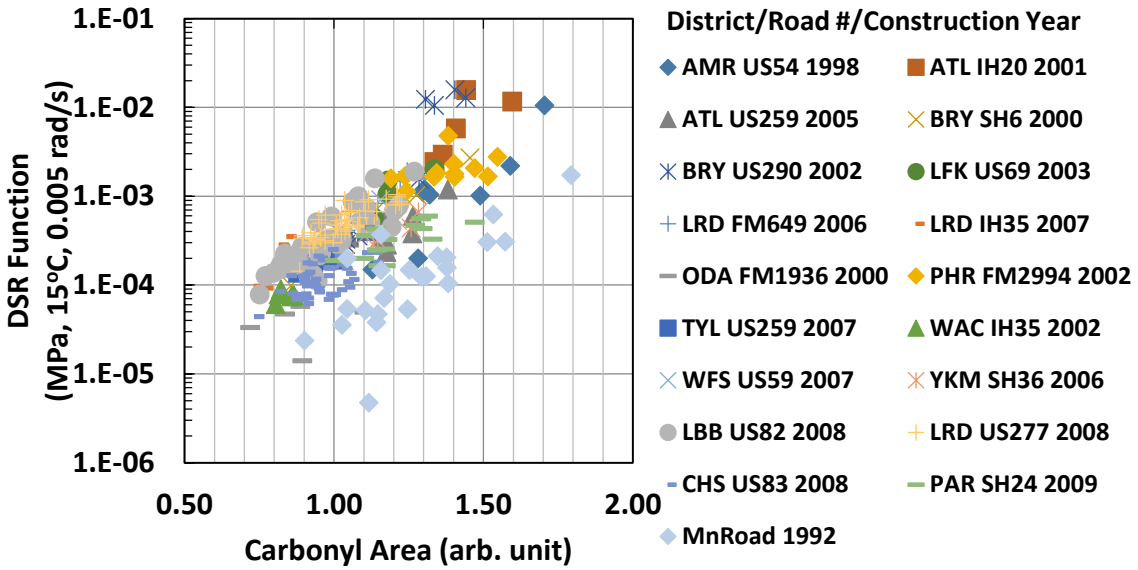

Figure 20 DSR Function versus Carbonyl Area of all Recovered Binders.

Data of DSR Function versus CA for all of the pavements are shown in Figure 20. Because of the tremendous numbers of data points, it becomes impossible to recognize each point in the figure. The hardening susceptibility and hardening intercept data for each recovered binder are given in Appendix A.

Conclusions

Based upon the discussion above, a number of conclusions of asphalt aging in pavement could be made as follows:

- Aging rates are different with depth of the pavement. This is a result of the accessibility of oxygen to the binder through the accessible air voids. From the pavement surface to the center, the amount of aging is reduced by the progressively

lower accessible air voids. And then that increasing level of accessible air voids towards the pavement bottom increases the aging.

- The significant impact of temperature results the binder aging in Minnesota occurs much lower than in Texas. That makes the oxidative aging not an important issue in the cold regions.
- A few pavements appear to experience a degree of oxidation decreases over time. But it definitely relates to some uncontrolled variables. In most of the cases, the binders oxidize and harden continuously in the pavement in an irreversible way.
- Generally, pavements with seal coat treatments appear to be under aged relative to the same pavement without this kind of maintenance. This phenomenon might relate to the application of a seal coat. Detailed data and discussion will be reported in Chapter V.

This study includes much more measurements of field binder aging than any previous studies. The collection of pavement cores provides massive of field data. Those data are used to assess the effects of accessible air voids, pavement temperatures and binder oxidation and hardening properties. However, two common problems suffer every study on pavement aging, limited numbers of field cores due to the expense and time and the uncontrolled variables different from one pavement site to another. So it is still far from summarizing a quantitative evaluation on the effects of various variables on asphalt aging in pavements. With studies keeps moving forward, more data would be added into the database. A complete picture of pavement aging will become clear in the future.

CHAPTER III

ASPHALT AGING STUDY ON FIELD AND LABORATORY AGED ASPHALT CONCRETE SAMPLES

Introduction

Except the measurements on binder kinetics and hardening, the pavement oxidation model also requires measurements on field asphalt concrete cores to determine the diffusion depth and to adjust the field calibration factor (*fcf*). An asphalt concrete mixture is a heterogeneous complex material composed of air voids, aggregates and asphalt binder. The selection of the materials and design is strongly dependent on a series of experimental tests in the laboratory. Although many previous studies on asphalt concrete mixtures point out that asphalt concrete performance strongly relates to asphalt binder properties, aging in asphalt concrete is not the same as aging in asphalt binder (Clark 1958, Halstead 1963, Welborn 1984, Walubita et al. 2005, Walubita et al. 2006). Performing aging tests only on asphalt binders could shorten the experiment period and simplify the experimental procedure, but there are very important data those experiments could not provide, especially the information on the interaction between the asphalt binders and the aggregates on aging (Petersen, Barbaar, and Dorrence 1974). Therefore, there is a need to study the asphalt aging in concrete. However, because of the field aging is very slow, it always takes years to measure an aging rate. Moreover, the fact that no field sample is available before pavement construction seriously limits applications of the pavement oxidation model.

Laboratory aged asphalt concrete samples are expected to replace the field samples in the measurements. First, laboratory samples have exactly the same materials and design as field ones, there should be no difference in mechanical properties. Second, comparing with the aging in pavements, laboratory aging at higher temperatures shorten the required time from years to months. Third, the aging conditions are controlled precisely in laboratory. Fourth, in case of a prediction before the pavement construction, there is no field core at all and testing on laboratory samples is the only choice. Although the laboratory aged sample has so much advantages, a commitment of efforts is needed to establish a correlation between the aging rates under field and laboratory conditions first.

Objectives

The goal of this study is to establish a correlation of asphalt concrete aging rates in field conditions and laboratory conditions and to propose a new model prediction method using laboratory aged cores instead of field cores.

Experimental Methods

Materials

Field Samples

Field samples were collected from three pavement sites in Texas, US 277 in the Laredo (LRD) District, US 83 in the Childress (CHS) District, and SH 24 in the Paris (PAR) District of the Texas Department of Transportation (TxDOT). The selection of those pavement sites was considered representative of the different climate zones in Texas as shown in Figure 21.

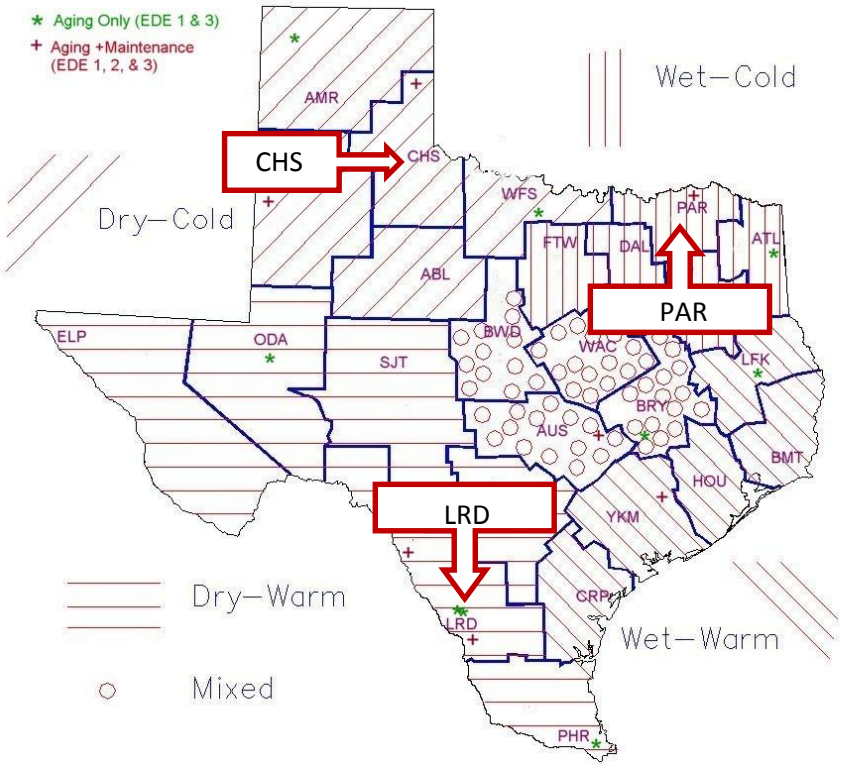

Figure 21 Field Sites Locations and Climate Zone in Texas.

In this map, LRD US 277 in the lower-left corner represents the field aging in Dry-Warm Zone. CHS US 83 in upper-left corner represents the field aging in Dry-Cold Zone. PAR SH 24 in upper-right corner gives an example of field aging in Wet-Cold Zone. The effect of climate--mainly the temperature effect--on pavement aging in different climate zone was compared. For all field cores collected from pavements each year, one from the wheel path and one from the shoulder, the air void content (AV) was determined first, then binders extracted from the concrete and tested for their characteristics. Information for test section US 277 is given in Table 2.

Table 2 Construction and Sampling Information of US 277.

Information	Details
District	Laredo, Texas
Texas Climate Zone	Dry-Warm
Binder Supplier	Valero Marketing and Supply Company
Binder PG Grade	PG 70-22
Construction Time	April/May 2008
1st Coring	July 2008
2nd Coring	December 2009
3rd Coring	December 2010
4th Coring	January 2012

Lab Mix Lab Compacted (LMLC) Samples

Raw materials collected during pavement construction were kept in laboratory. For the fabrication of LMLC samples, the exact same aggregates and binders were used as in field samples.

Aggregates used for the LMLC samples were placed in an oven at the mixing temperature of 149 ℃ and left overnight in order to remove moisture. The binder was also heated to the same mixing temperature for 2 hours just prior to mixing. The mixture was then short term oven aged at the compaction temperature of 135 ℃ for 4 hours as prescribed by AASHTO R30 for performance testing.

Samples were compacted using the Superpave Gyratory Compacter (SGC) to a 6 in (152.4 mm) diameter by 6 in height to meet the specified AV content. To obtain more uniform AV distributions that better represent field samples, LMLC samples were compacted at a higher AV content and then cored from 6 in to a 4 in (101.6 mm) diameter. The sample then had 1 in (25.4 mm) trimmed from each end to produce the final 4 in diameter by 4 in height sample with the correct AV content.

Finally, cores were aged in a 60 ºC environmental room with 0, 6, 9, and 12 month aging periods.

Binder Extraction and Recovery

The binder extraction for the field samples was executed layer by layer from the top surface to the bottom. First, all field samples were sawed into layers, with each layer approximately 0.5 in (12.7 mm) thick. Then, these layers were broken into small pieces ready for extraction. Note that the test results for each layer are in the Appendices; only the average values are reported in this chapter.

Unlike field samples, in which oxygen starts transporting from the top surface only, oxygen transports through all the surfaces exposed to air in LMLC samples. Considering the different oxidative levels throughout the core, a special procedure guarantees the final extracted binder presents the average property of the whole. The core was cut vertically into two equal pieces. Only one of the half-circle cores was broken into small pieces and then the small pieces were well blended. Only a portion of the amount was used in binder extraction.

The extraction used successive washes of a mixture of 15 % ethanol plus 85 % toluene by volume, approximately 85 ml solvent each wash for 250 g mixture samples. After extraction, the solution was centrifuged and filtered to remove all the aggregate particles. Then the binder was recovered from the solvent with a Büchi RE111 Rotovap. During solvent removal, the bath temperature was kept at 100 ℃ to avoid hardening or softening of the asphalt in dilute solution and nitrogen was used to carry off the solvent and to prevent any further oxidation. To ensure total solvent removal, the bath temperature

was increased to 174 ℃ for 50 min after the condensing solvent could no longer be detected visually.

Test Method

To determine the degree of oxidation, recovered binders were analysed by a Nicolet 6700 FTIR spectrometer with an attenuated total reflection (ATR) zinc selenide prism by measuring the carbonyl area (CA).

A Carri-Med CSL 500 Controlled Stress Rheometer was used to record and analyse the rheological properties, including limiting viscosity at 60 ^{o}C and DSR Function.

Results and Discussion

In this study, the asphalt concrete LMLC samples and field samples were aged separately under laboratory conditions (Environmental Room) and field conditions. The Environmental Room keeps a constant high temperate (60 ^{o}C) and a constant low humidity, which provides the LMLC samples in an accelerated aging condition with no external interference. However, for the samples aged in field conditions, except the temperature and humidity are changing every minute, many interfering factors affects its performance, like traffic loading, freezing and thawing, and so forth.

Binders in the asphalt concretes were extracted and recovered, and then the extent of aging was determined by FTIR. Aging rates under laboratory and field conditions were evaluated individually first and then combined together in order to provide a preliminary evaluation (see Figure 22, Comparison 1).

A pavement oxidation model was brought into this study to predict binder performance in the particular pavement. Two input factors, the field calibration factor (*fcf*)

and diffusion depth, were determined from LMLC samples instead of field samples. Results from field samples were used to verify the correctness of the model calculation (see Figure 22, Comparison 2).

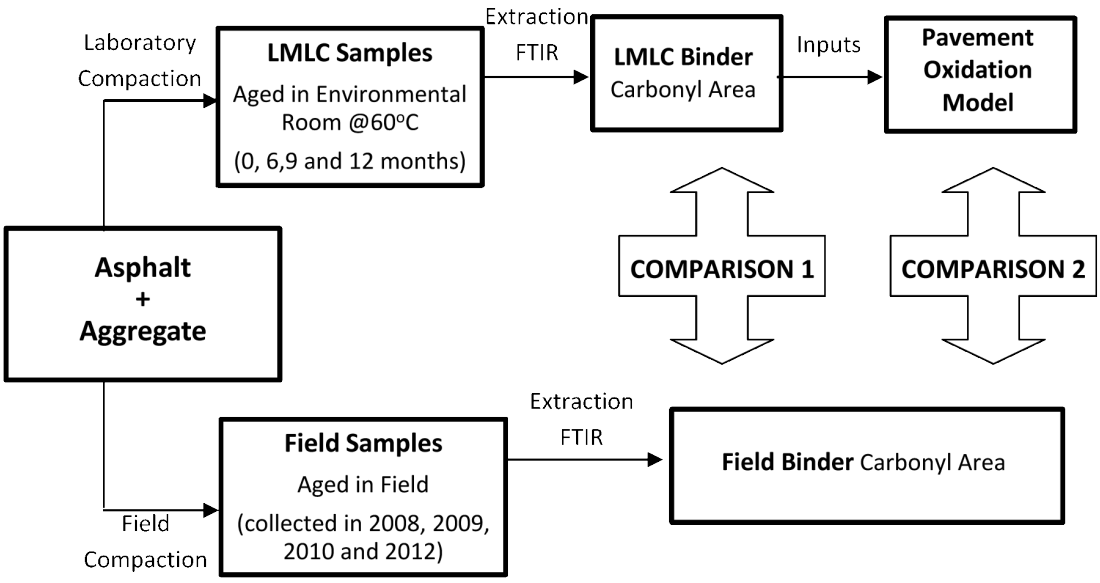

Figure 22 Testing Protocol for Field Samples and LMLC Samples.

Field Sample Test Results

With respect to the field samples, after the extraction and recovery, the extents of binder aging were tested by FTIR. CA growth rates were measured from the wheel path and shoulder samples collected from 2008 to 2012. CA value for each layer are reported in Table A21 and A22 in Appendix A. Average CA values are plotted in Figure 23. While the CA value for each location (shoulder and wheel path) increases from year to year, CA increased by about 0.07 (arb. unit) in the first year for both locations, indicating that much of the aging occurs during the first year. But there is no evident difference between the

wheel path and the shoulder until 2010. Since 2010, the oxidation accumulated in wheel path is slightly less than that in the shoulder.

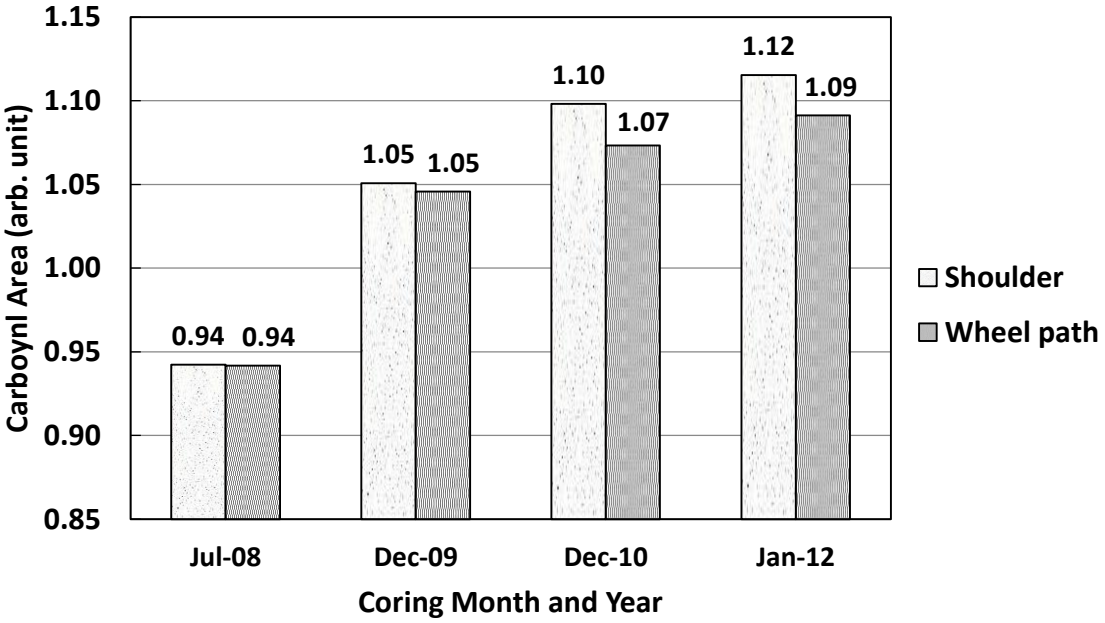

Figure 23 Average Carbonyl Area for All Sections of US 277.

Comparison of LMLC and Field Sample Results (Comparison 1)

After analysis on field aging, the performances of LMLC core and the field core were connected. It should be noted that LMLC samples were only exposed to accelerated laboratory aging conditions and experienced no traffic loading prior to testing. Therefore, to make an equivalent comparison, samples taken from pavement shoulder, which had no exposure to traffic loading, were compared with LMLC samples. Figure 24 shows this comparison of the CA values. The age of LMLC samples in months listed at the top of the graph, and the months that the field samples were aged listed at the bottom. By plotting

the two lines representing the linear fit of CA for LMLC samples and field samples on the same graph, the relationship is clear. The ratio is around 10 between the field and laboratory aging rates. This result is less than the value of 13 to 19 on hardening rates ratio, given by previous study on a pavement site in Refugio County, Texas (Woo et al., 2007). However, the climate in the Laredo area, in the southwest corner of Texas, features extreme heat, which definitely affected the rate of field aging. Because the temperature in environmental room is fixed, but pavement temperature varies with location, this ratio around 10 is not universal for every pavement.

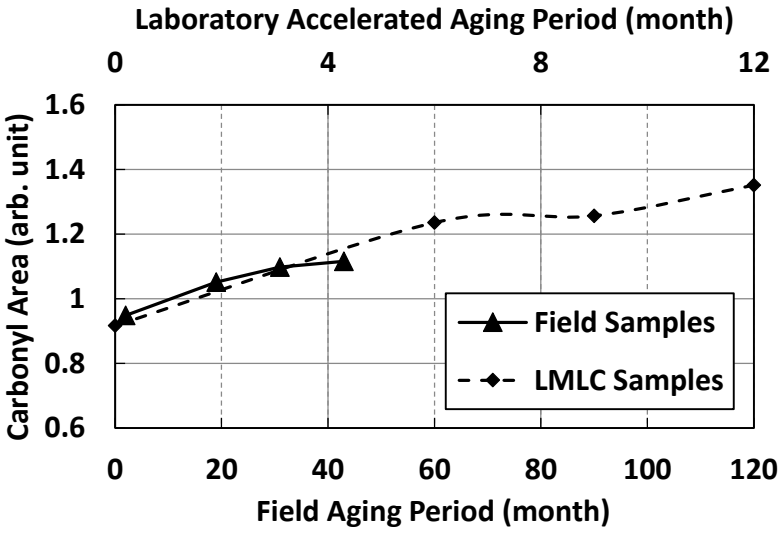

Figure 24 Laboratory to Field CA Comparison.

Pavement Oxidation Modelling Results (Comparison 2)

A pavement oxidation model (Jin, Cui, and Glover 2013) could predict the degree of binder oxidation in pavements, but has its limits. This model is specific to a pavement

location and incorporates elements of the particular pavement structural design and materials. There are two input factors in this model, diffusion depth and field calibration factor (*fcf*), are related to pavement structural design. Previous method to obtain the diffusion depth was to use X-ray CT scanning on the field core. And to fit the *fcf*, at least two field samples from the same location but collected in different years are required. Therefore, to make an oxidation prediction using this model, field sampling is unavoidable. This pre-requirement makes the prediction before pavement construction impossible and strongly limits the application of this model.

Aging simulation on LMLC samples solves this problem by calibrating diffusion depth and *fcf* in the process of oxidation prediction on LMLC samples. Binder film thickness, a similar concept to diffusion depth but already widely used in pavement design, was brought in. Both binder film thickness and diffusion depth give the thickness of an asphalt binder film. Film-thickness is defined as the thickness of the asphalt film around aggregates. Diffusion depth assumes that asphalt binder only spreads on air void surfaces. Therefore, the value of film thickness should be much less than diffusion depth. In order to convert the film thickness to diffusion depth, a new empirical factor, film thickness factor (*ftf*), was proposed. Film thickness factor is calibrated by comparing the measurements of LMLC samples and the model prediction on LMLC samples. Moreover, *fcf*, which is used to calibrate the difference between measurements and model predictions on field samples, could be replaced by this *ftf*, because, in general, both *fcf* and *ftf* calibrate effect of aggregates on asphalt binder aging. So this new diffusion depth is defined as:

$$\text{Diffusion Depth} = \text{Film Thickness} \times ftf$$

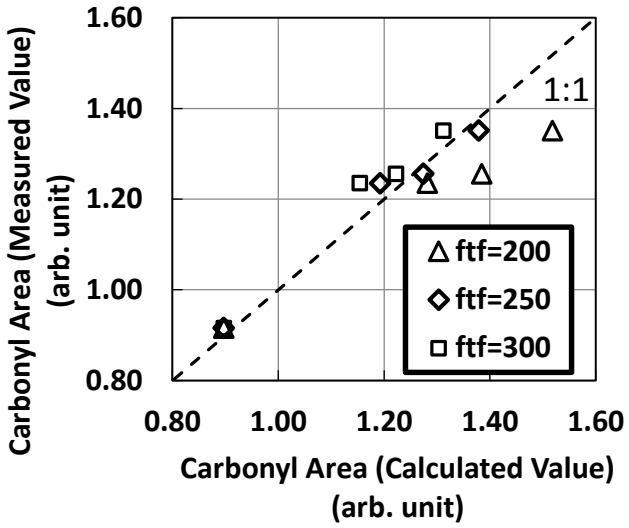

Figure 25 Comparison between Measured LMLC CA and Model Calculated LMLC CA.

In the LMLC model calculation, the aging temperature was set as constant, 60 ^{o}C, the same as the aging temperature in Environmental Room. According to the pavement design, the film thickness was 6.59 μm, and this value was used in the model calculations on both field and LMLC samples. Figure 25 shows that when *ftf* equals 250, this estimate gives a minimum average percent error as low as 2.3 %. When *fcf* = 200, the average percent error is 7.1 % and when *fcf* = 300, the average percent error is 3.6 %. Thus, based on the model prediction on LMLC samples, *ftf* is determined as 250. In the next step, *ftf* equals 250 would be used in oxidation prediction on field samples. The definition of percent error as follows:

Percent Error = $\left|\right.$ (Measured Value − Calculated Value) / Measured Value $\left|\right.$ ·100 %

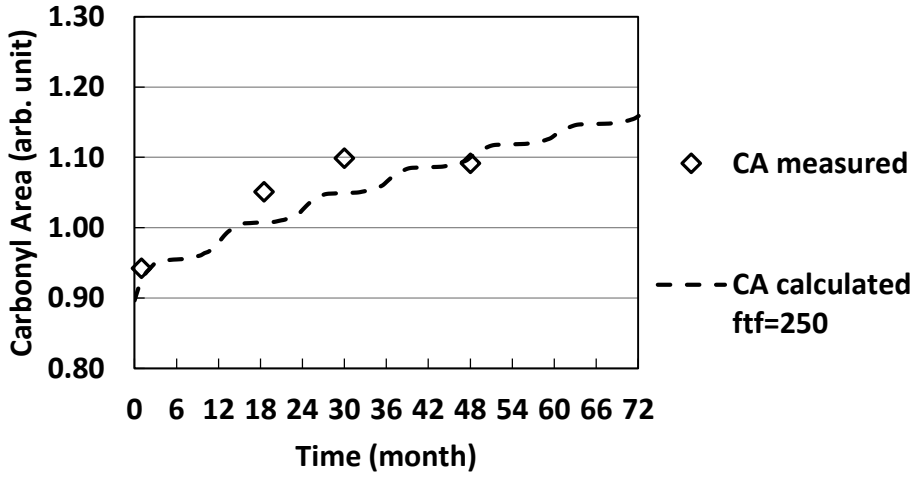

Figure 26 Comparison between Field Measured CA and Model Calculated CA (*ftf* = 250).

Figure 26 compares the field measured and model calculated CA values. Open diamonds present the average CA values for field cores collected in different years. In model calculation, the aging starts from a CA value of 0.90 (arb. unit). This number is the CA of 0 month LMLC samples. CA grows much faster in summer due to the high temperatures, so in the graph, calculated CA shows a ladder-type growth. Based on the model calculation, the average CA of the pavement would approach around 1.15 (arb. unit) after 72 months (6 years) in field. The average error percentage of this prediction is only 2.9 %.

Conclusions

Results from the laboratory and field aged asphalt concretes lead to some important conclusions.

- For US Route 277, much of the asphalt concrete aging occurs during the first year and the aging rate decreases over time. Based on the observations, the shoulder ages slightly faster than the wheel path.
- A ratio between the aging rates of LMLC and field samples varies with pavement locations. But using the pavement oxidation model, predictions on the LMLC samples could help to calibrate the predictions on the field samples. From this, a pavement oxidation prediction would be made even before the pavement construction.

CHAPTER IV

APPLYING RECOVERED BINDER IN ASPHALT AGING TEST

Introduction

One common problem in oxidation model application is the unavailability of the original binder. Accelerated aging tests on original asphalts are needed for kinetics and hardening properties of the asphalt binder, which are required by the model. But not all original binders are collected during the pavement construction and stored for a long time. Moreover, different batches of binders from same manufactures may have different characteristics, which eliminates the possibility of producing more original binder after construction. For an already constructed pavement, the lack of the original binder seriously hinders the model application. There is a great need for an alternate binder source.

Recovered binder, which is extracted from field cores, becomes the best candidate for an asphalt aging test (Burr et al. 1991, Cipione et al. 1991). There are three advantages of using recovered binder. First, recovered binder comes from the field cores, and those cores could be collected at any time after pavement construction. Second, recovered binder is the binder used in the pavement, and results from it are expected to provide the same aging information on the binder that remains in the pavement. Third, recovered binder has already experienced plant mixing and paving, which makes this binder better reflection of the short term aging in those processes than any laboratory simulations on the original binder. However, the possibility whether the extraction and recovery process changes the kinetics and hardening properties in the asphalt binder needs to be better understood. If

this concern can be eliminated, then recovered binder can be used as a new asphalt binder source for determining the pavement binder's hardening and kinetics parameters.

Objectives

The objective of this study was to test the possibility of using recovered binder in the asphalt accelerated aging test. The aging test determines the kinetics and hardening properties of the binder, which are required for oxidation prediction. A successful aging test using the recovered binder would be extremely useful when no original binder is available.

Experimental Methods

Material

Field Core

In this study, asphalt binder was extracted from the field cores collected in LRD US 277 after different years of aging in the pavement. Only the binder from cores in year two was further aged to test its kinetics and hardening properties. Former research on Texas pavements has showed that, after two years usage, the asphalt binder should have passed the fast aging period already (Woo et al. 2007). Thus, the kinetics studied here should only represent constant period kinetics of the asphalt. Construction and cores information for LRD US 277 are given in Table 2 in Chapter III. Measurements, including carbonyl area and DSR Function results, are shown in the Results and Discussion section.

Binder Extraction and Recovery

Field cores were cut by an electric saw into layers from top to bottom. Each layer was about 0.5 in (12.7 mm), and then broken into smaller pieces ready for extraction. The

extraction used successive washes, a mixture of 15 % ethanol plus 85 % toluene by volume, until the solvent was light brown. After the extraction, the solvent was centrifuged and filtered to remove all the aggregate particles from the binder solution. Then the asphalt binder was recovered from the solvent with a Büchi RE111 Rotovap. Nitrogen carried off the solvent and prevented any further oxidation in recovery. During solvent removal, the bath temperature was kept at 100 ℃ to avoid hardening or softening of the asphalt in dilute solution. To ensure the solvent removal, after no more condensing solvent could be detected visually, the temperature was increased to 174 ℃ and kept for 50 min.

Test Methods

Pressure Oxygen Vessel (POV) Test

The cores used in POV test were taken in December 2009 (Year 2), almost two years after construction. After measuring the degree of oxidation, the recovered binder was placed into POV to continue aging. The POV is a device which keeps asphalt samples age at constant temperatures in a range of 60 to 100 ℃ under atmospheric air. The vessel is immersed in a constant temperature bath, using triethylene glycol and water for temperature control. The asphalt was placed into several 4 cm × 7 cm aluminum trays to form a film with a uniform 0.8 mm thickness. This thickness has been proven to minimize the effects of diffusion (Lunsford 1994, Domke et al. 1997), and to provide enough sample to do the next measurements. Trays were removed from POV on chosen days, depending on the temperature.

Fourier Transform Infrared Spectrometer (FTIR)

A Nicolet 6700 FT-IR spectrometer with an attenuated total reflection (ATR) zinc selenide prism was used to track the oxidation progress in carbonyl area (CA). The carbonyl area was recorded as the area under the absorbance peak from 1650-1820 cm^{-1}.

Dynamic Shear Rheometer (DSR)

A Carri-Med CSL 500 controlled stress rheometer was used to record and analyze the rheological property in DSR Function This characteristic is calculated from storage modulus (G') and dynamic viscosity (η') both at 44.7 ℃ and 10 rad/s in time sweep mode.

Results and Discussion

Asphalt Binder Aging in Pavement

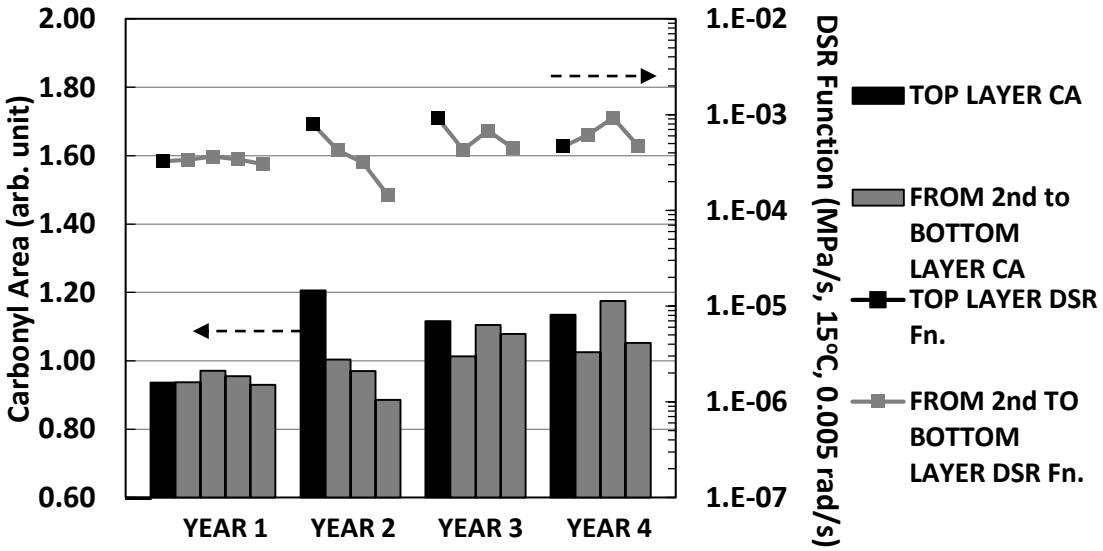

Figure 27 Carbonyl Area and DSR Function of LRD US 277 Wheel Path.

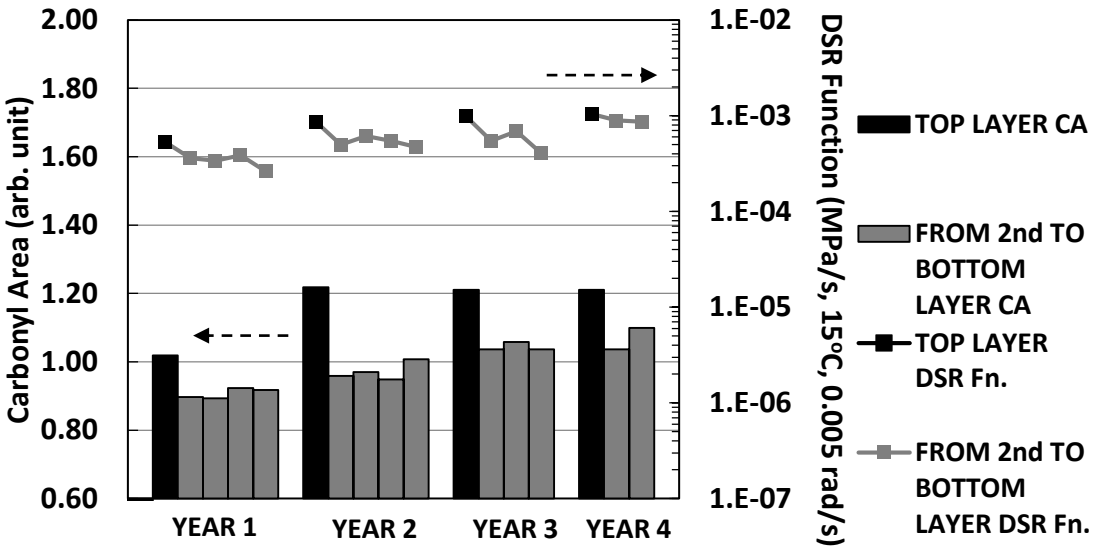

Figure 28 Carbonyl Area and DSR Function of LRD US 277 Shoulder.

Figure 27 and Figure 28 show the CA and DSR Function distribution layer-by-layer in each field cores collected in different years. Figure 27 shows data for the four cores from the wheel path, and Figure 28 shows data for the four cores from the shoulder. In each core, it is clear that the lower the degree of oxidation (carbonyl area), the lower the level of binder hardening (DSR Function). Generally, both the degree of oxidation and binder hardening increase with service time.

Recovered Asphalt Binder Aging in POV

The recovered binder was further aged in POV at three different temperatures. The carbonyl area formation rate at each constant temperature could be described in Arrhenius form:

$$k_c = A_c' e^{-E_{ac}/RT}$$

where k_c is carbonyl area formation rate in constant-rate period, $A_c^{'}$ is pre-exponential factor, and E_{ac} is activation energies; both are temperature independent. R is universal gas constant and T is temperature.

Figure 29 shows the CA growth with time at actual measured temperatures in the aging vessels. The reaction rate (or CA growth rate) is constant at a certain temperature, and this constant rate increases with increased temperature. The reaction rate values were obtained as the slope of the constant-rate lines at each temperature in the graph.

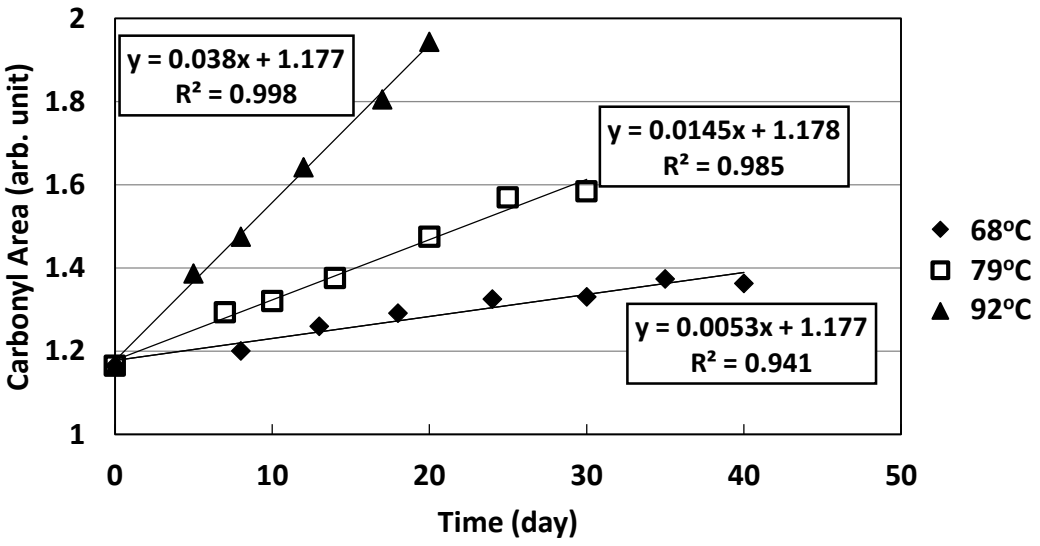

Figure 29 Carbonyl Area Growth of Recovered Binder at Three Temperatures in POV.

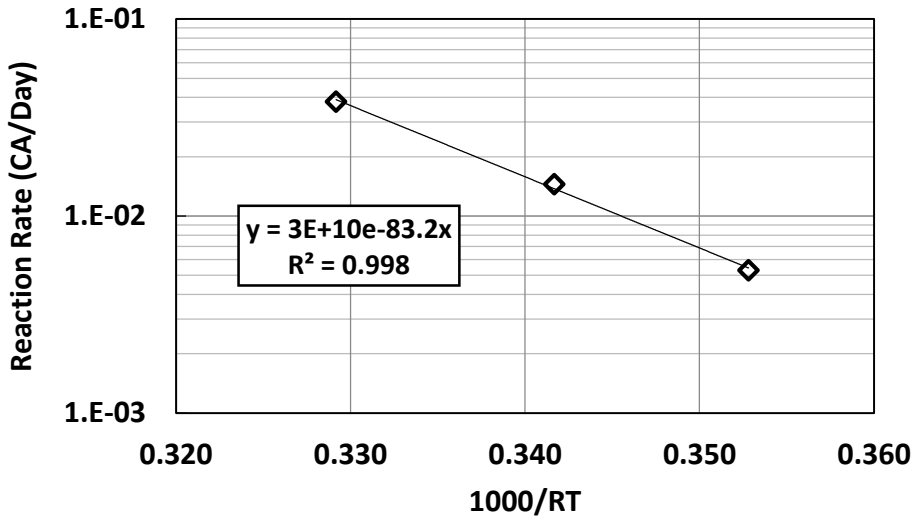

Figure 30 Temperature Dependency of Reaction Rate for Recovered Binder.

In Figure 30, the slope in the plot of the temperature dependency of reaction rate gives the activation energy. This experimentally determined parameter is independent of temperature and for a given asphalt, it can be thought of the sensitivity of the reaction rate to temperature. Of the recovered binder, it shows the activation energy is 83.2 kJ/mol. For comparison, the work reported in Jin et al. (2011) showed the original Valero PG 70-22 binder with a constant rate activation energy of 75.2 kJ/mol, which is close to the results from the same test on recovered binder.

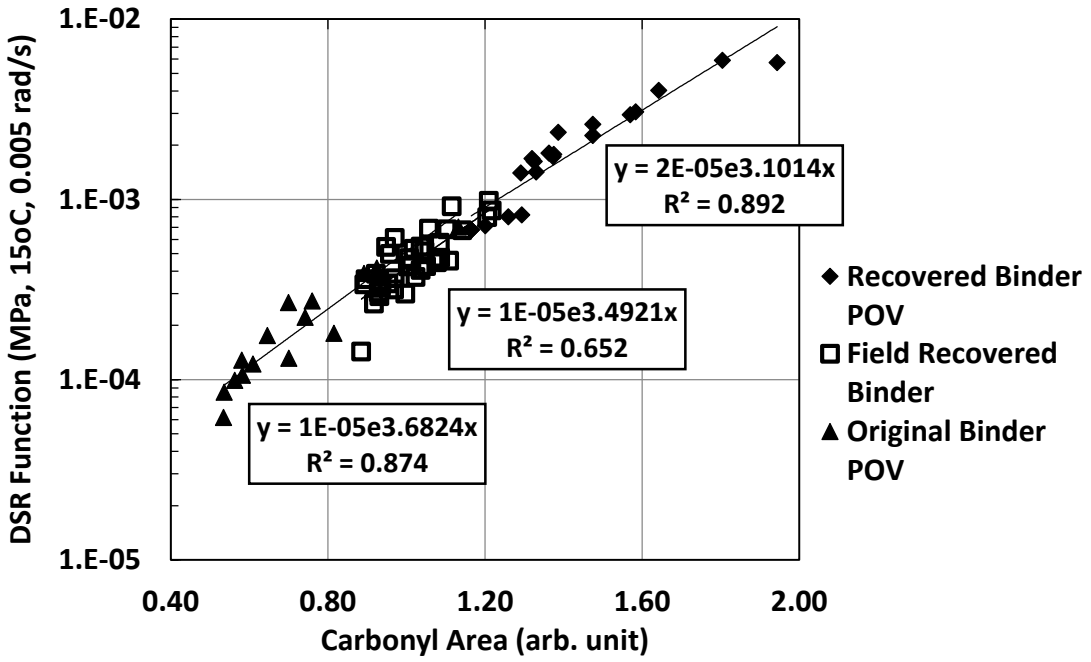

Figure 31 DSR Function Hardening Susceptibility of Three Binders.

Figure 31 compares the DSR Function hardening susceptibility of three binders: (1) original binder supplied by manufacturer, (2) recovered binder from field samples (labeled as Field Recovered Binder), and (3) recovered binder after additional aging in POV (labeled as Recovered Binder POV). Data of the original binder was reported in Jin et al. (2011) and results of the recovered binder are determined in this study. It is important to note that recovered binder with and without additional aging follow the same DSR Function hardening paths as the original binder. Statistical analysis shows the two slopes of Original Binder POV and Recovered Binder POV are not significantly different (p = 0.2083 > 0.05), so that assuming a common slope is valid. Then using a common slope equals 3.2851 as a correction, the difference between the adjusted means in natural logarithm of DSR Function is 0.0191 and it is not statistically significant too (p = 0.9101 >

0.05). It is a strong evidence to refute an argument that the rheology properties of the binder may be changed after the extraction and recovery process.

Conclusions

An alternate binder source has been tested for evaluating asphalt kinetics and hardening. Recovered binder, extracted from field cores, was further oxidized in laboratory to determine its activation energy and hardening susceptibility. Measurement results on this binder compare well with results on original binder. Moreover, a comparison on DSR Function hardening susceptibilities showed that the extraction and recovery process did not change the binder hardening. Kinetics and hardening properties from recovered binder allows an oxidation prediction on a pavement without any original binder.

CHAPTER V

TOWARDS AN OXIDATIVE AGING STUDY AND PREDICTION ON A SEAL COAT TREATED PAVEMENT*

Introduction

There is a need to better understand binder oxidation in seal coat treated pavements and to predict pavement performance as affected by seal coat applications. Oxidation of asphalt leads to rheological hardening and this effort could only be seen after a long-term aging period. However, most of the research has just focused on immediate effects of restoring pavement properties, known as surface cracks healing (McLeod et al. 1969, Alsuleiman, Sinha, and Riverson 1991), surface raveling (O'Brien 1989) and surface waterproofing (Brown 1988). However, seal coat failures such as loss of aggregate are obviously related to the asphalt aging in the seal coat. Even for a pavement successfully applied seal coat, the serviceability of the seal coat and underlying pavement eventually will fall below acceptable levels after a combination of traffic loading and asphalt oxidative hardening over time.

The complication of a long-term performance study on a seal coat treated pavement is because of different kinds of binders used in seal coat layer and pavement. Different oxidation rates and hardening rates would be expected. Moreover, on the

* Part of this chapter is reprinted with permission from "An Oxidative Aging Study of Seal Coat Treated Pavement" (Manuscript ID: LPET-2014-0281.R2) by Yuanchen Cui, Jin, X., Liu, G. and Glover, C. J. *Petroleum Science and Technology*. In press. Copyright by Taylor & Francis Group.

contacting surface (seal coat layer and original pavement surface), whether there is a mixing of those two binders (seal coat binder and pavement binder) is also of interest. Similar binder aging test, used on original binders, would be applied on the recovered binders to determine the kinetics and hardening properties of those binders.

Once the kinetics and hardening properties are known, another interest is to predict the future performance of the binders in pavements. This goal could be achieved by several aging models have been proposed (Lunsford 1994, Prapaitrakul et al. 2009, Han 2011, Jin, Cui, and Glover 2013). In those models, the most important concepts have been well considered, e.g., pavement temperatures, air void, binder content, oxygen diffusion, asphalt oxidation kinetics and hardening. In this study, a model calculation based on Jin's work has been applied on a seal coat treated pavement. The aging patterns for each binder were found to be significantly different. The future performance of the pavement (including the seal coat layer) was determined by the weakest layer of the pavement. Based on those calculation results, an aging study on the seal coat treated pavement is proven to be meaningful.

Objectives

The objectives of this study were (1) to evaluate the oxidation levels in a seal coat treated pavement; (2) to characterize the kinetics and hardening properties of the binders in the seal coat and pavement layers by the aging test developed in Chapter IV; (3) to do a layer-by-layer oxidation prediction on the seal coat treated pavement and validate it with field data.

Experimental Methods

Material

Field Core

Field samples for this study were collected in Texas, US 82 in Lubbock (LBB) District of the Texas Department of Transportation (TxDOT). This road was built in July 2008 and the asphalt binder used in this pavement was ALON PG 76-22. During the construction in 2008, loose mix was collected. One month later, the sample cores were taken a few days before seal coat application on certain sections of the road in August 2008. The seal coat binder used was AC 20-5TR and spay rate was 2 L/m^2. In 2009, sample collection included both seal coat treated and untreated cores on different sections of the pavement. The first step for the cores with a seal coat layer on top was to cut this layer off by knife with care. The seal coat layer was a single course layer only about 0.25 in (6.4 mm) thick. After the seal coat removal, all the cores were sliced into 0.5 in (12.7 mm) thick layers from top to bottom.

Binder Extraction and Recovery

The extraction used successive washes: a blend of 15 % ethanol plus 85 % toluene by volume, until the last wash appeared a color of light brown instead of black. After the binder was completely extracted, the solution was first settled in a beaker for 30 seconds and then distributed into serial 15 mL conical type tubes to do the centrifuge at 3100 rpm for 10 min to remove the big particles. After the centrifuge, the solution was filtered using a basket coffee filter to remove all particles. The asphalt binder was recovered from the solvent with a Büchi Re 111 Rotovap. During the recovery, nitrogen gas was introduced

into the vessel to drive off any remaining solvent and to prevent asphalt contacting with oxygen. The bath temperature was kept at 100 ^{o}C to avoid hardening or softening of asphalt in the dilute solution. When no more tiny drops of solvent could be detected visually on condense column, the bath temperature was increased to 174 ^{o}C for an additional 50 min to ensure sufficient solvent removal. The total time for the extraction and recovery procedure is 5 to 6 hours for each sample.

Test Methods

Extract-Recovered Binder Pressure Oxygen Vessel (POV) Test

Only binders recovered from samples collected in 2009 were further oxidized in the Pressure Oxygen Vessel (POV) test. POV is a device could keep asphalt samples aged at specific temperatures in a range of 60 to 100 ^{o}C under atmospheric air. Vessel immersed in a constant temperature bath, using triethylene glycol and water for temperature control. Binders were placed into several 4 cm × 7 cm aluminum trays to form a 0.8 mm-thickness uniform film. Several replicate trays removed from the POV on chosen days, and the length of aging period depended on the aging temperatures.

The asphalt binders were classified into three groups. Binder in the seal coat layer is seal coat binder. Binder in the 1st layer (0 to 0.5 in or 0 to 12.7 mm below seal coat layer) was studied separately, which is called 1st layer binder. Binder in the other pavement layers, underneath 0.5 in (12.7 mm) deep below seal coat layer, is pavement binder.

Fourier Transform Infrared Spectrometer (FTIR)

A Nicolet 6700 FT-IR spectrometer with an attenuated total reflectance ZnSe prism was used to measure the Carbonyl Area (CA), which tracked the oxidation progress

in asphalt samples. The value of Carbonyl Area, reported in arbitrary units, equals to the area under the absorbance peak from 1650 to 1820 cm^{-1}.

Dynamic Shear Rheometer (DSR)

A Carri-Med CSL 500 Controlled Stress Rheometer was used to record and analyze the rheological property, DSR function. The value of DSR function, which combines both elastic and viscous properties, is calculated from storage modulus (G') and dynamic viscosity (η') both at 44.7°C and 10 rad/s in time sweep mode.

Results and Discussion

Oxidation Evaluation

The first objective of this work was to test the levels of oxidation and stiffness of recovered binder.

Previous work on asphalt field aging in Texas Highways (Woo et al. 2007), provided evidence that binder oxidation occurred over many inches of depth into the pavement. This work was directed at addressing the specific impact of seal coats on this binder oxidation and hardening process and in the context of these various tools. It should be noted that measuring and interpreting the effectiveness of seal coats is always problematic because of the unknown extent to which seal coats penetrate into the pavement and blend *in-situ* with the original binder. The discussion that follows includes data for both wheel path and shoulder lanes and both treated and untreated sections of pavement.

This study on US 82 in the Lubbock District of TxDOT tracks chemical and rheological property changes due to field aging and seal coat treatment. Untreated cores

were collected in 2008, 2009, and 2010, and seal coat treated cores were collected only in 2009 and 2010.

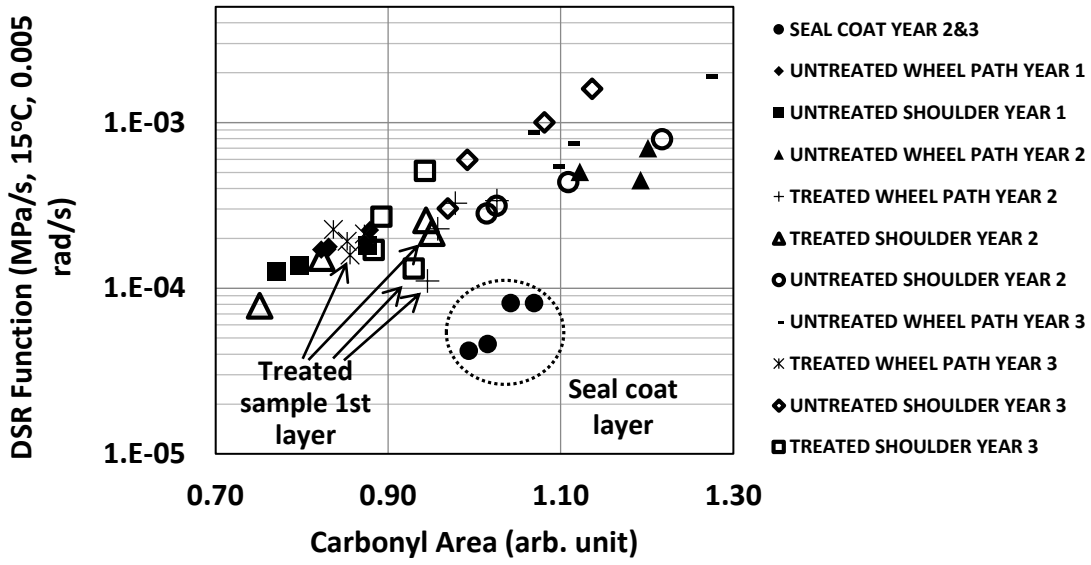

Figure 32 DSR Function Hardening Susceptibility for Each Layer in Field Cores.

The slope of logarithmic scale viscosity versus CA is termed the DSR Function hardening susceptibility and is characteristic of each asphalt. In Figure 32, recovered binder DSR function vs. CA data are plotted for each layer for the various treated and untreated cores. For example, the data labeled "Untreated Shoulder Year 2" shows four data points for the four layers in that core, each layer aged for the same amount of time according to when the core was sampled. The asphalt in different layers aged to different CA levels and the DSR function corresponding to each CA generally is higher or lower, consistent with a higher or lower value of the CA. Other untreated pavement cores do not

provide as consistent a relationship of increasing oxidation over time, but the trend is clear, nonetheless.

For the treated pavements, other observations are noted. First, the seal coat layer binder (all points inside the circle) shows CA values that are offset well below the pavement binder data for a given CA. Second, a linear correlation based on all the layers from the untreated section cores plus the all layers from treated section cores except seal coat layers is:

$$\text{DSR Function} = 3.85\times10^{-6}\cdot\exp(4.59\cdot CA),\ R^2 = 0.78$$

While there is significant scatter to these data (R^2 = 0.78), the correlation is consistent with those in Figure 33. Third, for the first layers (beneath the seal coat) in two of the treated cores (Treated Wheel Path Year 2 and Treated Shoulder Year 3), the points clearly lie between pure pavement asphalt and seal coat asphalt, likely indicating penetration of the seal coat into the top of the original pavement.

Extract-Recovered Binder Pressure Oxygen Vessel Test

Work has been reported previously on the development of an apparatus and procedure for oxidizing unaged asphalt under atmospheric air pressure and at several elevated temperatures in order to evaluate binder oxidation kinetics and hardening. An asphalt oxidation kinetics model was established to describe the formation rate of carbonyl during the constant-rate period, following classical Arrhenius reaction kinetics (Lau et al. 1992).

Kinetics Parameters

Field binder recovered from field cores was characterized using this POV method in order to determine binder oxidation kinetics parameters. Such an approach can be used on pavements as a forensics tool, potentially making every pavement a test section, even when the original binder is not available.

The kinetics parameters of all three binders are given in Table 3. The result is evidently proving the binder in the 1st layer of seal coat treated cores is a blend of two binders that activation energy of 1st layer binder is in the middle of pavement binder and seal coat binder.

Extract-Recovered Binder DSR Function Hardening

DSR function hardening susceptibility values were also determined from the POV aging data of the recovered binders. DSR Function hardening parameters are given in Table 3. The pavement binder has greater DSR Function values for a given CA compared to the seal coat binder, in agreement with the previous observation in Figure 32. Again, the binder recovered from the first pavement layer of treated cores shows a mixed property with the hardening intercept lying between the pavement binder and seal coat binder. Probably coincidentally, the hardening susceptibility values of the three binders are nearly the same.

DSR Function Hardening Comparison

Figure 33 compares the DSR function hardening susceptibility of binder recovered from untreated cores for Years 1, 2, and 3, both as-recovered (labeled as field recovered binder) and after additional aging in the POV. Also shown are data for the original binder

(supplied by the manufacturer), both unaged and after POV aging to various levels. Recovered binder with additional aging in the POV follows the same DSR function hardening path as the binder recovered from field cores and as the original binder. This result has been seen before for binder aging in the field and is important because it means that the original binder is not necessary for predicting pavement future performance, even for pavements for which original binder is unavailable.

Table 3 Kinetics Parameters of the Three Kinds of Asphalt in Seal Coat Treated US 82.

Binder Type	Pre-exponential Factor (CA/Day)	Activation Energy (kJ/mol)	Hardening Susceptibility	Hardening Intercept (MPa/s)
Pavement binder	3.87×10^{8}	69.8	4.00	6.67×10^{-6}
1st layer binder	2.89×10^{9}	76.0	4.01	2.68×10^{-6}
Seal coat binder	6.57×10^{9}	78.0	3.82	9.97×10^{-7}

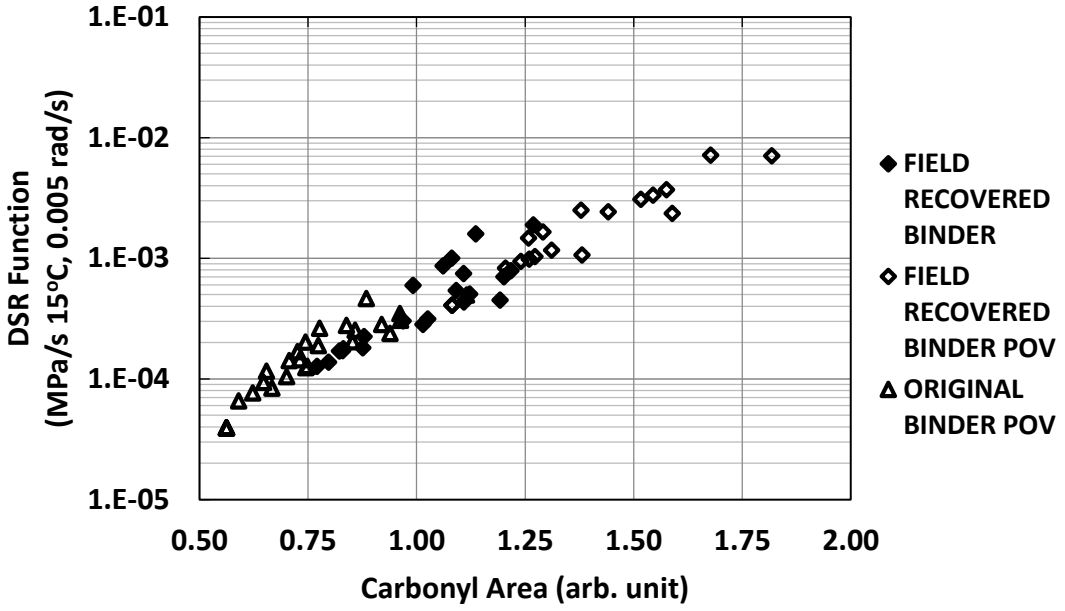

Figure 33 DSR Function Hardening for Extract-recovered Pavement Binder and Original Pavement Binder.

Pavement Oxidation Prediction

A precise prediction could tell us when and how to better build and maintain a pavement. In this research, a pavement oxidation model proposed by Jin, Cui, and Glover (2013) was used to predict oxidation aging in pavement. Important concepts have been well considered in this model, e.g., pavement temperature, air void distribution, binder content, oxygen diffusion, asphalt oxidation kinetics, and hardening. Applying this model for pavement degree of oxidation as a function of time and depth, estimates were calculated of binder oxidation in pavements knowing the recovered asphalt binder oxidation kinetic parameters and hardening parameters.

Including the binder properties, all the information, such as air void structure, binder film thickness, are following the pavement design or the measurement on field samples of US Route 82 in Lubbock, Texas. Pavement life was set as 89 months (from Aug. 2008 to Dec. 2015). Pavement temperature was calculated based on solar radiation, air temperature, and wind speed (Han, Jin, and Glover 2011).

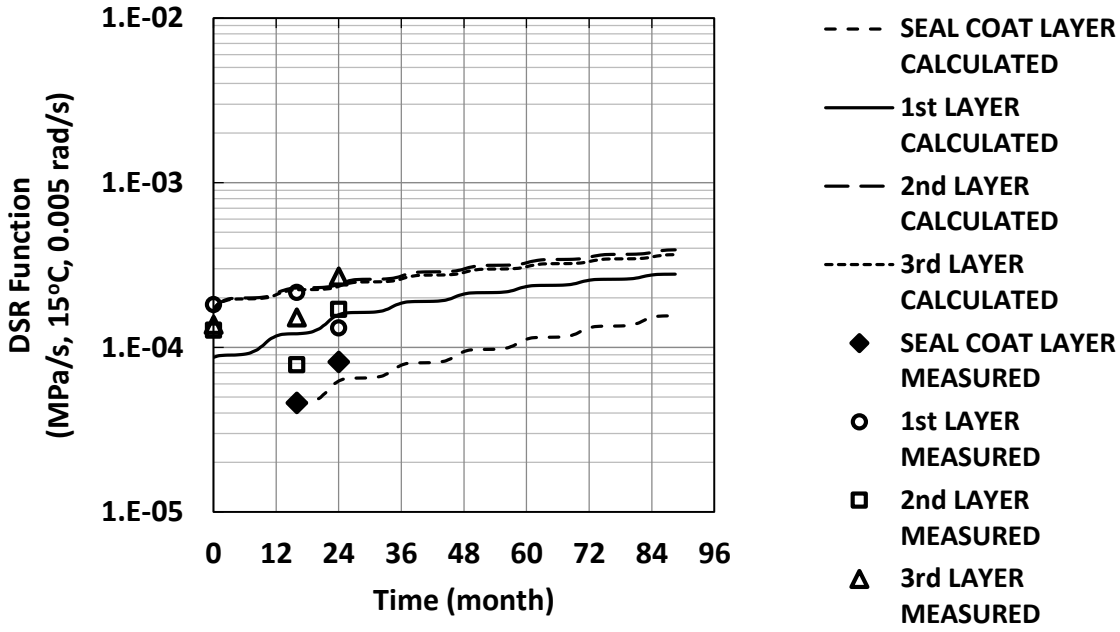

Figure 34 Calculated and Measured DSR Function Growth.

Figure 34 shows calculated and measured binder DSR Function growth over time. Note that calculations made for the seal coat layer, 1st layer and two more layers below (2nd and 3rd layers of the pavement are 0.5 to 1 in (12.7 to 25.4 mm) and 1 to 1.5 in (25.4

mm to 38.1 mm) below the seal coat-pavement interface) are using their own binder properties, including kinetics and hardening properties.

For the different layers, the first measured DSR Function values from the field cores were used as the starting points. For the seal coat layer, although it was applied one month after construction, the first seal coat treated core was collected 16 months after. Because the DSR Function hardening susceptibilities are almost the same for those three binders, the only factor matters the hardening rates is the kinetics. In the graph, the DSR Function growth rate of the seal coat layer is significantly higher than the DSR Function growth rate of the 1st layer, and the other pavement layers grow at a similar rate, which is much lower than the seal coat layer and slight lower than the 1st layer. One of the most important reasons is that the seal coat layer has lowest activation energy, which gives this binder a property easy to react with oxygen. The pavement binder has the highest activation energy, so pavement binder reacts with oxygen much slower. The binder in the 1st layer is a blend of the seal coat binder and the pavement binder, and activation energy of the 1st layer binder is in between, as showed in Table 3. Another reason for the difference of the DSR Function growth rates is the temperature distribution. Daily temperature changes much greater on the surface of the pavement than the lower layers. Because of a low hardening intercept, the seal coat binder still has a lower DSR Function value after 89 months of aging.

Based on the results above, recovered binder POV could be trusted as a reliable extended accelerated aging test. With this test, the further changes of binder properties

happened in field become predictable. The advantages to utilize the recovered binder to collect the kinetics and hardening properties are:

- Comparing with original binder, recovered binder is more accessible. Field cores could be collected from the pavements at any time. And recovered binder is the same binder used in the pavement. Moreover, two batches of asphalt sharing the same PG grade may perform differently due to the different crude oil sources;
- Study on the recovered binder could provide the real time aging situation as the starting point. This starting point plus the kinetics and hardening properties could be used in the pavement oxidation model to predict future performance of the pavement.

Conclusions

This study provides a systematic method to evaluate seal coat treated pavement oxidation and predict future changes to the binder rheology. DSR function hardening susceptibility, the ratio between increases in natural logarithm of DSR function and carbonyl area, is a characteristic of asphalt materials that relates chemical and rheological properties and that is sensitive enough to be used to identify blends of original binder and seal coat material. As such, it can be used to assess seal coat penetration below the pavement surface. Binder extracted and recovered from field cores can be further oxidized in laboratory accelerated aging to determine oxidation kinetics, allowing the possibility of analyzing oxidation kinetics as a forensics study of pavements where no original binder is available.

This work has demonstrated a method for evaluating seal coat effectiveness with respect to binder oxidation and hardening. This strategy therefore provides a very cost-effective strategy for predicting the service life of a seal coat treated pavement.

CHAPTER VI

AN ACCELERATED METHOD FOR DETERMINING ASPHALT OXIDATION KINETICS PARAMETERS*

Introduction

Numerous accelerated aging tests have been developed to simulate long-term field aging by raising either temperature or pressure or both (Liu et al. 1996, Huh and Robertson 1996). One widely accepted aging method is the pressure aging vessel (PAV) test, which is conducted at an elevated air pressure, 20 times atmospheric pressure, and at temperatures elevated above pavement conditions. Inevitably, these conditions change the balance of reactions among the many hydrocarbon species present in asphalt, causing binder aging comparisons obtained from these aging tests to deviate from comparisons at pavement aging conditions (Domke, Davison, and Glover 2000). On the other hand, oxidation occurs so slowly at atmospheric air pressure and pavement temperatures that laboratory tests at these conditions requires an inordinately long test time. Thus the dilemma has been to choose between either long test times that provide correct information or short test times that provide incorrect information. Therefore, a laboratory test or procedure that provides information on pavement oxidation and hardening that is correct at pavement temperature and pressure and in an accelerated test time has been a long-sought but very elusive goal of asphalt materials testing.

---

* Part of this chapter is reprinted with permission from "An Accelerated Method for Determining Asphalt Oxidation Kinetics Parameters for Use in Pavement Oxidation and Performance Modeling" (Manuscript ID: LPET-2014-0010.R2) by Yuanchen Cui, Jin, X., Han, R. and Glover, C. J. *Petroleum Science and Technology*. In press.

The fundamental difficulty with using laboratory tests to predict pavement performance is that different asphalt materials inevitably have different oxidation kinetics and hardening properties. Thus, two binders subjected to the same accelerating test conditions, will oxidize and harden in the test to different degrees. Equivalently, over years of pavement service (which, by design, are at conditions of temperature and pressure that are different from the accelerating laboratory aging test) individual test results will transform to pavement oxidation and hardening rates in ways that are not consistent from asphalt to asphalt, and that are not predictable.

So, instead of making problematic direct comparisons of binder oxidation and hardening after a prescribed aging test, this work considered a fundamentally different approach to an aging test. This approach recognizes that an Arrhenius kinetics function of both temperature and pressure that requires asphalt-specific parameters describes r_c, the carbonyl formation rate at constant temperature and pressure in asphalt materials (Lau et al. 1992, Liu et al. 1996):

$$r_c = A_c' \cdot exp(-E_{ac}/RT)$$

where A' is the pre-exponential factor, E_{ac} is the activation energy during the constant-rate oxidation period, R is the gas constant, and T is the absolute temperature (K) at which the reaction occurs. Jin et al. (2011) showed that the fast-rate oxidation period also is governed by Arrhenius activation parameters (E_{af} and A_f'), and that given E_{ac} and A_c', both E_{af} and A_f' can be estimated from correlations among kinetics parameters obtained at one atmosphere.

In order to use Jin's work at one atmosphere in an accelerated PAV aging test, a correlation between parameters at 20.7 atm air pressure and parameters at one atmosphere was needed. Thus, the principal objective of this study, was to obtain kinetics parameters for multiple asphalt materials at both PAV and atmospheric pressure and then to assess whether a correlation existed between the two sets of parameters. Such a correlation would support a strategy of using accelerated PAV aging to determine kinetics parameters and then converting them to pavement conditions to model pavement oxidation over time.

This is a fundamentally new and innovative approach to using accelerated binder aging tests to predict oxidative hardening and consequent loss of durability at pavement service conditions. Based on oxidation kinetics and thermal and oxygen transport fundamentals, the strategy offers the promise of a much more accurate and robust prediction tool than any previously proposed accelerated method and with significant but reasonable (considering the improved fundamental information and predictive potential that is obtained) increases in test time and effort compared to the traditional PAV test.

Experimental Methodology

Eight asphalt materials obtained from four different suppliers are shown in Table 4. The selected binders covered four PG grades with two binders being unmodified (PG 64-22) and six being polymer modified (PG 70-22, PG 70-28, and PG 76-22). All of the binders were supplied unaged, directly from the supplier.

Table 4 Details of Asphalts.

Name	Modification	Name	Modification
Lion PG64-22	None	**Martin PG64-22**	None
Lion PG70-22	Yes	**Martin PG70-22**	Yes
Alon PG70-22	Yes	**SEM PG70-22**	Yes
Alon PG76-22	Yes	**SEM PG70-28**	Yes

Pressure Aging Vessel

The standard PAV apparatus was designed to simulate binder oxidation in pavements over a number of years of service, suggested to be from 4 to 8 years (Anderson et al. 1994). According to AASHTO R 28, Accelerated Aging of Asphalt Binder using a Pressurized Aging Vessel, several 3.2-mm thick asphalt film samples are placed in a cylindrical chamber containing dry, clean compressed air at 20.7 atm (305 psi) air pressure and different temperatures.

For the purposes of this study, this standard test was modified to obtain asphalt kinetics parameters. The oxidation reactions at 110 °C, at which the final product may exhibit a measurably significant weight loss, are not considered to be adequately representative of the reactions that occur at pavement service temperatures. To avoid such effects, only 90 °C and 100 °C were adopted from the standard PAV test. An additional modification of the standard method was to use a number of 38 mm diameter tin containers instead of the standard pans (140 mm diameter) described in AASHTO R 28, to place up to six times the number of samples in each PAV batch. In these containers, asphalt samples of 3.65 grams form a 3.2 mm film, the same thickness as required by the standard method. Another modification was to obtain samples aged for several different periods at the same

aging condition in order to measure the oxidation rate. Each sample, subjected to aging in the PAV was removed after its appropriate specified time and measured for chemical (FTIR) property changes to obtain oxidation and hardening rates as functions of temperature.

Pressure Oxidation Vessel (POV)

Pressure Oxidation Vessels (POV) were immersed in a triethylene glycol bath, each at a different temperature. The baths provide a constant flow of preheated replacement air at one atmosphere pressure and constant temperatures for binder oxidation. The fixed temperatures ranged from 60 to 100 °C. Asphalt, 2.4 gram samples, were placed in a 4 cm × 7 cm aluminum tray to form a film about 0.8 mm thick. This thickness reduced the effects of diffusion at one atm to an acceptable level (Lunsford 1994). A number of trays were removed from each POV at prescribed intervals according to the POV temperature.

Fourier Transform Infrared Spectrometer (FTIR)

Carbonyl area was measured using a Nicolet 6700 Fourier Transform Infrared Spectrometer (FTIR) with an attenuated total reflectance zinc selenide prism. Carbonyl area, reported in arbitrary units, is the area under the absorbance peak from 1650 to 1820cm^{-1}, and provides a direct measurement of the oxidation level in asphalt (Liu et al., 1998a).

Results and Discussion

Reaction Rate Comparisons

Figure 35 shows example PAV (20.7 atm air gauge) and POV (1 atm air absolute) data for SEM PG 70-28. The constant-temperature reaction rate (the slope of the trend line) is higher with high temperatures in both apparatuses and at the higher air pressure of the PAV compared to the POV. Note that the time unit in Figure 35 is hours whereas for Figure 36, the time unit is days.

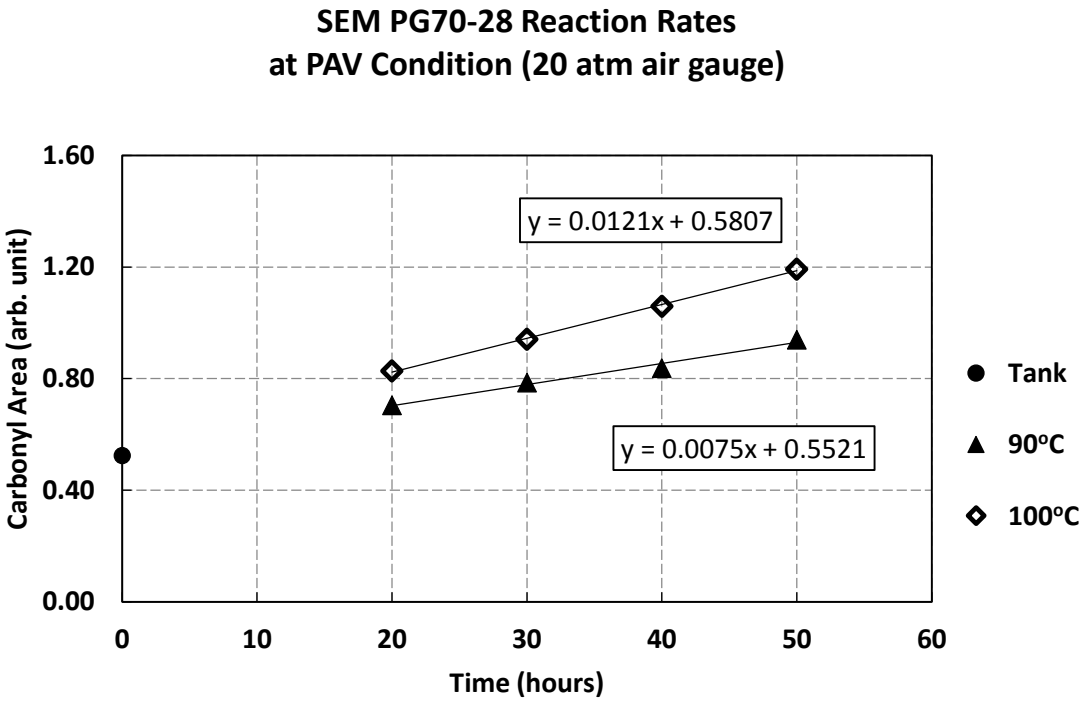

Figure 35 Carbonyl Area Increases with Hours of PAV Aging.

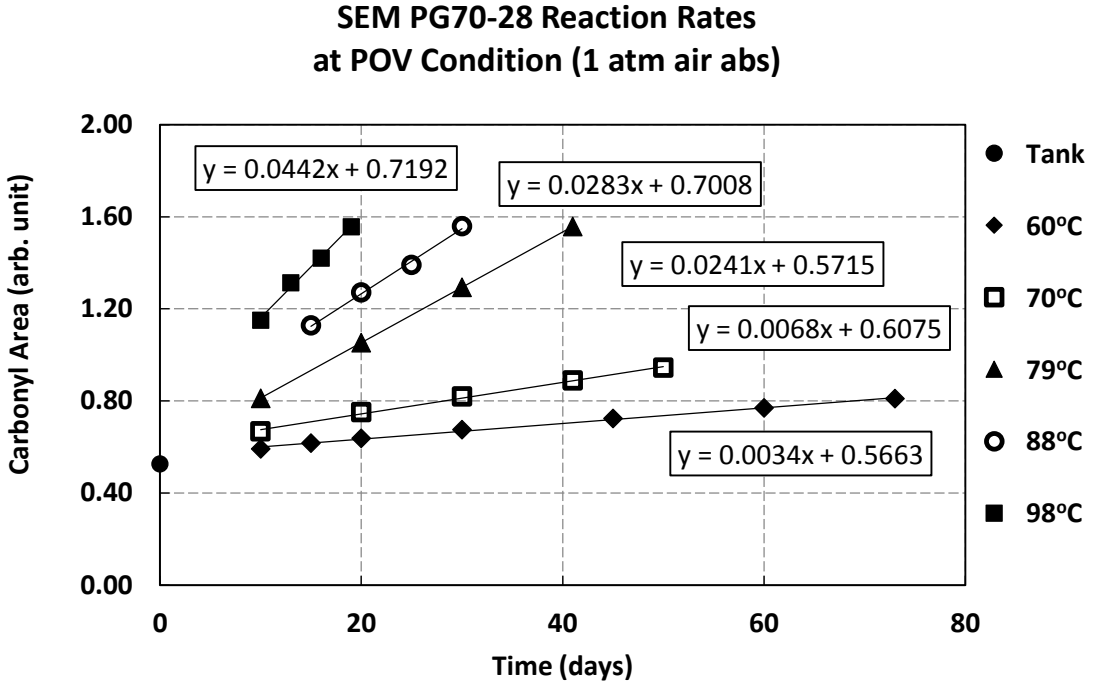

Figure 36 Carbonyl Area Increases with Days of POV Aging.

Using this kinetics relation and the data shown in Figure 35 and corresponding data for the other suppliers materials, values for $A_c^{'}$ and E_{ac} for both PAV and POV pressures were obtained and are reported in the top half of Table 5.

A direct comparison of POV and PAV oxidation at two temperatures is instructive and demonstrates the fallacy of using PAV data directly to infer pavement aging rates. However, because the POV data were not measured at exactly 90 °C and 100 °C, a calculation procedure was performed first. The POV constant-rate period kinetics parameters in Table 5 were used to calculate reaction rates in the POV at both 90 °C and 100 °C (rather than the measured rates at 88 °C and 98 °C). Then these rates were

compared to PAV rates that were measured at 90 °C and 100 °C. These comparisons are shown in the bottom half of Table 5 for all eight materials.

Two observations are noted from Table 5 by comparing reaction rates among binders. First, at a fixed temperature (90 °C or 100 °C), the reaction rate rankings of each binder in the two different devices are different because of the different oxygen pressures. For example, at 90 °C, of the eight asphalts evaluated in this study, Martin PG 70-22 binder has the highest oxidation rate in the POV but the lowest in the PAV. Second, at different temperatures, the reaction rate ranking of a binder was not always the same in a particular device. For example, Lion PG 64-22 has the highest oxidation rate in the PAV at 90 °C but the lowest rate at 100 °C. Those two effects are the results of the different activation energies for the different asphalts and different activation energies under different oxygen pressures. This phenomenon emphasizes the futility of measuring the relative reaction rates of asphalts at an elevated temperature and using those rates to predict rankings at pavement conditions (or, equivalently, comparing the amount of aging by two different asphalts that is obtained at the same accelerating condition and assuming that that comparison will hold at pavement conditions).

Table 5 Summary of Constant-Rate Kinetics at POV and PAV Conditions.

Binder	POV Kinetics Parameters[a]		PAV Kinetics Parameters[b]	
	Pre-exponential Factor (A') (CA/day)	Activation Energy (E_{ac}) (kJ/mol)	Pre-exponential Factor (A') (CA/day)	Activation Energy (E_{ac}) (kJ/mol)
Lion PG 64-22	3.0×10^{6}	56.1	1.2	14.4
Lion PG 70-22	5.1×10^{8}	70.0	1.0×10^{3}	34.7
Alon PG 70-22	6.5×10^{9}	78.3	5.5×10^{4}	47.1
Alon PG 76-22	4.7×10^{9}	77.0	1.2×10^{6}	56.6
Martin PG 64-22	8.8×10^{8}	72.5	4.5×10^{4}	47.0
Martin PG 70-22	2.0×10^{11}	88.0	4.0×10^{8}	74.5
SEM PG 70-22	1.1×10^{10}	79.9	1.1×10^{7}	63.5
SEM PG 70-28	1.0×10^{9}	72.5	3.3×10^{5}	53.1
Binder	**POV Reaction Rates[a]**		**PAV Reaction Rates[b]**	
	90 °C (CA/Day)	**100 °C (CA/Day)**	**90 °C (CA/Day)**	**100 °C (CA/Day)**
Lion PG 64-22	0.0273	0.0458	0.247	0.281
Lion PG 70-22	0.0412	0.0749	0.240	0.326
Alon PG 70-22	0.041	0.0766	0.223	0.338
Alon PG 76-22	0.329	0.0612	0.203	0.336
Martin PG 64-22	0.0315	0.0543	0.188	0.286
Martin PG 70-22	0.0487	0.1014	0.176	0.350
SEM PG 70-22	0.0367	0.0611	0.186	0.326
SEM PG 70-28	0.0293	0.0543	0.181	0.310

[a]POV conditions: 1 atm air absolute, 0.8 mm film
[b]PAV conditions: 20.7 atm air gauge, 3.2 mm film

Activation Energy Correlation

From the reaction rates for both POV and PAV apparatuses, constant-rate period activation energy and pre-exponential factors were determined (Table 5). E_{ac} is assumed independent of temperature for a given asphalt but the values vary from one asphalt to the next. Domke, Davison, and Glover (2000) reported that oxidation rates also are affected by the nature of the oxygen supply (pure oxygen versus air) and the total pressure. Understanding such relationships within the context of fundamental principles of binder oxidation is essential to developing an oxidative aging test capable of providing relatively rapid predictions of binder pavement performance.

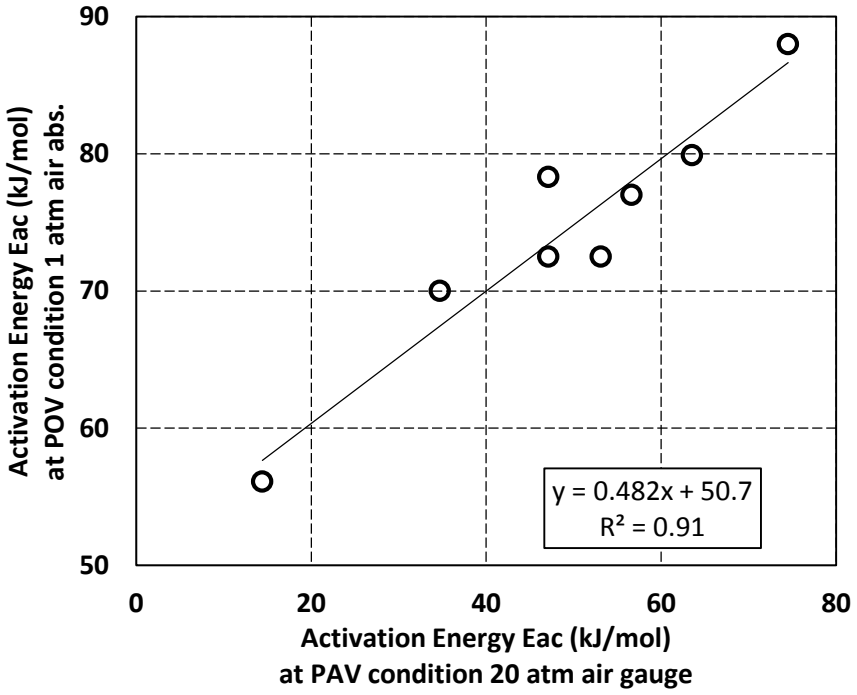

Figure 37 POV (1 atm air abs) versus PAV (20.7 atm air gauge) Activation Energy.

For this work, we used both PAV and POV apparatuses to measure oxidation kinetics parameters for the same asphalts at two oxidation conditions. Figure 37 compares the activation energies from both the POV (1 atm air absolute, 0.8 mm thick films) and PAV (20.7 atm air gauge, 3.2 mm thick films) oxidation conditions. Thus the results in Figure 37 include effects of the film thickness differences to the extent they affect reaction rates (and therefore activation energies) through mass transfer resistance. From Figure 37 the correlation between activation energies (kJ/mol) measured at the two pressures is linear according to:

$E_{ac,POV}=0.482\times E_{ac,PAV}+50.7,\ R^2=0.91$

An Accelerated Binder Aging Test

This work provides an accelerated method of determining an asphalt material's oxidation kinetics and hardening parameters for use in a pavement oxidation and performance model. The method can provide comparative estimates of each binder's pavement oxidation and hardening over time that is specific to each pavement (air voids, e.g.) and location (climate). Additionally, if it is known how a binder's oxidative hardening affects pavement performance (fatigue resistance, e.g.), then the impact of oxidation on mixture and pavement performance can also be predicted. Such an aging test used to predict aspects of pavement performance consists of laboratory measurements (using PAV, FTIR, DSR, and other binder and mixture characterization tests) and computer simulation. Not discussed in this paper, the procedure also requires determining the fast-rate period initial jump M (Jin et al., 2011) and the rheological hardening susceptibility (HS) parameters (Lau et al., 1992; Ruan et al., 2003), also necessary for pavement

oxidation model calculations of binder hardening. Climate data for the pavement location also are required, as described by Jin et al. (2013).

Binder kinetics parameters determined using this approach for the eight binders evaluated in this work are summarized in Table 6. For these data, measured POV data are shown for comparison to the calculated POV values (based on the PAV measurements).

Independent Literature Comparisons

Data for six SHRP asphalts (AAA-1, AAB-1, AAD-1, AAF-1, AAG-1, and AAM-1) from two independent literature reports were used to further investigate the PAV-POV activation energy correlation. The POV data (1 atm air, 0.8 mm thick films) are from Domke et al. (2000), and the PAV data (20.7 atm air, 3.2 mm thick films) are from Huh and Robertson (1996). In Table 6, measured POV activation energies are listed, as are the values calculated (predicted) by using the PAV measured activation energies as input. The predicted (calculated) POV values match quite well the measured POV activation energies, also reported in Table 6.

Table 6 Kinetics parameters Based on PAV Activation Energies and Fast-Rate-Constant-Rate Correlations.

Binder	POV Condition[a] (Measured)						PAV Cond[b] (Meas)	POV Condition[a] (Calculated)			
	E_{ac} (kJ/mol)	A_c (CA/day)	E_{af} (kJ/mol)	A_f (CA/day)	M (CA)	HS (1/CA)	E_{ac} (kJ/mol)	E_{ac} (kJ/mol)	A_c (CA/day)	E_{af} (kJ/mol)	A_f (CA/day)
Lion PG 64-22	56.1	$3.0x10^6$	37.3*	$1.3x10^5$*	0.162	2.33	14.4	56.0	$3.9x10^6$	37.2	$2.6x10^5$
Lion PG 70-22	70.0	$5.1x10^8$	49.1*	$6.5x10^6$*	-	2.46	34.7	66.8	$1.4x10^8$	46.4	$2.6x10^6$
Alon PG 70-22	78.3	$6.5x10^9$	60.8	$3.5x10^8$	0.156	3.04	47.1	73.3	$1.2x10^9$	51.9	$1.7x10^7$
Alon PG 76-22	77.0	$4.7x10^9$	52.6	$2.2x10^7$	0.267	5.03	56.6	78.4	$6.5x10^9$	56.2	$6.9x10^7$
Martin PG 64-22	72.5	$8.8x10^8$	51.9	$7.4x10^6$	0.131	5.12	47.0	73.3	$1.2x10^9$	51.9	$1.6x10^7$
Martin PG 70-22	88.0	$2.0x10^{11}$	60.9	$2.6x10^8$	0.147	5.02	74.5	87.8	$1.5x10^{11}$	64.3	$1.0x10^9$
SEM PG 70-22	79.9	$1.1x10^{10}$	54.4	$3.8x10^7$	0.236	4.51	63.5	82.0	$2.2x10^{10}$	59.3	$1.9x10^8$
SEM PG 70-28	72.5	$1.0x10^9$	49.1	$3.3x10^7$	0.205	3.22	53.1	76.5	$3.5x10^9$	54.6	$4.1x10^7$
AAA-1	85.6[c]						74.0[d]	86.4 (+0.9 %)			
AAB-1	90.2[c]						71.8[d]	85.3 (-5.42 %)			
AAD-1	92.3[c]						71.1[d]	85.0 (-7.94 %)			
AAF-1	82.9[c]						67.6[d]	83.3 (+0.46 %)			
AAG-1	83.1[c]						68.8[d]	83.9 (+0.92 %)			
AAM-1	84.8[c]						63.1[d]	81.1 (-4.35 %)			

[a]POV condition: 1 atm air absolute, 0.8 mm film
[b]PAV condition: 20.7 atm air gauge, 3.2 mm film
[c]Domke et al. (2000)
[d]Calculated from the data of Huh and Robertson (1996)
*These values for these asphalts were calculated from measured E_{ac} and measured A_c at 1 atm air, using fast-rate-constant-rate kinetics parameters correlation (Jin et al., 2011). Other calculated values in this table (for all asphalts) were based on the 1 atm-air – 20 atm-air activation energy correlation from this study and the fast-rate-constant-rate kinetics parameters correlation by Jin et al. (2011).

Summary

This work developed and demonstrated an accelerated method for comparing binder pavement aging and hardening characteristics. The strategy uses a 2-temperature, 50-hour PAV determination of a binder's constant-rate activation energy at PAV pressure. With the PAV – POV activation energy correlation developed in this study, plus the work of Jin et al. (2011), a complete set of binder oxidation fast-rate and constant-rate kinetics parameters can be estimated.

Thus, the accelerated PAV method for determining binder oxidation kinetics parameters, coupled with the thermal and oxygen transport model of pavement oxidation plus data on the impact of binder oxidative hardening on mixture durability, provides an innovative comprehensive, and fundamentals-based accelerated aging test of a binder's performance.

CHAPTER VII

FURTHER EXPLORATION OF THE PAVEMENT OXIDATION MODEL —DIFFUSION-REACTION BALANCE IN ASPHALT

Introduction

Over the years, there have been efforts to predict the pavement long term performance in need of the design and maintenance purposes and a series of models have been developed. The increasing numbers of findings on the asphalt aging is the driving force encouraging the scientists to refine those models. Lunsford (1994) proposed his pavement aging model, which includes many important concepts such as asphalt oxidation kinetics, asphalt binder content and air voids structure. Prapaitrakul et al. (2009) refined this model by introducing a new concept, average shell thickness, and using hourly pavement temperatures. Han (2011) replaced the average shell thickness with five pore radii from X-ray CT measurements of pore size distribution and also quantified the effort of asphalt viscosity on oxygen diffusion. The latest and most advanced model is developed by Jin, Cui, and Glover (2013) with two significantly improvements: (1) introducing the concept of diffusion depth to better define the oxygen diffusion region in the asphalt-aggregate mastic; (2) incorporating both fast-rate and constant-rate asphalt oxidation kinetics to better describe the aging in the pavement. In previous studies, the only use of the models was to predict the pavement aging statues and the results described particularly in the literatures already prove their capability and accuracy. But, the role of the model should not be limited just to oxidation predicting. Of even greater importance to asphalt

scientists is how to use the model to better understand the controlling factors in pavement aging.

These findings in field and in laboratory, are believed to play the most important roles in pavement aging, and are included as seven fundamental elements in the model:

1. Pavement design information, including the basic information such as designed air voids and asphalt binder content;
2. Accessible air void distributions, derived from X-ray CT analysis on field cores, providing the exposed surface area of asphalt to air;
3. Hourly pavement temperatures, calculated by pavement temperature model (Han, Jin, and Glover 2011);
4. Asphalt oxidation kinetics, obtained from laboratory accelerated aging tests on original binders. With the kinetics parameters, the formation rates of carbonyl could be described as a function of temperature and oxygen partial pressure;
5. Asphalt hardening properties, obtained from laboratory accelerated aging tests on original binders, reflect the physicochemical relationships between carbonyl components and binder stiffness. The hardening can be tracked with measurement of the binder viscosity or DSR Function;
6. Oxygen diffusivity in asphalt, determined by both temperature and binder viscosity;
7. Oxygen concentration, determined by oxygen diffusion-reaction process. The concentration changes as a function of position and time in the asphalt

film, influenced by oxygen diffusion in asphalt and oxidative reaction with asphalt.

The understanding on those aging elements are still limited. Only the effect of each element on asphalt aging has been well studied whereas the effects of the other have been eliminated. But, toward deeper levels of thinking, it is necessary to consider those elements simultaneously and to further discover the relative importance of those elements. With current experimental methods, this issue could not be addressed without designing a series of complicated experiments. At this time, the pavement oxidation model could be used as a good tool to solve this problem with those two reasons: First, the model is a complex product, which combines all the individual aging factors together; Second, much less time and workload is required by the model than the experiments.

Among all the aging elements, one relationship is extremely important that is to determine which has more determination in the whole aging process, oxidative reaction or oxygen diffusion. This issue has been discussed all the time but no real experimental provident has been post out yet. An exploration of the model application is to discover the interactions between oxygen diffusion and oxidative reaction. And there are four topics in this issue.

First, as mentioned in the section of model elements, oxygen diffusion and oxidative reaction occur simultaneously. Oxygen molecules penetrate through asphalt film to a certain depth first and then react with the asphalt at that position. If the oxygen diffusion runs much faster than the reaction, there should be plenty of oxygen molecules in the asphalt film that makes the reaction runs at its maximum level at all depth and all

time. On the other hand, if the reaction runs much faster than the diffusion, the oxygen concentration keeps at a very low level or in extreme cases there is almost no oxygen molecule in the asphalt film. It would seriously limit the reaction. Moreover, in the latter case, the oxygen "black hole" would create a large oxygen concentration gap between the atmosphere and the asphalt film. This gap gives a high diffusion driving force, which enforces the diffusion as feedback. Of course, there is still a big chance that the rates of diffusion and reaction are at similar levels. Therefore neither of them fully controls the aging.

Second, this study only focuses on the aging process in a long time range that is because the balance between oxygen diffusion and oxidative reaction changes every second. The reaction hardens the asphalt and the increased asphalt stiffness results the oxygen diffusivity decreasing over time. In return, decreased diffusion slows the reaction. This negative feedback makes the research interest not focus on an instantaneous correlation at a given second, but an accumulated effort in a long period.

Third, another issue needs to be considered is the effect of temperature. Since temperature plays extremely important roles in both diffusion and reaction, the sensitivity of the diffusion-reaction balance to temperature needs to be determined. In most of the cases concerning the pavement aging, the temperature range is from 20 to 60 ^{o}C. In this study, two extreme temperatures, 0 and 80 ^{o}C, were added to expand the range covering all the field aging situations.

Forth, the nature characteristics of the asphalt, e.g., asphalt oxidation kinetics, asphalt hardening, all contributes to the diffusion-reaction balance. Using the oxidation

model, combinations of different asphalt characteristics are included in this work without a huge amount of experimental workload.

Objectives

The purpose of this research is to use the pavement oxidation model developed by Jin, Cui, and Glover (2013) to discover the diffusion-reaction balance in a long term pavement aging. Several issues are also studied, including the temperature sensitivity of the balance and the contributions of the asphalt properties.

Methodology

Asphalt Oxidative Reaction

From experimental results, both oxidative reaction and oxygen diffusion could be described as functions of asphalt properties, temperature and time.

Previous studies on asphalt oxidative reaction concluded that there are two parallel reactions: a first order reaction that terminates when the limiting amount of quick reaction components is depleted and a zero-order constant-rate reaction that occurs indefinitely throughout the pavement service life. The period consists of both first order reaction and zero order reaction is called fast-rate period, and after that is the constant-rate period (only zero order reaction). A schematic graph is given in Figure 38 . In this graph, the asphalt aging growth in carbonyl area is under a constant temperature without considering any oxygen diffusion resistance.

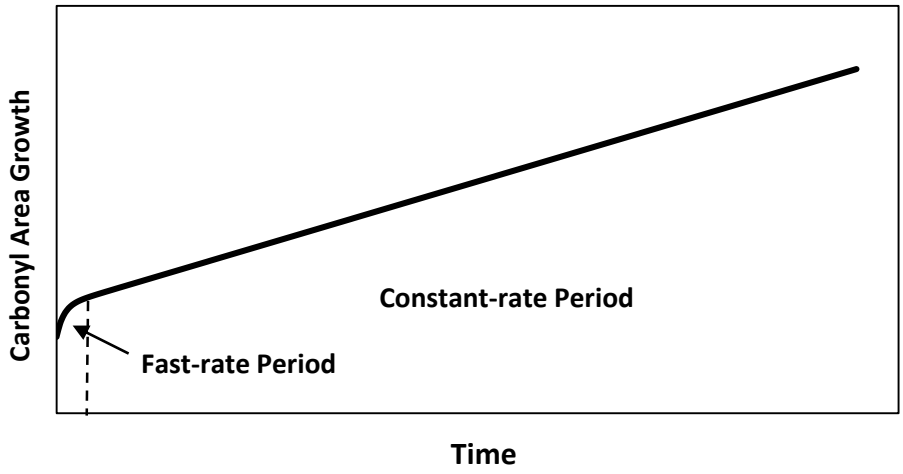

Figure 38 A Schematic Graph of a Typical Carbonyl Area Growth without Oxygen Diffusion Resistance.

Oxygen Diffusion

In Jin's pavement oxidation model, the equation for oxygen concentration (in oxygen partial pressure) is as following.

$$\frac{\partial P(x,t)}{\partial t} = \frac{\partial}{\partial x}\left(fcf \cdot D_{O_2} \cdot \frac{\partial P}{\partial x}\right) - \frac{c}{h} \cdot \frac{\partial CA(x,t)}{\partial t}$$

where D_{O_2} is the oxygen diffusivity in asphalt, c is a factor that converts rate of carbonyl area growth to rate of oxygen consumption, h is the solubility constant of oxygen. *fcf* is the field calibration factor adjusting D_{O_2} to match the measured field data.

The oxygen diffusivity is a function of temperature and asphalt viscosity (Han, Jin, and Glover 2011):

$$D_{O_2}=5.21\times10^{-12}\ LSV^{-0.55}\cdot T$$

where T is the temperature, and LSV is the low shear rate limiting viscosity, which is a function of carbonyl area.

$$LSV=e^{HI+HS\cdot CA}$$

where HI is the hardening intercept of natural logarithm of LSV versus CA, and HS is the hardening susceptibility, which relates asphalt oxidation to hardening (Martin et al. 1990a).

Asphalt Oxidative Reaction with Effect of Oxygen Diffusion

In this study, model simulation is used as a tool to study the asphalt oxidation with oxygen diffusion. The information of binder properties and pavement design are given in Table 7 (bold numbers are the default values used in the model calculation).

Table 7 Information of Binder Properties and Pavement Design as Inputs in Model Simulation.

Information Type	Information Name (Unit)	Input Values
Binder Property	Constant-Rate Activation Energy (kJ/mol)	**60**,110
	Hardening Susceptibility (HS) (arb. unit)	2,**3**,4
	Hardening Intercept (HI) (Hypothetical Viscosity when CA=0) (Pa s)	800,**2400**,7200
	M_{RTFO} (arb. unit)	**0.3**
Pavement Design	Diffusion Depth (μm)	**650**
	Field Calibration Factor (*fcf*) (arb. unit)	**1**

Table 7 Continued.

Information Type	Information Name (Unit)	Input Values
Temperature	(^{o}C)	0, 20, 30, 40, 50, 60, 80 and annul hourly temperatures in Laredo, Texas and in MnRoad Test Site, Minnesota
Aging Period	(Month)	**114** (From 0 Year's August to 9th Year's December)

Figure 39 gives a typical aging path simulated by the pavement oxidation model showing the CA growth under a constant temperature with oxygen diffusion resistance. By introducing oxygen diffusion resistance, the aging path in the constant-rate period is no longer a straight line as shown in Figure 38. The capability of oxygen diffusion controls the oxygen supply to the reaction, and it suffers from the asphalt hardening. And asphalt hardening is a result of the oxidative reaction. Therefore the reaction results a deceleration of diffusion and slows down in return. But this phenomenon only appears after a high oxidation level reaches.

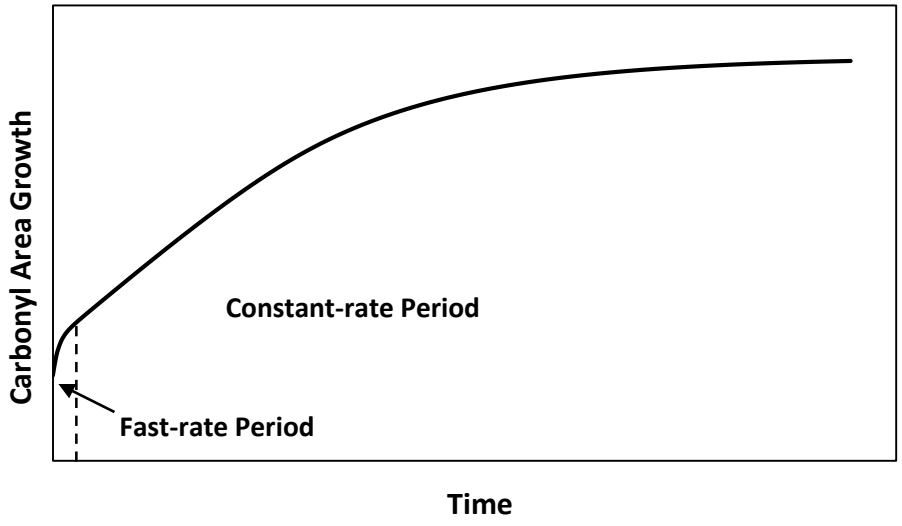

Figure 39 A Schematic Graph of a Typical Carbonyl Area Growth with Oxygen Diffusion Resistance.

Results and Discussion

Comparison of Maximum Reaction Amounts

The maximum reaction amount means the total asphalt oxidative reaction occurs in a long period (114 months) with the hypothesis that there is no oxygen diffusion resistance or diffusivity is infinite in the asphalt film. Under this circumstance, the oxygen penetrates into any depth of asphalt film freely and reacts with asphalt at the maximum rate. In model simulations, the value of oxygen diffusivity has been magnified up to 10^5 times to eliminate the oxygen diffusion resistance. The simulation results are given in Figure 40.

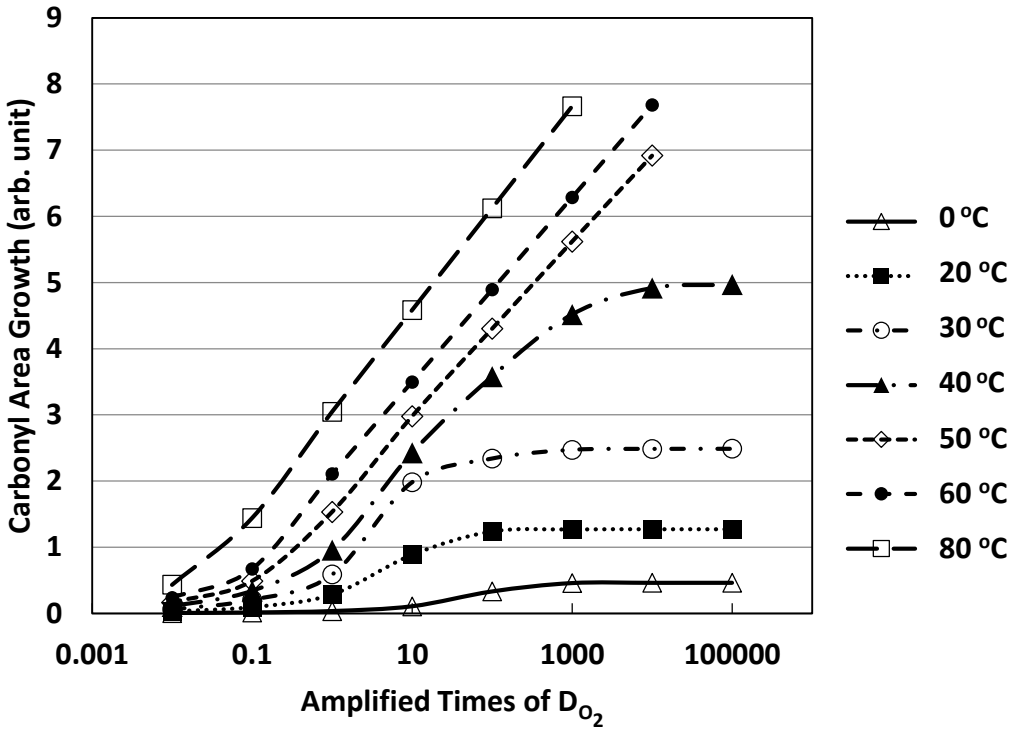

Figure 40 CA Growth with Amplified Times of Oxygen Diffusivity at Different Temperature.

The points shown in Figure 40 are the increased amounts of carbonyl area after 114 months aging under different constant temperatures with different oxygen diffusivities. The diffusivity range is from 10^2 to 10^5 time the actual value at each temperature. It is clear that at one constant temperature, the amount of CA growth increases with diffusivity until a maximum CA value has been reached. This maximum CA appears under extremely high oxygen diffusivities, which matches the concept of the maximum reaction amount with infinite diffusivity (or no diffusion resistance), and the values are independent of oxygen diffusivity at each temperature. The maximum CA under such temperatures, 0, 20,

30, and 40 ^{o}C could be read in the figure directly. Unfortunately, for the higher temperatures, such as 50, 60, and 80 ^{o}C, the values of maximum CA could not be read from the figure directly because the diffusivity still is not large enough.

To estimate the maximum reaction amount at each temperature, a method simpler than model simulation has been proposed. Formulas describing the oxidative reaction (see Chapter I), was summarized under a circumstance that only lightly aging occurred on very thin asphalt films, so the oxygen diffusion resistance was low enough to be ignored. Thus the calculated CA values based on those formulas could be considered as same as the maximum reaction amounts. The values from two methods, formula calculation and model simulation (with an extremely high diffusivity), have been compared in Table 8. Note that the so called maximum CA growth read from Figure 40 under those high temperatures, 50, 60, and 80 ^{o}C, marked in italic, are not the actual maximum CA values, but they are the closest values could be accessed by the model simulation.

Table 8 Comparison of the Maximum CA Increases from Two Methods.

Temperature (^{o}C)	**Maximum CA Increase by Formulas Calculation**	**Maximum CA Increase by Oxidation Model with Amplified D_{O_2}**	$\frac{\textbf{Max CA (Model)}}{\textbf{Max CA (Formulas)}} \times 100$ **%**
0	0.461	0.460	99.8
20	1.276	1.272	99.7
30	2.497	2.487	99.6
40	4.995	4.968	99.5
50	9.873	*6.917*	70.1
60	19.003	*7.682*	40.4
80	64.013	*7.662*	12.0

Comparing the results at 0, 20, 30, and 40 ^{o}C, the maximum CA growths calculated from the formulas are almost the same as the values from the model simulation. In the following sections, the value calculated by formulas is taken as the maximum reaction amount, or called maximum CA growth.

Instead of the hyperbolic condition, which makes the asphalt oxidation runs at the maximum rate, regular aging condition with actual oxygen diffusivity is more of interest. The gap between the maximum CA growth with no oxygen diffusion resistance and the regular CA growth with actual diffusion resistance contributes to discover which of the two steps, oxygen diffusion or oxidative reaction, dominates the aging process.

Effect of Activation Energy on Diffusion-Reaction Balance

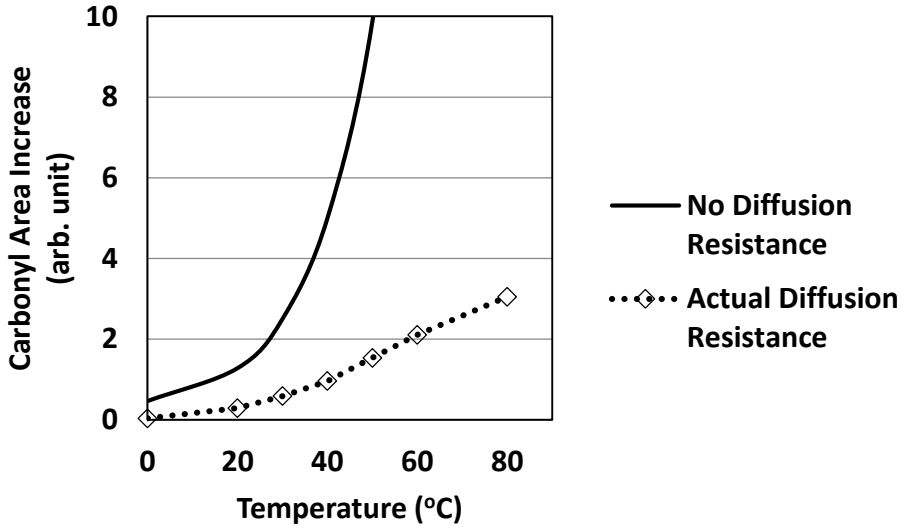

Figure 41 CA Growth at Different Temperatures with No Diffusion Resistance and Actual Diffusion Resistance, E_{ac} = 60 kJ/mol.

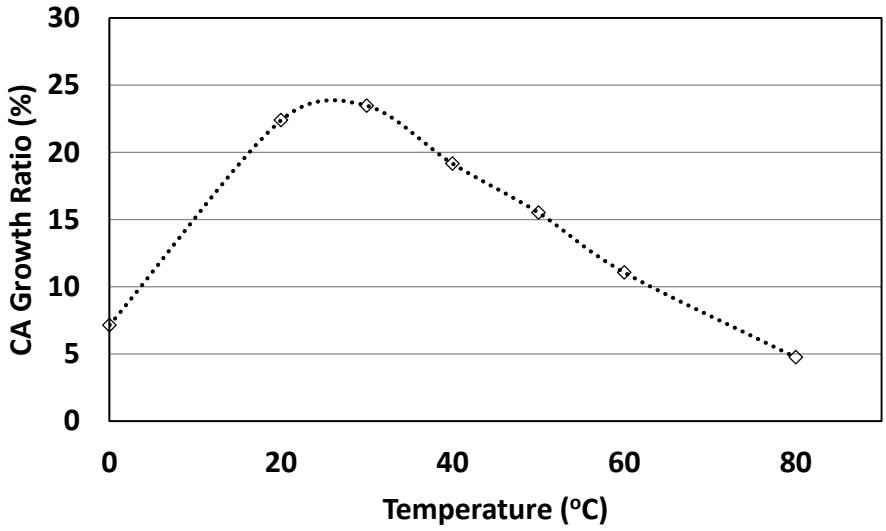

Figure 42 Ratio between CA Growths with and without Diffusion Resistance, E_{ac} = 60 kJ/mol.

Both CA growth with no diffusion resistance (solid line) and CA growth with actual diffusion resistance (dash line) are plotted with temperature in Figure 41. The CA growth ratio over temperature is plotted in Figure 42 and the definition of this ratio is the value of actual CA growth divided by the value of maximum CA growth at a particular temperature. In the simulations, the constant-rate activation energies were fixed as 60 kJ/mol, which is relatively low among the known asphalt binders. The other model inputs are listed in Table 7. In these figures it has been shown that under this circumstance, all the actual CA growth values are much less than the maximum CA values. The highest ratio appears at 30 °C, but is still lower than a quarter. That means the oxidation runs in actual conditions is much slower than the maximum reaction rate with no diffusion resistance. The oxygen concentrations in the asphalt films are far from saturated. The oxygen diffusion rate strongly restricts the reaction rate. The whole aging process is absolutely

determined by oxygen diffusion.

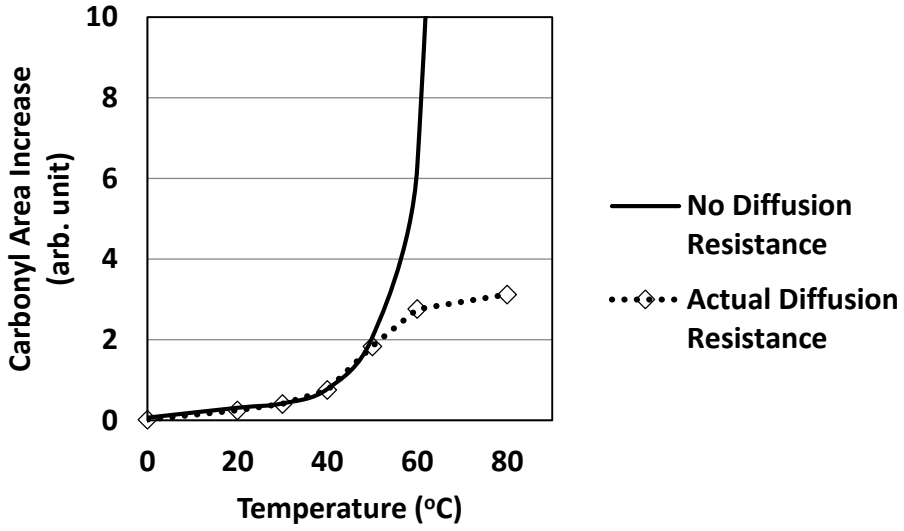

Figure 43 CA Growth at Different Temperatures with No Diffusion Resistance and Actual Diffusion Resistance, E_{ac} = 110 kJ/mol.

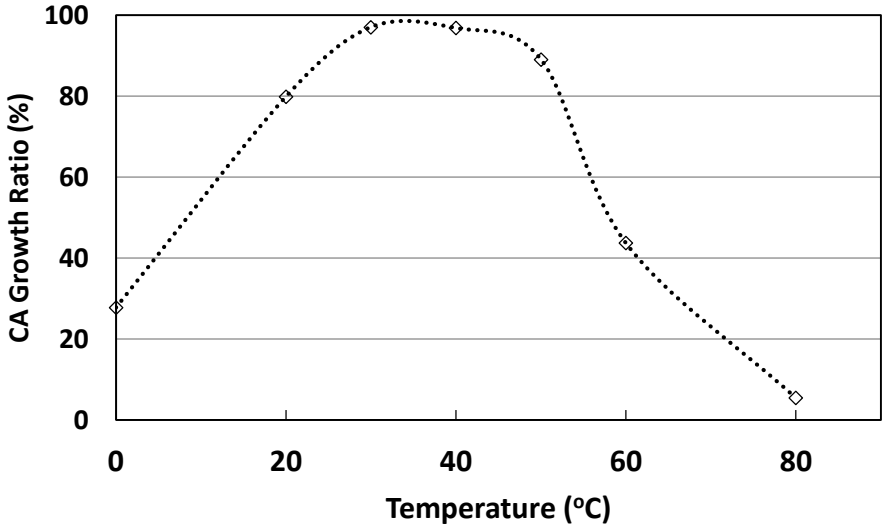

Figure 44 Ratio between CA Growths with and without Diffusion Resistance, E_{ac} = 110 kJ/mol.

Figure 43 shows a similar comparison as Figure 41, but under the case of constant-rate activation energy equals 110 kJ/mol. In Figure 44, the ratios between the actual and maximum CA growths indicate that, in the range of 25 to 50 ^{o}C, the reaction rates under actual conditions reach the maximum rates (ratio above 90 %). Therefore, at least in this temperature range, the amount of oxygen supplied by diffusion is much more than the amount consumed by the reaction and the aging process is fully determined by the reaction. However, in temperature ranges lower than 0 ^{o}C and above 70 ^{o}C, the actual CA growths only reach less than 25 % of maximum. It indicates that at those temperatures, the oxygen diffusion still mainly controls the aging process, which is the same as the case shown in Figure 42. For the temperatures fall into the ranges from 0 to 25 ^{o}C and from 50 to 70 ^{o}C, the ratio is above 25 % and less than 90 %, the aging process should be controlled by both oxygen diffusion and oxidative reaction.

Effect of Hardening Properties (Hardening Susceptibility and Hardening Intercept) on Diffusion-Reaction Balance

Figure 45 shows the simulation results on asphalt with different hardening susceptibilities. Figure 46 gives the ratio between the actual CA growth and maximum CA growth. The hardening susceptibility correlates the asphalt chemical components changes with its viscosity increase. Low hardening susceptibility gives slower viscosity increase comparing with high hardening susceptibility. And the asphalt hardening slows down the oxygen diffusion significantly, which decelerates the overall aging process. It has been proven in Figure 45 that under actual diffusivity conditions, the CA growth drops with hardening susceptibility increases.

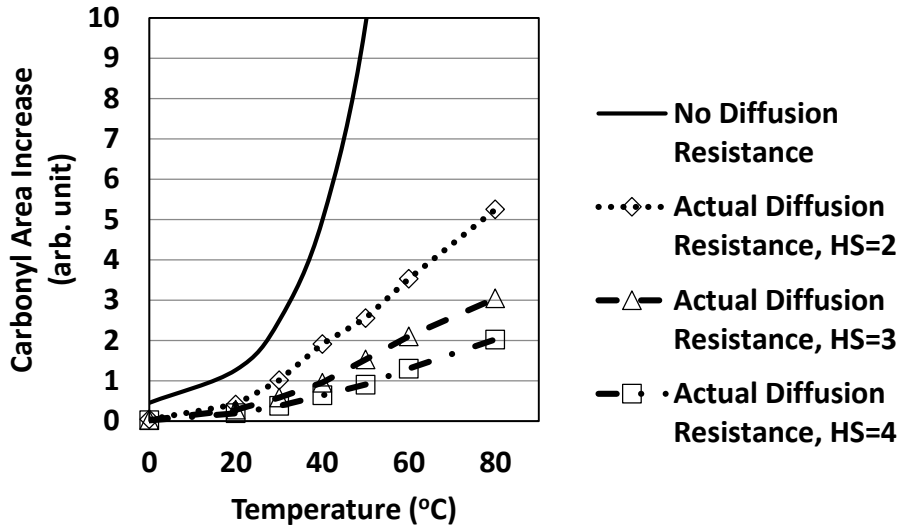

Figure 45 CA Growth at Different Temperatures with Different Hardening Susceptibilities with No Diffusion Resistance or Actual Diffusion Resistance.

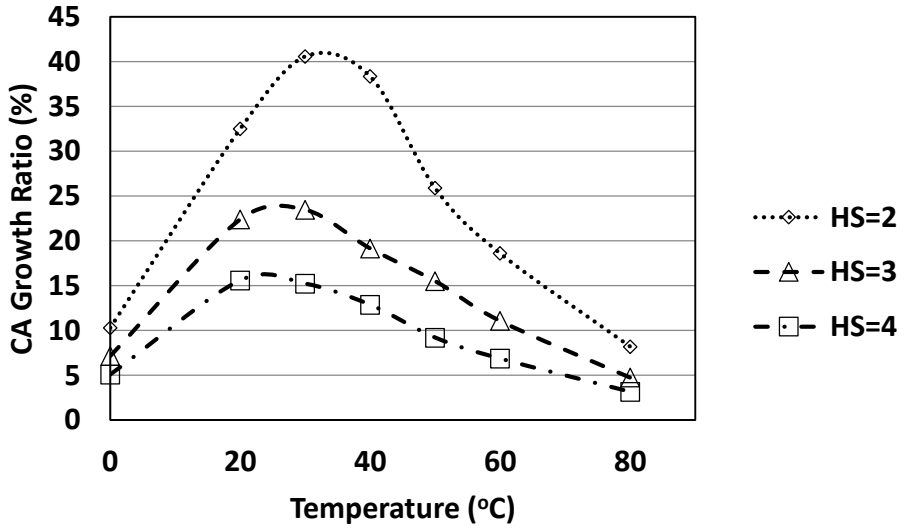

Figure 46 Ratio between CA Growths with and without Actual Diffusion Resistance.

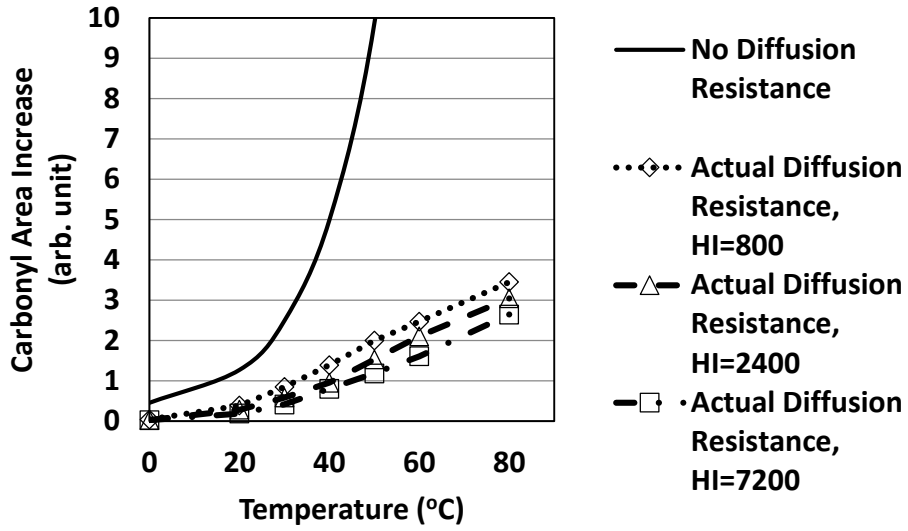

Figure 47 CA Growth at Different Temperatures with Different Asphalt Hardening Intercepts with or without Actual Diffusion Resistance.

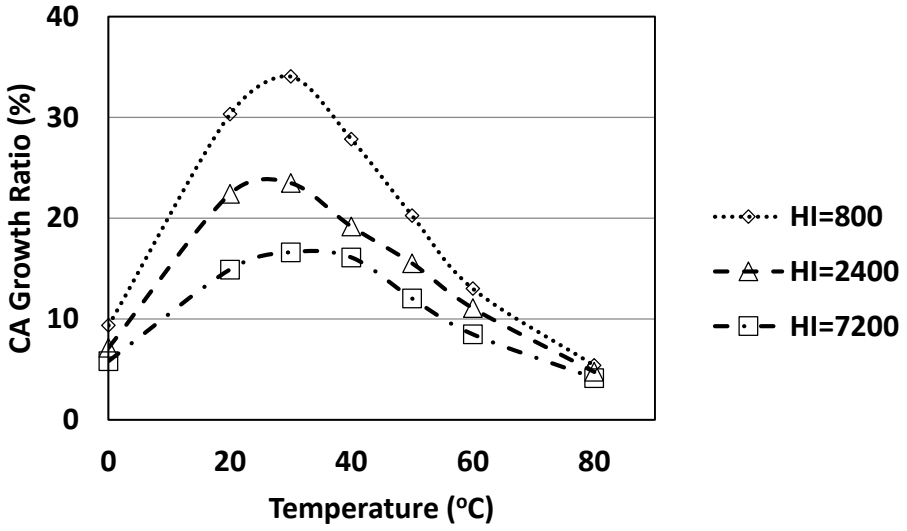

Figure 48 Ratio between CA Growth with and without Actual Diffusion Resistance.

Figure 47 studies the effect of the hardening intercept on diffusion-reaction balance. Figure 48 gives the ratio between the actual CA growth and maximum CA growth. The concept of the hardening intercept is a hypothetical viscosity at 60 ^{o}C when CA equals to zero, so the hardening intercept performs as an ideal starting point of asphalt binder hardening. When two binders with the same hardening susceptibility and the same oxidation level (same CA), the binder with a higher hardening intercept has a higher viscosity. And as discussed in the paragraph above, the oxygen diffusion suffers from the asphalt hardening, therefore hardening intercept has a negative effort on asphalt aging, which is shown in Figure 47.

Discussion about Kinetics and Hardening Properties of a "Good" Binder

Based on what has been discussed above, a new standard from the aspect of aging could be proposed to judge an asphalt binder "good" or not. One direct thought would be a binder with a low reaction rate, which could be translated into high activation energy. Except high activation energy, results in this study has proven that the oxygen diffusion also plays an extremely important role in asphalt aging. In some cases, diffusion even controls the aging process (see Figure 42). Thus, to slow down the aging, the asphalt properties, which relates to oxygen diffusion, should be carefully checked as well. From Han's work (2011), oxygen diffusivity is a function of viscosity, and viscosity is a function of oxidation level, hardening susceptibility and hardening intercept. Thus to enhance the diffusion resistance or to eliminate the oxygen supply, the binder should have a high viscosity at a relatively low oxidation level, which means high hardening susceptibility and high hardening intercept. High hardening susceptibility can result in a big viscosity

increase, which slows down the oxygen diffusion significantly. However, at the same time, high hardening susceptibility makes the asphalt binder reach the stiffness limitation much quickly, thus shortens the pavement life significantly. Comparing with hardening susceptibility, high hardening intercept only gives a high starting point to asphalt viscosity, and makes the oxygen diffusion run at a low level since the beginning of aging. With a combination of the high hardening intercept and low hardening susceptibility, the asphalt viscosity could be high at the beginning, but increase slowly within the road service life. Thus this combination gives the best solution to reduce the oxygen diffusion.

To sum up, to evaluate a good asphalt binder merely from the aspect of aging, those features are preferred:

1. High activation energy;
2. High hardening intercept;
3. Low hardening susceptibility.

Effect of Pavement Temperatures on Diffusion-Reaction Balance

Unlike the constant-temperature conditions discussed above, the actual pavement temperature may change fast and largely, daily and annually. This fact makes the diffusion-reaction balance hard to detect, but an overall ratio between the actual CA growth and maximum CA growth could still be defined. To give a general idea of the effect of pavement temperatures on the diffusion-reaction balance, two pavement locations have been chosen, Laredo District in Texas and MnRoad Test Site in Minnesota. Profiles of the annul hourly temperatures from these two sites, calculated by a pavement temperature model (Han, Jin, and Glover 2011), is given in Table 9.

Table 9 Annual Hourly Temperature Distribution.

Site	Total Annual Hours	<20 ºC (%)	20 to 30 ºC (%)	30 to 40 ºC (%)	40 to 50 ºC (%)	50 to 60 ºC (%)	>60 ºC (%)
TX	8760	35.5	30.5	15.5	8.6	7.3	2.7
MN	8760	73.5	16.0	8.7	1.8	0.0	0.0

The next step is to study the effect of actual pavement temperatures on the diffusion-reaction balance. Binders with two activation energies, 60 kJ/mol and 110 kJ/mol, were used in the model simulation. The maximum increased CA amounts (no diffusion resistance) and actual increased CA amounts after 114 months are given in Table 10. It could be seen that for the binder with the activation energy equals 60 kJ/mol, the overall ratios are around 40 %. This means the aging process is controlled by both diffusion and reaction in most of the time. For the binder with the activation energy equals 110 kJ/mol, the overall ratios are above 90 % that means the reaction is the only limitation for the aging process. One issue should be mentioned again that the pavement temperature changes every moment. At each time point, there is a specific ratio between the maximum and actual reaction rates, and the aging process could be controlled by diffusion, reaction, both of them at this moment. The overall ratio in Table 10 only gives an average value of the ratios in this long aging period (114 months).

Table 10 CA Growth at Field Temperatures.

Site + Binder's Constant- Rate Activation Energy (kJ/mol)	Maximum CA Growth (arb. unit)	Actual CA Growth (arb. unit)	$100\ \% \times \frac{\text{Actual CA Growth}}{\text{Maximum CA Growth}}$ Overall Ratio=
TX 60	3.641	1.505	41.3
MN 60	1.143	0.452	39.5
TX 110	0.916	0.889	97.1
MN 110	0.335	0.312	93.1

Retarding Asphalt Aging by Reducing Oxygen Diffusivity

Instead of evaluating the existing asphalt, the discussion above could instruct the scientists to develop new methods to slow down the binder aging. There are two existing and widely used methods: (1) blending with some binders age slowly; (2) adding anti-oxidant into the binder. This anti-oxidant could react with oxygen instead of asphalt, but there is a limitation for the anti-oxidant that is once they all consumed by the oxygen, the protection is over.

From the new understandings on the role of oxygen diffusion in asphalt aging, new methods could be developed to retard the aging. It could be achieved by either increasing binder stiffness to reduce the oxygen diffusivity or building a network structure by additives to increase the oxygen diffusion distance. The benefits would be: (1) applicable for every binder; (2) no time limitation (not consumed like traditional anti-oxidant).

Figure 49 gives an example about the amount of benefit could be obtained. In each individual case, the CA growth after 114 months with actual diffusivity is set as 100 %, and the ratios are defined as the amounts with reduced diffusivities divided by the amounts with actual diffusivity. In the figure, these ratios are always less than 100 %, so it is clear

that reducing the diffusion capability could definitely slow the aging process. And for each case, the effect of reducing diffusivity is not equal. First, for the case that the binder has a low activation energy (60 kJ/mol), the aging process is mainly controlled by diffusion (see Table 10), thus the effort of reducing diffusivity would be evidently. The total CA growth would be reduced to 95 % by reducing diffusivity to 90 %, to about 85 % by reducing diffusivity to 70 %, to only about 35 % by reducing diffusivity to 10 %. So there is an approximate 5 % aging amount reduced for every 10 % diffusivity reducing. Second, for the case that the binder has a high activation energy (110 kJ/mol), the whole process is fully controlled by the reaction not the diffusion (see Table 10). The approximate 5 % reducing rate is not suitable for this case. It could not affect the whole aging process much by reducing the diffusivity in a small range (10 or 30 %). Only when the diffusivity is an extremely low value (to 10 % of original value), the effect could be seen clearly (to 35 % of original value). Only at this time, diffusion could play a role important enough to bring the whole aging out of reaction determination.

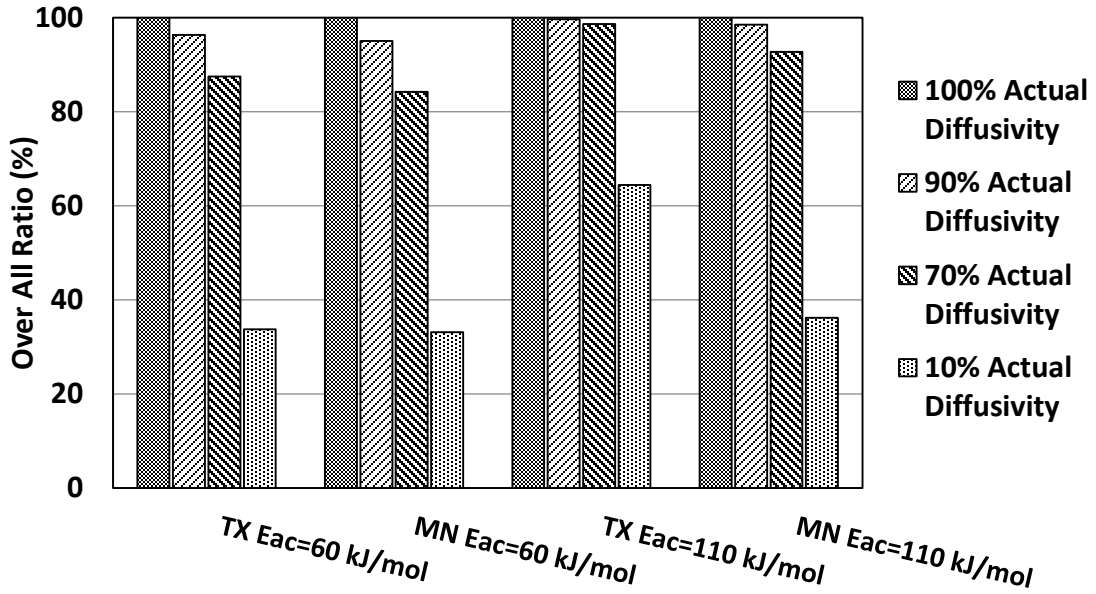

Figure 49 Remained CA Growth Percent at Different Reduced Actual Diffusivity.

Conclusions

The balance between oxygen diffusion and oxidative reaction controls the asphalt aging. However, it could not be easily studied by experimental methods due to its comprehensiveness. With the help of the pavement oxidation model, the effects of temperature and asphalt properties on this balance were carefully studied. Conclusions are given as following:

- The oxygen diffusion suffers from the asphalt hardening seriously at a high oxidative level that slows down the whole process of asphalt aging.
- If the asphalt has a low activation energy (60 kJ/mol), in the temperature range from 0 to 80 ^{o}C, the oxygen diffusion mainly controls the whole aging process. If the asphalt has a high activation energy (110 kJ/mol), the

determination step switches from oxygen diffusion to oxidative reaction and then back to oxygen diffusion while the temperature increases from 0 to 80 ^{o}C;

- Both high hardening susceptibility and high hardening intercept have negative efforts on oxygen diffusion.
- From asphalt aging aspect, the evaluation of a good binder would be: (1) high activation energy; (2) high hardening intercept; (3) low hardening susceptibility.
- By using pavement temperatures in the model simulation, an overall ratio is given to tell the determination step in field aging. And the binder activation energy plays a much more important role than pavement temperatures.
- A new method has been proposed to retard the asphalt aging by reducing the oxygen diffusivity. The potential effect of this new idea has been proven by model simulations.

CHAPTER VIII

SUMMARY

Summary and Conclusions

After verifying the fact that asphalt oxidation occurs in pavements, predicting the oxidation level after years of usage becomes essential. In recent ten years, asphalt scientists have developed serial oxidation models based on the understandings on asphalt aging. All the models aim to simulate the asphalt aging in field conditions, predict asphalt performance in future and consequently give answers to pavement service life.

In this dissertation, an exploration has been conducted on the issue of the model application. Topics include the investigation of asphalt field aging and the new developments of laboratory accelerated aging tests. The problems of applying this model in two special cases, no original binder and no field sample, were successfully solved. On one hand, original binder is not always available after the construction. On the other hand, field sample is impossible to be obtained before the construction. To solve those problems, new methods were proposed and alternated materials were tested in laboratory. Information from those tests were inputted in the model and simulation results were verified by field data. In the meanwhile, with the help of the model, a fundamentals-based study was conducted on the issue of diffusion-reaction balance in asphalt aging. A summary of major research findings for each individual task follows.

Asphalt Aging in Field Conditions

This study includes much more measurements than any previous studies on pavement aging. The pavement cores, which were collected all over Texas and one pavement site in Minnesota, provide a massive of field data. Several conclusions were obtained, including the effects of depth, air void distribution, pavement temperature, and asphalt properties on pavement aging. First, aging rates are different with depth, and they are results of the accessibility of oxygen to the binder through the accessible air voids. Second, the impact of temperature in asphalt aging is significant. The binder ages slower in Minnesota than in Texas due to the pavement temperature difference. Third, pavements with seal coat treatment appear to be under aged relative to the same pavement without this kind of maintenance. This is definitely related to the application of seal coat.

Recovered Binder POV Tests

An alternate binder source has been proposed and tested in the asphalt aging tests. Recovered binder, extracted from field cores, was further oxidized in laboratory to determine its kinetics and hardening properties. Measurement results from recovered binder match well with results from original binder, which confirms the fact that extraction and recovery process does not change the binder kinetics and hardening properties. This new method provides a binder source allowing oxidation analysis on some pavements with no original binder.

Aging in a Seal Coat Treated Pavement

A systematic method has been established to determine and to predict the degree of oxidative aging in a seal coat treated pavement. Seal coat penetrates below the pavement

surface and a mixed binder of pavement binder and seal coat binder was identified by binder hardening property. Different aging rates are expected in different depth of the pavement. Recovered binders from different depth were further oxidized in laboratory for their kinetics and hardening properties. With this essential information, the future performance of this seal coat treated pavement was predicted by pavement oxidation model.

Asphalt Concrete Aging in Laboratory and in Field

The aim of this work was to establish a relation between LMLC sample and field sample to apply the model on a pavement before construction. Based on the observation on field samples, much of the asphalt concrete aging occurs during the first year, and the aging rate decreases over time. In LMLC samples, the binder stiffness increases with time, which coordinates well with findings in field samples. Based on the measurements on LMLC binders, a prediction could be given to a pavement before construction by pavement oxidation model.

Fast Aging Test

This work developed and demonstrated an accelerated method for comparing binder pavement aging characteristics. The strategy determines a binder's constant-rate activation energy at PAV pressure. With the PAV – POV activation energy correlation developed in this study, plus the work of Jin et al. (2011), a complete set of binder oxidation fast-rate and constant-rate kinetics parameters can be estimated. The accelerated PAV method for determining binder oxidation kinetics parameters, coupled with the thermal and oxygen transport model of pavement oxidation plus data on the impact of

binder oxidative hardening on mixture durability, provides an innovative comprehensive, and fundamentals-based accelerated aging test of a binder's performance.

Diffusion-Reaction Balance in Asphalt Aging

A balance between oxygen diffusion and oxidative reaction was discovered by model simulation. This issue could not be easily studied by experimental methods due to its comprehensiveness. In some special cases, oxygen diffusion or oxidative reaction becomes the determination step. And binder hardening has a significant role, which suffers the oxygen diffusion seriously and consequently slows down the whole process of asphalt aging. With the help of the model, the efforts of binder properties and temperatures on this balance have been discussed in detail. A new standard for asphalt binder, solely from aging aspect, includes high activation energy, low hardening susceptibility and high hardening intercept. And an overall diffusion-reaction ratio was given by the analysis on the effort of pavement temperatures. This ratio provides a general idea of the balance in field conditions.

Recommendations

More Samples from the Field

Study on pavement aging is still far from summarizing a quantitative evaluation on the effects of various variables. Limited numbers of field cores could be obtain due to the expense and time. Uncontrolled variables vary from one pavement site to another. To have a complete picture of the pavement aging, more field data needs to be added into the database.

Aging in a Standard Core

In the process of model validation, there appears a problem raised by air void disparity in field cores. The air void distributions were widely different in different cores, although they were collected from the same pavement. An overall aging rate for a pavement seriously suffers from this discrepancy. However, the pavement oxidation model already considered the effects of air voids on asphalt aging. With the help of the model, testing results from different cores may be transformed into oxidation levels in a standard core, which has a fixed air void distribution. By eliminating the effect of air voids, the oxidation increase would be only determined by pavement temperature, service time and nature of asphalt. The rate in this standard core may better represent the pavement aging and this rate would be much more objective than any approximated rate ranges obtained from field cores with different air void distributions.

Analysis of Aging Factors

A better characterization of the aging elements in the model is still an ongoing process. There are up to seven fundamental elements in the model. Those elements could be classified into two main groups, pavement design and asphalt properties. To better predict the asphalt aging, the effort of every element needs to be better understood. And relations between those elements are essentially more important. In this dissertation, only one case was fully analysed, which is the balance between oxygen diffusion and oxidative reaction. A very limited number of simulations were conducted due to time issue. This could only be called as a starting point, more works on aging element analysis are strongly recommended.

REFERENCES

1. Al-Azri, N. A., Jung, S. H., Lunsford, K. M., Ferry, A., Bullin, J. A., Davison, R. R., and Glover C. J. (2006). Binder Oxidative Aging in Texas Pavements: Hardening Rates, Hardening Susceptibilities, and Impact of Pavement Depth. *Transportation Research Record: Journal of the Transportation Research Board.* 1962: 12-20.

2. Al-Suleiman, T. I., Sinha, K. C., and Riverson, J. D. (1991). Effects of Pavement Age and Traffic on Maintenance Effectiveness. *Journal of Transportation Engineering.* 117: 644-659.

3. Anderson, D. A., Christensen, D. W., Bahia, H. U., Dongre, R., Sharma, M. G., Antle, C. E., and Button, J. (1994). *Binder Characterization and Evaluation, Volume 3: Physical Characterization.* SHRP Report A-369. Washington, D.C.: Strategic Highway Research Program/National Research Council.

4. Branthaver, J. F., Petersen, J. C., Robertson, R. E., Duvall, J. J., Kim, S. S., Harnsberger, P. M., Mill, T., Ensley, E. K., Barbour, F. A., and Scharbron, J. F. (1993). *Binder Characterization and Evaluation. Volume 2: Chemistry*. SHRP Report A-368. Washington, D.C.: Strategic Highway Research Program/National Research Council.

5. Brown, E. R. (1988). Preventative Maintenance of Asphalt Concrete Pavements. *Transportation Research Record: Journal of the Transportation Research Board.* 1205: 6-11.

6. Buchanan, M. S., and White, T. D. (2005). Hot Mix Asphalt Mix Design Evaluation Using the Corelok Vacuum-Sealing Device. *Journal of Materials in Civil Engineering.* 17: 137-142.

7. Burr, B. L., Davison, R. R., Jemison, H. B., Glover, C. J., and Bullin, J. A. (1991). Asphalt Hardening in Extraction Solvents. *Transportation Research Record: Journal of the Transportation Research Board.* 1323: 70-76.

8. Cipione, C. A., Davison, R. R., Burr, B. L., Glover, C. J., and Bullin, J. A. (1991). Evaluation of Solvents for Extraction of Residual Asphalt from Aggregates. *Transportation Research Record: Journal of the Transportation Research Board.* 1323: 47-52.

9. Clark, R. C. (1958). Practical Results of Asphalt Hardening on Pavement Life. *Proceedings, Association of Asphalt Paving Technologists.* 27: 196.

10. Cooley, L. A., Prowell, B. D., Hainin, M. R., Buchanan, M. S., and Harrington J. (2002). *Bulk Specific Gravity Round-Robin Using the Corelok Vacuum Sealing Device*. Washington, D.C.: Office of Pavement Technology Applications, Federal Highway Administration.

11. Coons, R. F., and Wright, P. H. (1965). An Investigation of the Hardening of Asphalt Recovered from Pavements of Various Ages. Master's thesis. Atlanta, GA: Georgia Institute of Technology.

12. Dickinson, E. J. (1984). The Diffusion Controlled Reaction of Oxygen with Films of Bituminous Binders. *Australian Road Research.* 14: 121-132.

13. Domke, C. H., Davison, R. R., and Glover, C. J. (2000). Effect of Oxygen Pressure on Asphalt Oxidation Kinetics. *Industrial & Engineering Chemistry Research.* 39: 592-598.

14. Domke, C. H., Liu, M., Davison, R. R., Bullin, J. A., and Glover, C. J. (1997). Study of Strategic Highway Research Program Pressure Aging Vessel Procedure Using Long-Term, Low-Temperature Aging Experiments and Asphalt Kinetics. *Transportation Research Record: Journal of the Transportation Research Board.* 1586: 10-15.

15. Doyle, P. C. (1958). Cracking Characteristics of Asphalt Cement. *Association of Asphalt Paving Technologists Proceedings.* 27: 581-597.

16. Glover, C. J., Davison, R. R., Domke, C. H., Ruan, Y., Juristyarini, P., Knorr, D. B., and Jung. S. H. (2005). *Development of a New Method for Assessing Asphalt Binder Durability with Field Validation*. FHWA/TX-05/1872-2. College Station, TX: Texas Transportation Institute, Texas A & M University System.

17. Gransberg, D. D., and James D. M. (2005). *Chip Seal Best Practices*. NCHRP Synthesis 342. Washington, D.C.: Transportation Research Board.

18. Hagos, E. T., Molenaar, A. A. A., and van de Ven, M. K. C. (2009). Chemical Characterization of Laboratory and Field Bitumen Aging in Porous Asphalt Concrete. *Advanced Testing and Characterization of Bituminous Materials.* pp. 173-184. Taylor & Francis Group, London.

19. Halstead, W. J. (1963). The Relation of Asphalt Ductility to Pavement Performance. *Association of Asphalt Paving Technologists Proceedings.* 32: 247-270.

20. Han, R. (2011). *Improvement to a Transport Model of Asphalt Binder Oxidation in Pavements: Pavement Temperature Modeling, Oxygen Diffusivity in Asphalt Binders and Mastics, and Pavement Air Void Characterization*. Ph.D. dissertation. College Station, TX: Texas A&M University.

21. Han, R., Jin, X., and Glover, C. J. (2011). Modeling Pavement Temperature for Use in Binder Oxidation Models and Pavement Performance Prediction. *Journal of Materials in Civil Engineering.* 23: 351-359.

22. Herrington, P. R. (1998). Oxidation of Bitumen in the Presence of a Constant Concentration of Oxygen. *Petroleum Science and Technology.* 16: 743-765.

23. Huh, J. D., and Robertson, R. E. (1996). Modeling of Oxidative Aging Behavior of Asphalts from Short-Term, High-Temperature Data as a Step toward Prediction of Pavement Aging. *Transportation Research Record: Journal of the Transportation Research Board.* 1535: 91-97.

24. Jemison, H. B., Burr, B. L., Davison, R. R., Bullin, J. A., and Glover, C. J. (1992). Application and Use of the ATR, FT-IR Method to Asphalt Aging Studies. *Fuel Science & Technology International.* 10: 795-808.

25. Jin, X., Cui, Y., and Glover, C. J. (2013). Modeling Asphalt Oxidation in Pavement with Field Validation. *Petroleum Science and Technology.* 31: 1398-1405.

26. Jin, X., Han, R., Cui, Y., and Glover, C. J. (2011). Fast-Rate–Constant-Rate Oxidation Kinetics Model for Asphalt Binders. *Industrial & Engineering Chemistry Research.* 50: 13373-13379.

27. Juristyarini, P., Davison, R. R., and Glover, C. J. (2011). Oxidation Hardening Kinetics of the Rheological Function G′/(η′/G′) in Asphalts. *Petroleum Science and Technology.* 29: 2027-2036.

28. Kandhal, P. S. (1977). Low-Temperature Ductility in Relation to Pavement Performance. *ASTM Selected Technical Papers.* 628: 95-106.

29. Kandhal, P. S., and Koehler, W. C. (1984). Significant Studies on Asphalt Durability: Pennsylvania Experience (Discussion). *Transportation Research Record: Journal of the Transportation Research Board.* 999: 41-50.

30. Kandhal, P. S., and Wenger, M. E. (1975). Asphalt Properties in Relation to Pavement Performance. *Transportation Research Record: Journal of the Transportation Research Board.* 544: 1-13.

31. King, G., Anderson, M., Hanson, D., and Blankenship, P. (2012). Using Black Space Diagrams to Predict Age-Induced Cracking. *7th RILEM International Conference on Cracking in Pavements*. 453-463. Delft, Netherlands.

32. Knotnerus, J. (1972). Bitumen Durability-Measurement by Oxygen Absorption. *Industrial & Engineering Chemistry Product Research and Development.* 11: 411-422.

33. Lau, C. K., Lunsford. K. M., Glover, C. J., Davison, R. R, and Bullin, J. A. (1992). Reaction Rates and Hardening Susceptibilities as Determined from Pressure Oxygen Vessel Aging of Asphalts. *Transportation Research Record: Journal of the Transportation Research Board.* 1342: 50-57.

34. Lawson, W. D., and Senadheera, S. (2009). Chip Seal Maintenance. *Transportation Research Record: Journal of the Transportation Research Board.* 2108: 61-68.

35. Lee, D. Y., and Huang, R. J. (1973). Weathering of Asphalts as Characterized by Infrared Multiple Internal Reflection Spectra. *Applied Spectroscopy.* 27: 435-440.

36. Liu, M. M., Lin, M. S., Chaffin, J. M., Davison, R. R., Glover, C. J., and Bullin, J. A. (1998). Oxidation Kinetics of Asphalt Corbett Fractions and Compositional Dependence of Asphalt Oxidation. *Petroleum Science and Technology.* 16: 827-850.

37. Liu, M., Lunsford, K. M., Davison, R. R., Glover, C. J., and Bullin, J. A. (1996). The Kinetics of Carbonyl Formation in Asphalt. *AIChE Journal.* 42: 1069-1076.

38. Lunsford, K. M. (1994). *The Effect of Temperature and Pressure on Laboratory Oxidized Asphalt Films with Comparison to Field Aging*. Ph.D. dissertation. College Station, TX: Texas A & M University.

39. Martin, K. L., Davison, R. R., Glover, C. J., and Bullin, J. A. (1990). Asphalt Aging in Texas Roads and Test Sections. *Transportation Research Record: Journal of the Transportation Research Board.* 1269: 9-19.

40. McLeod, N. W., Chaffin, C. W., Holberg, A. E., Parker, C. F., Obrcian, V., Edwards, J. M., Campen, W. H., and Kari, W. J. (1969). A General Method of Design for Seal Coats and Surface Treatments. *Association of Asphalt Paving Technologists Proceedings*. 38: 537-628.

41. Mill, T., Tse, D. S., Loo, B., Yao, C. C. D., and Canavesi, E. (1992). Oxidation Pathways for Asphalt. *Prepr. Pap- ACS Division Fuel Chemistry.* 37:1367-1375.

42. NAPA. Asphalt Pavement Overview. Accessed June 05, 2014. Web address: https://www.asphaltpavement.org/index.php?option=com_content&view=article&id=14&Itemid=33.

43. O'Brien, L. G. (1989). *Evolution and Benefits of Preventive Maintenance Strategies*. Washington D.C.: Transportation Research Board.

44. Petersen, J. C. (1975). Quantitative Method Using Differential Infrared Spectrometry for the Determination of Compound Types Absorbing in the

Carbonyl Region in Asphalts. *Analytical Chemistry.* 47: 112-117.

45. Petersen, J. C., Robertson, R. E., Branthaver, J. F., Harnsberger, P. M., Duvall, J. J., Kim, S. S., Anderson, D. A., Christiansen, D. W., and Bahia, H. U. (1994). *Binder Characterization and Evaluation*. SHRP-A-367. Washington D.C.: Transportation Research Board.

46. Petersen, J. C., Barbaar, F. A., and Dorrence, S. M. (1974). Catalysis of Asphalt Oxidation by Mineral Aggregate Surfaces and Asphalt Components. *Association of Asphalt Paving Technologists Proceedings.*43: 162-177.

47. Petersen, J. C., Branthaver, J. F., Robertson, R. E., Harnsberger, P. M., Duvall, J. J., and Ensley, E. K. (1993). Effects of Physicochemical Factors on Asphalt Oxidation Kinetics. *Transportation Research Record: Journal of the Transportation Research Board.* 1391: 1-10.

48. Petersen, J. C., and Harnsberger, P. M. (1998). Asphalt Aging: Dual Oxidation Mechanism and Its Interrelationships with Asphalt Composition and Oxidative Age Hardening. *Transportation Research Record: Journal of the Transportation Research Board.* 1638: 47-55.

49. Prapaitrakul, N., Han, R., Jin, X., and Glover, C. J. (2009). A Transport Model of Asphalt Binder Oxidation in Pavements. *Road Materials and Pavement Design.* 10: 95-113.

50. Roberts, F. L., Kandhal, P. S., Brown. E. R., Lee, D. Y., and Kennedy, T. W. (1996). *Hot Mix Asphalt Materials, Mixture Design and Construction*. Lanham, MD: National Asphalt Pavement Association Research and Education Foundation.

51. Ruan, Y., Davison, R. R., and Glover, C. J. (2003). An Investigation of Asphalt Durability: Relationships between Ductility and Rheological Properties for Unmodified Asphalts. *Petroleum Science and Technology.* 21: 231-254.

52. Walubita, L. F., Epps Martin, A., Jung, S. H., Glover, C. J., and Park, E. S. (2006). *Application of Calibrated Mechanistic Fatigue Analysis with Aging Effects*. FHWA/TX-06/0-4468-3. College Station, TX: Texas Transportation Institute, Texas A&M University System.

53. Epps Martin, A., Jung, S. H., Glover, C. J., Park, E. S., Chowdhury, A., and Lytton, R. L. (2005). *Comparison of Fatigue Analysis Approaches for Two Hot Mix Asphalt Concrete (HMAC) Mixtures*. FHWA/TX-05/0-4468-2. College Station, TX: Texas Transportation Institute, Texas A&M University System.

54. Welborn, J. (1984) Physical Properties as Related to Asphalt Durability: State of the Art. *Transportation Research Record: Journal of the Transportation Research*

Board. 999: 31-36.

55. Woo, W. J., Chowdhury, A., and Glover, C. J. (2008). Field Aging of Unmodified Asphalt Binder in Three Texas Long-Term Performance Pavements. *Transportation Research Record: Journal of the Transportation Research Board.* 2051: 15-22.

56. Woo, W. J., Ofori-Abebresse E., Chowdhury A., Hilbrich, J. M., Kraus Z., Epps Martin, A., and Glover, C. J. (2007). *Polymer Modified Asphalt Durability in Pavements*. FHWA/TX-07/0-4688-1. College Station, TX: Texas Transportation Institute, Texas A&M University System.

APPENDIX A

TABLES OF REHEOLOGICAL PROPERTIES, CARBONYL AREA, AND DSR FUNCTION HARDENING WITH PAVEMENT SERVICE TIME DATA

List of pavement test sites and binders information are shown in Table 1 (Page 13). The locations of the sites in Texas are shown in Figure 1 **(Page 15). The sites range from the Northern Panhandle to the Southern Rio Grande Valley and from Odessa in the West to the Lufkin and Atlanta districts in the East. Moreover, some of the Texas pavements applied seal coat maintenance on the surface. Cores were also collected in Minnesota by Mn/DOT (Minnesota Department of Transportation). The MnRoad test site used to be studied in previous projects, named as MnRoad Cell 1, and results on its original binders are also available in FHWA/TX-07/0-4468-1 Report. For the field cores with seal coat treatment, the seal coat layer was removed first if possible, but for some of those cores, the seal coat layer was too thin to remove, binder from the layer, including seal coat and 1st layer, was extracted and tested.**

Table A1. AMR US54 Field Core (Wheel Path)

Binder: Unknown Activation Energy: 81.5 kJ/mol Cons.: 1998		η* (Poise) @60ºC 0.1 rad/s	G'/(η'/G') (MPa/s) @15ºC 0.005 rad/s	Carbonyl Area
1st Core Seal coat Treated (07/2008)	Seal coat and 1st layer	60000	0.0002	1.282
	2nd	1200000	0.0106	1.705
	3rd	300000	0.0022	1.590
	4th	160000	0.001	1.489
	1st to 4th	219000	0.0015	1.508

Table A2. AMR US54 Field Core (Shoulder)

Binder: Unknown Activation Energy: 81.5 kJ/mol Cons.: 1998		η* (Poise) @60ºC 0.1 rad/s	G'/(η'/G') (MPa/s) @15ºC 0.005 rad/s	Carbonyl Area
1st Core Seal coat Treated (07/2008)	Seal coat and 1st layer	60000	0.0001	1.128
	2nd	300000	0.0011	1.296
	3rd	280000	0.0012	1.303
	4th	280000	0.001	1.320
	1st to 4th	280000	0.0006	1.245

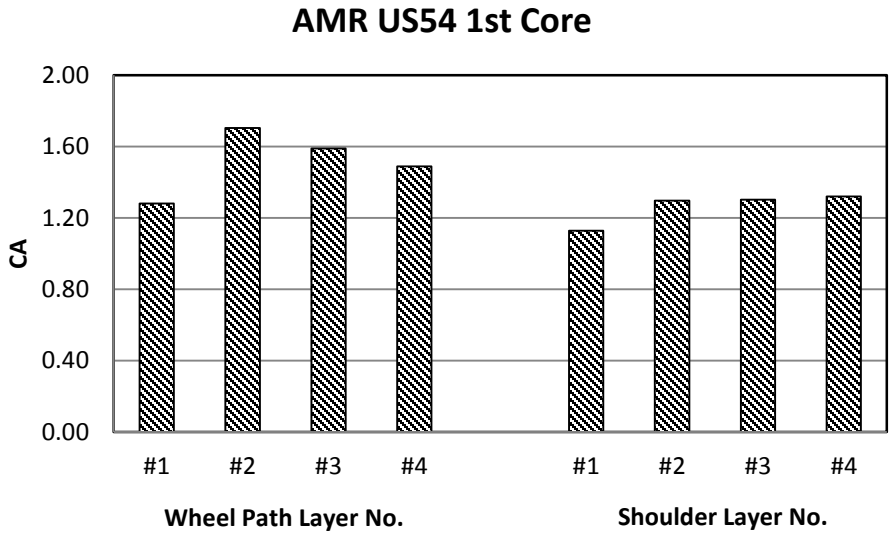
AMR US54 1st Core
2.00
1.60
1.20
0.80
0.40
0.00
CA
#1
#2
#3
#4
#1
#2
#3
#4
Wheel Path Layer No.
Shoulder Layer No.

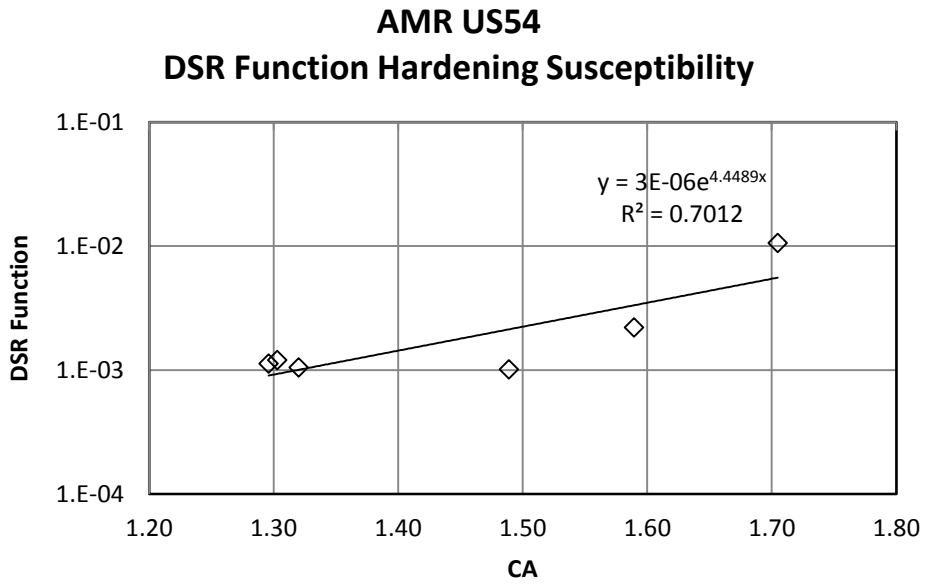
AMR US54
DSR Function Hardening Susceptibility
1.E-01
1.E-02
1.E-03
1.E-04
DSR Function
y = 3E-06e4.4489x
R2 = 0.7012
1.20
1.30
1.40
1.50
1.60
1.70
1.80
CA

Table A3. ATL IH20 Field Core (Wheel Path)

Binder: Wright PG76-22 Activation Energy: Unknown Cons.: 2003		η* (Poise) @60ºC 0.1 rad/s	G'/(η'/G') (MPa/s) @15ºC 0.005 rad/s	Carbonyl Area
1st Core (07/2008)	1st layer	Too high to measure	Too high to measure	1.531
	2nd	Too high to measure	Too high to measure	1.653
	3rd	1300000	0.0117	1.596
	4th	2000000	0.0157	1.442
	1st to 4th	-	-	1.568

Table A4. ATL IH20 Field Core (Shoulder)

Binder: Wright PG76-22 Activation Energy: Unknown Cons.: 2003		η* (Poise) @60ºC 0.1 rad/s	G'/(η'/G') (MPa/s) @15ºC 0.005 rad/s	Carbonyl Area
1st Core (07/2008)	1st layer	Too high to measure	Too high to measure	1.7445
	2nd	180000	0.0024	1.336
	3rd	210000	0.0029	1.364
	4th	320000	0.0058	1.407
	1st to 4th	-	-	1.489

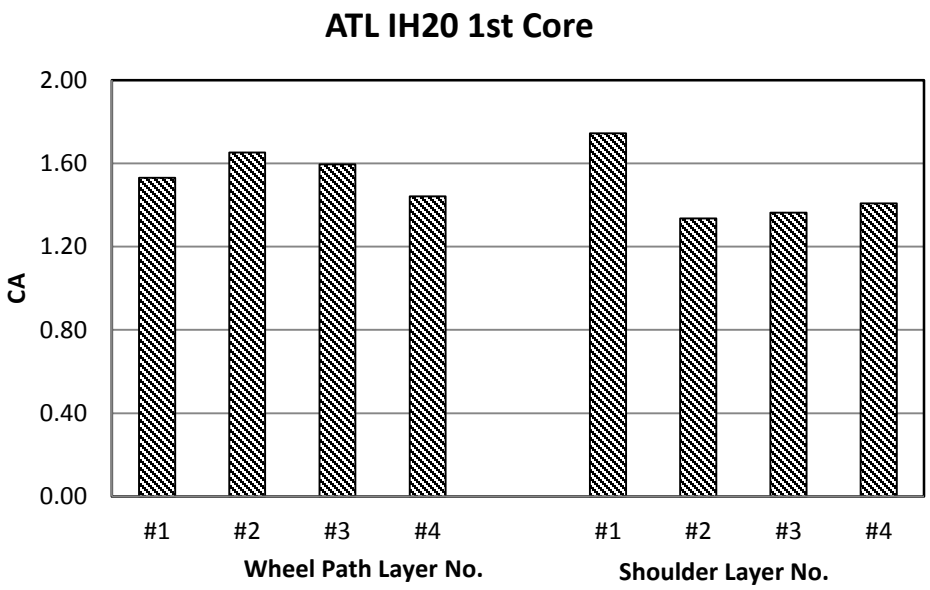
ATL IH20 1st Core
2.00
1.60
1.20
0.80
0.40
0.00
CA
#1
#2
#3
#4
#1
#2
#3
#4
Wheel Path Layer No.
Shoulder Layer No.

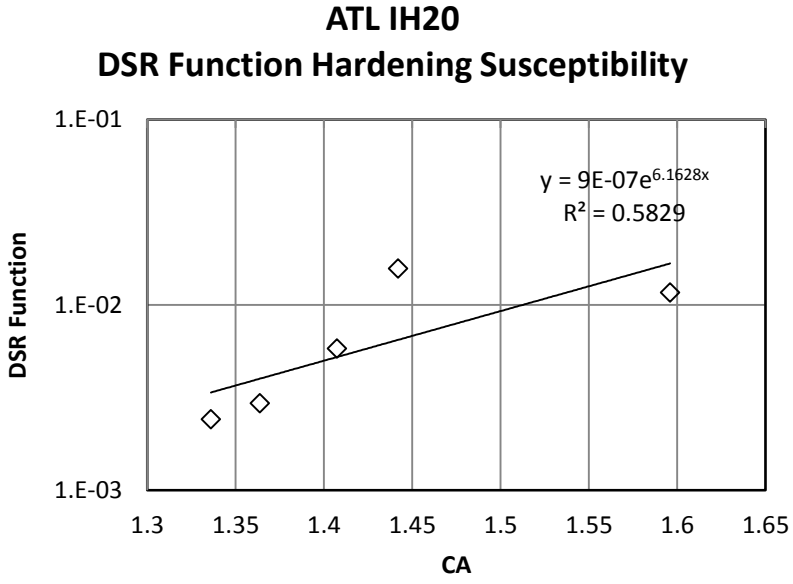
ATL IH20
DSR Function Hardening Susceptibility
1.E-01
1.E-02
1.E-03
DSR Function
y = 9E-07e6.1628x
R² = 0.5829
1.3
1.35
1.4
1.45
1.5
1.55
1.6
1.65
CA

Table A5. ATL US259 Field Core (Wheel Path)

Binder: Lion PG76-22 Activation Energy: 97.4 kJ/mol Cons.: 2005		η* (Poise) @60°C 0.1 rad/s	G'/(η'/G') (MPa/s) @15°C 0.005 rad/s	Carbonyl Area
1st Core (12/2008)	1st layer	16000	0.0012	1.381
	2nd	100000	0.00060	1.264
	3rd	100000	0.00050	1.168
	4th	80000	0.00032	1.051
	5th	65000	0.00031	1.157
	1st to 5th	50000	0.00071	1.257
2nd Core (10/2010)	1st to 5th	121000	0.00070	1.271

Table A6. ATL US259 Field Core (Shoulder)

Binder: Lion PG76-22 Activation Energy: 97.4 kJ/mol Cons.: 2005		η* (Poise) @60°C 0.1 rad/s	G'/(η'/G') (MPa/s) @15°C 0.005 rad/s	Carbonyl Area
1st Core (12/2008)	1st layer	38000	0.0004	1.263
	2nd	33000	0.0003	1.167
	3rd	30000	0.0003	1.177
	4th	28000	0.0002	1.176
	1st to 4th	30000	0.0003	1.202
2nd Core (10/2010)	1st to 4th	50500	0.00046	1.191

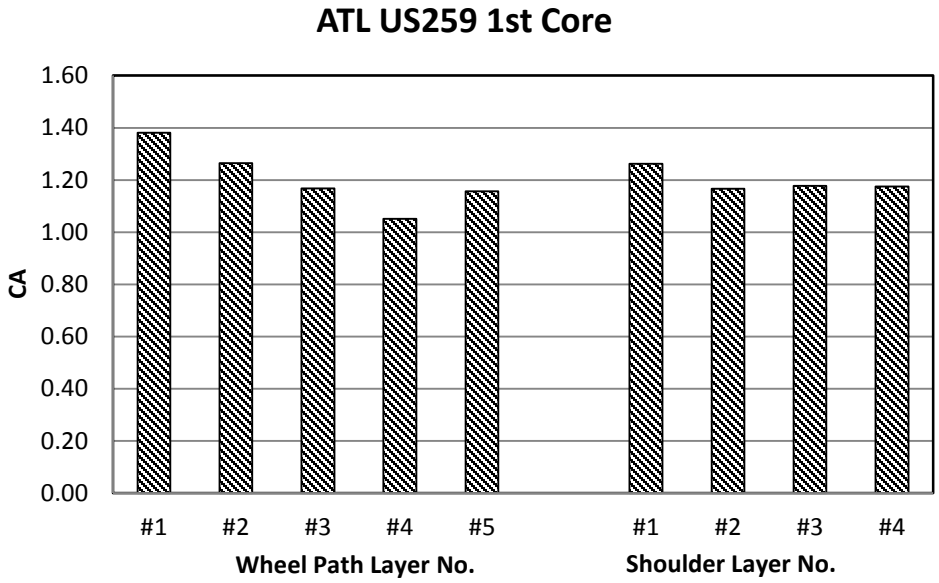
ATL US259 1st Core
1.60
1.40
1.20
1.00
0.80
0.60
0.40
0.20
0.00
CA
#1
#2
#3
#4
#5
#1
#2
#3
#4
Wheel Path Layer No.
Shoulder Layer No.

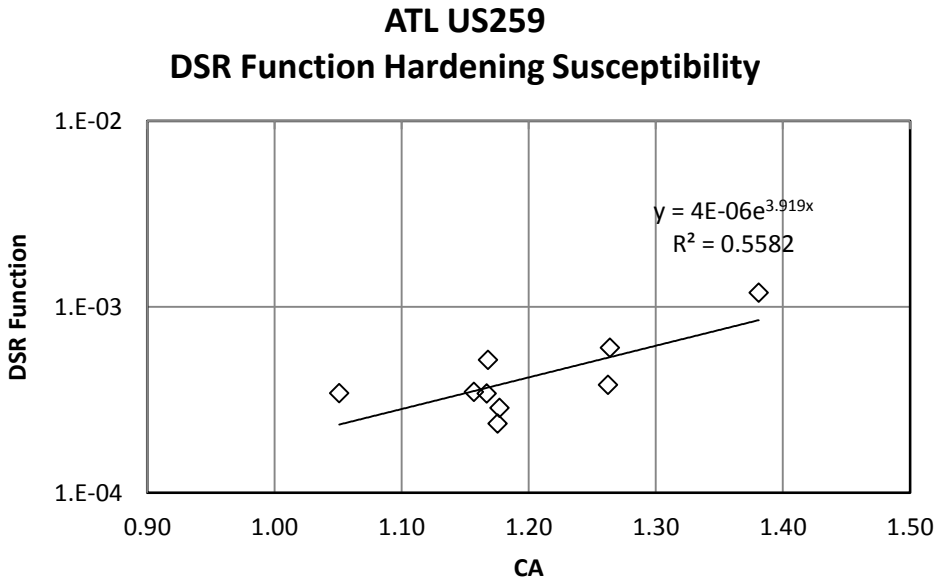
ATL US259
DSR Function Hardening Susceptibility
1.E-02
1.E-03
1.E-04
DSR Function
y = 4E-06e3.919x
R² = 0.5582
0.90
1.00
1.10
1.20
1.30
1.40
1.50
CA

Table A7. BRY SH6 Field Core (Wheel Path)

Binder: Unknown Activation Energy: 52.6 kJ/mol Cons.: 2000		η* (Poise) @60°C 0.1 rad/s	G'/(η'/G') (MPa/s) @15°C 0.005 rad/s	Carbonyl Area
1st Core (08/2008)	1st layer	100000	0.001	1.277
	2nd	45000	0.0003	1.020
	3rd	19000	0.0001	0.856
	1st to 3rd	44000	0.0003	1.051
2nd Core (12/2010)	1st to 3rd	87000	0.00072	1.178

Table A8. BRY SH6 Field Core (Shoulder)

Binder: Unknown Activation Energy: 52.6 kJ/mol Cons.: 2000		η* (Poise) @60°C 0.1 rad/s	G'/(η'/G') (MPa/s) @15°C 0.005 rad/s	Carbonyl Area
1st Core (08/2008)	1st layer	220000	0.0027	1.455
	2nd	110000	0.0011	1.224
	3rd	70000	0.0007	1.133
	1st to 3rd	119000	0.0012	1.271

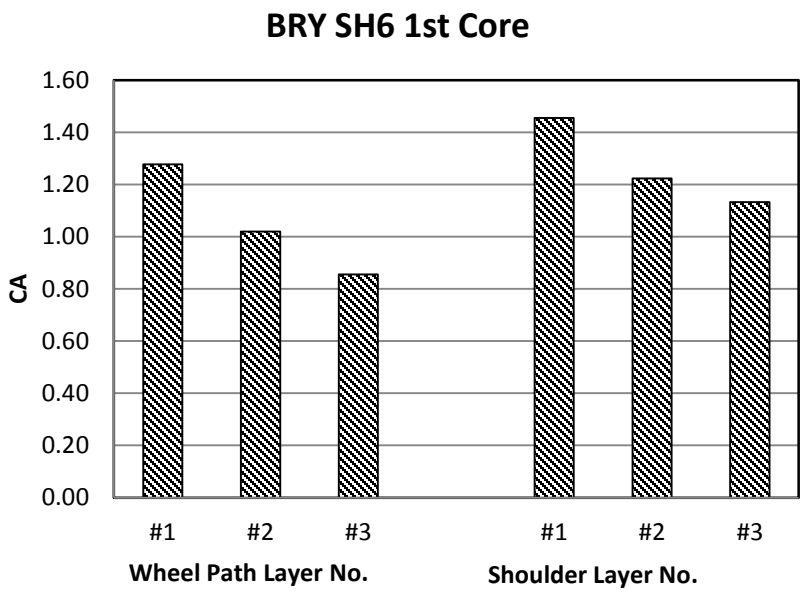
BRY SH6 1st Core
1.60
1.40
1.20
1.00
0.80
0.60
0.40
0.20
0.00
CA
#1
#2
#3
#1
#2
#3
Wheel Path Layer No.
Shoulder Layer No.

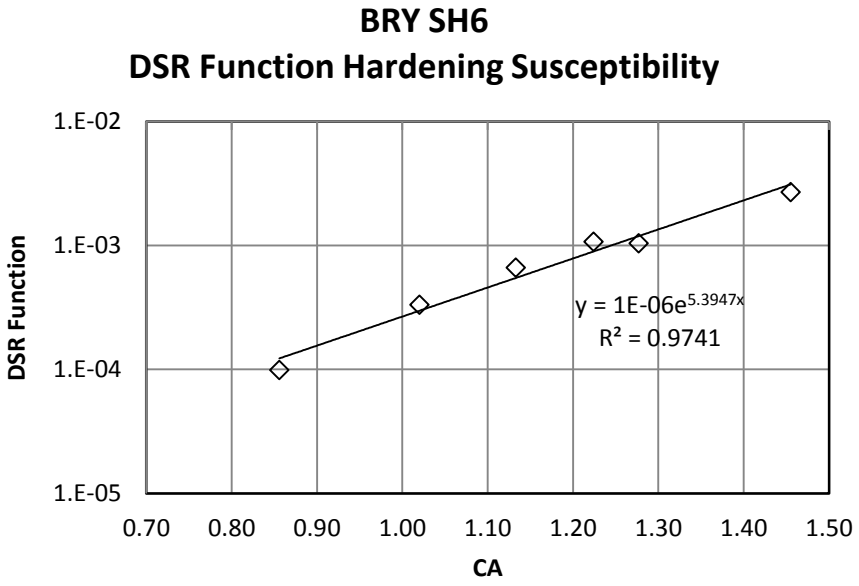
BRY SH6
DSR Function Hardening Susceptibility
1.E-02
1.E-03
1.E-04
1.E-05
DSR Function
y = 1E-06e5.3947x
R² = 0.9741
0.70
0.80
0.90
1.00
1.10
1.20
1.30
1.40
1.50
CA

Table A9. BRY US290 Field Core (Wheel Path)

Binder: Eagle PG64-22 Activation Energy: 84.8 kJ/mol Cons.: 2002		η* (Poise) @60°C 0.1 rad/s	G'/(η'/G') (MPa/s) @15°C 0.005 rad/s	Carbonyl Area
1st Core (08/2008)	1st layer	80000	0.0006	1.087
	2nd	1000000	0.0106	1.336
	3rd	1100000	0.0123	1.306
	4th	1000000	0.0128	1.441
	5th	800000	0.0159	1.404
	1st to 5th	425000	0.0045	1.269
2nd Core (12/2010)	1st to 5th	54000	0.00026	0.940

Table A10. BRY US290 Field Core (Shoulder)

Binder: Eagle PG64-22 Activation Energy: 84.8 kJ/mol Cons.: 2002		η* (Poise) @60°C 0.1 rad/s	G'/(η'/G') (MPa/s) @15°C 0.005 rad/s	Carbonyl Area
1st Core (08/2008)	1st layer	200000	0.0016	1.285
	2nd	60000	0.0003	1.039
	3rd	58000	0.0003	1.038
	4th	60000	0.0004	1.080
	1st to 4th	89000	0.0005	1.128
2nd Core (12/2010)	1st to 4th	64000	0.00033	0.996

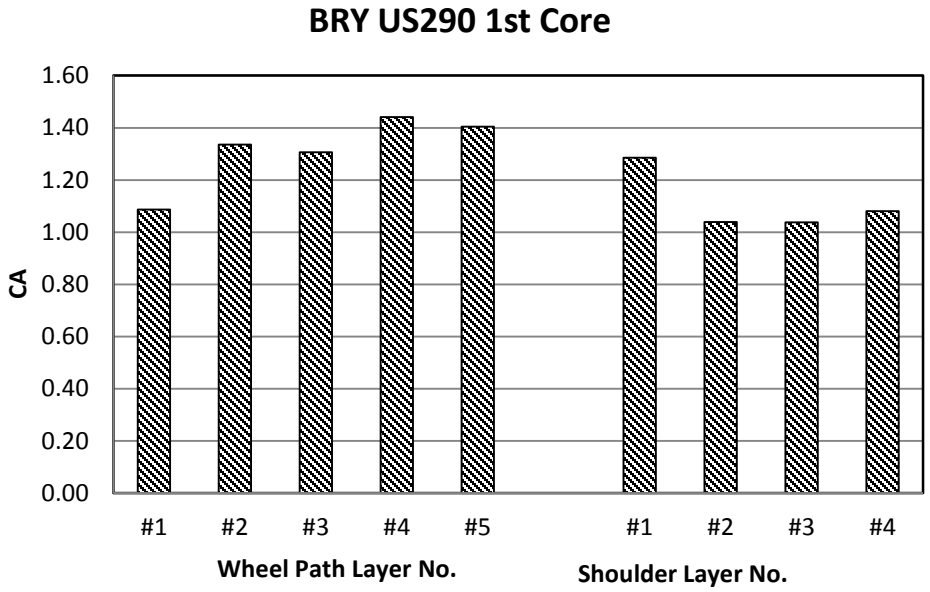
BRY US290 1st Core
1.60
1.40
1.20
1.00
0.80
0.60
0.40
0.20
0.00
CA
#1
#2
#3
#4
#5
#1
#2
#3
#4
Wheel Path Layer No.
Shoulder Layer No.

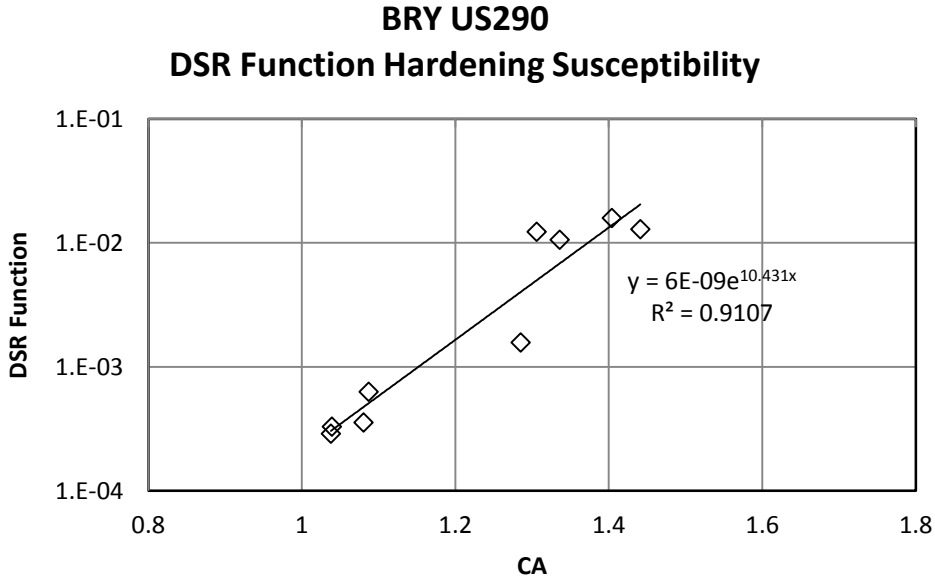
BRY US290
DSR Function Hardening Susceptibility
1.E-01
1.E-02
1.E-03
1.E-04
DSR Function
y = 6E-09e10.431x
R² = 0.9107
0.8
1
1.2
1.4
1.6
1.8
CA

Table A11. CHS US83 Field Core (Wheel Path)

Binder: SEM PG70-28 Activation Energy: 65.6 kJ/mol Cons.: 2008		η* (Poise) @60ºC 0.1 rad/s	G'/(η'/G') (MPa/s) @15ºC 0.005 rad/s	Carbonyl Area
1st Core (08/2008)	1st layer	60000	0.00013	0.968
	2nd	36000	0.00008	0.867
	3rd	31000	0.00007	0.871
	1st to 3rd	40600	0.00009	0.902
2nd Core (10/2009)	1st layer	139000	0.00023	1.129
	2nd	103000	0.00017	1.012
	3rd	86000	0.00016	1.029
	1st to 3rd	107000	0.00018	1.056
3rd Core (08/2010)	1st layer	135000	0.00023	1.097
	2nd	141000	0.00013	1.043
	3rd	112000	0.00021	0.934
	1st to 3rd	128000	0.00019	1.024
4th Core (11/2011)	1st layer	109600	0.00018	1.134
	2nd	93000	0.00015	0.971
	3rd	100000	0.00020	0.946
	1st to 3rd	100000	0.00018	1.017
2nd Core Seal coat Treated (10/2009)	Seal coat layer	20000	0.000043	1.311
	1st layer	62000	0.00011	1.034
	2nd	58000	0.000079	0.975
	3rd	64000	0.000092	0.936
	4th	45000	0.000069	0.884
	5th	56000	0.000088	1.012
	1st to 5th	58000	0.000089	0.984
3rd Core Seal coat Treated (08/2010)	Seal coat layer	45000	0.00016	1.329
	1st layer	40000	0.000079	0.990
	2nd	82000	0.00013	0.842
	3rd	57000	0.000085	0.807
	1st to 3rd	49000	0.000095	0.880
4th Core Seal coat Treated (11/2011)	Seal coat layer	37000	0.00012	1.523
	1st layer	61000	0.00012	1.052
	2nd	103000	0.00016	0.982
	3rd	103000	0.00014	0.905
	1st to 3rd	86000	0.00014	0.980

Table A12. CHS US83 Field Core (Shoulder)

Binder: SEM PG70-28 Activation Energy: 65.6 kJ/mol Cons.: 2008		η* (Poise) @60ºC 0.1 rad/s	G'/(η'/G') (MPa/s) @15ºC 0.005 rad/s	Carbonyl Area
1st Core (08/2008)	1st layer	45000	0.0001	0.924
	2nd	35000	0.00007	0.860
	3rd	35000	0.00007	0.861
	4th	36000	0.00008	0.885
	5th	35000	0.00007	0.900
	1st to 5th	38000	0.00008	0.889
2nd Core (10/2009)	1st layer	270000	0.00045	1.105
	2nd	28000	0.000084	0.937
	3rd	53000	0.000077	0.983
	4th	63000	0.000095	1.039
	5th	54000	0.000080	0.892
	1st to 5th	96000	0.00015	1.004
3rd Core (08/2010)	1st layer	80000	0.00016	0.967
	2nd	72000	0.00012	0.887
	3rd	69000	0.00010	0.894
	4th	92000	0.00018	0.897
	5th	48000	0.000076	0.878
	6th	66000	0.00012	0.925
	1st to 6th	73000	0.00013	0.917
4th Core (11/2011)	1st layer	140000	0.00025	0.983
	2nd	80000	0.00013	0.898
	3rd	71000	0.00013	0.882
	1st to 3rd	92000	0.00016	0.921
2nd Core Seal coat Treated (10/2009)	Seal coat layer	20000	0.000042	1.080
	1st layer	41000	0.000069	0.968
	2nd	48000	0.000062	0.900
	3rd	50000	0.000076	0.859
	1st to 3rd	46000	0.000069	0.909
3rd Core Seal coat Treated (08/2010)	Seal coat layer	70000	0.000098	1.313
	1st layer	61000	0.000098	0.895
	2nd	55000	0.000081	0.847
	3rd	74000	0.00011	0.919
	4th	100000	0.00017	0.914
	1st to 4th	66000	0.00010	0.886

Table A12. CHS US83 Field Core (Shoulder) (Continued)

Binder: SEM PG70-28 Activation Energy: 72.5 kJ/mol Cons.: 2008		η* (Poise) @60°C 0.1 rad/s	G'/(η'/G') (MPa/s) @15°C 0.005 rad/s	Carbonyl Area
4th Core Seal coat Treated (11/2011)	Seal coat layer	50000	0.00022	1.483
	1st layer	100000	0.00021	1.005
	2nd	33000	0.000044	0.734
	3rd	68000	0.00011	0.887
	4th	110000	0.00019	0.950
	1st to 4th	66000	0.00011	0.886

CHS US83 1st Core Wheel Path

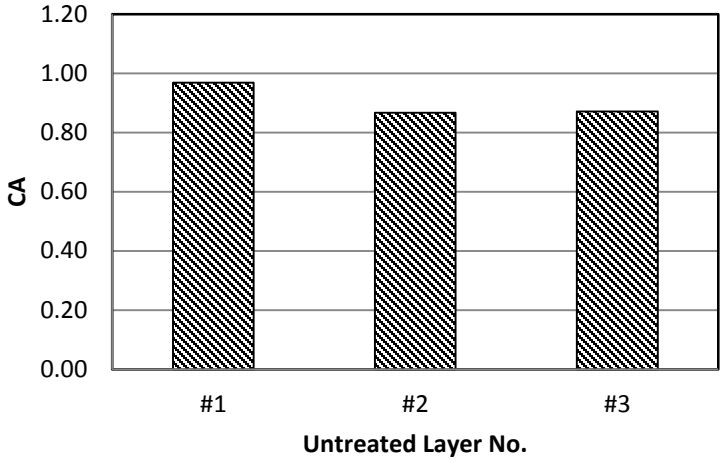

CHS US83 2nd Core Wheel Path

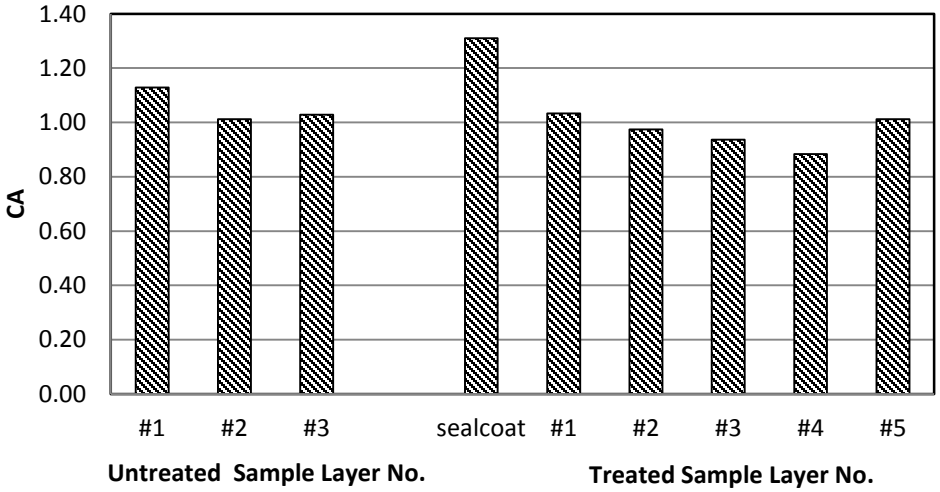

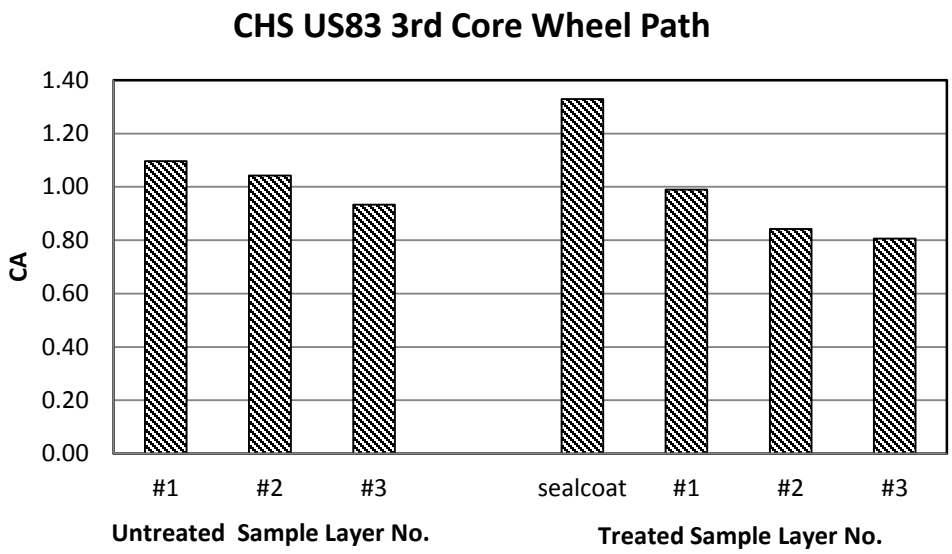
CHS US83 3rd Core Wheel Path
1.40
1.20
1.00
0.80
0.60
0.40
0.20
0.00
CA
#1
#2
#3
sealcoat
#1
#2
#3
Untreated Sample Layer No.
Treated Sample Layer No.

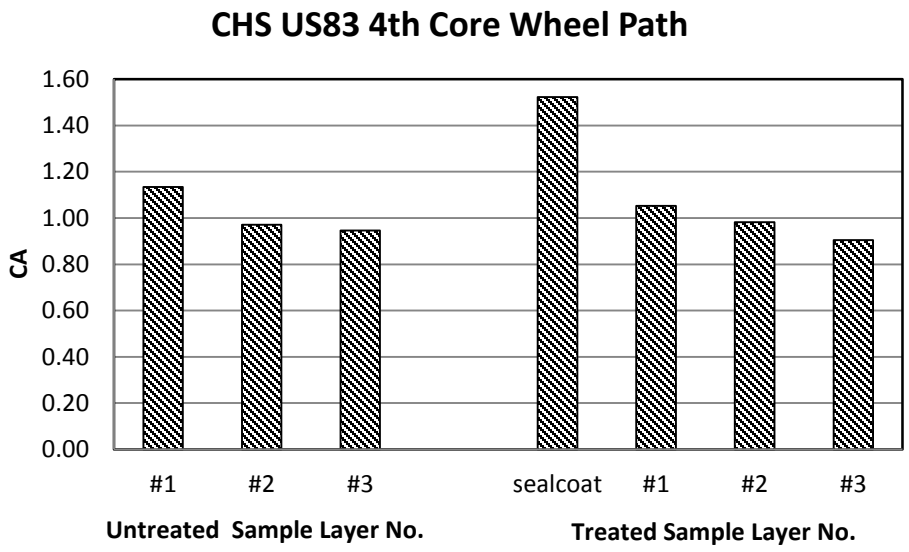
CHS US83 4th Core Wheel Path
1.60
1.40
1.20
1.00
0.80
0.60
0.40
0.20
0.00
CA
#1
#2
#3
sealcoat
#1
#2
#3
Untreated Sample Layer No.
Treated Sample Layer No.

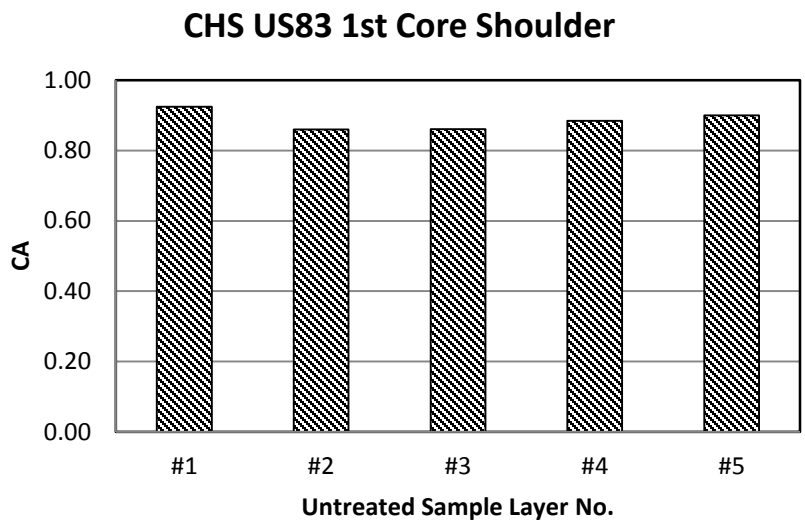
CHS US83 1st Core Shoulder
1.00
0.80
0.60
0.40
0.20
0.00
CA
#1
#2
#3
#4
#5
Untreated Sample Layer No.

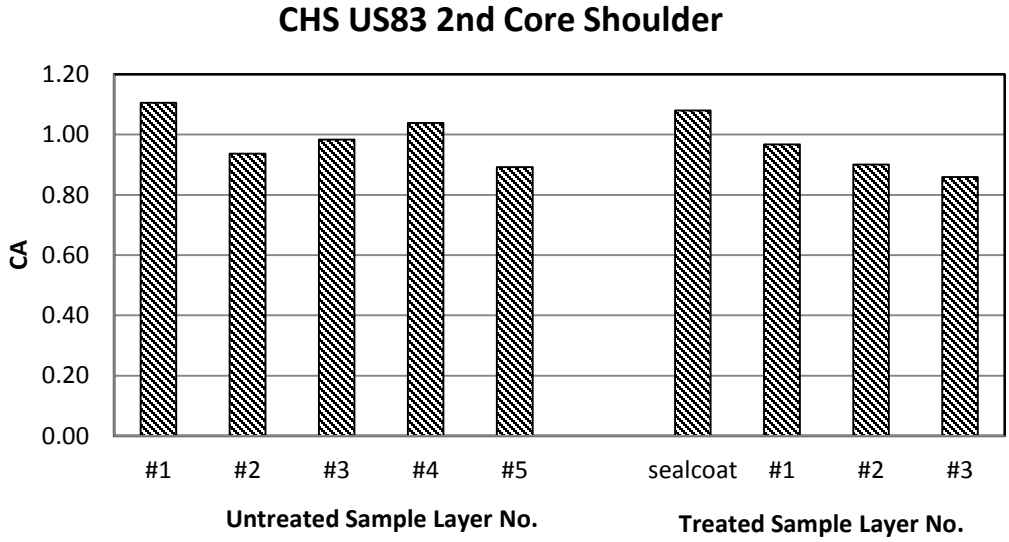
CHS US83 2nd Core Shoulder
1.20
1.00
0.80
0.60
0.40
0.20
0.00
CA
#1
#2
#3
#4
#5
sealcoat
#1
#2
#3
Untreated Sample Layer No.
Treated Sample Layer No.

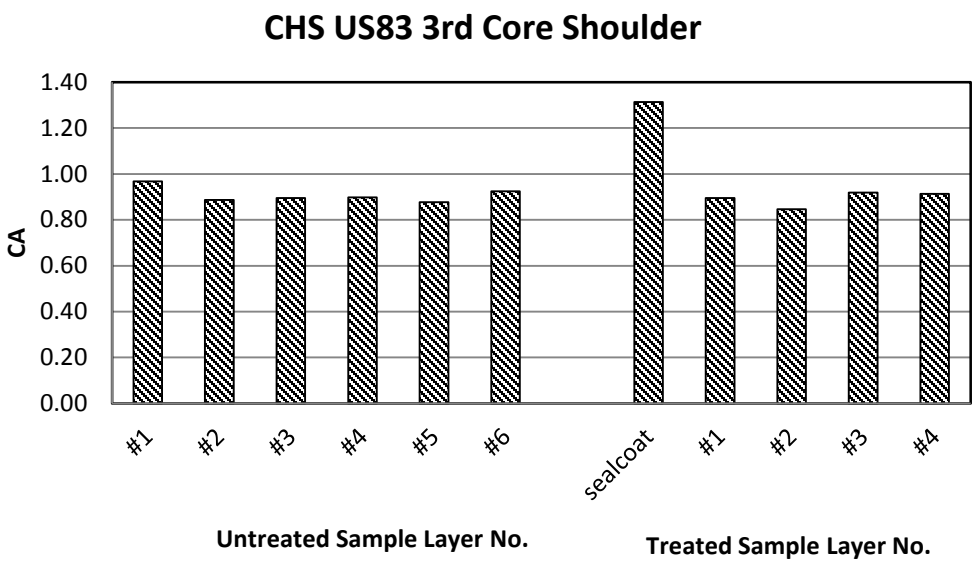
CHS US83 3rd Core Shoulder
1.40
1.20
1.00
0.80
0.60
0.40
0.20
0.00
CA
#1
#2
#3
#4
#5
#6
sealcoat
#1
#2
#3
#4
Untreated Sample Layer No.
Treated Sample Layer No.

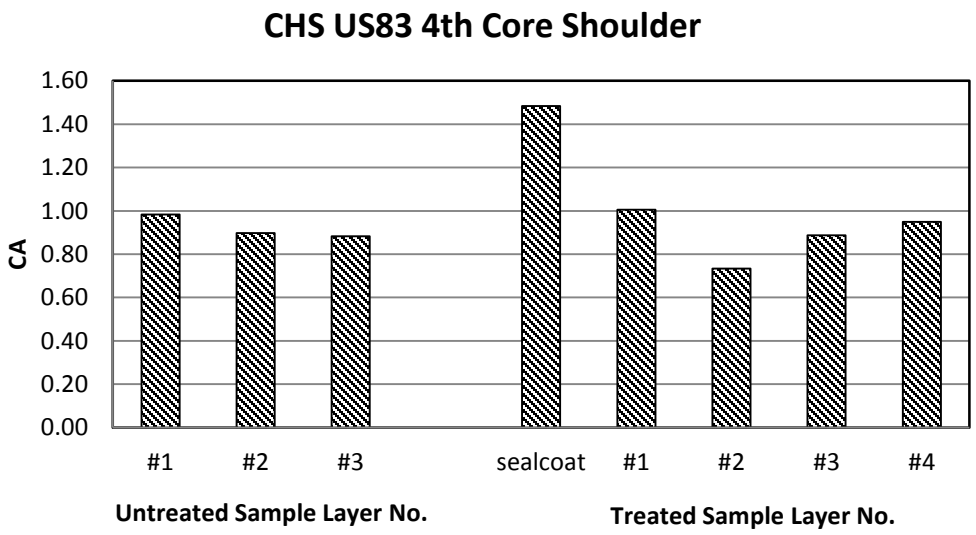
CHS US83 4th Core Shoulder
1.60
1.40
1.20
1.00
0.80
0.60
0.40
0.20
0.00
CA
#1
#2
#3
sealcoat
#1
#2
#3
#4
Untreated Sample Layer No.
Treated Sample Layer No.

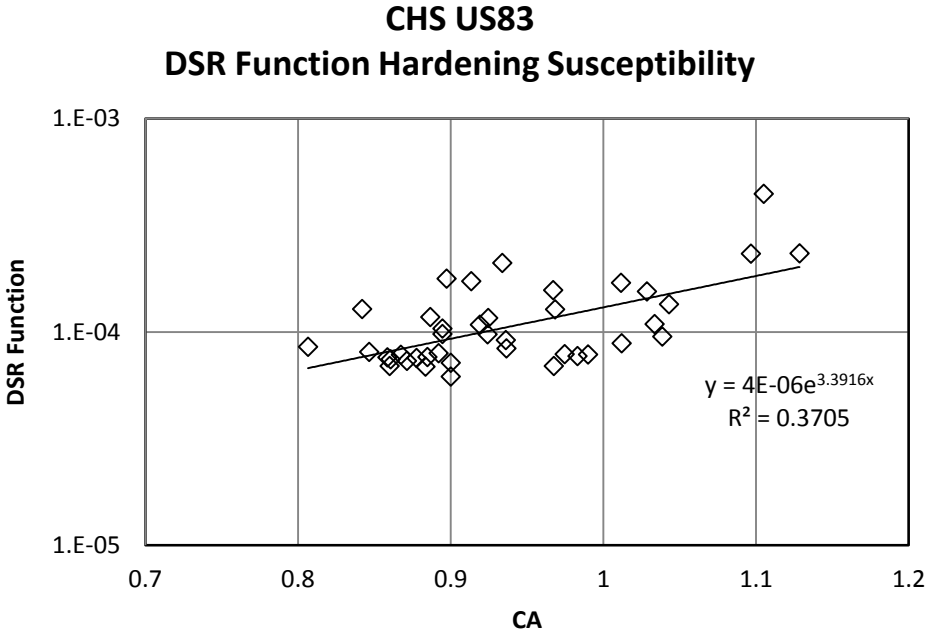
CHS US83
DSR Function Hardening Susceptibility
1.E-03
1.E-04
1.E-05
DSR Function
0.7
0.8
0.9
1
1.1
1.2
CA
y = 4E-06e3.3916x
R² = 0.3705

Table A13. LBB US82 Field Core (Wheel Path)

Binder: Alon PG76-22 Activation Energy: 69.8 kJ/mol Cons.: 2008		η* (Poise) @60ºC 0.1 rad/s	G'/(η'/G') (MPa/s) @15ºC 0.005 rad/s	Carbonyl Area
1st Core (08/2008)	1st layer	80000	0.0002	0.879
	2nd	65000	0.0002	0.830
	3rd	70000	0.0002	0.823
	4th	65000	0.0002	0.831
	1st to 4th	70000	0.0002	0.845
2nd Core (12/2009)	1st layer	230000	0.00070	1.201
	2nd	200000	0.00050	1.122
	3rd	170000	0.00045	1.193
	1st to 3rd	190000	0.00053	1.172
3rd Core (08/2010)	1st layer	400000	0.0019	1.269
	2nd	170000	0.00054	1.092
	3rd	230000	0.00075	1.108
	4th	240000	0.00087	1.062
	1st to 4th	250000	0.00090	1.148
2nd Core Seal coat Treated (12/2009)	Seal coat layer	19000	0.000042	0.994
	1st layer	62000	0.00011	0.946
	2nd	160000	0.00034	1.026
	3rd	110000	0.00023	0.958
	4th	150000	0.00033	0.978
	1st to 4th	110000	0.00023	0.980
3rd Core Seal coat Treated (08/2010)	Seal coat layer	30000	0.000082	1.042
	1st layer	78000	0.00016	0.856
	2nd	100000	0.00019	0.853
	3rd	110000	0.00021	0.873
	4th	120000	0.00022	0.837
	1st to 4th	100000	0.00020	0.854

Table A14. LBB US82 Field Core (Shoulder)

Binder: Alon PG76-22 Activation Energy: 69.8 kJ/mol Cons.: 2008		η* (Poise) @60ºC 0.1 rad/s	G'/(η'/G') (MPa/s) @15ºC 0.005 rad/s	Carbonyl Area
1st Core (08/2008)	1st layer	70000	0.0002	0.876
	2nd	52000	0.0001	0.771
	3rd	60000	0.0001	0.798
	1st to 3rd	60000	0.0001	0.815
2nd Core (12/2009)	1st layer	260000	0.00079	1.218
	2nd	130000	0.00028	1.015
	3rd	150000	0.00031	1.026
	4th	170000	0.00044	1.109
	1st to 4th	180000	0.00043	1.100
3rd Core (08/2010)	1st layer	Too high to measure	0.00160	1.137
	2nd	130000	0.00030	0.969
	3rd	210000	0.00059	0.992
	4th	300000	0.0010	1.081
	1st to 4th	-	0.00073	1.047
2nd Core Seal coat Treated (12/2009)	Seal coat layer	20000	0.000046	1.016
	1st layer	100000	0.00022	0.951
	2nd	69000	0.000078	0.751
	3rd	120000	0.00015	0.823
	4th	150000	0.00025	0.944
	1st to 4th	100000	0.00016	0.887
3rd Core Seal coat Treated (08/2010)	Seal coat layer	25000	0.000082	1.069
	1st layer	67000	0.00013	0.930
	2nd	95000	0.00017	0.884
	3rd	120000	0.00027	0.893
	4th	180000	0.00051	0.943
	1st to 4th	110000	0.00023	0.910

LBB US82 1st Core Wheel Path

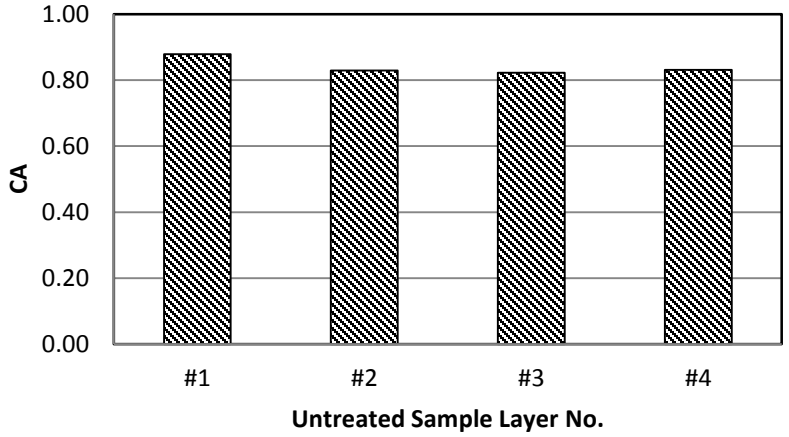

LBB US82 2nd Core Wheel Path

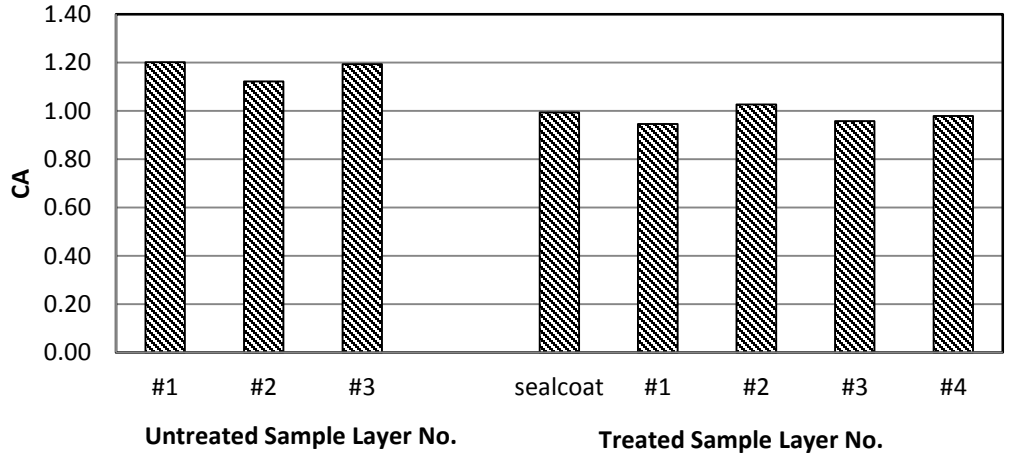

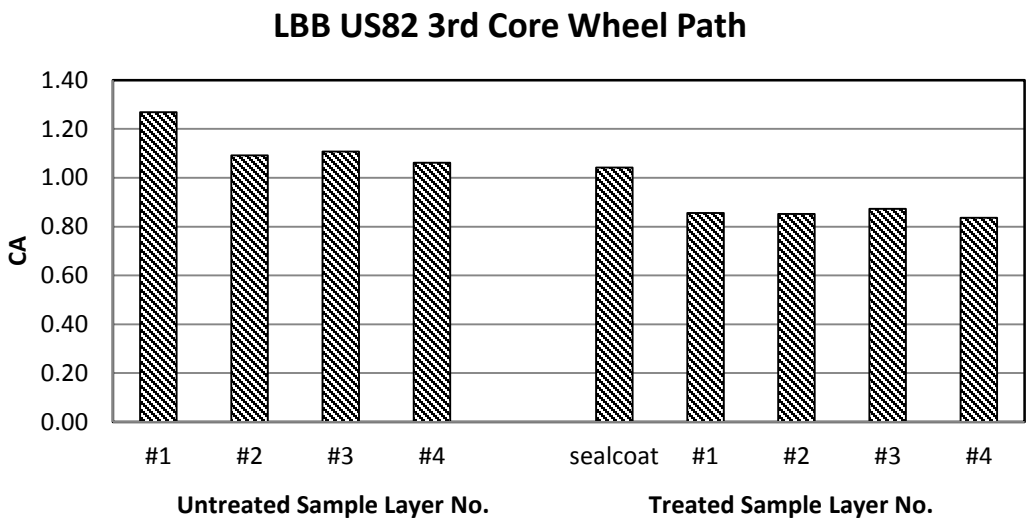
LBB US82 3rd Core Wheel Path
1.40
1.20
1.00
0.80
0.60
0.40
0.20
0.00
CA
#1
#2
#3
#4
sealcoat
#1
#2
#3
#4
Untreated Sample Layer No.
Treated Sample Layer No.

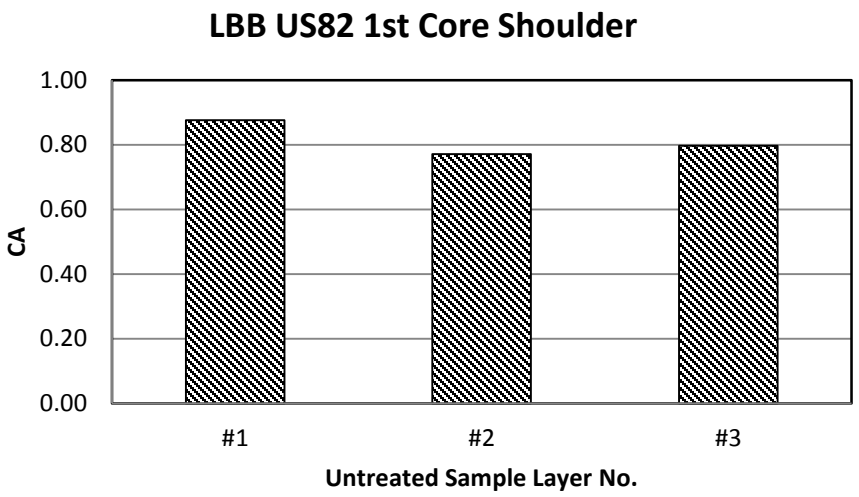
LBB US82 1st Core Shoulder
1.00
0.80
0.60
0.40
0.20
0.00
CA
#1
#2
#3
Untreated Sample Layer No.

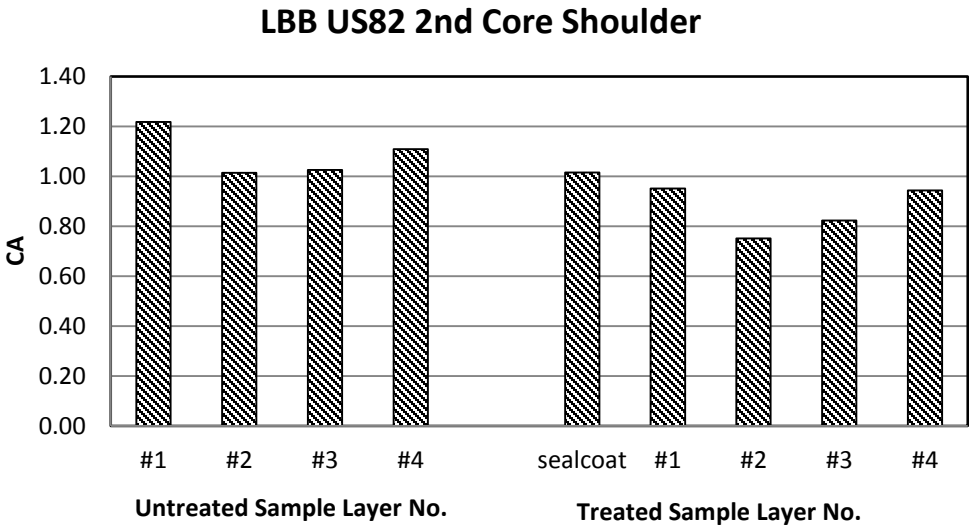
LBB US82 2nd Core Shoulder
1.40
1.20
1.00
0.80
0.60
0.40
0.20
0.00
CA
#1
#2
#3
#4
sealcoat
#1
#2
#3
#4
Untreated Sample Layer No.
Treated Sample Layer No.

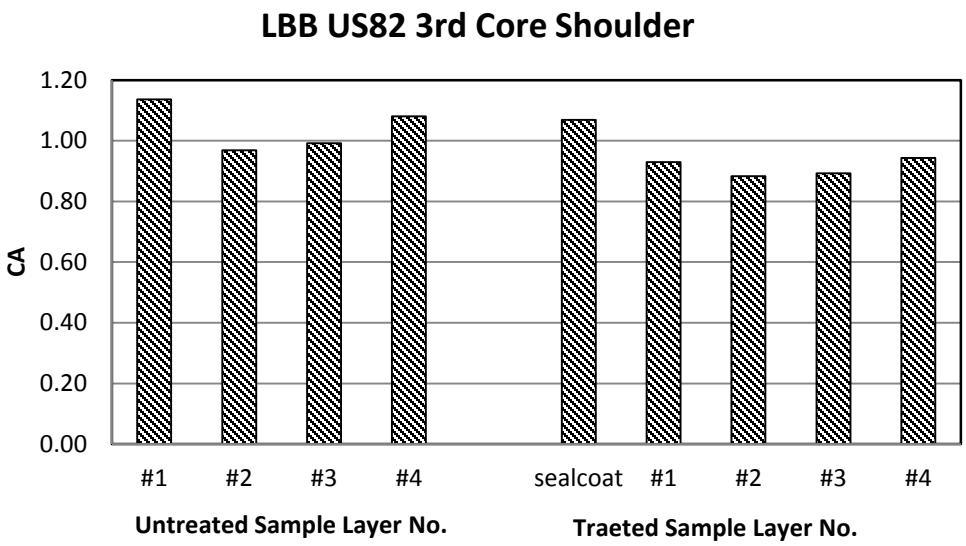
LBB US82 3rd Core Shoulder
1.20
1.00
0.80
0.60
0.40
0.20
0.00
CA
#1
#2
#3
#4
sealcoat
#1
#2
#3
#4
Untreated Sample Layer No.
Traeted Sample Layer No.

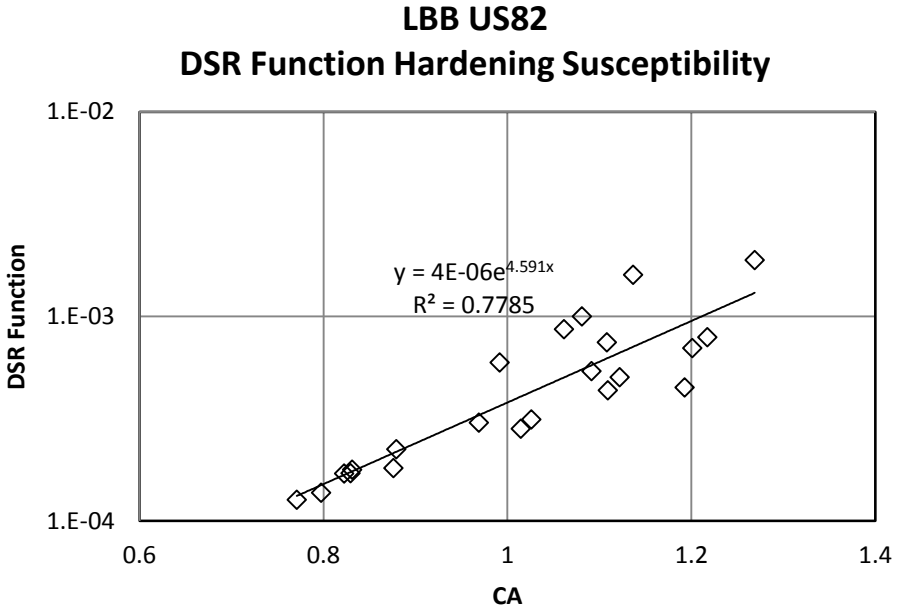
LBB US82
DSR Function Hardening Susceptibility
1.E-02
1.E-03
1.E-04
DSR Function
y = 4E-06e4.591x
R² = 0.7785
0.6
0.8
1
1.2
1.4
CA

Table A15. LFK US69 Field Core (Wheel Path)

Binder: Martin PG70-22 Activation Energy: 64.3 kJ/mol Cons.: 2003		η* (Poise) @60°C 0.1 rad/s	G'/(η'/G') (MPa/s) @15°C 0.005 rad/s	Carbonyl Area
1st Core (06/2008)	1st layer	Too high to measure	Too high to measure	1.491
	2nd	200000	0.0015	1.180
	3rd	160000	0.0011	1.179
	1st to 3rd	-	-	1.283

Table A16. LFK US69 Field Core (Shoulder)

Binder: Martin PG70-22 Activation Energy: 64.3 kJ/mol Cons.: 2003		η* (Poise) @60°C 0.1 rad/s	G'/(η'/G') (MPa/s) @15°C 0.005 rad/s	Carbonyl Area
1st Core (06/2008)	1st layer	500000	0.002	1.336
	2nd	120000	0.00057	1.134
	1st to 2nd	240000	0.0011	1.235

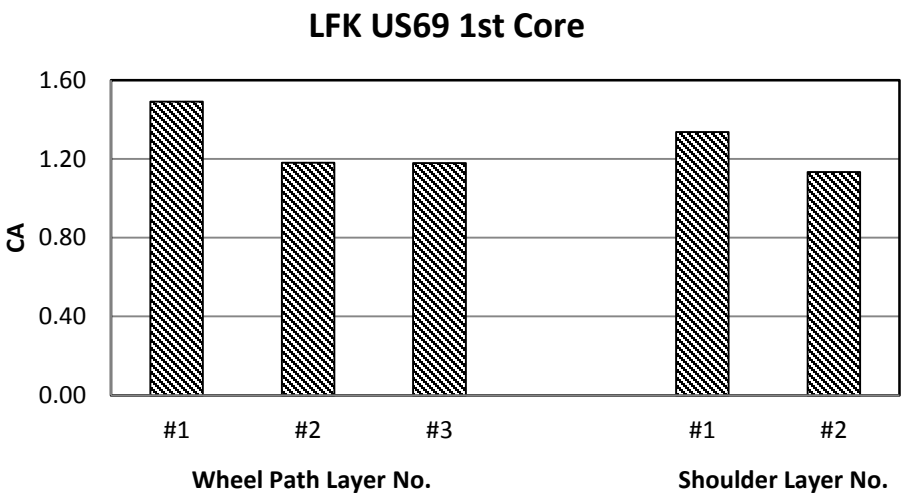
LFK US69 1st Core
1.60
1.20
0.80
0.40
0.00
CA
#1
#2
#3
#1
#2
Wheel Path Layer No.
Shoulder Layer No.

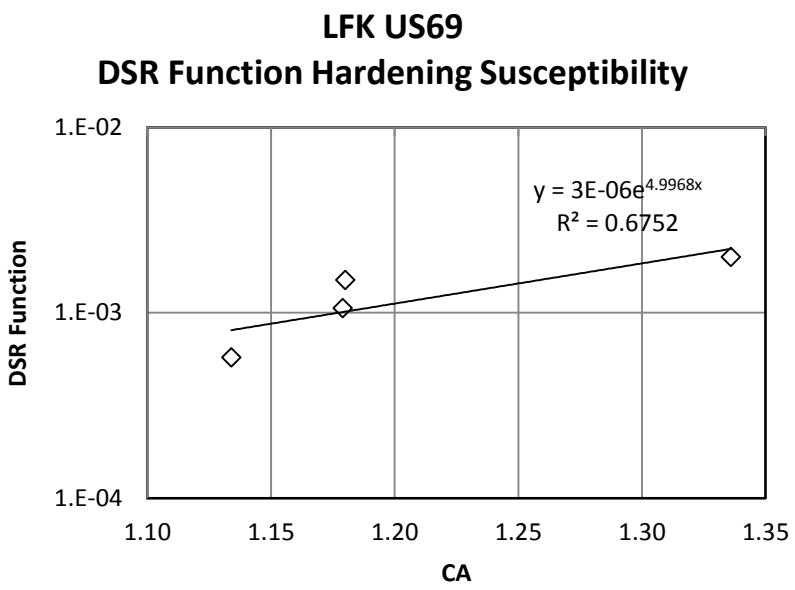
LFK US69
DSR Function Hardening Susceptibility
1.E-02
1.E-03
1.E-04
DSR Function
y = 3E-06e4.9968x
R² = 0.6752
1.10
1.15
1.20
1.25
1.30
1.35
CA

Table A17. LRD FM649 Field Core (Wheel Path)

Binder: Valero-Corpus PG76-22 Activation Energy: 80.8 kJ/mol Cons.: 2006		η* (Poise) @60°C 0.1 rad/s	G'/(η'/G') (MPa/s) @15°C 0.005 rad/s	Carbonyl Area
1st Core (06/2008)	1st layer	500000	0.0015	1.221
	2nd	220000	0.0009	1.093
	3rd	200000	0.0008	1.147
	1st to 3rd	280000	0.001	1.154

Table A18. LRD FM649 Field Core (Shoulder)

Binder: Valero-Corpus PG76-22 Activation Energy: 80.8 kJ/mol Cons.: 2006		η* (Poise) @60°C 0.1 rad/s	G'/(η'/G') (MPa/s) @15°C 0.005 rad/s	Carbonyl Area
1st Core (06/2008)	1st layer	520000	0.0019	1.245
	2nd	200000	0.0007	1.056
	3rd	160000	0.0006	1.078
	1st to 3rd	255000	0.0009	1.126
2nd Core (02/2010)	1st to 3rd	180000	0.00068	1.096

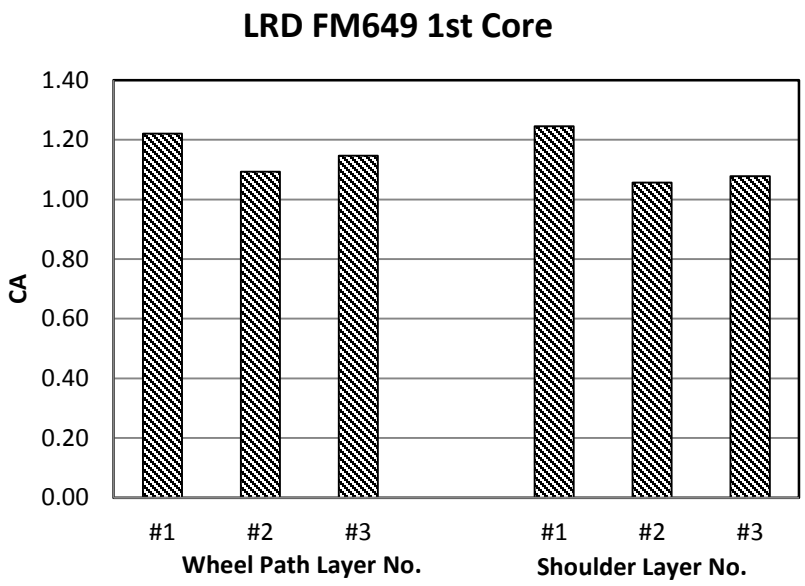
LRD FM649 1st Core
1.40
1.20
1.00
0.80
0.60
0.40
0.20
0.00
CA
#1
#2
#3
#1
#2
#3
Wheel Path Layer No.
Shoulder Layer No.

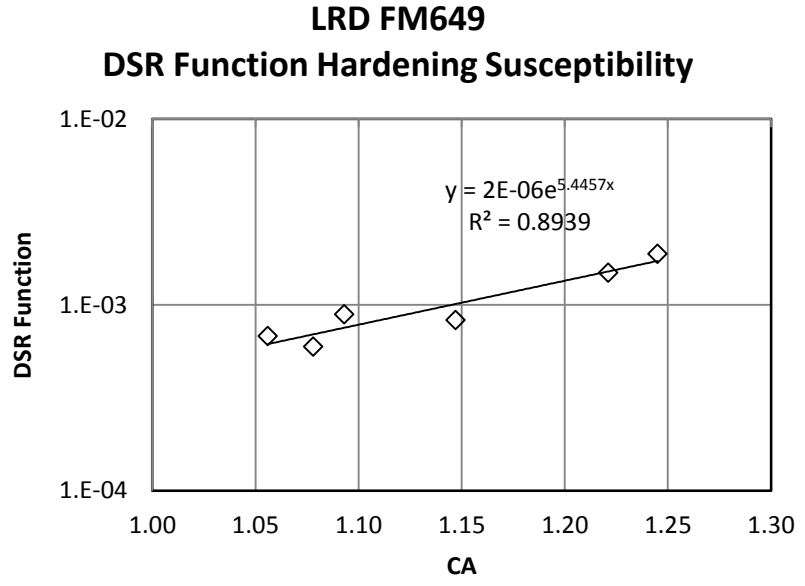
LRD FM649
DSR Function Hardening Susceptibility
1.E-02
1.E-03
1.E-04
DSR Function
y = 2E-06e5.4457x
R² = 0.8939
1.00
1.05
1.10
1.15
1.20
1.25
1.30
CA

Table A19. LRD04 IH35 #3 Field Core (Shoulder)

Binder: Valero-Corpus PG76-22 Activation Energy: 72.9 kJ/mol Cons.: 2007		η* (Poise) @60°C 0.1 rad/s	G'/(η'/G') (MPa/s) @15°C 0.005 rad/s	Carbonyl Area
1st Core (06/2008)	1st layer	100000	0.00028	0.817
	2nd	80000	0.00027	0.820
	3rd	80000	0.00023	0.808
	4th	80000	0.00019	0.862
	5th	150000	0.00035	0.842
	6th	70000	0.00024	0.892
	1st to 6th	90000	0.00027	0.829
2nd Core (12/2010)	1st to 6th	56000	0.00014	0.631

Table A20. LRD04 IH35 #5 Field Core (Shoulder)

Binder: Valero-Corpus PG70-22 Activation Energy: 103.8 kJ/mol (Original Binder) Cons.: 2007		η* (Poise) @60°C 0.1 rad/s	G'/(η'/G') (MPa/s) @15°C 0.005 rad/s	Carbonyl Area
1st Core (06/2008)	1st layer	30000	0.000092	0.764
	2nd	31000	0.000097	0.733
	1st to 2nd	30500	0.000093	0.749

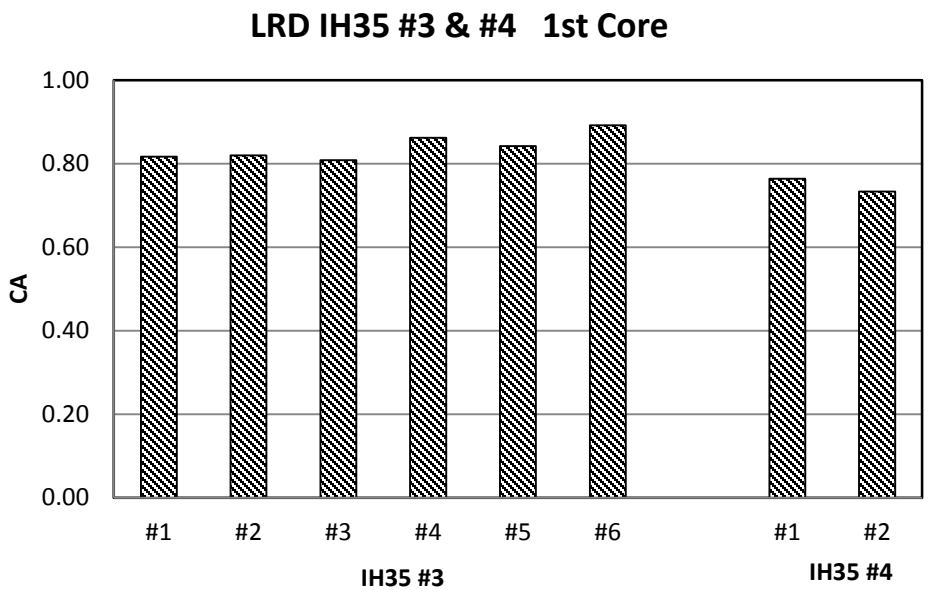
LRD IH35 #3 & #4 1st Core
1.00
0.80
0.60
0.40
0.20
0.00
CA
#1
#2
#3
#4
#5
#6
#1
#2
IH35 #3
IH35 #4

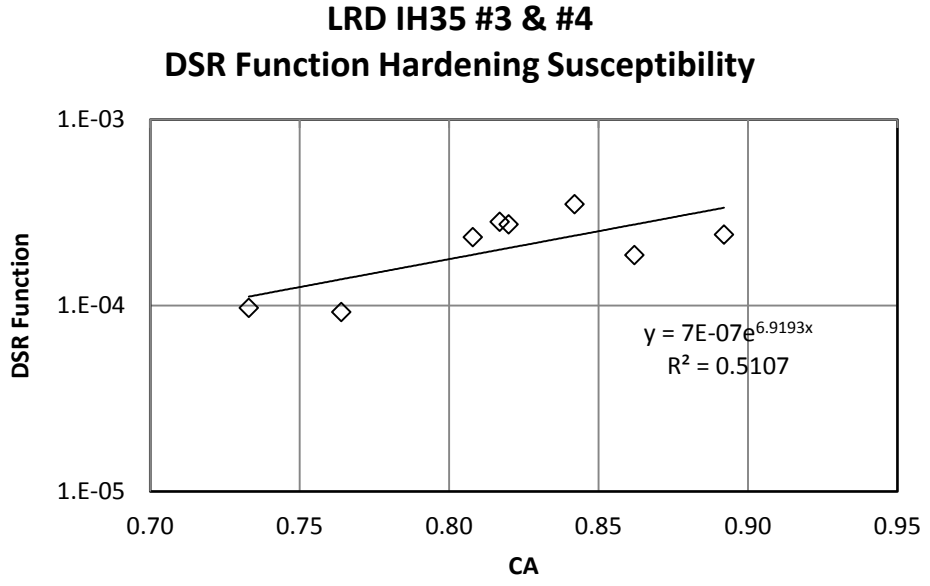
LRD IH35 #3 & #4
DSR Function Hardening Susceptibility
1.E-03
1.E-04
1.E-05
DSR Function
y = 7E-07e6.9193x
R² = 0.5107
0.70
0.75
0.80
0.85
0.90
0.95
CA

Table A21. LRD US277 Field Core (Wheel Path)

Binder: Valero-Corpus PG70-22 Activation Energy: 83.2 kJ/mol Cons.: 2008		η* (Poise) @60°C 0.1 rad/s	G'/(η'/G') (MPa/s) @15°C 0.005 rad/s	Carbonyl Area
1st Core (07/2008)	1st layer	82000	0.0003	0.936
	2nd	100000	0.0003	0.937
	3rd	120000	0.0004	0.971
	4th	100000	0.0003	0.954
	5th	80000	0.0003	0.930
	1st to 5th	93000	0.0003	0.942
2nd Core (12/2009)	1st layer	160000	0.00080	1.206
	2nd	150000	0.00042	1.004
	3rd	120000	0.00032	0.970
	4th	37000	0.00014	0.886
	1st to 4th	120000	0.00042	1.046
3rd Core (12/2010)	1st layer	320000	0.00091	1.116
	2nd	150000	0.00043	1.013
	3rd	230000	0.00068	1.104
	4th	140000	0.00045	1.079
	1st to 4th	200000	0.00060	1.073
4th Core (01/2012)	1st layer	140000	0.00046	1.135
	2nd	200000	0.00062	1.026
	3rd	280000	0.00093	1.175
	4th	130000	0.00047	1.053
	1st to 4th	170000	0.00057	1.091
2nd Core Seal coat Treated (12/2009)	Seal coat layer	Too high to measure	0.0030	1.218
	1st layer	170000	0.00047	1.087
	2nd	160000	0.00051	1.047
	3rd	160000	0.00047	1.081
	4th	140000	0.00043	1.051
	5th	83000	0.00029	0.932
	1st to 5th	150000	0.00045	1.052

Table A21. LRD US277 Field Core (Wheel Path) (Continued)

Binder: Valero-Corpus PG70-22 Activation Energy: 83.2 kJ/mol Cons.: 2008		η* (Poise) @60°C 0.1 rad/s	G'/(η'/G') (MPa/s) @15°C 0.005 rad/s	Carbonyl Area
3rd Core Seal coat Treated (12/2010)	Seal coat layer	Too high to measure	0.0027	1.541
	1st layer	110000	0.00037	1.024
	2nd	170000	0.00057	1.086
	3rd	140000	0.00046	1.109
	4th	190000	0.00067	1.143
	5th	72000	0.00030	0.998
4th Core Seal coat Treated (01/2012)	Seal coat and 1st layer	250000	0.00081	1.226
	2nd	140000	0.00047	1.043
	3rd	170000	0.00066	1.050
	1st to 3rd	180000	0.00063	1.106

Table A22. LRD US277 Field Core (Shoulder)

Binder: Valero-Corpus PG70-22 Activation Energy: 83.2 kJ/mol Cons.: 2008		η* (Poise) @60°C 0.1 rad/s	G'/(η'/G') (MPa/s) @15°C 0.005 rad/s	Carbonyl Area
1st Core (07/2008)	1st layer	120000	0.0005	1.019
	2nd	85000	0.0004	0.897
	3rd	100000	0.0003	0.894
	4th	100000	0.0004	0.923
	5th	80000	0.0003	0.918
	1st to 5th	98000	0.0004	0.942
2nd Core (12/2009)	1st layer	Too high to measure	0.00087	1.218
	2nd	170000	0.00050	0.959
	3rd	190000	0.00061	0.971
	4th	200000	0.00054	0.949
	5th	160000	0.00047	1.008
	1st to 5th	-	0.00062	1.051
3rd Core (12/2010)	1st layer	310000	0.00098	1.211
	2nd	160000	0.00055	1.037
	3rd	200000	0.00069	1.058
	4th	82000	0.00041	1.037
	1st to 4th	180000	0.00066	1.098
4th Core (01/2012)	1st layer	340000	0.00104	1.211
	2nd	250000	0.00089	1.037
	3rd	250000	0.00087	1.099
	1st to 3rd	280000	0.00093	1.115

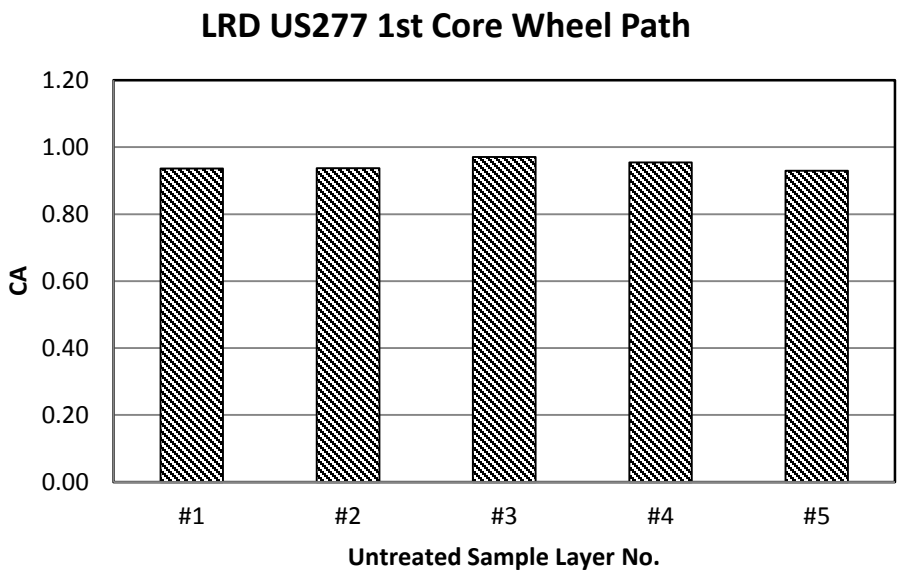
LRD US277 1st Core Wheel Path
1.20
1.00
0.80
0.60
0.40
0.20
0.00
CA
#1
#2
#3
#4
#5
Untreated Sample Layer No.

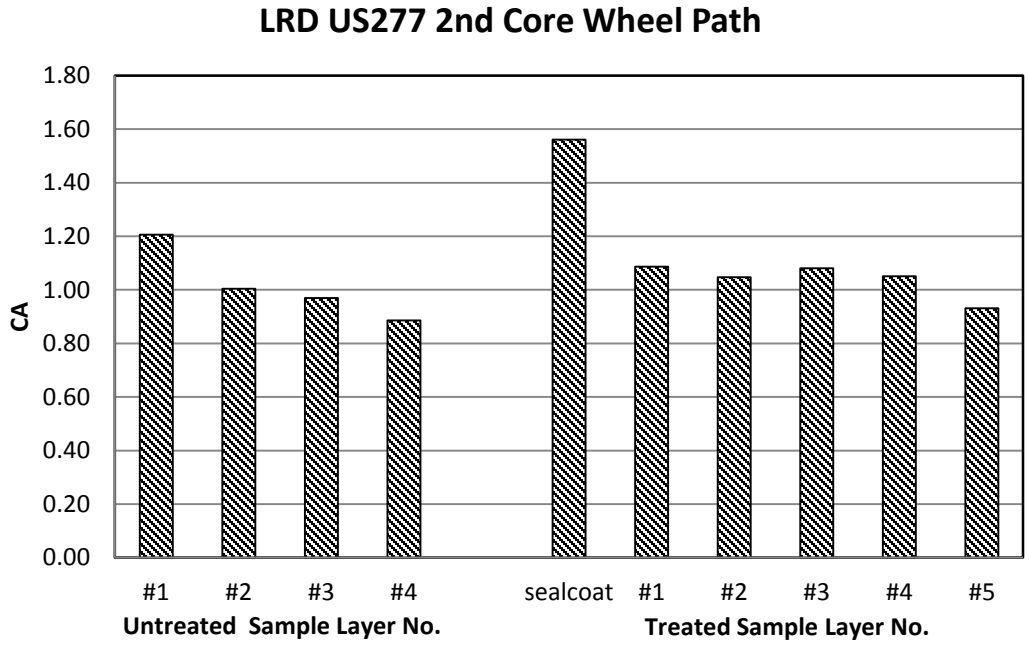
LRD US277 2nd Core Wheel Path
1.80
1.60
1.40
1.20
1.00
0.80
0.60
0.40
0.20
0.00
CA
#1
#2
#3
#4
sealcoat
#1
#2
#3
#4
#5
Untreated Sample Layer No.
Treated Sample Layer No.

LRD US277 3rd Core Wheel Path

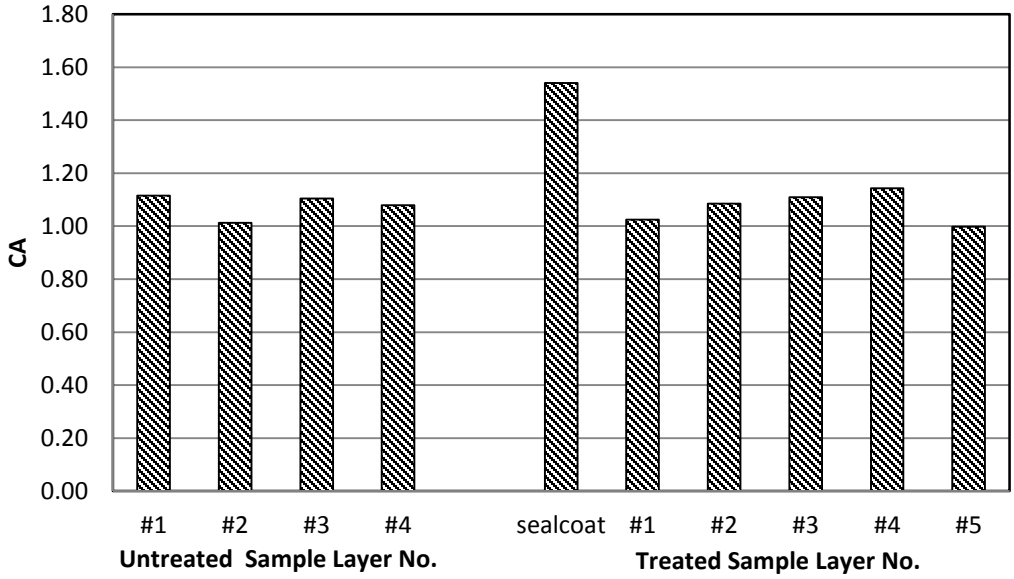

LRD US277 4th Core Wheel Path

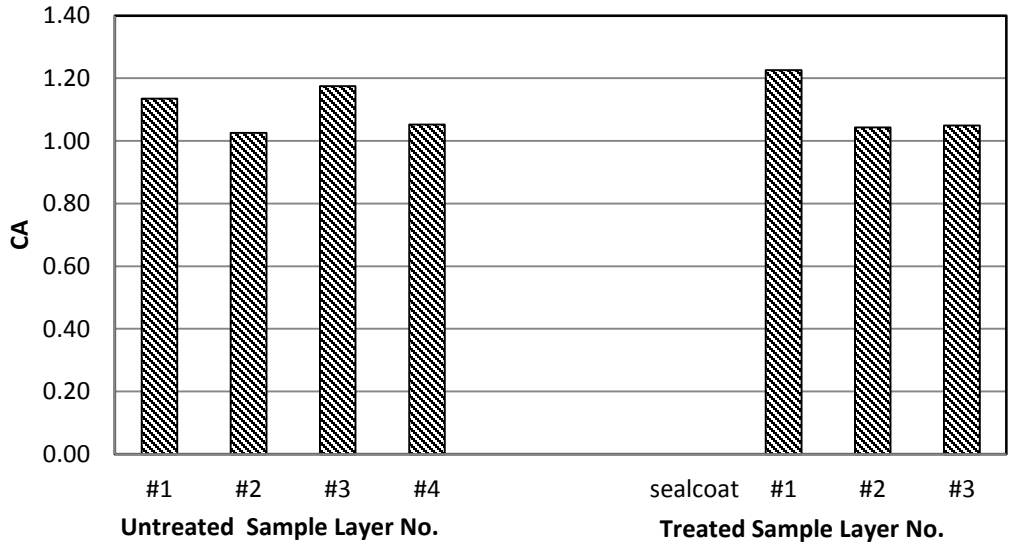

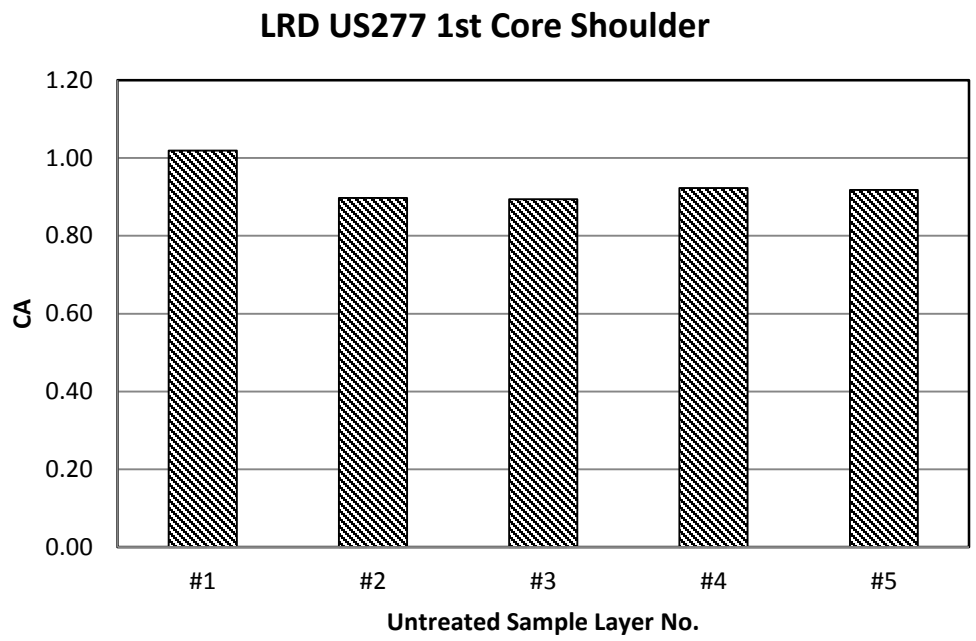
LRD US277 1st Core Shoulder
1.20
1.00
0.80
0.60
0.40
0.20
0.00
CA
#1
#2
#3
#4
#5
Untreated Sample Layer No.

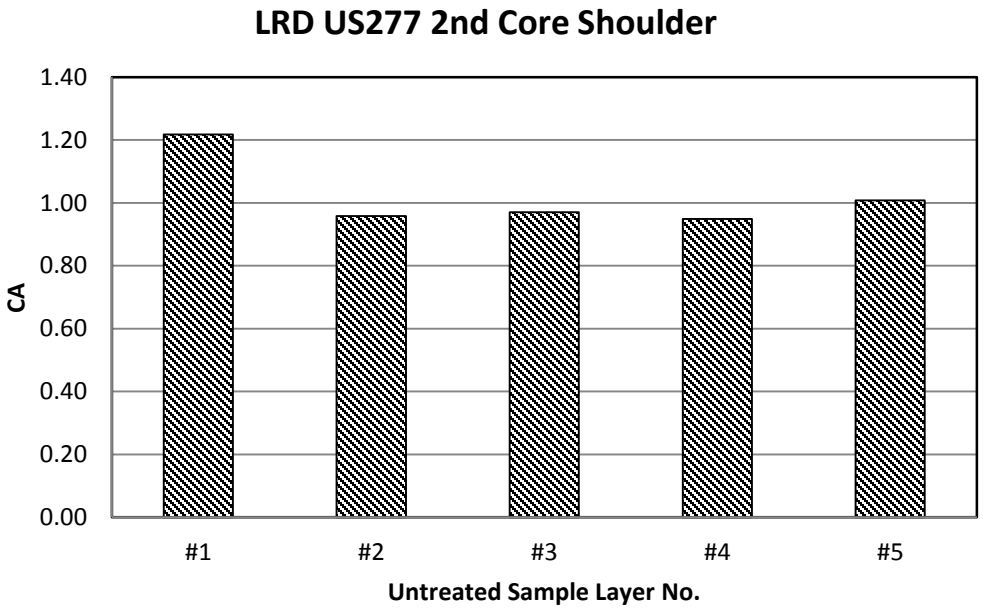
LRD US277 2nd Core Shoulder
1.40
1.20
1.00
0.80
0.60
0.40
0.20
0.00
CA
#1
#2
#3
#4
#5
Untreated Sample Layer No.

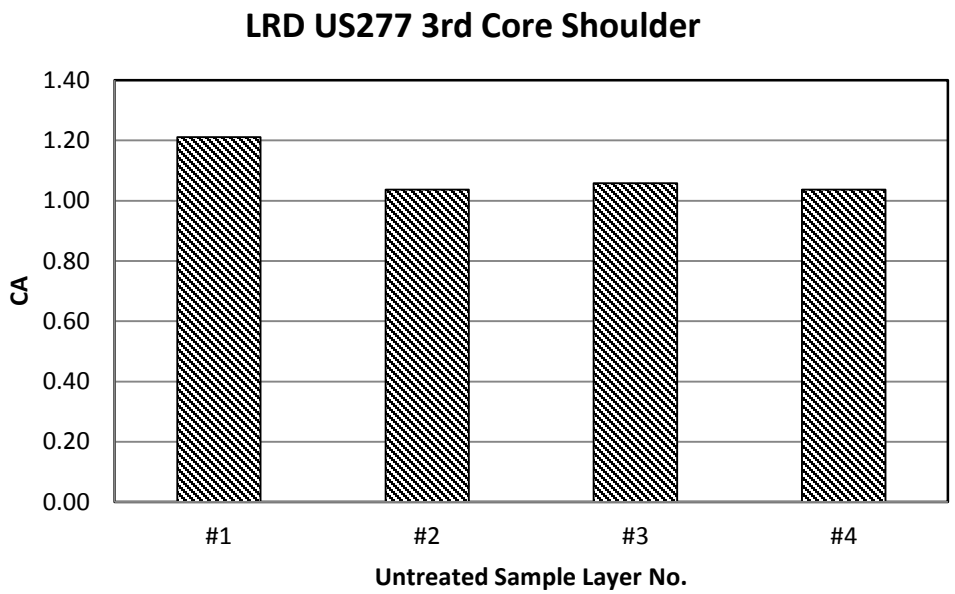
LRD US277 3rd Core Shoulder
1.40
1.20
1.00
0.80
0.60
0.40
0.20
0.00
CA
#1
#2
#3
#4
Untreated Sample Layer No.

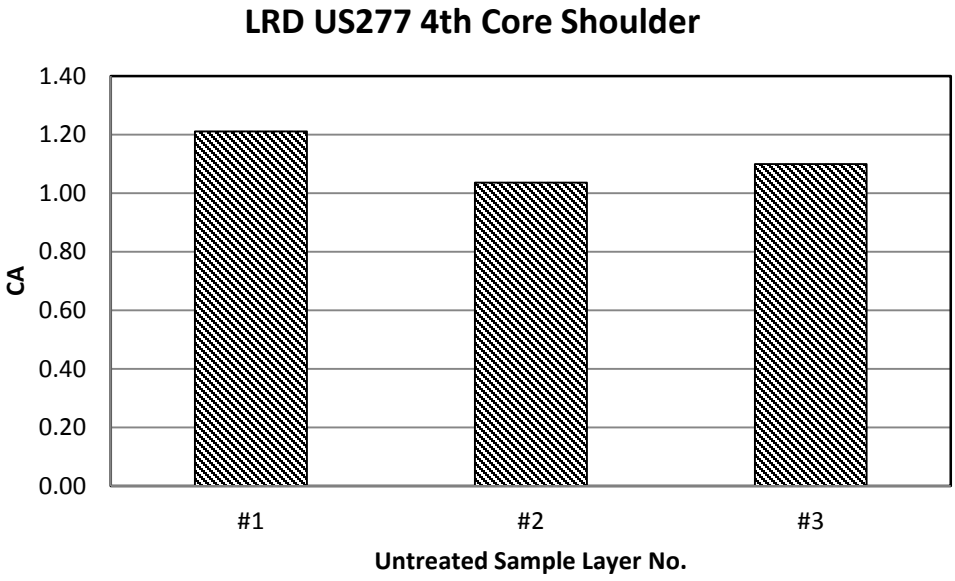
LRD US277 4th Core Shoulder
1.40
1.20
1.00
0.80
0.60
0.40
0.20
0.00
CA
#1
#2
#3
Untreated Sample Layer No.

LRD US277
DSR Function Hardening Susceptibility

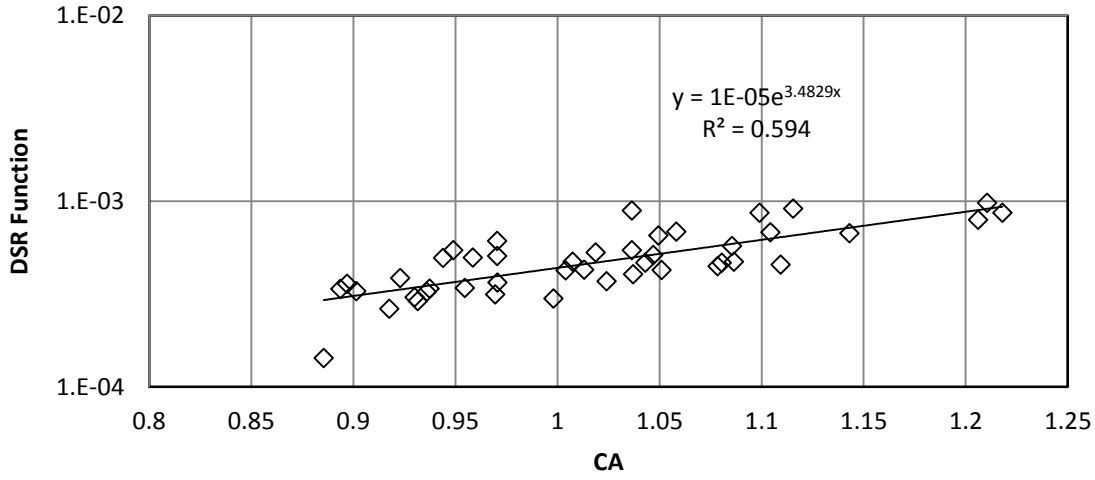

Table A23. MnRoad Field Core

Binder: Unknown Activation Energy: 69.5 kJ/mol Cons.: 1992		η* (Poise) @60ºC 0.1 rad/s	G'/(η'/G') (MPa/s) @15ºC 0.005 rad/s	Carbonyl Area
1st Core (Wheel Path) (11/2008)	1st layer	40000	0.00030	1.513
	2nd	20000	0.00012	1.294
	3rd	11000	0.000054	1.246
	4th	11000	0.000052	1.105
	5th	9000	0.000038	1.142
	6th	13000	0.000072	1.168
	7th	17000	0.00011	1.382
	8th	22000	0.00016	1.378
	9th	27000	0.00021	1.347
	1st to 9th	23000	0.00015	1.286
2nd Core (Wheel Path) (2010)	1st layer	30000	0.000204	1.377
	2nd	12000	0.0000537	1.044
	3rd	6600	0.0000237	0.901
	4th	8600	0.0000355	1.027
	5th	23000	0.000147	1.157
	6th	27000	0.000201	1.044
	7th	120000	0.00173	1.793
	1st to 7th	32400	0.00034	1.192
2nd Core (Shoulder) (2010)	1st layer	40000	0.000307	1.573
	2nd	21000	0.000125	1.308
	3rd	11500	0.0000473	1.146
	4th	24000	0.0000473	1.117
	5th	17000	0.000103	1.187
	6th	24000	0.000149	1.252
	7th	43000	0.000369	1.157
	8th	59000	0.000623	1.533
	1st to 8th	30000	0.00022	1.284

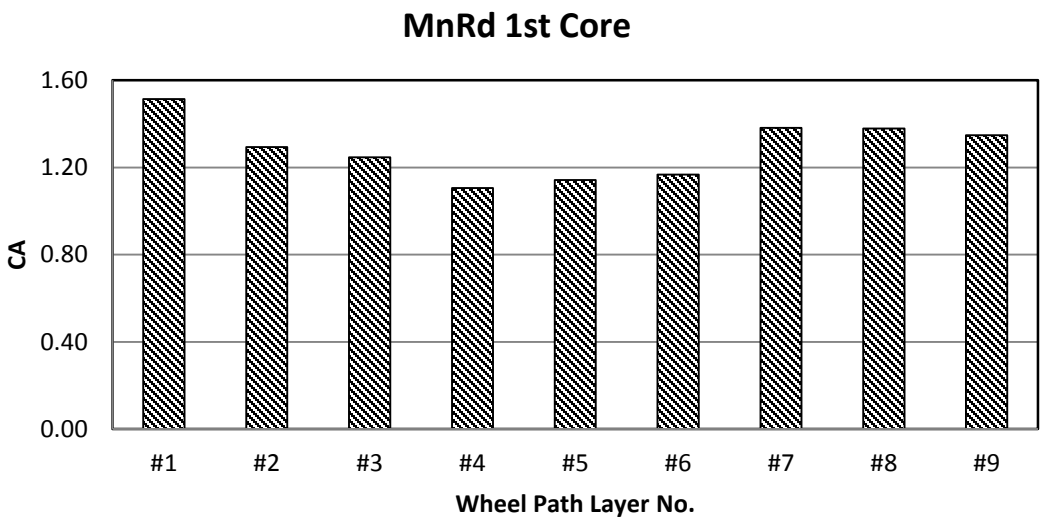
MnRd 1st Core
1.60
1.20
0.80
0.40
0.00
CA
#1
#2
#3
#4
#5
#6
#7
#8
#9
Wheel Path Layer No.

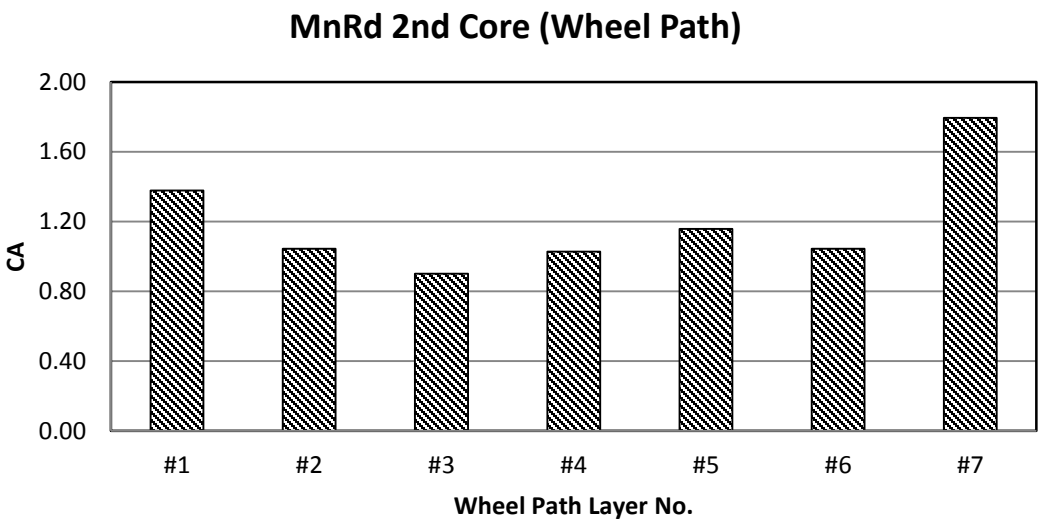
MnRd 2nd Core (Wheel Path)
2.00
1.60
1.20
0.80
0.40
0.00
CA
#1
#2
#3
#4
#5
#6
#7
Wheel Path Layer No.

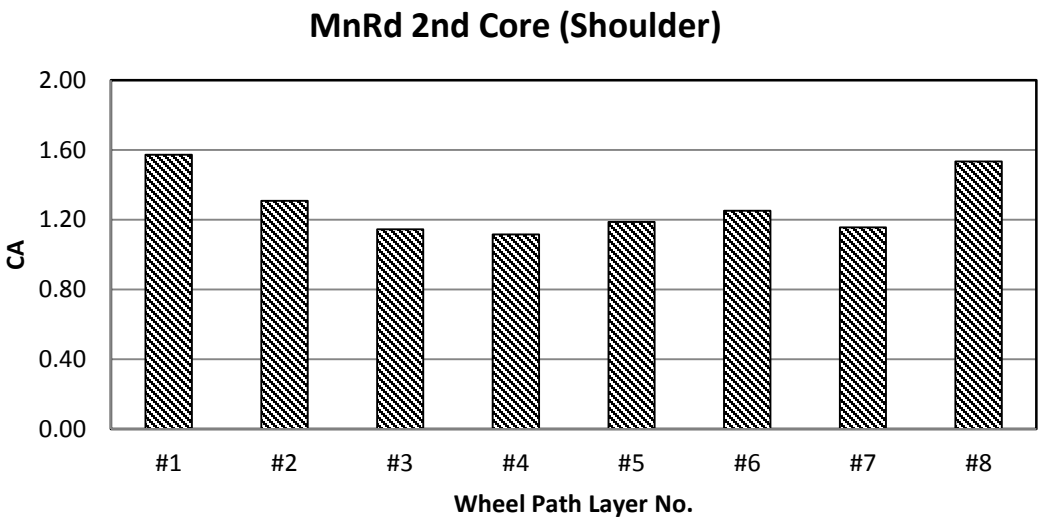
MnRd 2nd Core (Shoulder)
2.00
1.60
1.20
0.80
0.40
0.00
CA
#1
#2
#3
#4
#5
#6
#7
#8
Wheel Path Layer No.

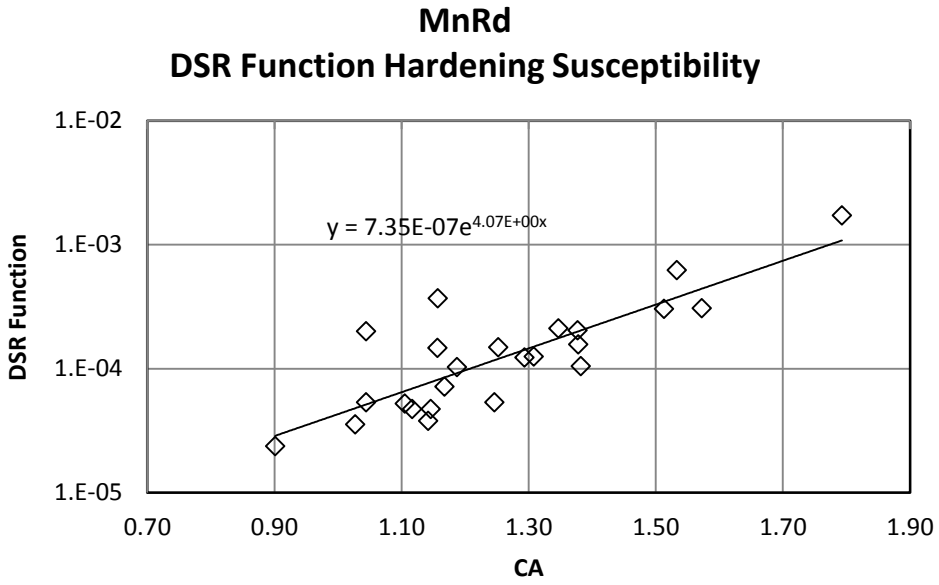
MnRd
DSR Function Hardening Susceptibility
1.E-02
1.E-03
1.E-04
1.E-05
DSR Function
y = 7.35E-07e4.07E+00x
0.70
0.90
1.10
1.30
1.50
1.70
1.90
CA

Table A24. ODA FM1936 Field Core (Wheel Path)

Binder: Alon PG70-22 Activation Energy: 47.2 kJ/mol Cons.: 2002		η* (Poise) @60°C 0.1 rad/s	G'/(η'/G') (MPa/s) @15°C 0.005 rad/s	Carbonyl Area
1st Core (05/2008)	1st layer	140000	0.00163	1.279
	2nd	30000	0.000157	0.966
	3rd	7900	0.0000141	0.894
	4th	21000	0.0000576	0.887
	1st to 4th	38000	0.00019	1.045

Table A25. ODA FM1936 Field Core (Shoulder)

Binder: Alon PG70-22 Activation Energy: 47.2 kJ/mol Cons.: 2002		η* (Poise) @60°C 0.1 rad/s	G'/(η'/G') (MPa/s) @15°C 0.005 rad/s	Carbonyl Area
1st Core (05/2008)	1st layer	55000	0.00038	1.124
	2nd	13000	0.000033	0.920
	3rd	15000	0.000047	0.836
	4th	19000	0.000050	1.101
	1st to 4th	23000	0.000085	0.937
2nd Core (12/2010)	1st to 4th	23000	0.00066	0.733

ODA FM1936 1st Core

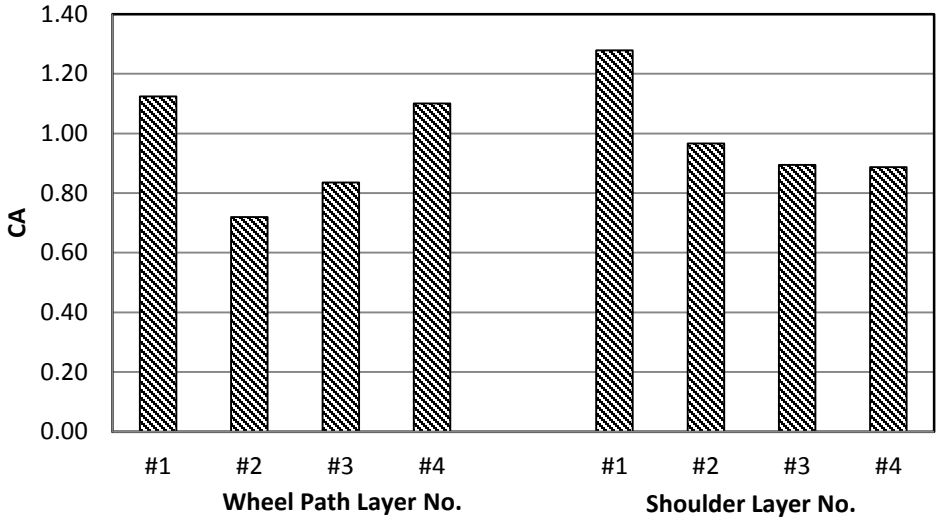

ODA FM1936
DSR Function Hardening Susceptibility

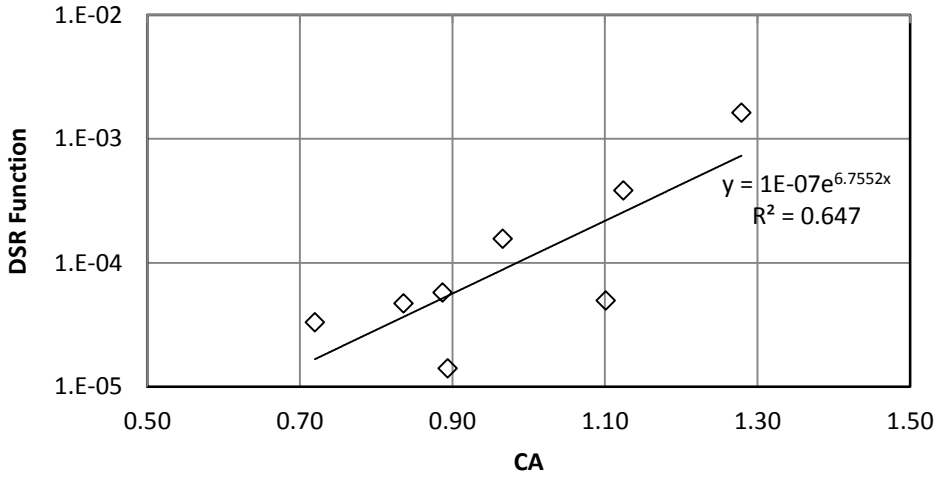

Table A26. PAR SH24 Field Core (Wheel Path)

Binder: Lion PG64-22 Activation Energy: 56.1 kJ/mol (Original Binder) Cons.: 2009		η* (Poise) @60°C 0.1 rad/s	G'/(η'/G') (MPa/s) @15°C 0.005 rad/s	Carbonyl Area
1st Core (07/2009)	1st layer	32000	0.00025	1.171
	2nd	37000	0.00033	1.330
	3rd	44000	0.00043	1.142
	1st to 3rd	37000	0.00033	1.214
2nd Core (12/2010)	1st layer	50000	0.00051	1.471
	2nd	50700	0.00056	1.292
	3rd	41400	0.00036	1.107
	1st to 3rd	47000	0.00047	1.290

Table A27. PAR SH24 Field Core (Shoulder)

Binder: Lion PG64-22 Activation Energy: 56.1 kJ/mol (Original Binder) Cons.: 2009		η* (Poise) @60°C 0.1 rad/s	G'/(η'/G') (MPa/s) @15°C 0.005 rad/s	Carbonyl Area
1st Core (06/2009)	1st layer	25000	0.00016	1.149
	2nd	33000	0.00025	1.144
	3rd	25000	0.00016	1.173
	4th	48000	0.00047	1.272
	1st to 4th	30000	0.00022	1.172
2nd Core (12/2010)	1st layer	44000	0.00043	1.296
	2nd	38000	0.00033	1.179
	3rd	57000	0.00060	1.315
	1st to 3rd	45000	0.00044	1.263

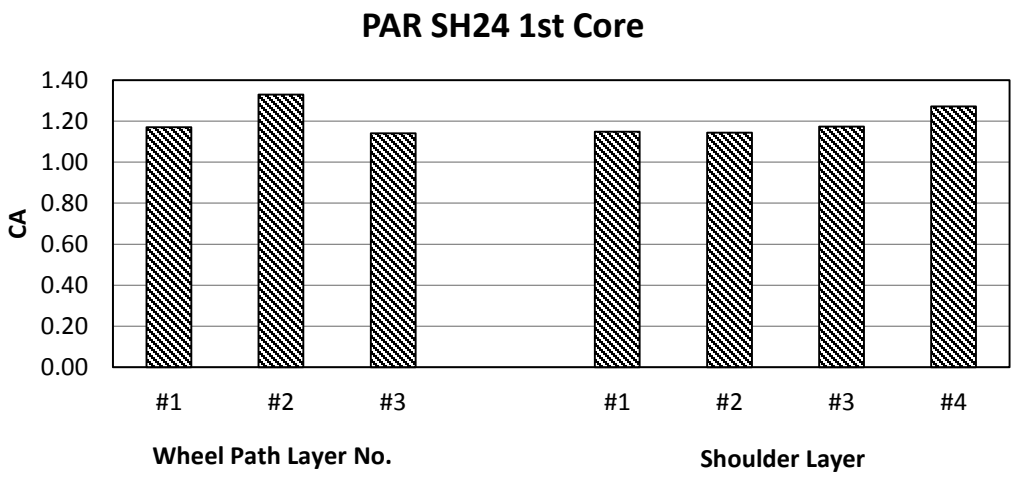
PAR SH24 1st Core
1.40
1.20
1.00
0.80
0.60
0.40
0.20
0.00
CA
#1
#2
#3
#1
#2
#3
#4
Wheel Path Layer No.
Shoulder Layer

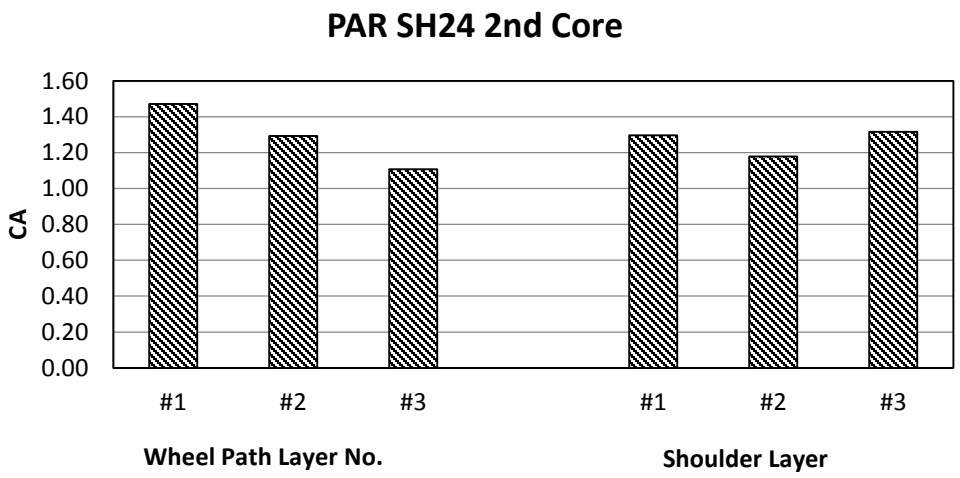
PAR SH24 2nd Core
1.60
1.40
1.20
1.00
0.80
0.60
0.40
0.20
0.00
CA
#1
#2
#3
#1
#2
#3
Wheel Path Layer No.
Shoulder Layer

PAR SH24
DSR Function Hardening Susceptibility

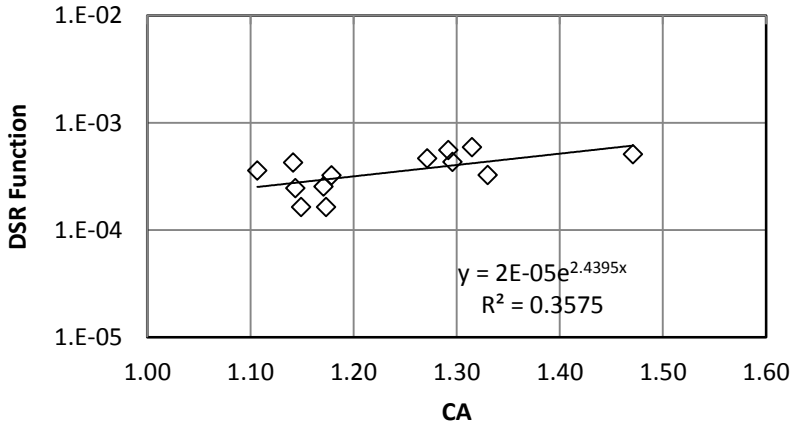

Table A28. PHR FM2994 Field Core (Wheel Path)

Binder: Eagle PG70-22 Activation Energy: 55.0 kJ/mol Cons.: 2002		η* (Poise) @60°C 0.1 rad/s	G'/(η'/G') (MPa/s) @15°C 0.005 rad/s	Carbonyl Area
1st Core (05/2008)	1st layer	700000	0.0023	1.402
	2nd	300000	0.0011	1.242
	3rd	400000	0.0018	1.344
	4th	300000	0.0017	1.335
	5th	400000	0.0018	1.403
	6th	300000	0.0017	1.515
	1st to 6th	420000	0.0017	1.347
2nd Core (11/2010)	1st to 6th	330000	0.0019	1.301

Table A29. PHR FM2994 Field Core (Shoulder)

Binder: Eagle PG70-22 Activation Energy: 55.0 kJ/mol Cons.: 2002		η* (Poise) @60°C 0.1 rad/s	G'/(η'/G') (MPa/s) @15°C 0.005 rad/s	Carbonyl Area
1st Core (05/2008)	1st layer	1100000	0.0048	1.382
	2nd	400000	0.0016	1.190
	3rd	400000	0.0017	1.237
	4th	400000	0.0021	1.471
	5th	300000	0.0017	1.403
	6th	300000	0.0028	1.547
	1st to 6th	530000	0.0025	1.329
2nd Core (11/2010)	1st to 6th	540000	0.0029	1.240

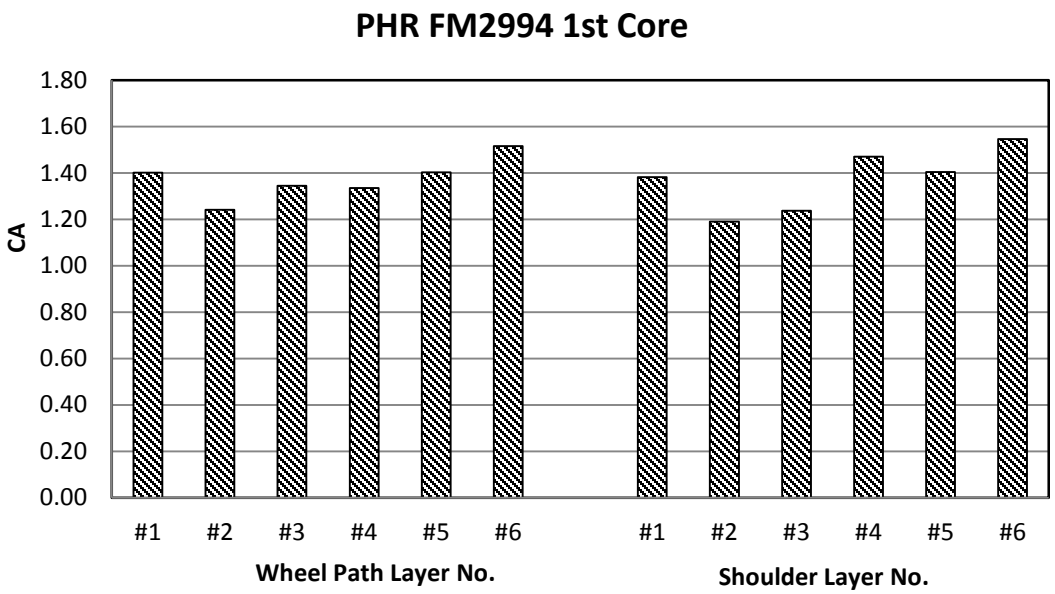
PHR FM2994 1st Core
CA
1.80
1.60
1.40
1.20
1.00
0.80
0.60
0.40
0.20
0.00
#1
#2
#3
#4
#5
#6
Wheel Path Layer No.
Shoulder Layer No.

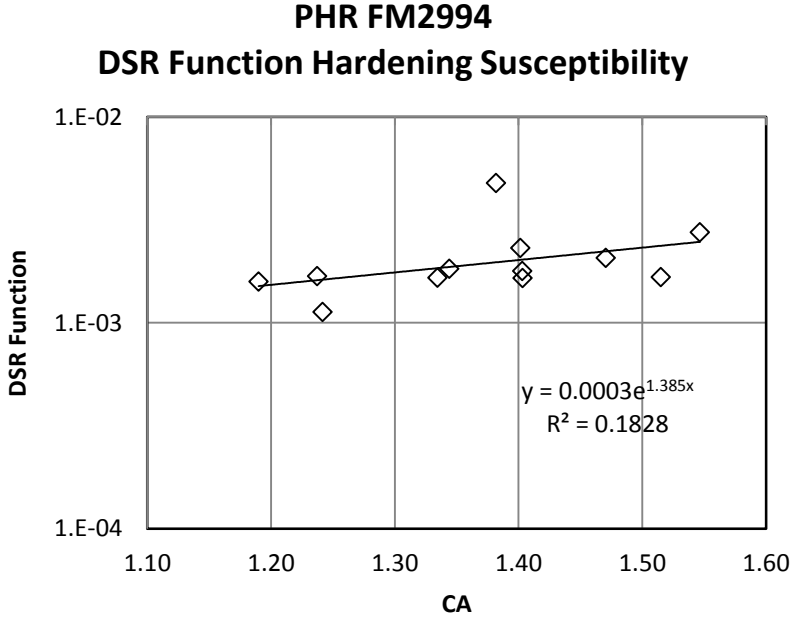
PHR FM2994
DSR Function Hardening Susceptibility
DSR Function
1.E-02
1.E-03
1.E-04
y = 0.0003e1.385x
R² = 0.1828
1.10
1.20
1.30
1.40
1.50
1.60
CA

Table A30. TYL US259 Field Core (Wheel Path)

Binder: Lion PG70-22 Activation Energy: 70.2 kJ/mol (Original Binder) Cons.: 2007		η* (Poise) @60°C 0.1 rad/s	G'/(η'/G') (MPa/s) @15°C 0.005 rad/s	Carbonyl Area
1st Core (07/2008)	1st layer	50000	0.00041	1.110
	2nd	32000	0.00020	0.927
	3rd	27000	0.00015	0.902
	4th	26000	0.00014	0.880
	1st to 4th	35000	0.00023	0.976

Table A31. TYL US259 Field Core (Shoulder)

Binder: Lion PG70-22 Activation Energy: 70.2 kJ/mol (Original Binder) Cons.: 2007		η* (Poise) @60°C 0.1 rad/s	G'/(η'/G') (MPa/s) @15°C 0.005 rad/s	Carbonyl Area
1st Core (07/2008)	1st layer	40000	0.00026	0.993
	2nd	25000	0.00013	0.930
	3rd	30000	0.00019	0.995
	1st to 3rd	31000	0.00019	0.973
2nd Core (10/2010)	1st to 3rd	20000	0.000093	1.055

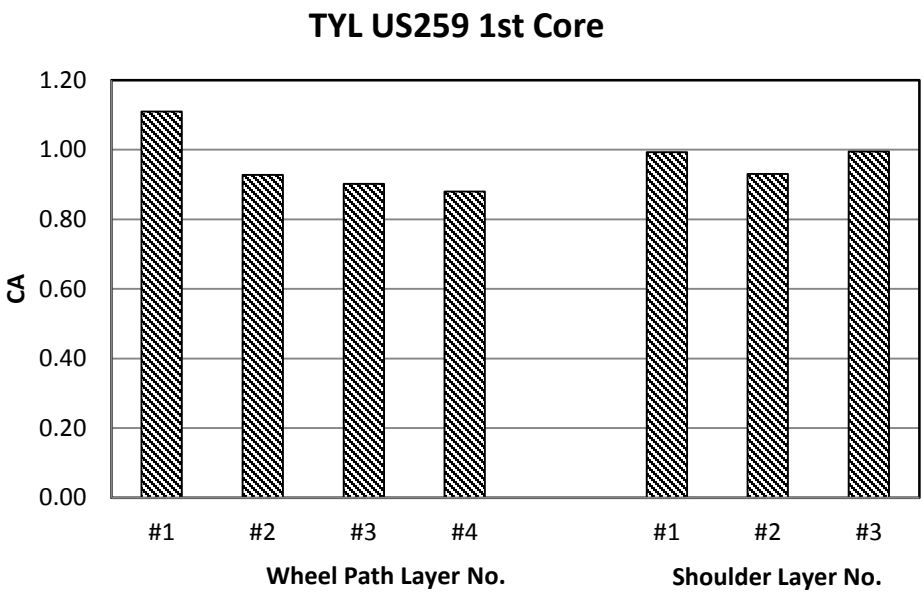
TYL US259 1st Core
1.20
1.00
0.80
0.60
0.40
0.20
0.00
CA
#1
#2
#3
#4
#1
#2
#3
Wheel Path Layer No.
Shoulder Layer No.

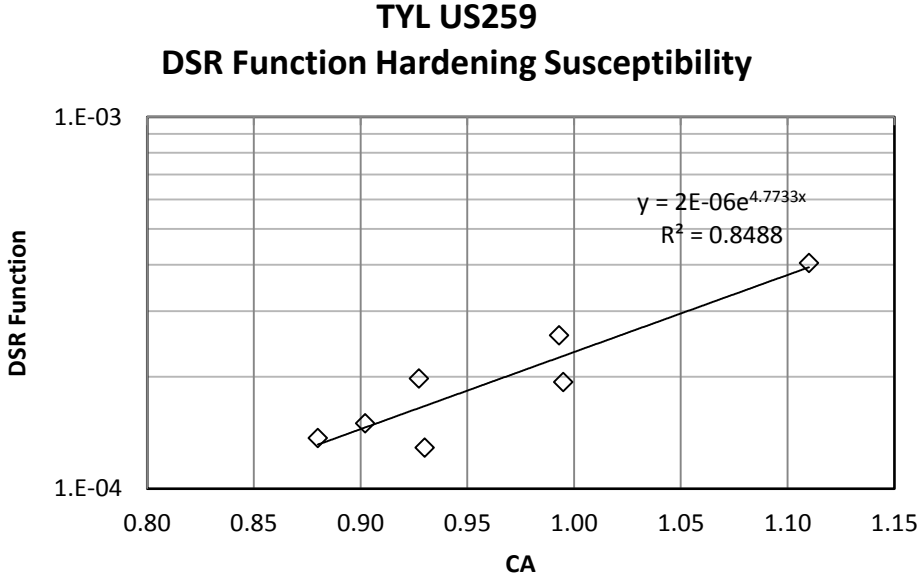
TYL US259
DSR Function Hardening Susceptibility
1.E-03
1.E-04
DSR Function
y = 2E-06e4.7733x
R² = 0.8488
0.80
0.85
0.90
0.95
1.00
1.05
1.10
1.15
CA

Table A32. WAC IH35 Field Core (Wheel Path)

Binder: Fina PG70-22 Activation Energy: 98.7 kJ/mol Cons.: 2003		η* (Poise) @60ºC 0.1 rad/s	G'/(η'/G') (MPa/s) @15ºC 0.005 rad/s	Carbonyl Area
1st Core (08/2008)	1st layer	26000	0.000075	0.859
	2nd	26000	0.000074	0.858
	3rd	26000	0.000077	0.866
	4th	26000	0.000078	0.815
	5th	31000	0.000090	0.822
	6th	25000	0.000061	0.805
	1st to 6th	26000	0.000075	0.848
2nd Core (02/2011)	1st to 6th	Too high to measure	0.00039	0.959

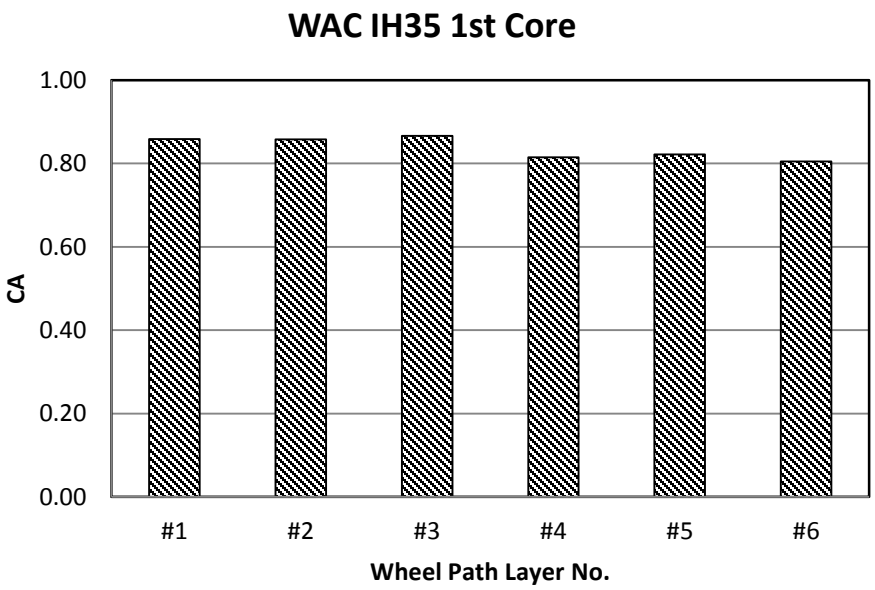
WAC IH35 1st Core
1.00
0.80
0.60
0.40
0.20
0.00
CA
#1
#2
#3
#4
#5
#6
Wheel Path Layer No.

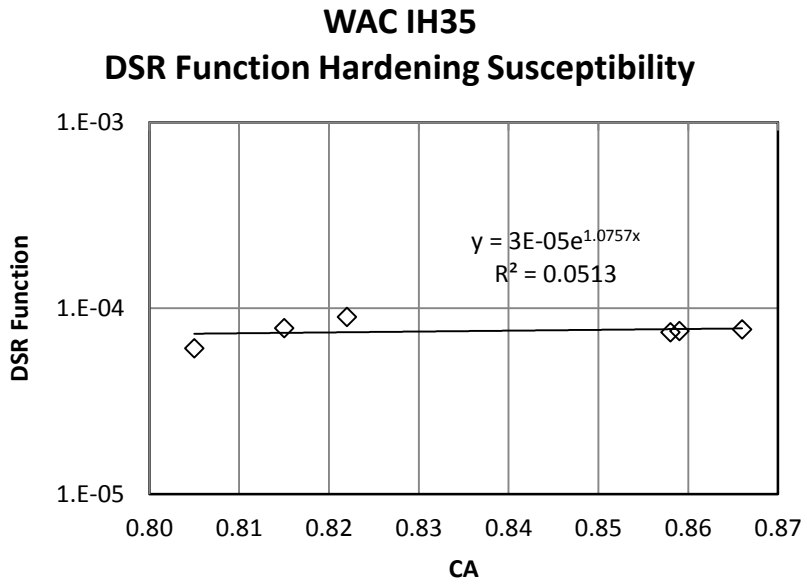
WAC IH35
DSR Function Hardening Susceptibility
1.E-03
1.E-04
1.E-05
DSR Function
y = 3E-05e1.0757x
R² = 0.0513
0.80
0.81
0.82
0.83
0.84
0.85
0.86
0.87
CA

Table A33. WFS US59 Field Core (Wheel Path)

Binder: SEM PG70-22 Activation Energy: 85.7 kJ/mol Cons.: 2007		η* (Poise) @60°C 0.1 rad/s	G'/(η'/G') (MPa/s) @15°C 0.005 rad/s	Carbonyl Area
1st Core (07/2008)	1st layer	58000	0.00050	1.069
	2nd	53000	0.00025	0.942
	3rd	52000	0.00026	0.920
	4th	50000	0.00022	0.896
	5th	50000	0.00020	0.911
	1st to 5th	54000	0.00031	0.973
2nd Core (10/2010)	1st to 5th	66000	0.00027	1.019

Table A34. WFS US59 Field Core (Shoulder)

Binder: SEM PG70-22 Activation Energy: 85.7 kJ/mol Cons.: 2007		η* (Poise) @60°C 0.1 rad/s	G'/(η'/G') (MPa/s) @15°C 0.005 rad/s	Carbonyl Area
1st Core (07/2008)	1st layer	80000	0.00092	1.156
	2nd	72000	0.00040	1.014
	3rd	50000	0.00044	1.020
	1st to 3rd	66000	0.00054	1.063
2nd Core (10/2010)	1st to 3rd	147000	0.00093	1.087

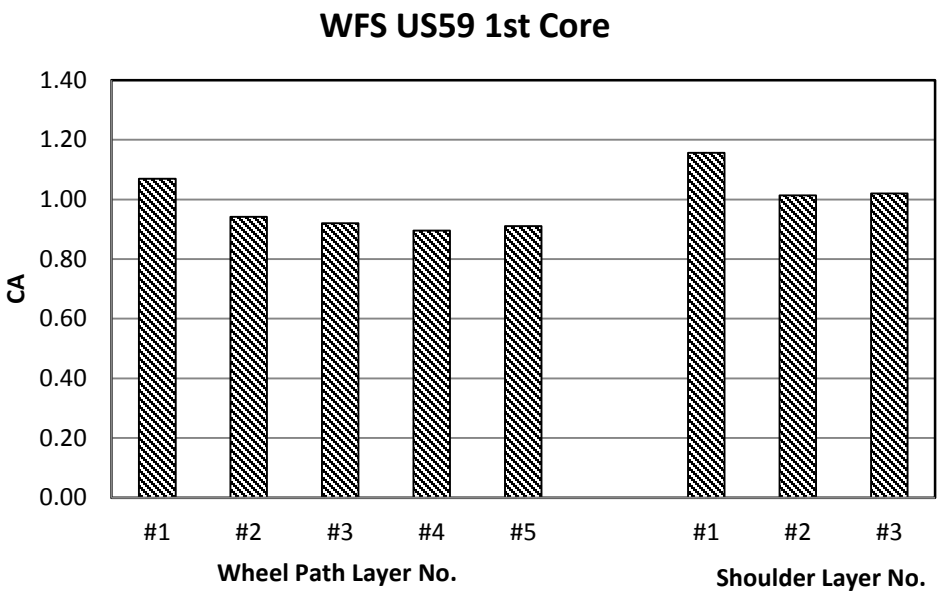
WFS US59 1st Core
1.40
1.20
1.00
0.80
0.60
0.40
0.20
0.00
CA
#1
#2
#3
#4
#5
#1
#2
#3
Wheel Path Layer No.
Shoulder Layer No.

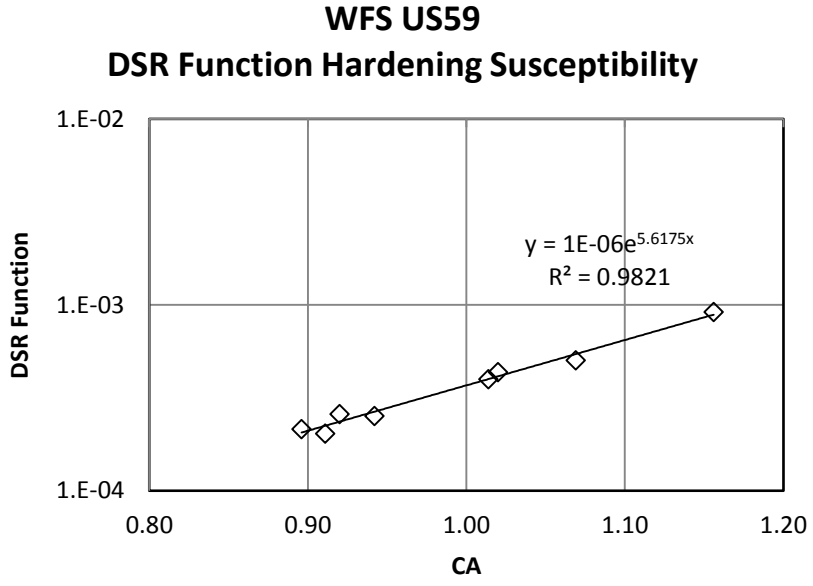
WFS US59
DSR Function Hardening Susceptibility
1.E-02
1.E-03
1.E-04
DSR Function
y = 1E-06e5.6175x
R² = 0.9821
0.80
0.90
1.00
1.10
1.20
CA

Table A35. YKM SH36 Field Core (Wheel Path)

Binder: Martin PG64-22 Activation Energy: 71.7 kJ/mol Cons.: 2006		η* (Poise) @60ºC 0.1 rad/s	G'/(η'/G') (MPa/s) @15ºC 0.005 rad/s	Carbonyl Area
1st Core (06/2008)	1st layer	70000	0.00054	1.212
	2nd	45000	0.00038	1.111
	3rd	30000	0.00030	0.951
	4th	27000	0.00019	1.036
	1st to 4th	45000	0.00035	1.077
2nd Core (01/2011)	1st to 4th	48000	0.00034	0.997

Table A36. YKM SH36 Field Core (Shoulder)

Binder: Martin PG64-22 Activation Energy: 71.7 kJ/mol Cons.: 2006		η* (Poise) @60ºC 0.1 rad/s	G'/(η'/G') (MPa/s) @15ºC 0.005 rad/s	Carbonyl Area
1st Core (06/2008)	1st layer	70000	0.00067	1.282
	2nd	40000	0.00032	1.146
	3rd	35000	0.00029	1.131
	4th	52000	0.00044	1.258
	1st to 4th	49000	0.00042	1.208

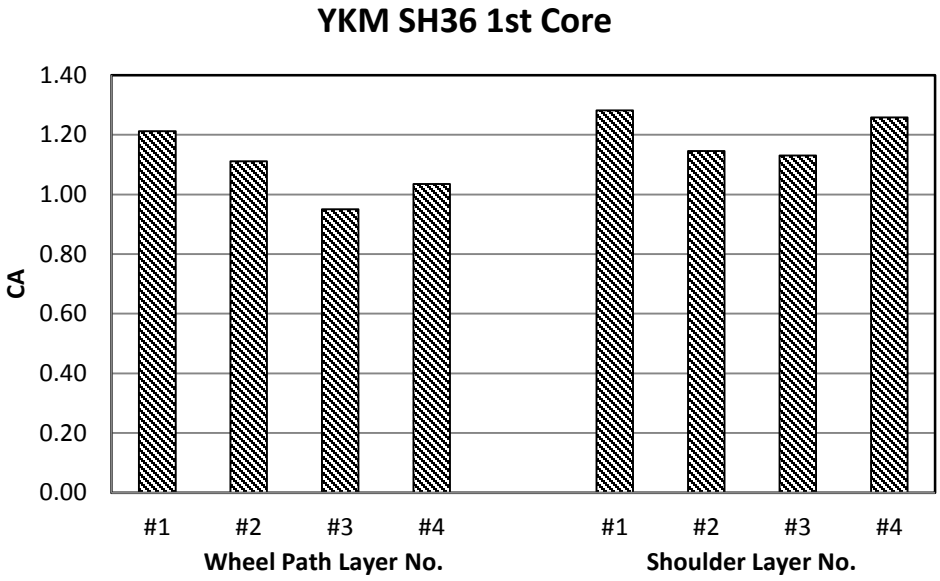
YKM SH36 1st Core
1.40
1.20
1.00
0.80
0.60
0.40
0.20
0.00
CA
#1
#2
#3
#4
#1
#2
#3
#4
Wheel Path Layer No.
Shoulder Layer No.

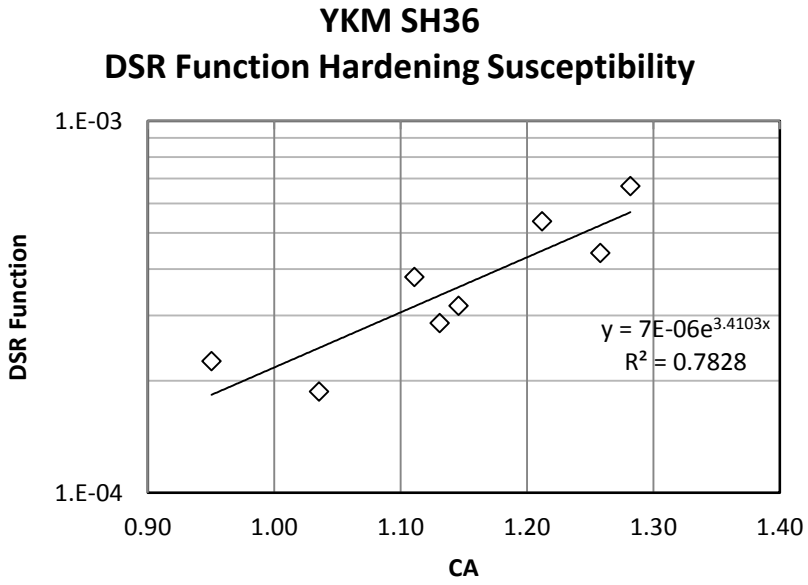
YKM SH36
DSR Function Hardening Susceptibility
1.E-03
1.E-04
DSR Function
y = 7E-06e3.4103x
R² = 0.7828
0.90
1.00
1.10
1.20
1.30
1.40
CA

APPENDIX B

TABLES OF BULK S.G., AIR VOID, AND BINDER CONTENT DATA

In the graphs below the following terms are used in their abbreviated forms: Total Air Void (TAV), Accessible Air Void by Corelok Method (AAV CL), and Accessible Air Void by Saturated Surface Dry Method (AAV SSD).

Table B1. AMR US54 Field Core (Wheel Path)

Cons.: 1998		Bulk S.G.	Maximum S.G.	Total Air Voids (vol. %)	Accessible A.V. (vol. %)		Binder Content (wt. %)
					Corelok	SSD	
1st Core Seal coat Treated (07/2008)	1st	2.03	2.32	12.36	12.27	4.20	- (Seal coat attached)
	2nd	2.21	2.46	10.26	10.40	8.23	2.0
	3rd	2.26	2.44	7.62	5.62	4.36	3.6
	4th	2.27	2.45	7.54	7.16	6.41	3.6

Table B2. AMR US54 Field Core (Shoulder)

Cons.: 1998		Bulk S.G.	Maximum S.G.	Total Air Voids (vol. %)	Accessible A.V. (vol. %)		Binder Content (wt. %)
					Corelok	SSD	
1st Core Seal coat Treated (07/2008)	1st	1.98	2.29	13.81	13.20	5.12	- (Seal coat attached)
	2nd	2.20	2.49	11.67	10.60	8.40	3.6
	3rd	2.20	2.49	11.67	10.72	8.79	3.6
	4th	2.21	2.50	11.82	10.66	8.17	4.3

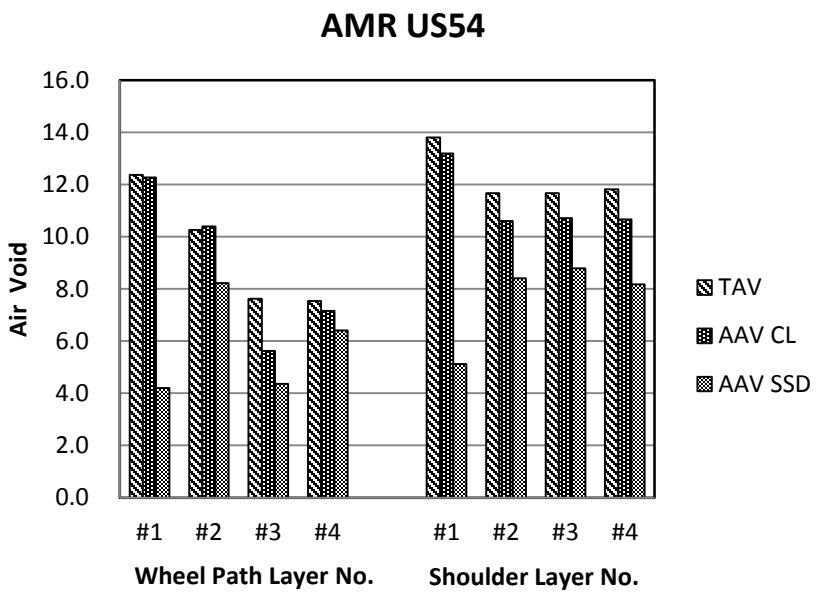
AMR US54
16.0
14.0
12.0
10.0
8.0
6.0
4.0
2.0
0.0
Air Void
#1
#2
#3
#4
#1
#2
#3
#4
Wheel Path Layer No.
Shoulder Layer No.
TAV
AAV CL
AAV SSD

Table B3. ATL IH20 Field Core (Wheel Path)

Cons.: 2003		Bulk S.G.	Maximum S.G.	Total Air Voids (vol. %)	Accessible A.V. (vol. %)		Binder Content (wt. %)
					Corelok	SSD	
1st Core (07/2008)	1st	2.02	2.39	15.62	14.87	12.00	4.8
	2nd	2.16	2.42	10.86	10.41	7.20	4.0
	3rd	2.16	2.43	10.90	9.81	8.09	4.0
	4th	2.06	2.41	14.30	13.88	9.13	3.2

Table B4. ATL IH20 Field Core (Shoulder)

Cons.: 2003		Bulk S.G.	Maximum S.G.	Total Air Voids (vol. %)	Accessible A.V. (vol. %)		Binder Content (wt. %)
					Corelok	SSD	
1st Core (07/2008)	1st	2.03	2.26	10.31	15.48	8.58	Average 4.1
	2nd	2.12	2.41	11.93	11.22	7.89	
	3rd	2.15	2.42	10.98	10.02	7.28	
	4th	2.05	2.37	13.48	13.08	7.56	

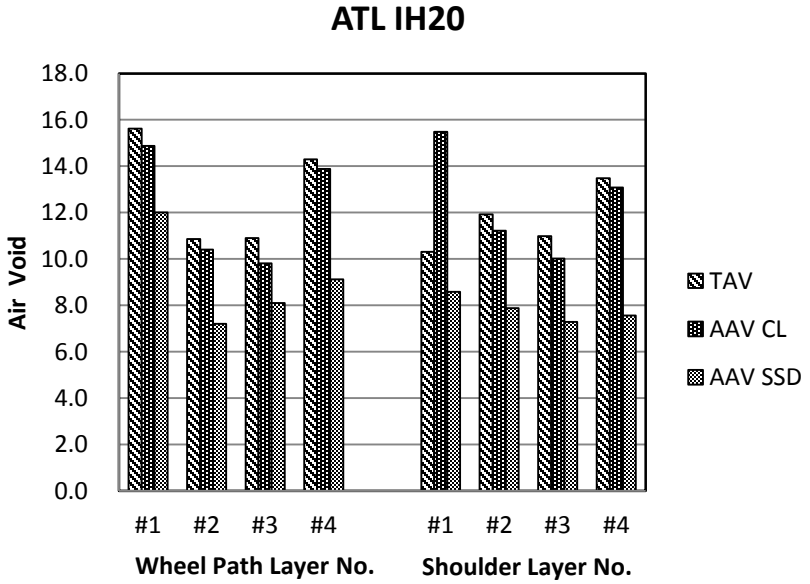

Table B5. ATL US259 Field Core (Wheel Path)

Cons.: 2005		Bulk S.G.	Maximum S.G.	Total Air Voids (vol. %)	Accessible A.V. (vol. %)		Binder Content (wt. %)
					Corelok	SSD	
1st Core (12/2008)	1st	2.20	2.42	9.16	7.94	5.41	4.8
	2nd	2.27	2.41	5.75	4.88	4.45	3.2
	3rd	2.28	2.42	5.85	4.93	4.24	4.4
	4th	2.28	2.41	5.48	4.26	4.01	4.8
	5th	2.22	2.42	8.16	7.65	6.33	4.0

Table B6. ATL US259 Field Core (Shoulder)

Cons.: 2005		Bulk S.G.	Maximum S.G.	Total Air Voids (vol. %)	Accessible A.V. (vol. %)		Binder Content (wt. %)
					Corelok	SSD	
1st Core (12/2008)	1st	2.20	2.42	9.39	9.03	6.79	4.8
	2nd	2.23	2.41	7.30	7.03	5.95	4.8
	3rd	2.26	2.42	6.83	6.55	5.45	4.8
	4th	2.23	2.41	7.15	7.27	6.00	4.4

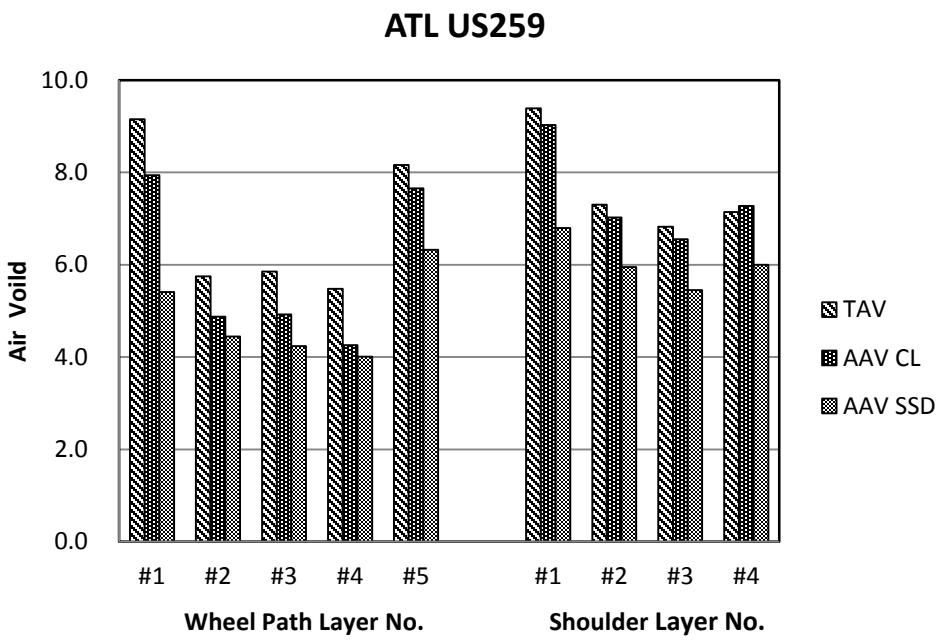
ATL US259
10.0
8.0
6.0
4.0
2.0
0.0
Air Voild
#1
#2
#3
#4
#5
#1
#2
#3
#4
Wheel Path Layer No.
Shoulder Layer No.
TAV
AAV CL
AAV SSD

Table B7. BRY SH6 Field Core (Wheel Path)

Cons.: 2000		Bulk S.G.	Maximum S.G.	Total Air Voids (vol. %)	Accessible A.V. (vol. %)		Binder Content (wt. %)
					Corelok	SSD	
1st Core (08/2008)	1st	2.26	2.46	7.91	6.52	4.12	Average 3.9
	2nd	2.32	2.47	5.91	5.35	3.83	
	3rd	2.33	2.47	5.87	4.52	3.63	

Table B8. BRY SH6 Field Core (Shoulder)

Cons.: 2000		Bulk S.G.	Maximum S.G.	Total Air Voids (vol. %)	Accessible A.V. (vol. %)		Binder Content (wt. %)
					Corelok	SSD	
1st Core (08/2008)	1st	2.14	2.46	12.88	13.20	6.62	Average 3.6
	2nd	2.20	2.47	10.67	9.74	5.86	
	3rd	2.23	2.45	8.95	9.48	6.82	

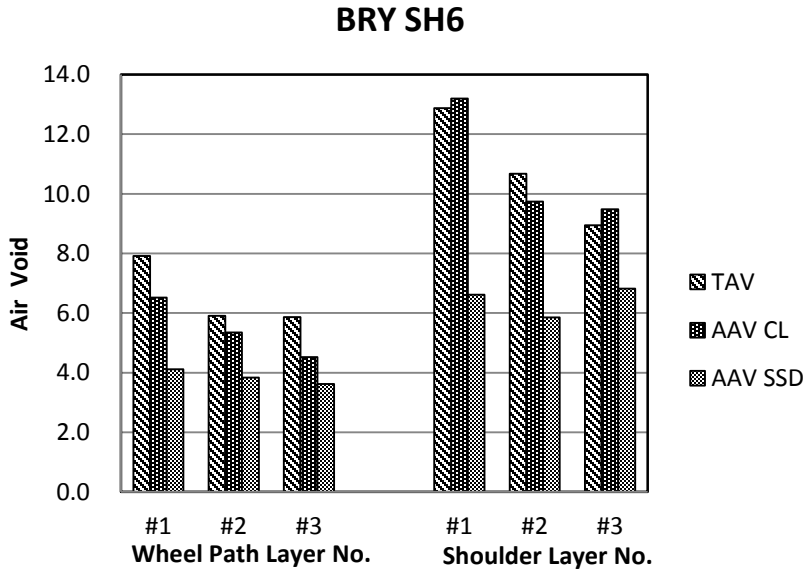

Table B9. BRY US290 Field Core (Wheel Path)

Cons.: 2002		Bulk S.G.	Maximum S.G.	Total Air Voids (vol. %)	Accessible A.V. (vol. %)		Binder Content (wt. %)
					Corelok	SSD	
1st Core (08/2008)	1st	1.84	2.13	13.71	11.54	7.13	-
	2nd	2.06	2.46	16.51	15.94	8.11	
	3rd	2.05	2.46	16.41	16.21	8.20	
	4th	2.03	2.35	13.39	16.56	9.16	
	5th	1.90	2.44	22.02	21.24	10.34	
2nd Core (12/2010)	1st to 5th	2.17	2.42	10.09	6.05	5.95	3.4

Table B10. BRY US290 Field Core (Shoulder)

Cons.: 2002		Bulk S.G.	Maximum S.G.	Total Air Voids (vol. %)	Accessible A.V. (vol. %)		Binder Content (wt. %)
					Corelok	SSD	
1st Core (08/2008)	1st	2.14	2.47	13.24	12.36	10.16	Average 3.2
	2nd	2.26	2.46	8.41	6.98	7.14	
	3rd	2.26	2.48	8.92	7.10	7.26	
	4th	2.21	2.48	10.66	9.62	8.86	
2nd Core (12/2010)	1st to 5th	2.18	2.43	10.53	8.54	7.98	3.5

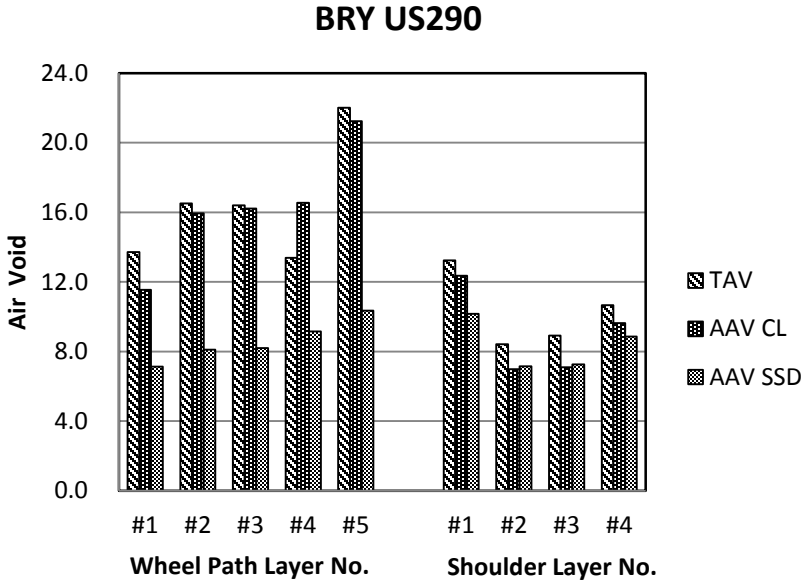
BRY US290
24.0
20.0
16.0
12.0
8.0
4.0
0.0
Air Void
#1 #2 #3 #4 #5
Wheel Path Layer No.
#1 #2 #3 #4
Shoulder Layer No.
TAV
AAV CL
AAV SSD

Table B11. CHS US83 Field Core (Wheel Path)

Cons.: 2008		Bulk S.G.	Maximum S.G.	Total Air Voids (vol. %)	Accessible A.V. (vol. %)		Binder Content (wt. %)
					Corelok	SSD	
1st Core (08/2008)	1st	2.18	2.43	9.99	10.32	7.99	Average 4.0
	2nd	2.25	2.40	6.53	7.45	6.86	
	3rd	2.25	2.43	7.45	7.33	6.62	
2nd Core (10/2009)	1st	2.20	2.43	9.55	8.77	6.03	3.6
	2nd	2.25	2.41	6.91	6.60	5.49	3.2
	3rd	2.26	2.40	5.90	5.08	4.02	4.7
3rd Core (08/2010)	1st	2.23	2.46	9.33	7.94	6.19	3.8
	2nd	2.27	2.46	7.39	5.97	4.76	3.5
	3rd	2.29	2.42	5.44	5.07	4.50	3.6
2nd Core Seal coat Treated (10/2009)	Seal coat layer and 1st layer	2.05	2.32	11.49	7.28	3.13	5.2
	2nd	2.24	2.41	7.09	5.25	3.69	3.6
	3rd	2.23	2.37	6.05	4.04	2.92	3.6
	4th	2.23	2.41	7.63	5.00	3.78	3.2
	5th	2.17	2.40	9.59	10.76	9.34	2.4
3rd Core Seal coat Treated (08/2010)	Seal coat layer and 1st layer	2.13	2.29	7.28	6.13	4.04	7.4
	2nd	2.25	2.42	6.96	6.26	5.03	4.0
	3rd	2.30	2.41	4.62	3.13	2.35	4.0

Table B12. CHS US83 Field Core (Shoulder)

Cons.: 2008		Bulk S.G.	Maximum S.G.	Total Air Voids (vol. %)	Accessible A.V. (vol. %)		Binder Content (wt. %)
					Corelok	SSD	
1st Core (08/2008)	1st	2.16	2.42	10.47	10.58	9.07	Average 4.4
	2nd	2.23	2.42	7.62	7.83	7.19	
	3rd	2.20	2.40	8.60	9.64	8.82	
	4th	2.15	2.42	11.38	11.46	10.01	
	5th	2.17	2.43	10.53	10.89	9.84	
2nd Core (10/2009)	1st	2.08	2.43	14.44	13.45	8.33	4.1
	2nd	2.20	2.37	7.02	8.36	7.36	3.4
	3rd	2.20	2.37	7.05	8.02	6.64	4.0
	4th	2.19	2.40	8.97	9.19	7.69	3.6
	5th	2.17	2.38	8.54	7.90	6.93	3.6
3rd Core (08/2010)	1st	2.20	2.44	10.06	9.62	7.92	3.8
	2nd	2.26	2.43	7.13	6.38	5.65	3.9
	3rd	2.25	2.44	7.82	6.59	5.20	3.8
	4th	2.11	2.40	12.16	11.68	8.89	4.6
	5th	2.20	2.42	9.17	9.40	7.50	3.8
	6th	2.22	2.41	7.52	7.84	6.38	3.9
2nd Core Seal coat Treated (10/2009)	Seal coat layer and 1st layer	2.11	2.31	8.46	6.16	3.02	6.5
	2nd	2.29	2.41	4.92	4.33	3.30	3.6
	3rd	2.32	2.40	3.28	2.76	2.52	4.0
3rd Core Seal coat Treated (08/2010)	Seal coat layer and 1st layer	2.19	2.40	8.41	5.55	4.28	4.4
	2nd	2.27	2.44	6.98	5.70	4.51	4.0
	3rd	2.22	2.44	8.94	9.07	7.68	4.2
	4th	2.11	2.43	12.97	12.65	10.83	3.4

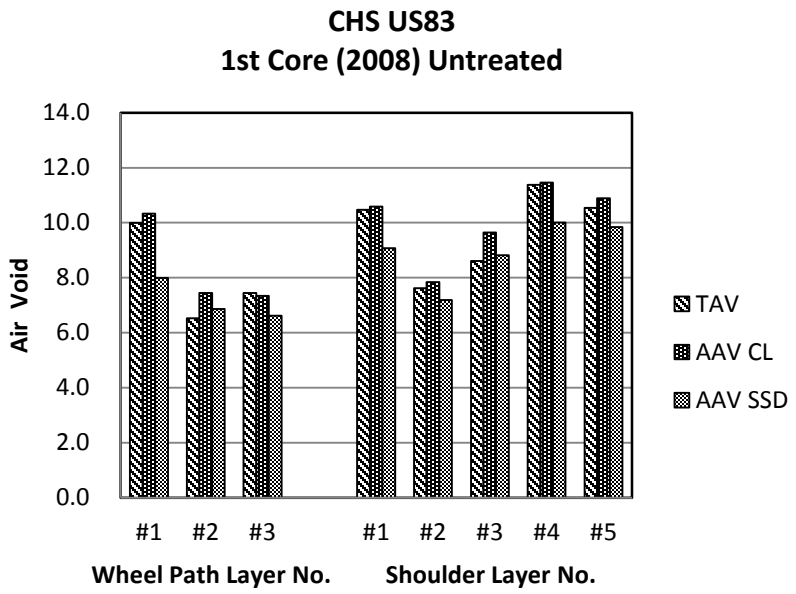
CHS US83
1st Core (2008) Untreated
14.0
12.0
10.0
8.0
6.0
4.0
2.0
0.0
Air Void
#1 #2 #3 #1 #2 #3 #4 #5
Wheel Path Layer No.
Shoulder Layer No.
TAV
AAV CL
AAV SSD

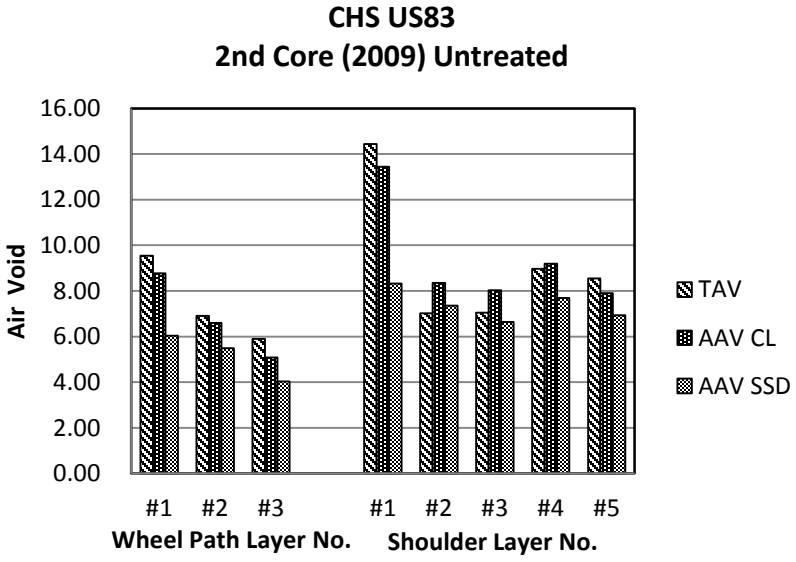
CHS US83
2nd Core (2009) Untreated
16.00
14.00
12.00
10.00
8.00
6.00
4.00
2.00
0.00
Air Void
#1 #2 #3 #1 #2 #3 #4 #5
Wheel Path Layer No.
Shoulder Layer No.
TAV
AAV CL
AAV SSD

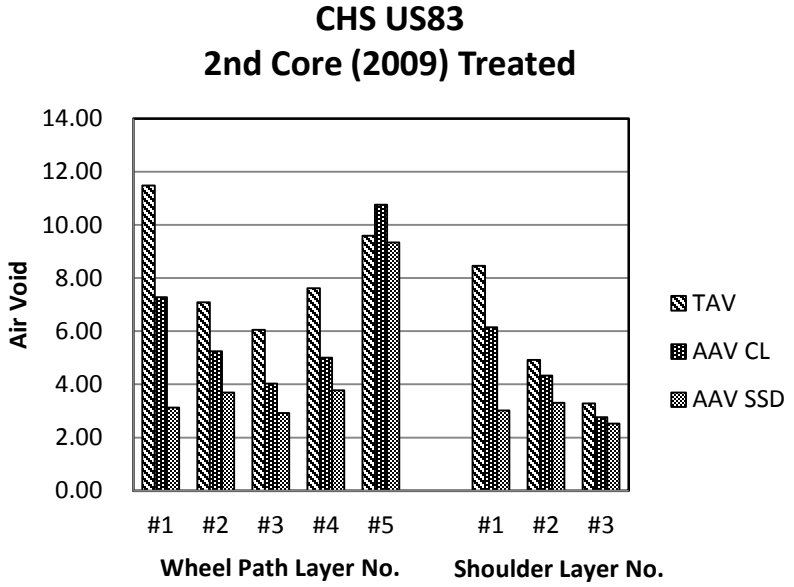
CHS US83
2nd Core (2009) Treated
14.00
12.00
10.00
8.00
6.00
4.00
2.00
0.00
Air Void
#1
#2
#3
#4
#5
#1
#2
#3
Wheel Path Layer No.
Shoulder Layer No.
TAV
AAV CL
AAV SSD

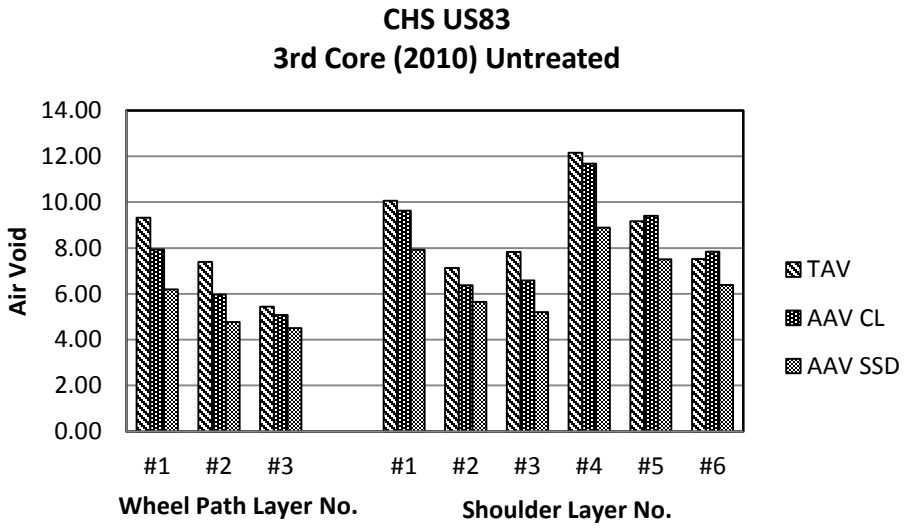
CHS US83
3rd Core (2010) Untreated
14.00
12.00
10.00
8.00
6.00
4.00
2.00
0.00
Air Void
#1
#2
#3
#1
#2
#3
#4
#5
#6
Wheel Path Layer No.
Shoulder Layer No.
TAV
AAV CL
AAV SSD

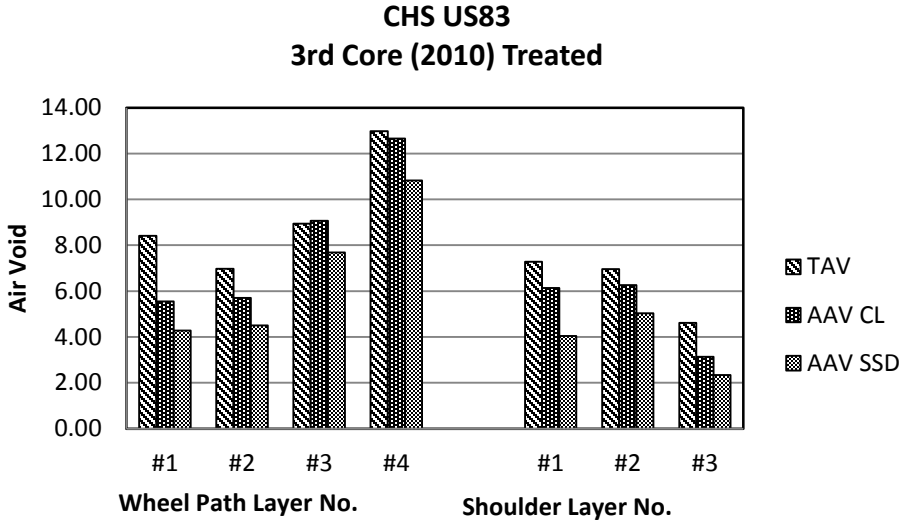
CHS US83
3rd Core (2010) Treated
14.00
12.00
10.00
8.00
6.00
4.00
2.00
0.00
Air Void
#1
#2
#3
#4
Wheel Path Layer No.
#1
#2
#3
Shoulder Layer No.
TAV
AAV CL
AAV SSD

Table B13. LBB US82 Field Core (Wheel Path)

Cons.: 2008		Bulk S.G.	Maximum S.G.	Total Air Voids (vol. %)	Accessible A.V. (vol. %)		Binder Content (wt. %)
					Corelok	SSD	
1st Core (08/2008)	1st	2.08	2.31	10.29	9.90	6.84	
	2nd	2.15	2.31	6.94	6.37	4.92	Average
	3rd	2.14	2.31	7.36	6.95	5.89	4.8
	4th	2.12	2.32	8.63	8.07	6.61	
2nd Core (12/2009)	1st	2.10	2.32	9.33	7.97	7.01	2.6
	2nd	2.14	2.33	8.32	7.25	6.52	2.8
	3rd	2.11	2.32	8.94	7.04	5.88	3.6
2nd Core Seal coat Treated (12/2009)	Seal coat layer and 1st layer	1.74	2.20	20.72	19.09	2.11	4.9
	2nd	2.04	2.32	11.83	10.55	7.72	4.0
	3rd	1.97	2.30	14.23	9.91	4.04	3.6
	4th	2.06	2.27	9.05	8.08	6.46	4.8

Table B14. LBB US82 Field Core (Shoulder)

Cons.: 2008		Bulk S.G.	Maximum S.G.	Total Air Voids (vol. %)	Accessible A.V. (vol. %)		Binder Content (wt. %)
					Corelok	SSD	
1st Core (08/2008)	1st	2.06	2.32	11.16	9.99	5.51	Average 4.8
	2nd	2.18	2.32	6.08	4.82	4.12	
	3rd	2.15	2.31	6.91	6.15	5.02	
2nd Core (12/2009)	1st	2.02	2.30	11.90	11.60	7.40	3.6
	2nd	2.15	2.31	7.02	6.64	6.03	4.0
	3rd	2.14	2.31	7.12	6.16	5.15	4.4
	4th	2.08	2.33	10.93	9.44	7.49	3.6
2nd Core Seal coat Treated (12/2009)	Seal coat layer and 1st layer	1.95	2.20	11.26	11.86	5.69	7.2
	2nd	1.99	2.32	13.88	13.10	9.51	3.6
	3rd	1.98	2.25	12.10	11.57	10.04	4.6

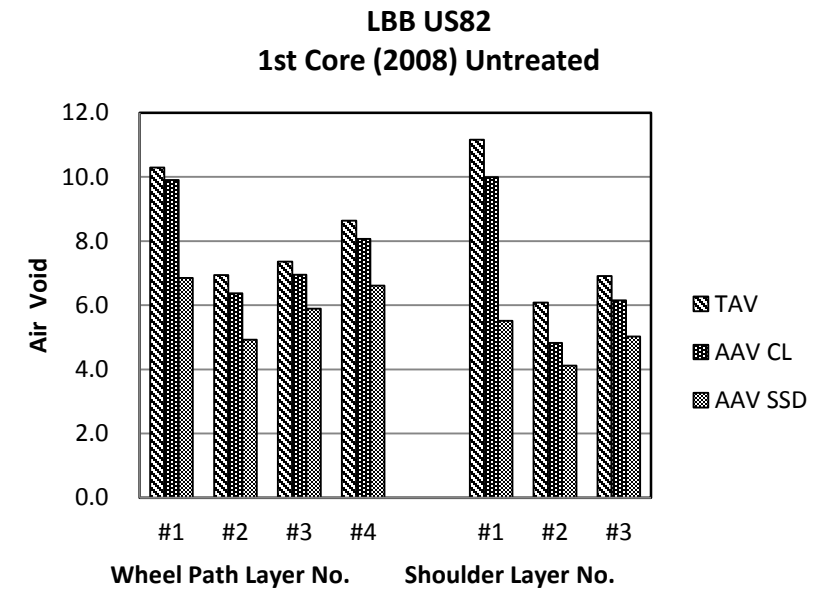
LBB US82
1st Core (2008) Untreated
12.0
10.0
8.0
6.0
4.0
2.0
0.0
Air Void
#1
#2
#3
#4
#1
#2
#3
Wheel Path Layer No.
Shoulder Layer No.
TAV
AAV CL
AAV SSD

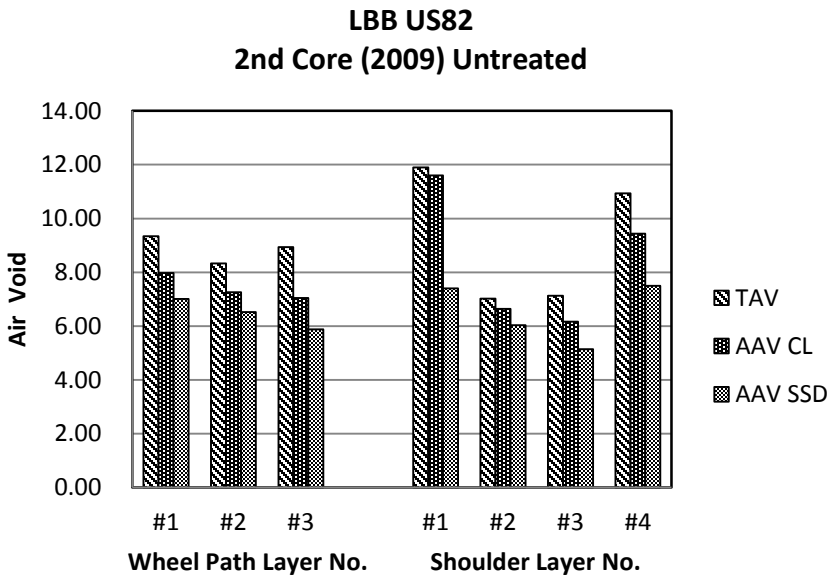
LBB US82
2nd Core (2009) Untreated
14.00
12.00
10.00
8.00
6.00
4.00
2.00
0.00
Air Void
#1
#2
#3
#1
#2
#3
#4
Wheel Path Layer No.
Shoulder Layer No.
TAV
AAV CL
AAV SSD

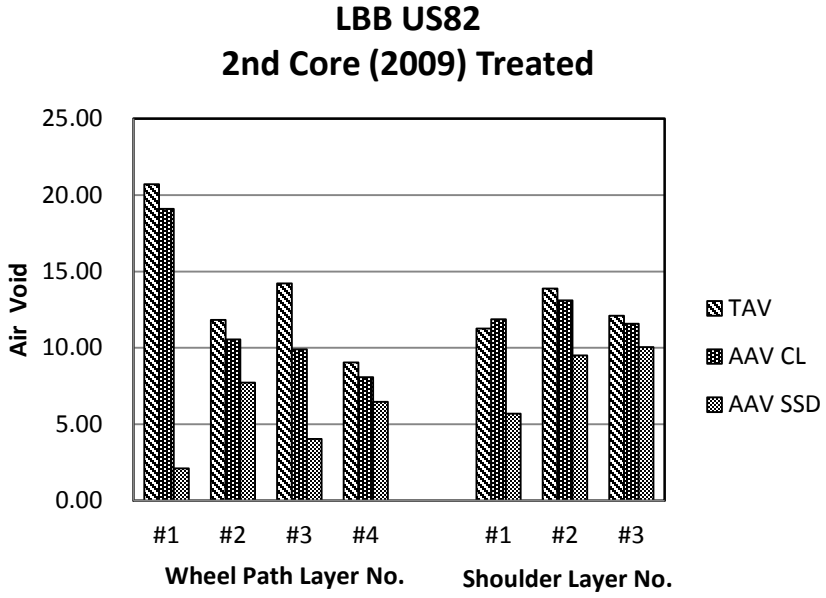
LBB US82
2nd Core (2009) Treated
25.00
20.00
15.00
10.00
5.00
0.00
Air Void
#1
#2
#3
#4
#1
#2
#3
Wheel Path Layer No.
Shoulder Layer No.
TAV
AAV CL
AAV SSD

Table B15. LFK US69 Field Core (Wheel Path)

Cons.: 2003		Bulk S.G.	Maximum S.G.	Total Air Voids (vol. %)	Accessible A.V. (vol. %)		Binder Content (wt. %)
					Corelok	SSD	
1st Core (06/2008)	1st	2.20	2.52	12.68	12.04	7.09	Average 5.6
	2nd	2.30	2.51	8.28	7.59	6.66	
	3rd	2.30	2.49	7.59	7.25	6.81	

Table B16. LFK US69 Field Core (Shoulder)

Cons.: 2003		Bulk S.G.	Maximum S.G.	Total Air Voids (vol. %)	Accessible A.V. (vol. %)		Binder Content (wt. %)
					Corelok	SSD	
1st Core (06/2008)	1st	2.18	2.49	12.61	12.65	9.65	Average 3.2
	2nd	2.26	2.48	8.90	8.54	8.12	

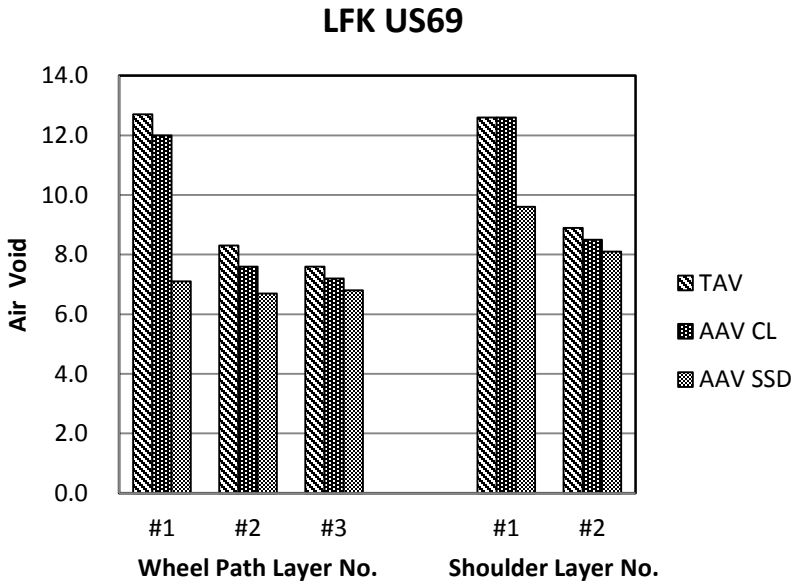

Table B17. LRD FM649 Field Core (Wheel Path)

Cons.: 2006		Bulk S.G.	Maximum S.G.	Total Air Voids (vol. %)	Accessible A.V. (vol. %)		Binder Content (wt. %)
					Corelok	SSD	
1st Core (06/2008)	1st	2.15	2.47	13.03	12.14	9.54	3.6
	2nd	2.17	2.47	12.20	11.34	10.49	3.6
	3rd	2.14	2.48	13.54	12.87	11.92	3.2

Table B18. LRD FM649 Field Core (Shoulder)

Cons.: 2006		Bulk S.G.	Maximum S.G.	Total Air Voids (vol. %)	Accessible A.V. (vol. %)		Binder Content (wt. %)
					Corelok	SSD	
1st Core (06/2008)	1st	2.04	2.47	17.29	16.63	12.20	3.6
	2nd	2.12	2.47	14.15	13.38	12.10	4.0
	3rd	2.14	2.47	13.36	12.97	11.81	3.6

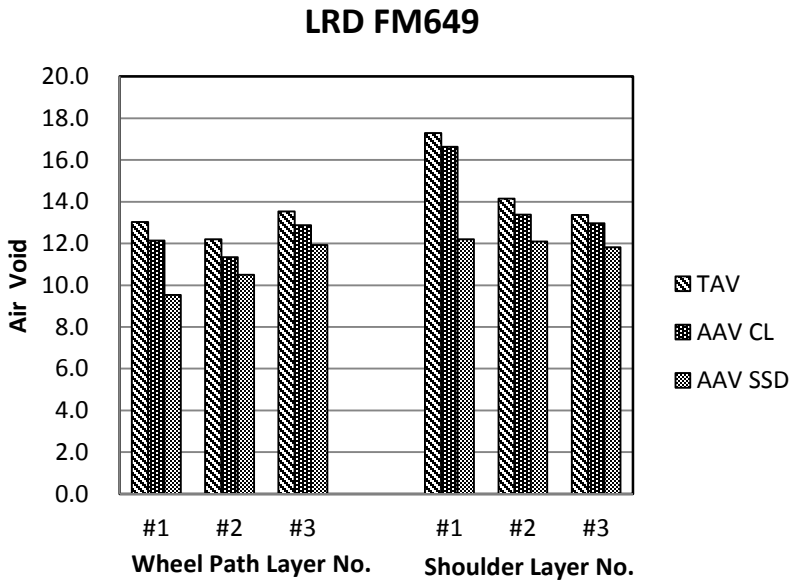

Table B19. LRD04 IH35 #3 Field Core (Shoulder)

Cons.: 2007		Bulk S.G.	Maximum S.G.	Total Air Voids (vol. %)	Accessible A.V. (vol. %)		Binder Content (wt. %)
					Corelok	SSD	
1st Core (06/2008)	1st	2.47	2.63	6.06	5.13	3.43	2.8
	2nd	2.48	2.59	4.36	3.46	2.35	4.0
	3rd	2.50	2.63	4.76	3.74	2.42	-
	4th	2.47	2.61	5.52	4.65	3.23	4.0
	5th	2.44	2.68	8.82	8.69	5.61	3.6
	6th	2.37	2.55	6.91	6.45	5.22	4.8

Table B20. LRD04 IH35 #5 Field Core (Shoulder)

Cons.: 2007		Bulk S.G.	Maximum S.G.	Total Air Voids (vol. %)	Accessible A.V. (vol. %)		Binder Content (wt. %)
					Corelok	SSD	
1st Core (06/2008)	1st	2.30	2.36	2.62	2.42	1.56	Average
	2nd	2.30	2.36	2.50	2.02	2.06	3.2

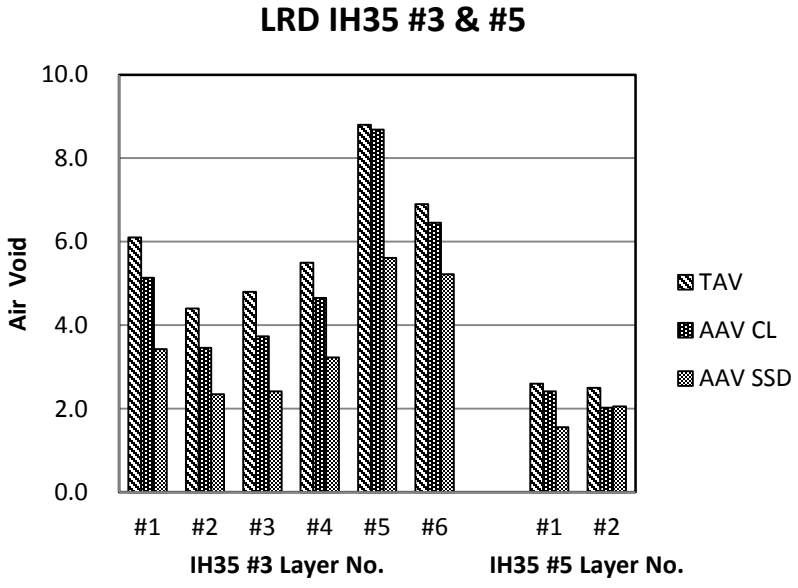

Table B21. LRD US277 Field Core (Wheel Path)

Cons.: 2008		Bulk S.G.	Maximum S.G.	Total Air Voids (vol. %)	Accessible A.V. (vol. %)		Binder Content (wt. %)
					Corelok	SSD	
1st Core (07/2008)	1st	2.33	2.56	8.99	7.40	6.15	2.8
	2nd	2.36	2.56	7.95	6.62	6.22	4.4
	3rd	2.34	2.57	8.78	7.18	6.60	4.0
	4th	2.31	2.55	9.24	8.40	7.76	4.0
	5th	2.29	2.53	9.36	8.36	7.97	6.0
2nd Core (12/2009)	1st	2.33	2.53	8.03	5.54	2.84	4.0
	2nd	2.35	2.55	7.69	6.12	4.18	3.6
	3rd	2.30	2.55	9.65	8.30	7.07	3.6
	4th	2.30	2.47	6.61	4.92	3.38	5.2
3rd Core (12/2010)	1st	2.39	2.56	6.81	3.97	2.82	3.6
	2nd	2.36	2.56	7.60	4.65	2.97	3.9
	3rd	2.37	2.56	7.60	4.74	4.29	3.6
	4th	2.32	2.55	9.15	7.49	6.46	3.4
4th Core (01/2012)	1st	2.19	2.34	6.78	3.36	2.99	-
	2nd	2.38	2.59	8.76	4.94	3.67	
	3rd	2.37	2.57	8.48	4.29	3.21	
	4th	2.34	2.55	8.97	5.91	5.59	
2nd Core Seal coat Treated (12/2009)	Seal coat and 1st layer	2.20	2.47	11.09	5.84	3.11	4.4
	2nd	2.31	2.54	9.20	7.66	5.32	4.0
	3rd	2.30	2.55	9.66	8.68	7.66	4.0
	4th	2.30	2.55	9.80	9.34	9.11	3.6
	5th	2.25	2.51	10.40	7.83	6.19	4.0
3rd Core Seal coat Treated (12/2010)	Seal coat and 1st layer	2.25	2.52	10.80	4.00	2.92	3.9
	2nd	2.30	2.56	10.24	8.11	7.31	3.4
	3rd	2.30	2.54	9.67	8.77	7.95	3.5
	4th	2.21	2.55	13.52	12.49	10.04	3.1
	5th	2.23	2.49	10.43	8.08	5.43	3.7
4th Core Seal coat Treated (01/2012)	Seal coat and 1st layer	2.13	2.28	7.25	4.02	2.58	-
	2nd	2.36	2.56	8.59	3.90	2.79	
	3rd	2.36	2.55	8.08	4.59	4.05	

Table B22. LRD US277 Field Core (Shoulder)

Cons.: 2008		Bulk S.G.	Maximum S.G.	Total Air Voids (vol. %)	Accessible A.V. (vol. %)		Binder Content (wt. %)
					Corelok	SSD	
1st Core (07/2008)	1st	2.28	2.56	10.83	9.22	7.88	4.0
	2nd	2.35	2.55	7.85	6.97	6.53	4.0
	3rd	2.33	2.55	8.50	7.68	7.43	4.0
	4th	2.32	2.55	8.83	7.86	7.73	4.0
	5th	2.33	2.49	6.40	5.33	5.02	6.0
2nd Core (12/2009)	1st	2.28	2.56	10.64	9.91	6.04	3.2
	2nd	2.39	2.56	6.48	5.28	4.18	2.8
	3rd	2.39	2.55	6.23	5.07	4.31	3.6
	4th	2.36	2.53	7.08	6.83	5.51	3.6
	5th	2.35	2.52	6.61	6.09	5.56	4.4
3rd Core (12/2010)	1st	2.32	2.56	9.29	8.10	7.36	3.6
	2nd	2.36	2.56	7.62	5.01	4.28	3.6
	3rd	2.34	2.55	8.17	6.00	5.18	3.6
	4th	2.26	2.43	7.04	5.74	4.98	5.7
4th Core (01/2012)	1st	2.33	2.57	10.22	7.25	5.34	
	2nd	2.37	2.57	8.18	5.06	3.79	-
	3rd	2.39	2.55	6.66	4.07	3.38	

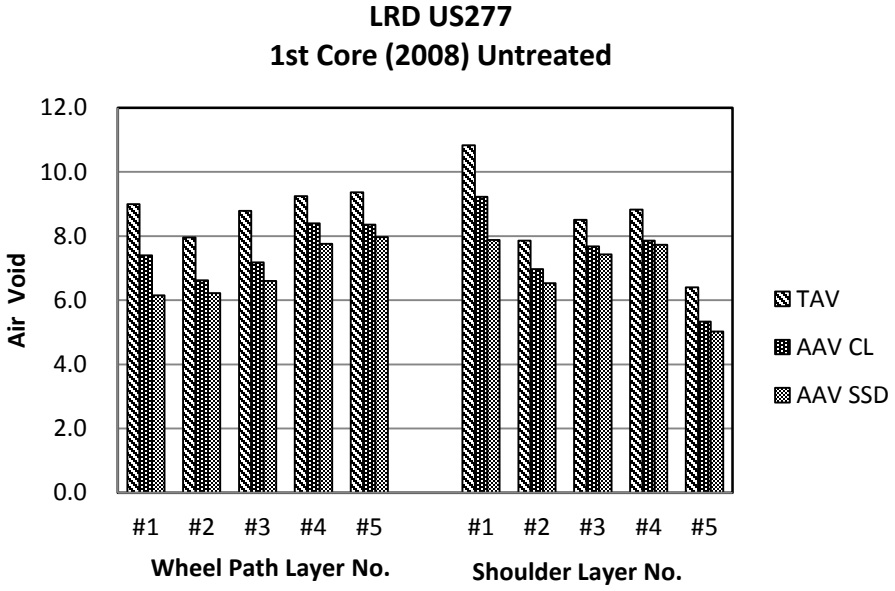
LRD US277
1st Core (2008) Untreated
12.0
10.0
8.0
6.0
4.0
2.0
0.0
Air Void
#1 #2 #3 #4 #5
Wheel Path Layer No.
#1 #2 #3 #4 #5
Shoulder Layer No.
TAV
AAV CL
AAV SSD

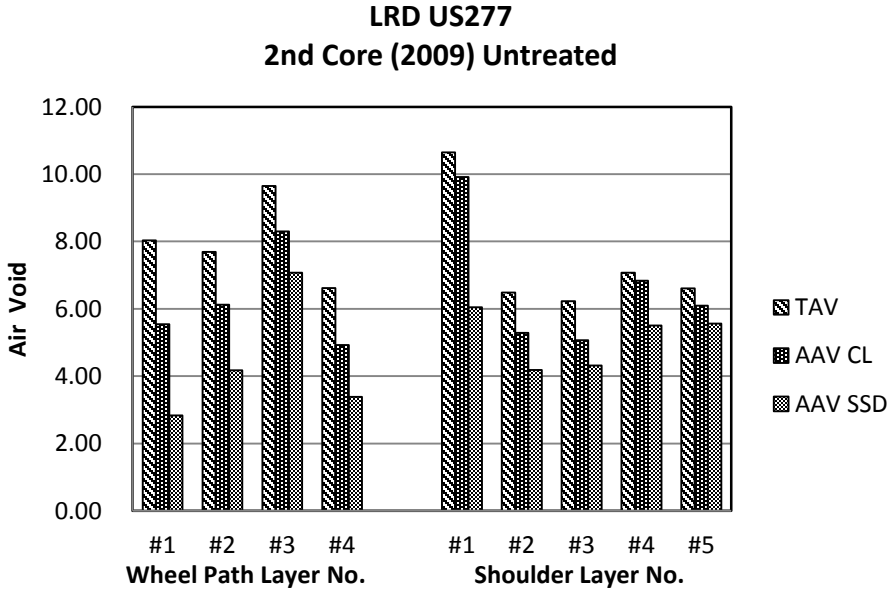
LRD US277
2nd Core (2009) Untreated
12.00
10.00
8.00
6.00
4.00
2.00
0.00
Air Void
#1 #2 #3 #4
Wheel Path Layer No.
#1 #2 #3 #4 #5
Shoulder Layer No.
TAV
AAV CL
AAV SSD

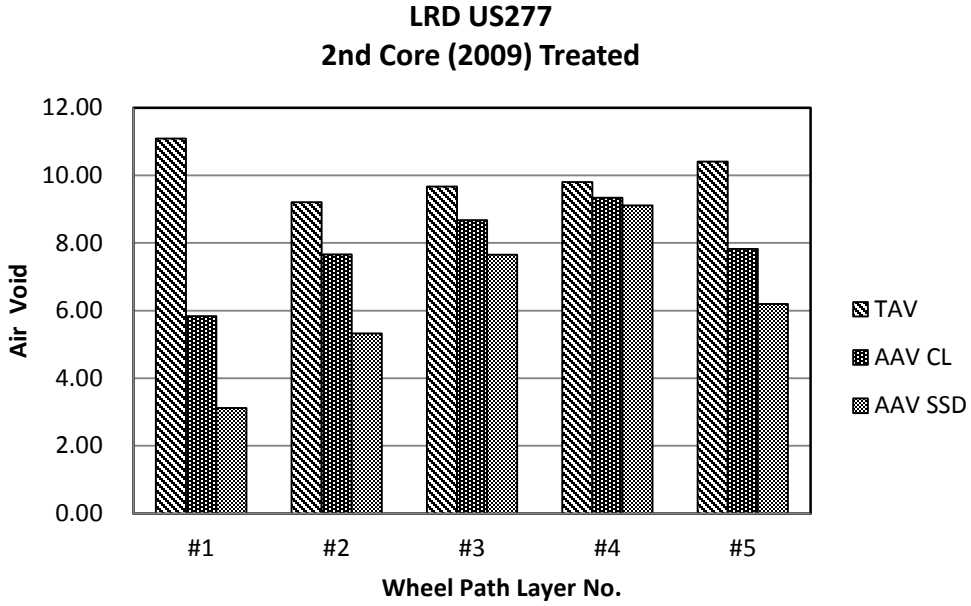
LRD US277
2nd Core (2009) Treated
12.00
10.00
8.00
6.00
4.00
2.00
0.00
Air Void
#1
#2
#3
#4
#5
Wheel Path Layer No.
TAV
AAV CL
AAV SSD

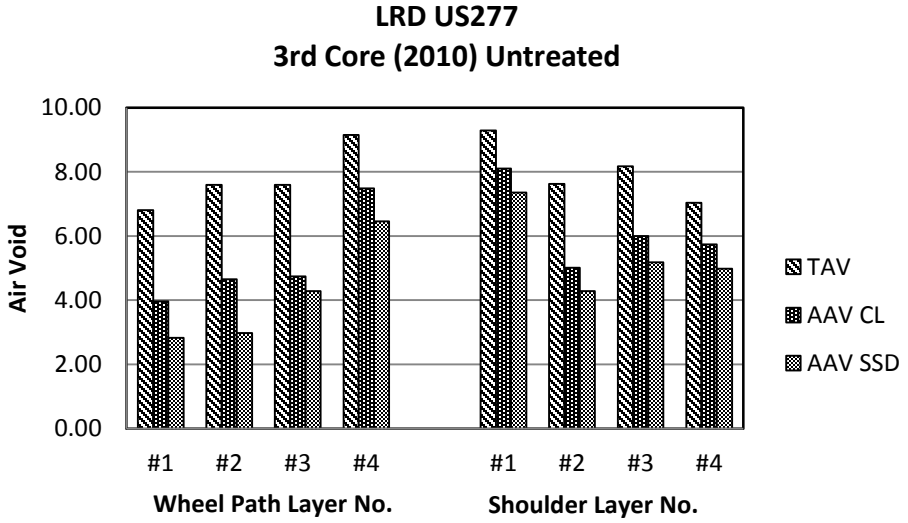
LRD US277
3rd Core (2010) Untreated
10.00
8.00
6.00
4.00
2.00
0.00
Air Void
#1
#2
#3
#4
#1
#2
#3
#4
Wheel Path Layer No.
Shoulder Layer No.
TAV
AAV CL
AAV SSD

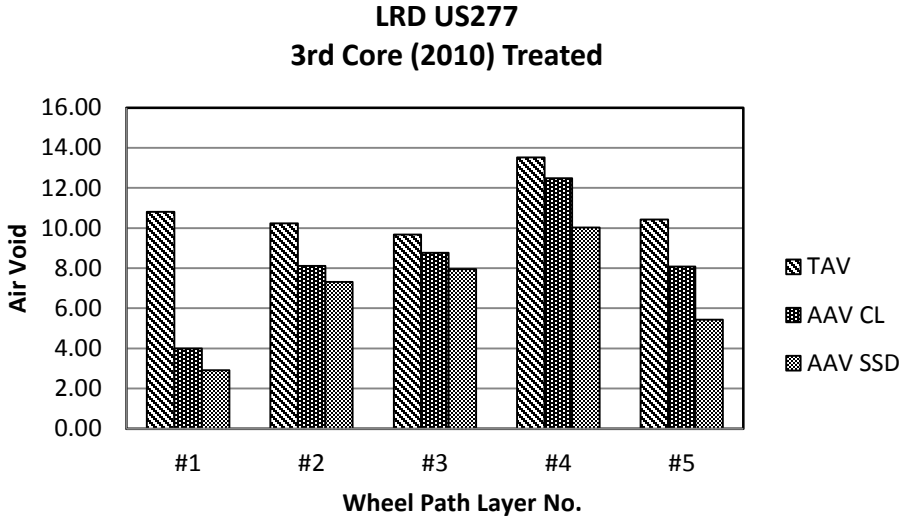
LRD US277
3rd Core (2010) Treated
16.00
14.00
12.00
10.00
8.00
6.00
4.00
2.00
0.00
Air Void
#1
#2
#3
#4
#5
Wheel Path Layer No.
TAV
AAV CL
AAV SSD

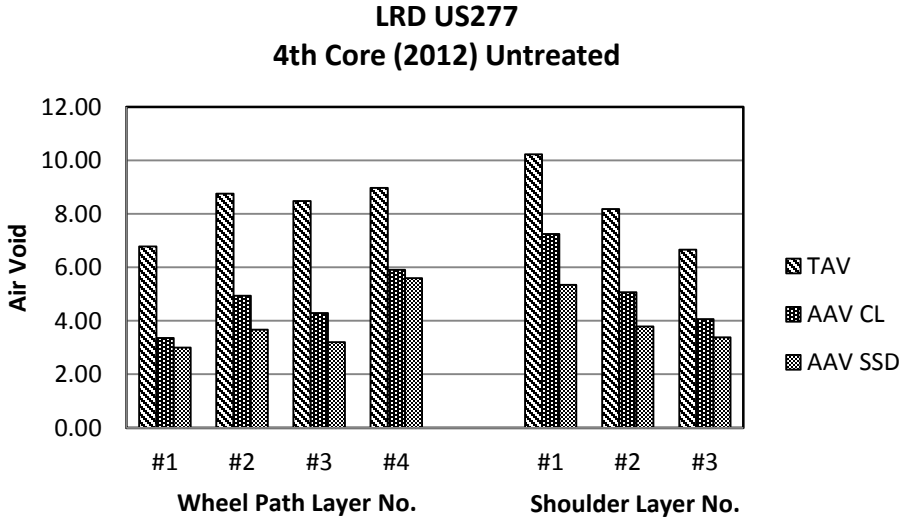
LRD US277
4th Core (2012) Untreated
12.00
10.00
8.00
6.00
4.00
2.00
0.00
Air Void
#1
#2
#3
#4
#1
#2
#3
Wheel Path Layer No.
Shoulder Layer No.
TAV
AAV CL
AAV SSD

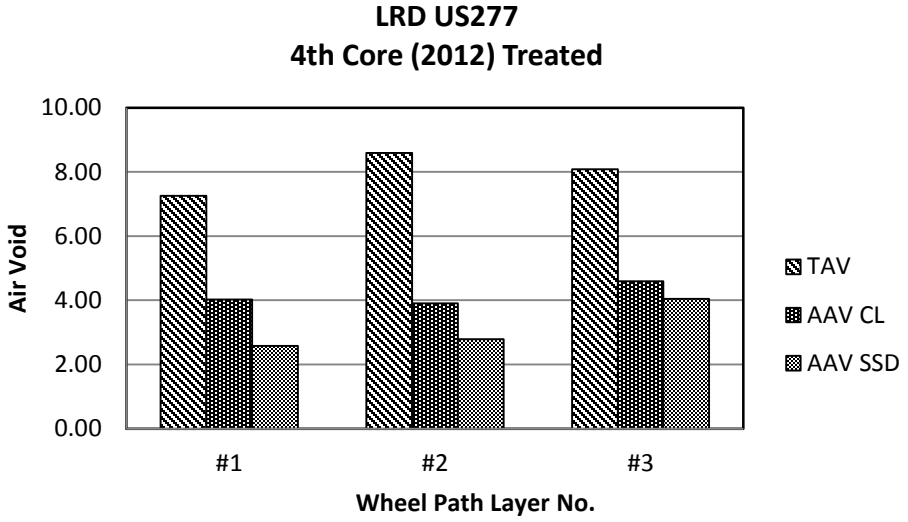
LRD US277
4th Core (2012) Treated
10.00
8.00
6.00
4.00
2.00
0.00
Air Void
#1
#2
#3
Wheel Path Layer No.
TAV
AAV CL
AAV SSD

Table B23. MnRoad Field Core

Cons.: Unknown		Bulk S.G.	Maximum S.G.	Total Air Voids (vol. %)	Accessible A.V. (vol. %)		Binder Content (wt. %)
					Corelok	SSD	
1st Core (Wheel Path) (11/2008)	1st	2.27	2.47	7.97	6.69	2.98	4.0
	2nd	2.33	2.45	4.71	2.71	2.04	4.8
	3rd	2.33	2.44	4.45	2.77	2.01	4.8
	4th	2.30	2.45	6.39	4.56	3.44	4.4
	5th	2.29	2.42	5.35	4.64	3.62	4.0
	6th	2.26	2.44	7.46	6.11	4.04	4.4
	7th	2.30	2.47	6.88	6.43	5.37	4.0
	8th	2.28	2.47	7.59	6.94	6.11	4.0
	9th	2.24	2.47	9.53	9.45	6.51	4.3
2nd Core (Wheel Path) (2010)	1st	2.27	2.45	7.57	5.02	2.41	5.0
	2nd	2.34	2.45	4.58	1.91	0.87	4.8
	3rd	2.31	2.48	6.99	3.73	3.05	4.9
	4th	2.24	2.45	8.36	3.51	1.03	5.3
	5th	2.26	2.48	8.59	5.95	4.24	4.9
	6th	2.27	2.46	7.97	5.50	4.48	5.1
	7th	2.18	2.49	12.68	11.44	7.78	4.9
2nd Core (Shoulder) (2010)	1st	2.26	2.48	8.80	6.21	4.68	4.9
	2nd	2.29	2.44	6.19	3.10	2.13	5.2
	3rd	2.28	2.45	7.10	5.01	4.17	5.0
	4th	2.29	2.47	7.45	6.58	6.01	4.8
	5th	2.32	2.49	6.76	5.79	5.71	5.0
	6th	2.32	2.49	7.06	5.83	5.52	4.5
	7th	2.33	2.50	7.08	6.85	6.03	4.0
	8th	2.23	2.53	12.14	11.83	7.85	4.1

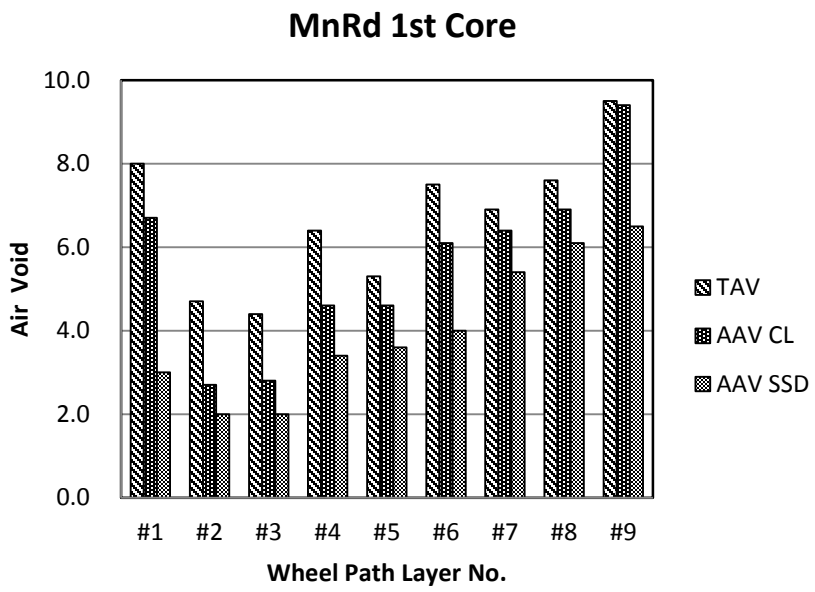
MnRd 1st Core
10.0
8.0
6.0
4.0
2.0
0.0
Air Void
#1
#2
#3
#4
#5
#6
#7
#8
#9
Wheel Path Layer No.
TAV
AAV CL
AAV SSD

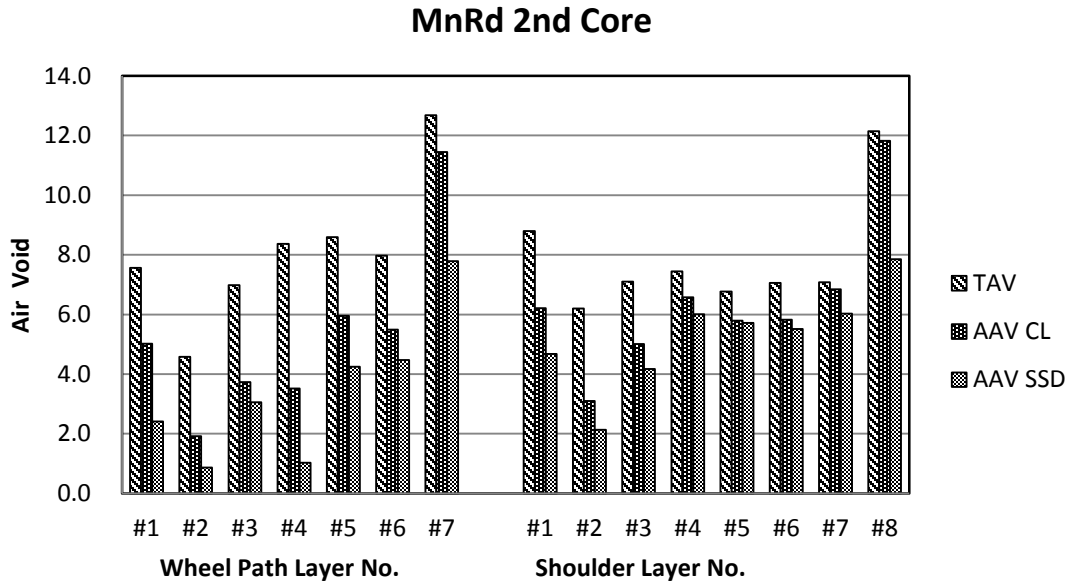
MnRd 2nd Core
14.0
12.0
10.0
8.0
6.0
4.0
2.0
0.0
Air Void
#1
#2
#3
#4
#5
#6
#7
Wheel Path Layer No.
#1
#2
#3
#4
#5
#6
#7
#8
Shoulder Layer No.
TAV
AAV CL
AAV SSD

Table B24. ODA FM1936 Field Core (Wheel Path)

Cons.: 2002		Bulk S.G.	Maximum S.G.	Total Air Voids (vol. %)	Accessible A.V. (vol. %)		Binder Content (wt. %)
					Corelok	SSD	
1st Core (05/2008)	1st	2.16	2.33	7.19	5.56	1.99	2.4
	2nd	2.26	2.34	3.53	1.76	1.06	6.0
	3rd	2.26	2.34	3.19	2.11	1.35	5.6
	4th	2.26	2.32	2.45	1.69	1.12	6.0

Table B25. ODA FM1936 Field Core (Shoulder)

Cons.: 2002		Bulk S.G.	Maximum S.G.	Total Air Voids (vol. %)	Accessible A.V. (vol. %)		Binder Content (wt. %)
					Corelok	SSD	
1st Core (05/2008)	1st	2.09	2.38	12.47	10.81	5.83	5.2
	2nd	2.21	2.34	5.90	4.76	2.90	6.0
	3rd	2.25	2.34	3.96	2.63	1.53	6.0
	4th	2.23	2.35	4.90	3.39	2.70	5.6

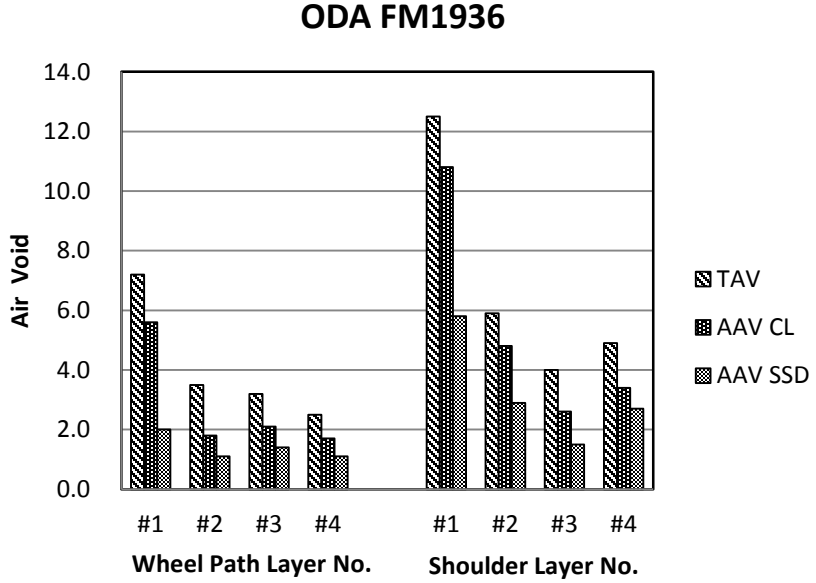

Table B26. PHR FM2994 Field Core (Wheel Path)

Cons.: 2002		Bulk S.G.	Maximum S.G.	Total Air Voids (vol. %)	Accessible A.V. (vol. %)		Binder Content (wt. %)
					Corelok	SSD	
1st Core (05/2008)	1st	2.12	2.44	13.13	11.47	4.37	3.2
	2nd	2.26	2.41	6.13	5.11	3.06	5.2
	3rd	2.23	2.40	6.96	6.33	3.89	4.8
	4th	2.22	2.44	8.89	7.86	4.42	4.8
	5th	2.23	2.40	7.01	6.86	4.49	4.8
	6th	2.21	2.37	6.49	5.49	2.25	4.0

Table B27. PHR FM2994 Field Core (Shoulder)

Cons.: 2002		Bulk S.G.	Maximum S.G.	Total Air Voids (vol. %)	Accessible A.V. (vol. %)		Binder Content (wt. %)
					Corelok	SSD	
1st Core (05/2008)	1st	2.09	2.46	14.84	14.16	8.33	4.4
	2nd	2.19	2.43	9.98	9.45	7.30	4.4
	3rd	2.19	2.45	10.47	10.21	7.34	4.0
	4th	2.13	2.43	12.53	11.93	8.14	4.4
	5th	2.15	2.42	11.11	10.99	7.35	4.4
	6th	2.15	2.41	10.86	11.99	7.38	4.0

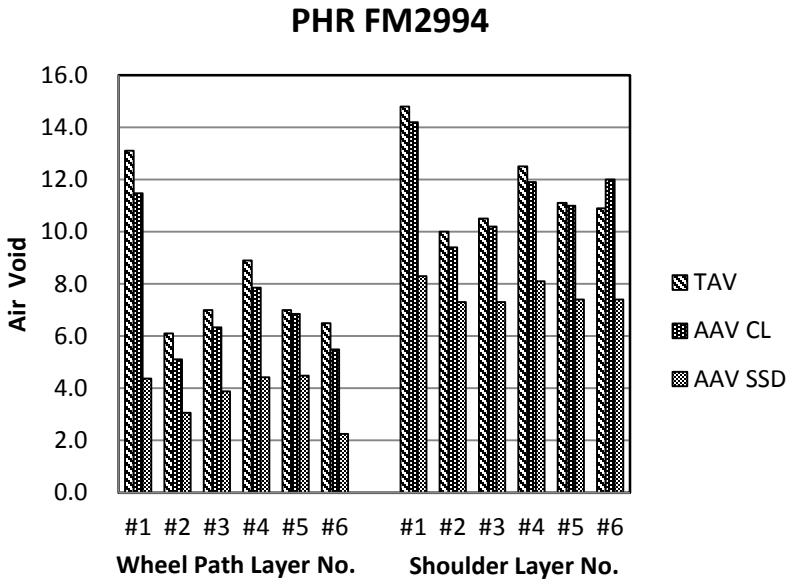
PHR FM2994
16.0
14.0
12.0
10.0
8.0
6.0
4.0
2.0
0.0
Air Void
#1 #2 #3 #4 #5 #6
#1 #2 #3 #4 #5 #6
Wheel Path Layer No.
Shoulder Layer No.
TAV
AAV CL
AAV SSD

Table B28. TYL US259 Field Core (Wheel Path)

Cons.: 2007		Bulk S.G.	Maximum S.G.	Total Air Voids (vol. %)	Accessible A.V. (vol. %)		Binder Content (wt. %)
					Corelok	SSD	
1st Core (07/2008)	1st	2.34	2.51	6.79	5.89	4.67	Average 3.1
	2nd	2.31	2.51	7.93	7.33	6.78	
	3rd	2.06	2.38	13.10	7.75	6.91	
	4th	2.22	2.51	11.58	10.98	8.19	

Table B29. TYL US259 Field Core (Shoulder)

Cons.: 2007		Bulk S.G.	Maximum S.G.	Total Air Voids (vol. %)	Accessible A.V. (vol. %)		Binder Content (wt. %)
					Corelok	SSD	
1st Core (07/2008)	1st	2.26	2.51	9.82	9.66	7.36	-
	2nd	2.35	2.50	6.02	5.32	5.18	
	3rd	2.32	2.51	7.43	6.42	5.94	

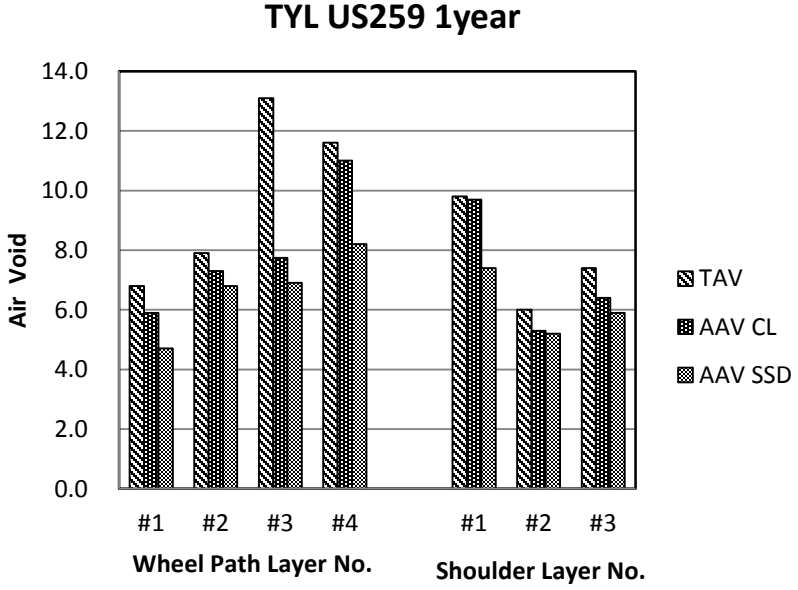

Table B30. WAC IH35 Field Core (Wheel Path)

Cons.: 2003		Bulk S.G.	Maximum S.G.	Total Air Voids (vol. %)	Accessible A.V. (vol. %)		Binder Content (wt. %)
					Corelok	SSD	
1st Core (08/2008)	1st	2.28	2.47	7.58	6.63	5.97	Average 4.4
	2nd	2.29	2.43	5.96	6.31	5.10	
	3rd	2.25	2.43	7.11	7.19	6.40	
	4th	2.28	2.44	6.61	6.08	5.50	
	5th	2.30	2.46	6.57	5.51	4.65	
	6th	2.29	2.44	6.19	5.99	4.98	

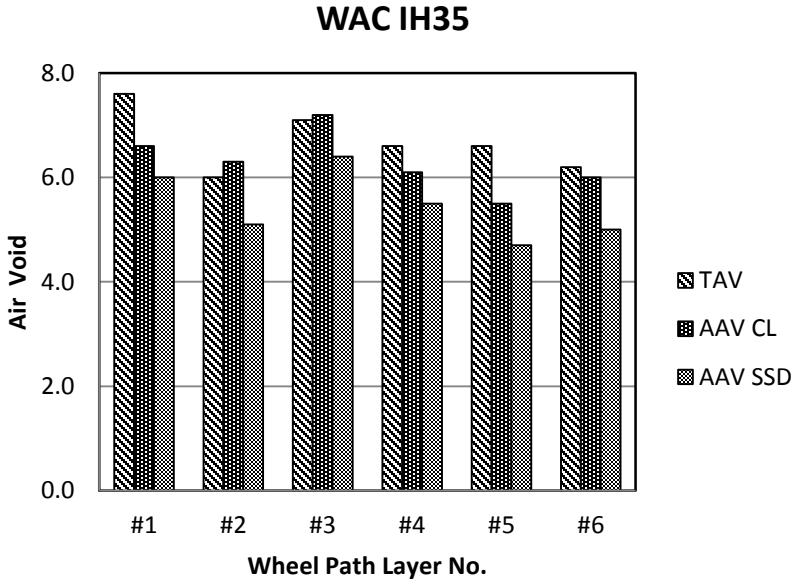

Table B31. WFS US59 Field Core (Wheel Path)

Cons.: 2007		Bulk S.G.	Maximum S.G.	Total Air Voids (vol. %)	Accessible A.V. (vol. %)		Binder Content (wt. %)
					Corelok	SSD	
1st Core (07/2008)	1st	2.23	2.52	11.52	10.46	7.61	Average 4.0
	2nd	2.30	2.51	8.35	7.65	7.15	
	3rd	2.32	2.49	6.91	6.76	6.32	
	4th	2.32	2.48	6.48	6.77	6.04	
	5th	2.24	2.51	10.62	8.75	5.30	

Table B32. WFS US59 Field Core (Shoulder)

Cons.: 2007		Bulk S.G.	Maximum S.G.	Total Air Voids (vol. %)	Accessible A.V. (vol. %)		Binder Content (wt. %)
					Corelok	SSD	
1st Core (07/2008)	1st	2.20	2.52	12.58	12.08	9.26	Average 3.6
	2nd	2.27	2.50	9.30	9.18	8.31	
	3rd	2.26	2.51	9.92	10.01	8.93	

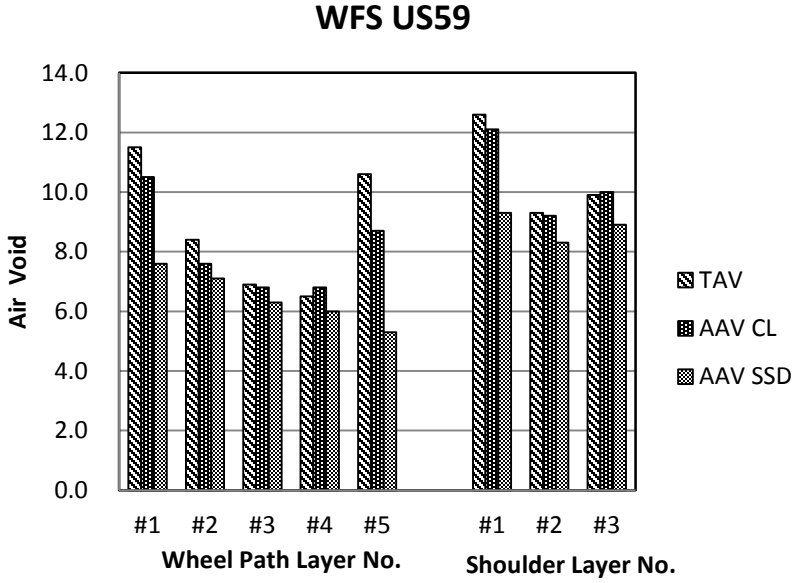

Table B33. YKM SH36 Field Core (Wheel Path)

Cons.: 2006		Bulk S.G.	Maximum S.G.	Total Air Voids (vol. %)	Accessible A.V. (vol. %)		Binder Content (wt. %)
					Corelok	SSD	
1st Core (06/2008)	1st	2.31	2.46	6.20	4.32	2.82	4.4
	2nd	2.35	2.44	3.54	3.07	2.51	4.0
	3rd	2.37	2.47	3.86	2.75	2.05	4.0
	4th	2.35	2.45	4.00	3.58	2.89	4.0

Table B34. YKM SH36 Field Core (Shoulder)

Cons.: 2006		Bulk S.G.	Maximum S.G.	Total Air Voids (vol. %)	Accessible A.V. (vol. %)		Binder Content (wt. %)
					Corelok	SSD	
1st Core (06/2008)	1st	2.19	2.46	10.99	10.48	8.27	4.4
	2nd	2.27	2.44	7.12	7.57	6.75	4.0
	3rd	2.27	2.45	7.35	7.40	6.20	4.0
	4th	2.23	2.44	8.44	9.02	7.21	4.8

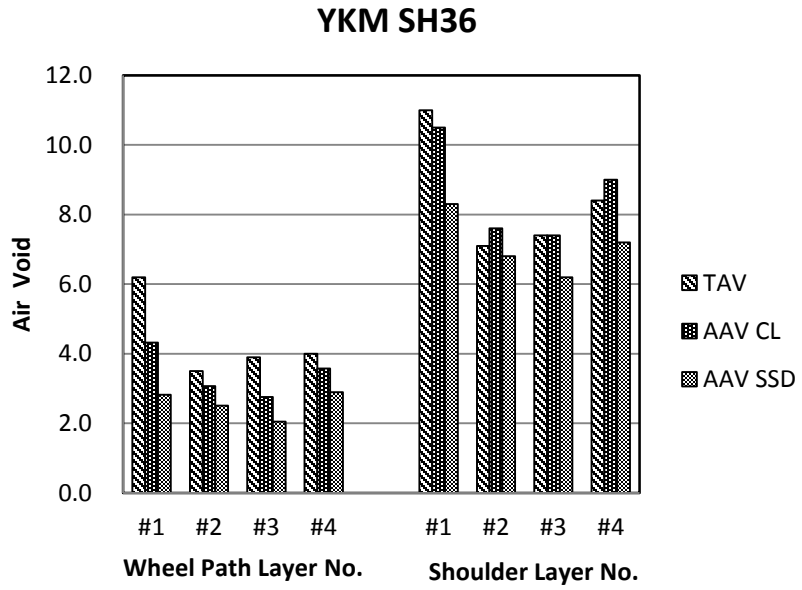

APPENDIX C

TABLES OF LMLC MIXTURE PROPERTY DATA

Table C1. HMAC LMLC Mixture Property Data (LRD US 277)

Sample #	SITE	Mix Type	Aggregate Material	Environmental Zone	Age (months)	BIND-ER CON-TENT (wt. %)	AV (vol. %)	FILM THICK NESS (microns)	DSR Function (MPa/s)	CA
1-1	**Laredo**	**Type C**	**Limestone w/TR Screening**	**DW**	**0**	4.0	3.8	5.1	2.34E-04	0.908
1-2	**Laredo**	**Type C**	**Limestone w/TR Screening**	**DW**	**0**	-	3.2	5.1	-	-
2-1	**Laredo**	**Type C**	**Limestone w/TR Screening**	**DW**	**0**	4.0	9.4	5.1	5.12E-04	0.949
2-2	**Laredo**	**Type C**	**Limestone w/TR Screening**	**DW**	**0**	-	8.5	5.1	-	-
3-1	**Laredo**	**Type C**	**Limestone w/TR Screening**	**DW**	**0**	5.0	5.5	6.9	1.84E-04	0.940
3-2	**Laredo**	**Type C**	**Limestone w/TR Screening**	**DW**	**0**	-	5.3	6.9	-	-

Table C1. HMAC LMLC Mixture Property Data (LRD US 277) (Continued)

Sample #	SITE	Mix Type	Aggregate Material	Environmental Zone	Age (months)	BINDER CONTENT (wt. %)	AV (vol. %)	FILM THICKNESS(microns)	DSR Function (MPa/s)	CA
4-1	**Laredo**	**Type C**	**Limestone w/TR Screening**	**DW**	**0**	5.0	8.1	6.9	8.13E-05	0.862
4-2	**Laredo**	**Type C**	**Limestone w/TR Screening**	**DW**	**0**	-	9.1	6.9	-	-
5-1	**Laredo**	**Type C**	**Limestone w/TR Screening**	**DW**	**0**	5.0	3.1	6.9	6.34E-05	0.826
5-2	**Laredo**	**Type C**	**Limestone w/TR Screening**	**DW**	**0**	-	2.9	6.9	-	-
6-1	**Laredo**	**Type C**	**Limestone w/TR Screening**	**DW**	**0**	4.5	5.6	6.0	4.03E-04	0.916
6-2	**Laredo**	**Type C**	**Limestone w/TR Screening**	**DW**	**0**	-	5.7	6.0	-	-

Table C1. HMAC LMLC Mixture Property Data (LRD US 277) (Continued)

Sample #	SITE	Mix Type	Aggregate Material	Environmental Zone	Age (months)	BINDER CONTENT (wt. %)	AV (vol. %)	FILM THICKNESS(microns)	DSR Function (MPa/s)	CA
7-1	**Laredo**	**Type C**	**Limestone w/TR Screening**	**DW**	**0**	4.5	9.3	6.0	3.69E-04	0.877
7-2	**Laredo**	**Type C**	**Limestone w/TR Screening**	**DW**	**0**	-	9.0	6.0	-	-
8-1	**Laredo**	**Type C**	**Limestone w/TR Screening**	**DW**	**6**	x	8.4	5.1	1.12E-03	1.202
8-2	**Laredo**	**Type C**	**Limestone w/TR Screening**	**DW**	**6**	-	8.2	5.1	-	-
9-1	**Laredo**	**Type C**	**Limestone w/TR Screening**	**DW**	**6**	4.0	5.5	5.1	6.90E-04	1.244
9-2	**Laredo**	**Type C**	**Limestone w/TR Screening**	**DW**	**6**	-	5.7	5.1	-	-

Table C1. HMAC LMLC Mixture Property Data (LRD US 277) (Continued)

Sample #	SITE	Mix Type	Aggregate Material	Environmental Zone	Age (months)	BINDER CONTENT (wt. %)	AV (vol. %)	FILM THICKNESS(microns)	DSR Function (MPa/s)	CA
10-1	**Laredo**	**Type C**	**Limestone w/TR Screening**	**DW**	**6**	5.0	3.2	6.9	6.11E-04	1.088
10-2	**Laredo**	**Type C**	**Limestone w/TR Screening**	**DW**	**6**	-	3.0	6.9	-	-
11-1	**Laredo**	**Type C**	**Limestone w/TR Screening**	**DW**	**6**	5.0	5.7	6.9	5.78E-04	1.179
11-2	**Laredo**	**Type C**	**Limestone w/TR Screening**	**DW**	**6**	-	5.4	6.9	-	-
12-1	**Laredo**	**Type C**	**Limestone w/TR Screening**	**DW**	**6**	4.5	8.4	6.0	1.01E-03	1.204
12-2	**Laredo**	**Type C**	**Limestone w/TR Screening**	**DW**	**6**	-	8.7	6.0	-	-

Table C1. HMAC LMLC Mixture Property Data (LRD US 277) (Continued)

Sample #	SITE	Mix Type	Aggregate Material	Environmental Zone	Age (months)	BINDER CONTENT (wt. %)	AV (vol. %)	FILM THICKNESS(microns)	DSR Function (MPa/s)	CA
13-1	**Laredo**	**Type C**	**Limestone w/TR Screening**	**DW**	**6**	4.5	2.5	6.0	5.75E-04	1.123
13-2	**Laredo**	**Type C**	**Limestone w/TR Screening**	**DW**	**6**	-	2.8	6.0	-	-
14-1	**Laredo**	**Type C**	**Limestone w/TR Screening**	**DW**	**6**	4.5	5.6	6.0	1.05E-03	1.235
14-2	**Laredo**	**Type C**	**Limestone w/TR Screening**	**DW**	**6**	-	5.7	6.0	-	-
15-1	**Laredo**	**Type C**	**Limestone w/TR Screening**	**DW**	**6**	4.0	8.3	5.1	1.20E-03	1.206
15-2	**Laredo**	**Type C**	**Limestone w/TR Screening**	**DW**	**6**	-	8.5	5.1	-	-

Table C1. HMAC LMLC Mixture Property Data (LRD US 277) (Continued)

Sample #	SITE	Mix Type	Aggregate Material	Environmental Zone	Age (months)	BINDER CONTENT (wt. %)	AV (vol. %)	FILM THICKNESS(microns)	DSR Function (MPa/s)	CA
16-1	**Laredo**	**Type C**	**Limestone w/TR Screening**	**DW**	**6**	4.0	5.5	5.1	1.44E-03	1.247
16-2	**Laredo**	**Type C**	**Limestone w/TR Screening**	**DW**	**6**	-	5.8	5.1	-	-
17-1	**Laredo**	**Type C**	**Limestone w/TR Screening**	**DW**	**6**	5.0	6.2	6.9	1.34E-03	1.276
17-2	**Laredo**	**Type C**	**Limestone w/TR Screening**	**DW**	**6**	-	6.1	6.9	-	-
18-1	**Laredo**	**Type C**	**Limestone w/TR Screening**	**DW**	**9**	5.0	2.6	6.9	9.87E-04	1.174
18-2	**Laredo**	**Type C**	**Limestone w/TR Screening**	**DW**	**9**	-	2.8	6.9	-	-

Table C1. HMAC LMLC Mixture Property Data (LRD US 277) (Continued)

Sample #	SITE	Mix Type	Aggregate Material	Environmental Zone	Age (months)	BINDER CONTENT (wt. %)	AV (vol. %)	FILM THICKNESS(microns)	DSR Function (MPa/s)	CA
19-1	**Laredo**	**Type C**	**Limestone w/TR Screening**	**DW**	**9**	5.0	8.7	6.9	9.19E-04	1.278
19-2	**Laredo**	**Type C**	**Limestone w/TR Screening**	**DW**	**9**	-	8.2	6.9	-	-
20-1	**Laredo**	**Type C**	**Limestone w/TR Screening**	**DW**	**9**	4.5	5.8	6.0	1.33E-03	1.256
20-2	**Laredo**	**Type C**	**Limestone w/TR Screening**	**DW**	**9**	-	5.5	6.0	-	-
21-1	**Laredo**	**Type C**	**Limestone w/TR Screening**	**DW**	**12**	4.0	5.5	5.1	2.07E-03	1.379
21-2	**Laredo**	**Type C**	**Limestone w/TR Screening**	**DW**	**12**	-	6.0	5.1	-	-

Table C1. HMAC LMLC Mixture Property Data (LRD US 277) (Continued)

Sample #	SITE	Mix Type	Aggregate Material	Environmental Zone	Age (months)	BINDER CONTENT (wt. %)	AV (vol. %)	FILM THICKNESS(microns)	DSR Function (MPa/s)	CA
22-1	**Laredo**	**Type C**	**Limestone w/TR Screening**	**DW**	**12**	4.0	3.1	5.1	2.10E-03	1.289
22-2	**Laredo**	**Type C**	**Limestone w/TR Screening**	**DW**	**12**	-	3.0	5.1	-	-
23-1	**Laredo**	**Type C**	**Limestone w/TR Screening**	**DW**	**12**	5.0	2.8	6.9	1.41E-03	1.270
23-2	**Laredo**	**Type C**	**Limestone w/TR Screening**	**DW**	**12**	-	3.1	6.9	-	-
24-1	**Laredo**	**Type C**	**Limestone w/TR Screening**	**DW**	**12**	5.0	9.0	6.9	1.25E-03	1.343
24-2	**Laredo**	**Type C**	**Limestone w/TR Screening**	**DW**	**12**	-	8.3	6.9	-	-

Table C1. HMAC LMLC Mixture Property Data (LRD US 277) (Continued)

Sample #	SITE	Mix Type	Aggregate Material	Environmental Zone	Age (months)	BINDER CONTENT (wt. %)	AV (vol. %)	FILM THICKNESS(microns)	DSR Function (MPa/s)	CA
25-1	**Laredo**	**Type C**	**Limestone w/TR Screening**	**DW**	**12**	4.5	3.2	6.0	2.29E-03	1.278
25-2	**Laredo**	**Type C**	**Limestone w/TR Screening**	**DW**	**12**	-	3.3	6.0	-	-
26-1	**Laredo**	**Type C**	**Limestone w/TR Screening**	**DW**	**12**	4.5	8.5	6.0	1.98E-03	1.311
26-2	**Laredo**	**Type C**	**Limestone w/TR Screening**	**DW**	**12**	-	8.6	6.0	-	-
27-1	**Laredo**	**Type C**	**Limestone w/TR Screening**	**DW**	**12**	4.5	5.8	6.0	3.05E-03	1.351
27-2	**Laredo**	**Type C**	**Limestone w/TR Screening**	**DW**	**12**	-	5.2	6.0	-	-

Table C2. HMAC LMLC Mixture Property Data (CHS US 83)

Sample #	SITE	Mix Type	Aggregate Material	Environmental Zone	Age (months)	BINDER CONTENT (wt. %)	AV (vol. %)	FILM THICKNESS(microns)	DSR Function (MPa/s)	CA
1-1	**Childress**	**Type D**	**Granite**	**DC**	**0**	4.8	2.7	8.8	8.36E-05	0.975
1-2	**Childress**	**Type D**	**Granite**	**DC**	**0**	-	2.5	8.8	-	-
2-1	**Childress**	**Type D**	**Granite**	**DC**	**0**	4.8	9.5	8.8	1.06E-04	1.068
2-2	**Childress**	**Type D**	**Granite**	**DC**	**0**	-	8.9	8.8	-	-
3-1	**Childress**	**Type D**	**Granite**	**DC**	**0**	5.8	5.9	10.7	8.26E-05	0.931
3-2	**Childress**	**Type D**	**Granite**	**DC**	**0**	-	6.7	10.7	-	-
4-1	**Childress**	**Type D**	**Granite**	**DC**	**0**	5.8	9.8	10.7	7.54E-05	0.951
4-2	**Childress**	**Type D**	**Granite**	**DC**	**0**	-	9.2	10.7	-	-
5-1	**Childress**	**Type D**	**Granite**	**DC**	**0**	5.8	3.6	10.7	1.61E-04	0.931
5-2	**Childress**	**Type D**	**Granite**	**DC**	**0**	-	3.5	10.7	-	-
6-1	**Childress**	**Type D**	**Granite**	**DC**	**0**	5.3	5.5	9.8	8.47E-05	0.952
6-2	**Childress**	**Type D**	**Granite**	**DC**	**0**	-	6.2	9.8	-	-

Table C2. HMAC LMLC Mixture Property Data (CHS US 83) (Continued)

Sample #	SITE	Mix Type	Aggregate Material	Environmental Zone	Age (months)	BINDER CONTENT (wt. %)	AV (vol. %)	FILM THICKNESS(microns)	DSR Function (MPa/s)	CA
7-1	**Childress**	**Type D**	**Granite**	**DC**	**0**	5.3	9.4	9.8	1.12E-04	1.041
7-2	**Childress**	**Type D**	**Granite**	**DC**	**0**	-	8.9	9.8	-	-
8-2	**Childress**	**Type D**	**Granite**	**DC**	**6**	4.8	9.4	8.8	3.14E-04	1.050
8-4	**Childress**	**Type D**	**Granite**	**DC**	**6**	-	10.4	8.8	-	-
9-3	**Childress**	**Type D**	**Granite**	**DC**	**6**	4.8	6.1	8.8	3.52E-04	1.059
9-4	**Childress**	**Type D**	**Granite**	**DC**	**6**	-	6.2	8.8	-	-
10-3	**Childress**	**Type D**	**Granite**	**DC**	**6**	5.8	3.3	10.7	1.96E-04	0.963
10-4	**Childress**	**Type D**	**Granite**	**DC**	**6**	-	3.2	10.7	-	-
11-2	**Childress**	**Type D**	**Granite**	**DC**	**6**	5.8	6.5	10.7	2.66E-04	1.004
11-4	**Childress**	**Type D**	**Granite**	**DC**	**6**	-	6.6	10.7	-	-
12-3	**Childress**	**Type D**	**Granite**	**DC**	**6**	5.3	11.6	9.8	2.27E-04	0.999
12-4	**Childress**	**Type D**	**Granite**	**DC**	**6**	-	10.3	9.8	-	-

Table C2. HMAC LMLC Mixture Property Data (CHS US 83) (Continued)

Sample #	SITE	Mix Type	Aggregate Material	Environmental Zone	Age (months)	BINDER CONTENT (wt. %)	AV (vol. %)	FILM THICKNESS(microns)	DSR Function (MPa/s)	CA
13-3	**Childress**	**Type D**	**Granite**	**DC**	**6**	5.3	3.3	9.8	2.97E-04	1.045
13-4	**Childress**	**Type D**	**Granite**	**DC**	**6**	-	3.3	9.8	-	-
14-3	**Childress**	**Type D**	**Granite**	**DC**	**6**	5.3	6.0	9.8	1.82E-04	1.075
14-4	**Childress**	**Type D**	**Granite**	**DC**	**6**	-	5.7	9.8	-	-
15-1	**Childress**	**Type D**	**Granite**	**DC**	**6**	4.8	9.8	8.8	2.99E-04	1.177
15-2	**Childress**	**Type D**	**Granite**	**DC**	**6**	-	9.1	8.8	-	-
16-1	**Childress**	**Type D**	**Granite**	**DC**	**6**	4.8	6.3	8.8	4.27E-04	1.191
16-2	**Childress**	**Type D**	**Granite**	**DC**	**6**	-	6.0	8.8	-	-
17-1	**Childress**	**Type D**	**Granite**	**DC**	**6**	5.8	6.0	10.7	3.10E-04	1.092
17-2	**Childress**	**Type D**	**Granite**	**DC**	**6**	-	6.2	10.7	-	-
18-1	**Childress**	**Type D**	**Granite**	**DC**	**9**	5.8	2.9	10.7	3.75E-04	1.055
18-2	**Childress**	**Type D**	**Granite**	**DC**	**9**	-	3.4	10.7	-	-
19-1	**Childress**	**Type D**	**Granite**	**DC**	**9**	5.8	9.3	10.7	2.18E-04	1.085

Table C2. HMAC LMLC Mixture Property Data (CHS US 83) (Continued)

Sample #	SITE	Mix Type	Aggregate Material	Environmental Zone	Age (months)	BINDER CONTENT (wt. %)	AV (vol. %)	FILM THICKNESS(microns)	DSR Function (MPa/s)	CA
19-2	**Childress**	**Type D**	**Granite**	**DC**	**9**	-	8.7	10.7	-	-
20-1	**Childress**	**Type D**	**Granite**	**DC**	**9**	5.3	6.2	9.8	3.41E-04	1.049
20-2	**Childress**	**Type D**	**Granite**	**DC**	**9**	-	6.1	9.8	-	-
21-1	**Childress**	**Type D**	**Granite**	**DC**	**12**	4.8	5.7	8.8	4.42E-04	1.146
21-2	**Childress**	**Type D**	**Granite**	**DC**	**12**	-	6.2	8.8	-	-
22-1	**Childress**	**Type D**	**Granite**	**DC**	**12**	4.8	2.7	8.8	4.16E-04	1.183
22-2	**Childress**	**Type D**	**Granite**	**DC**	**12**	-	2.8	8.8	-	-
23-1	**Childress**	**Type D**	**Granite**	**DC**	**12**	5.8	3.1	10.7	2.53E-04	1.042
23-2	**Childress**	**Type D**	**Granite**	**DC**	**12**	-	2.9	10.7	-	-
24-1	**Childress**	**Type D**	**Granite**	**DC**	**12**	5.8	9.5	10.7	3.99E-04	1.129
24-2	**Childress**	**Type D**	**Granite**	**DC**	**12**	-	9.6	10.7	-	-
25-1	**Childress**	**Type D**	**Granite**	**DC**	**12**	5.3	3.1	9.8	2.93E-04	1.038
25-2	**Childress**	**Type D**	**Granite**	**DC**	**12**	-	2.6	9.8	-	-

Table C2. HMAC LMLC Mixture Property Data (CHS US 83) (Continued)

Sample #	SITE	Mix Type	Aggregate Material	Environmental Zone	Age (months)	BINDER CONTENT (wt. %)	AV (vol. %)	FILM THICKNESS(microns)	DSR Function (MPa/s)	CA
26-1	**Childress**	**Type D**	**Granite**	**DC**	**12**	5.3	10.2	9.8	4.43E-04	1.154
26-2	**Childress**	**Type D**	**Granite**	**DC**	**12**	-	10	9.8	-	-
27-1	**Childress**	**Type D**	**Granite**	**DC**	**12**	5.3	5.8	9.8	4.21E-04	1.130
27-2	**Childress**	**Type D**	**Granite**	**DC**	**12**	-	5.8	9.8	-	-

Table C3. HMAC LMLC Mixture Property Data (PAR SH 24)

Sample #	SITE	Mix Type	Aggregate Material	Environmental Zone	Age (months)	BINDER CONTENT (wt. %)	AV (vol. %)	FILM THICKNESS(microns)	DSR Function (MPa/s)	CA
1-1	**Paris**	**Type D**	**Sandstone**	**WC**	**0**	4.9	3.7	6.6	2.47E-05	0.929
1-2	**Paris**	**Type D**	**Sandstone**	**WC**	**0**	-	3.2	6.6	-	-
2-1	**Paris**	**Type D**	**Sandstone**	**WC**	**0**	4.9	9.8	6.6	6.04E-05	0.998
2-2	**Paris**	**Type D**	**Sandstone**	**WC**	**0**	-	8.3	6.6	-	-
3-1	**Paris**	**Type D**	**Sandstone**	**WC**	**0**	5.9	6.7	8.2	3.63E-05	1.015
3-2	**Paris**	**Type D**	**Sandstone**	**WC**	**0**	-	6.2	8.2	-	-
4-1	**Paris**	**Type D**	**Sandstone**	**WC**	**0**	5.9	9.3	8.2	5.44E-05	1.028
4-2	**Paris**	**Type D**	**Sandstone**	**WC**	**0**	-	9.3	8.2	-	-
5-1	**Paris**	**Type D**	**Sandstone**	**WC**	**0**	5.9	3.3	8.2	2.58E-05	1.007
5-2	**Paris**	**Type D**	**Sandstone**	**WC**	**0**	-	3.4	8.2	-	-
6-1	**Paris**	**Type D**	**Sandstone**	**WC**	**0**	5.4	6.3	7.4	3.84E-05	1.020
6-2	**Paris**	**Type D**	**Sandstone**	**WC**	**0**	-	6.4	7.4	-	-

Table C3. HMAC LMLC Mixture Property Data (PAR SH 24) (Continued)

Sample #	SITE	Mix Type	Aggregate Material	Environmental Zone	Age (months)	BINDER CONTENT (wt. %)	AV (vol. %)	FILM THICKNESS(microns)	DSR Function (MPa/s)	CA
7-1	**Paris**	**Type D**	**Sandstone**	**WC**	**0**	5.4	10.0	7.4	3.41E-05	1.004
7-2	**Paris**	**Type D**	**Sandstone**	**WC**	**0**	-	9.9	7.4	-	-
8-1	**Paris**	**Type D**	**Sandstone**	**WC**	**6**	4.9	10.7	6.6	4.95E-04	1.273
8-2	**Paris**	**Type D**	**Sandstone**	**WC**	**6**	-	10.6	6.6	-	-
9-1	**Paris**	**Type D**	**Sandstone**	**WC**	**6**	4.9	6.9	6.6	6.46E-04	1.349
9-2	**Paris**	**Type D**	**Sandstone**	**WC**	**6**	-	7.4	6.6	-	-
10-1	**Paris**	**Type D**	**Sandstone**	**WC**	**6**	5.9	3.2	8.2	2.47E-04	1.129
10-2	**Paris**	**Type D**	**Sandstone**	**WC**	**6**	-	3.5	8.2	-	-
11-1	**Paris**	**Type D**	**Sandstone**	**WC**	**6**	5.9	7.2	8.2	5.52E-04	x
11-2	**Paris**	**Type D**	**Sandstone**	**WC**	**6**	-	7.0	8.2	-	-
12-1	**Paris**	**Type D**	**Sandstone**	**WC**	**6**	5.4	9.7	7.4	4.26E-04	1.238
12-2	**Paris**	**Type D**	**Sandstone**	**WC**	**6**	-	9.8	7.4	-	-
13-1	**Paris**	**Type D**	**Sandstone**	**WC**	**6**	5.4	3.1	7.4	1.03E-03	1.199

Table C3. HMAC LMLC Mixture Property Data (PAR SH 24) (Continued)

Sample #	SITE	Mix Type	Aggregate Material	Environmental Zone	Age (months)	BINDER CONTENT (wt. %)	AV (vol. %)	FILM THICKNESS(microns)	DSR Function (MPa/s)	CA
13-2	**Paris**	**Type D**	**Sandstone**	**WC**	**6**	-	3.3	7.4	-	-
14-1	**Paris**	**Type D**	**Sandstone**	**WC**	**6**	5.4	7.4	7.4	1.42E-03	1.206
14-2	**Paris**	**Type D**	**Sandstone**	**WC**	**6**	-	7.6	7.4	-	-
15-1	**Paris**	**Type D**	**Sandstone**	**WC**	**6**	4.9	9.1	6.6	1.43E-03	1.428
15-2	**Paris**	**Type D**	**Sandstone**	**WC**	**6**	-	10.4	6.6	-	-
16-1	**Paris**	**Type D**	**Sandstone**	**WC**	**6**	4.9	7.4	6.6	1.04E-03	1.454
16-2	**Paris**	**Type D**	**Sandstone**	**WC**	**6**	-	7.3	6.6	-	-
17-1	**Paris**	**Type D**	**Sandstone**	**WC**	**6**	5.9	7.1	8.2	5.45E-04	1.371
17-2	**Paris**	**Type D**	**Sandstone**	**WC**	**6**	-	7.0	8.2	-	-
18-1	**Paris**	**Type D**	**Sandstone**	**WC**	**9**	5.9	3.4	8.2	8.26E-04	1.485
18-2	**Paris**	**Type D**	**Sandstone**	**WC**	**9**	-	3.8	8.2	-	-
19-1	**Paris**	**Type D**	**Sandstone**	**WC**	**9**	5.9	10.2	8.2	6.98E-04	1.431
19-2	**Paris**	**Type D**	**Sandstone**	**WC**	**9**	-	9.6	8.2	-	-

Table C3. HMAC LMLC Mixture Property Data (PAR SH 24) (Continued)

Sample #	SITE	Mix Type	Aggregate Material	Environmental Zone	Age (months)	BINDER CONTENT (wt. %)	AV (vol. %)	FILM THICKNESS(microns)	DSR Function (MPa/s)	CA
20-1	**Paris**	**Type D**	**Sandstone**	**WC**	**9**	5.4	8.5	7.4	5.67E-04	1.264
20-2	**Paris**	**Type D**	**Sandstone**	**WC**	**9**	-	7.0	7.4	-	-
21-1	**Paris**	**Type D**	**Sandstone**	**WC**	**12**	4.9	6.8	6.6	4.56E-04	1.423
21-2	**Paris**	**Type D**	**Sandstone**	**WC**	**12**	-	6.7	6.6	-	-
22-1	**Paris**	**Type D**	**Sandstone**	**WC**	**12**	4.9	3.4	8.2	8.29E-04	1.444
22-2	**Paris**	**Type D**	**Sandstone**	**WC**	**12**	-	3.9	8.2	-	-
23-1	**Paris**	**Type D**	**Sandstone**	**WC**	**12**	5.9	2.9	8.2	3.39E-04	1.334
23-2	**Paris**	**Type D**	**Sandstone**	**WC**	**12**	-	3.2	8.2	-	-
24-1	**Paris**	**Type D**	**Sandstone**	**WC**	**12**	5.9	10.5	8.2	9.74E-04	1.372
24-2	**Paris**	**Type D**	**Sandstone**	**WC**	**12**	-	9.9	8.2	-	-
25-1	**Paris**	**Type D**	**Sandstone**	**WC**	**12**	5.4	3.9	7.4	9.18E-04	1.378
25-2	**Paris**	**Type D**	**Sandstone**	**WC**	**12**	-	3.8	7.4	-	-
26-1	**Paris**	**Type D**	**Sandstone**	**WC**	**12**	5.4	10.8	7.4	8.42E-04	x

Table C3. HMAC LMLC Mixture Property Data (PAR SH 24) (Continued)

Sample #	SITE	Mix Type	Aggregate Material	Environmental Zone	Age (months)	BINDER CONTENT (wt. %)	AV (vol. %)	FILM THICKNESS(microns)	DSR Function (MPa/s)	CA
26-2	**Paris**	**Type D**	**Sandstone**	**WC**	**12**	-	9.9	7.4	-	-
27-1	**Paris**	**Type D**	**Sandstone**	**WC**	**12**	5.4	7.5	7.4	9.20E-04	1.417
27-2	**Paris**	**Type D**	**Sandstone**	**WC**	**12**	-	7.4	7.4	-	-

APPENDIX D

TABLES OF RECOVERED BINDER CARBONYL AREA GROWTH, DSR FUNCTION HARDENING, AND ACTIVATION ENERGY IN POV AGING TEST

The cores used in POV test were taken in 2008, except three sites taken in 2009, LBB US82, CHS US83 (2nd round), and LRD US277 (2nd round). After measuring the degree of oxidation for each layer, the recovered binder was well blended and placed into POV to continue aging under atmospheric air. The vessel is immersed in a constant temperature bath, using triethylene glycol and water for temperature control. The asphalt was placed into several 4 cm × 7 cm aluminum trays to form a film with a uniform 0.8 mm thickness. Trays were removed from POV on chosen days, depending on the temperature. Because of the limited asphalt binder could be extracted from the field cores, reaction rates were determined by only two or three data points. For some of the cases (US 82, US 83 2nd round and US 277 2nd round), recovered binder were extracted from more field cores as well as the seal coat layers (on US 82 and US 83) and the layer underneath the seal coat layer (only on US 82), more binder samples were used in the test to determine the reaction rates. And based on those reaction rates, constant-rate activation energy for each recovered binder was calculated. Comparing with the POV test on original binder (unaged binder from manufacture), the limited amount of the recovered binder seriously suffers the accuracy of the activation energy. Therefore, it is strongly recommended to use kinetics parameters from original binder. Kinetics parameters from recovered binder are only recommended when no original binder is available. Except the constant-rate activation energy, other kinetics parameters can be calculated or measured following the instructions given in Jin (2011).

Table D1. AMR US54 Recovered Binder POV CA Growth

Tempe-rature (°C)	Time (Day)	CA (arb. unit)	Tempe-rature (°C)	Time (Day)	CA (arb. unit)	Tempe-rature (°C)	Time (Day)	CA (arb. unit)
	0	1.523		0	1.523		0	1.523
60	16	1.624	**80**	8	1.749	**98**	4	1.814
	32	1.604		16	1.833		8	1.890

Table D2. AMR US54 Recovered Binder POV CA Growth Rate

Temperature (°C)	1000/RT (mol/kJ)	Reaction Rate (CA/day)
60	0.3612	0.0025
80	0.3407	0.0194
98	0.3251	0.0458
Activation Energy (kJ/mol)	81.5 kJ/mol	

Table D3. ATL US259 Recovered Binder POV CA Growth

Tempe-rature (°C)	Time (Day)	CA (arb. unit)	Tempe-rature (°C)	Time (Day)	CA (arb. unit)	Tempe-rature (°C)	Time (Day)	CA (arb. unit)
60	0	1.247	**80**	0	1.247	**98**	0	1.247
	8	1.258		8	1.393		4	1.447
	16	1.276		16	1.528		8	1.719
	32	1.386						

Table D4. ATL US259 Recovered Binder POV CA Growth Rate

Temperature (°C)	1000/RT (mol/kJ)	Reaction Rate (CA/day)
60	0.3612	0.0018
80	0.3407	0.0176
98	0.3251	0.0590
Activation Energy (kJ/mol)	97.4 kJ/mol	

Table D5. BRY SH6 Recovered Binder POV CA Growth

Tempe-rature (°C)	Time (Day)	CA (arb. unit)	Tempe-rature (°C)	Time (Day)	CA (arb. unit)	Tempe-rature (°C)	Time (Day)	CA (arb. unit)
	0	1.202		0	1.202		0	1.202
60	16	1.422	**80**	8	1.385	**98**	4	1.468
	32	1.417		16	1.451		8	1.579

Table D6. BRY SH6 Recovered Binder POV CA Growth Rate

Temperature (°C)	1000/RT (mol/kJ)	Reaction Rate (CA/day)
60	0.3612	0.0069
80	0.3407	0.0156
98	0.3251	0.0472
Activation Energy (kJ/mol)	52.6 kJ/mol	

Table D7. BRY US290 Recovered Binder POV CA Growth

Tempe-rature (°C)	Time (Day)	CA (arb. unit)	Tempe-rature (°C)	Time (Day)	CA (arb. unit)	Tempe-rature (°C)	Time (Day)	CA (arb. unit)
	0	1.372		0	1.372		0	1.372
60	8	1.370	**80**	8	1.531	**98**	4	1.600
	16	1.422		16	1.584		8	1.917
	32	1.417						

Table D8. BRY US290 Recovered Binder POV CA Growth Rate

Temperature (°C)	1000/RT (mol/kJ)	Reaction Rate (CA/day)
60	0.3612	0.0031
80	0.3407	0.0133
98	0.3251	0.0681
Activation Energy (kJ/mol)	84.8 kJ/mol	

Table D9. CHS US83 Recovered Field Binder POV CA Growth

Tempe-rature (°C)	Time (Day)	CA (arb. unit)	Tempe-rature (°C)	Time (Day)	CA (arb. unit)	Tempe-rature (°C)	Time (Day)	CA (arb. unit)
	8	1.109		8	1.117		4	1.175
60	24	1.128	**80**	16	1.183	**98**	8	1.316
				24	1.278		12	1.534

(1st Round)

Table D10. CHS US83 Recovered Field Binder POV CA Growth Rate (1st Round)

Temperature (°C)	1000/RT (mol/kJ)	Reaction Rate (CA/day)
60	0.3612	0.0012
80	0.3407	0.0100
98	0.3251	0.0449
Activation Energy (kJ/mol)	75.2 kJ/mol	

Table D11. CHS US83 Recovered Field Binder POV CA Growth (2nd Round)

Temperature (ºC)	Time (Day)	CA (arb. unit)	Limiting Viscosity (rad/s, @60ºC)	DSR Function (MPa/s, 15ºC, 10 rad/s)
68	0	1.029	-	-
	8	1.053	148000	0.000236
	13	1.122	153000	0.000303
	18	1.148	-	-
	24	1.185	210600	0.000445
	30	1.232	267000	0.000488
	35	1.188	244000	0.000486
	40	1.281	214400	0.000468
79	0	1.029	-	-
	7	1.071	231000	0.000381
	10	1.112	198000	0.000400
	14	1.207	317000	0.000556
	20	1.440	-	0.000268
	25	1.353	-	0.00107
	30	1.431	-	0.00131
92	0	1.029	-	-
	5	1.194	339000	0.000562
	8	1.335	-	0.001022
	12	1.364	-	0.002678
	17	1.533	-	0.003382
	20	1.708	-	0.003951

Table D12. CHS US83 Recovered Field Binder POV CA Growth Rate (2nd Round)

Temperature (ºC)	1000/RT (mol/kJ)	Reaction Rate (CA/day)
68	0.3528	0.0067
79	0.3417	0.0142
92	0.3270	0.0316
Activation Energy (kJ/mol)	65.6 kJ/mol	

Table D13. CHS US83 Recovered Seal Coat Binder POV CA Growth (2nd Round)

Temperature (°C)	Time (Day)	CA (arb. unit)	Limiting Viscosity (rad/s, @60°C)	DSR Function (MPa/s, 15°C, 10 rad/s)
68	0	1.301	-	-
	24	1.466	69400	0.000317
92	0	1.301	-	-
	12	1.869	152000	0.000949

Table D14. CHS US83 Recovered Seal Coat Binder POV CA Growth Rate (2nd Round)

Temperature (°C)	1000/RT (mol/kJ)	Reaction Rate (CA/day)
68	0.3528	0.0069
92	0.3270	0.0474
Activation Energy (kJ/mol)	81.5 kJ/mol	

Table D15. LBB US82 Recovered Field Binder POV CA Growth

Temperature (°C)	Time (Day)	CA (arb. unit)	Limiting Viscosity (rad/s, @60°C)	DSR Function (MPa/s, 15°C, 10 rad/s)
68	0	1.082	-	0.000408
	8	1.205	-	0.000831
	13	1.241	-	0.000940
	18	1.260	-	0.000982
	24	1.291	-	0.00166
	30	1.381	-	-
	35	1.345	-	-
	40	1.441	-	0.00243
79	0	1.082	-	0.000408
	7	1.273	-	0.001035
	10	1.258	-	0.001467
	14	1.379	-	0.002500
	20	1.517	-	0.003073
	25	1.545	-	0.003329
	30	1.589	-	0.002353
92	0	1.082	-	0.000408
	5	1.311	-	0.001164
	8	1.576	-	0.003702
	12	1.678	-	0.007163
	17	1.818	-	0.007076
	20	1.913	-	-

Table D16. LBB US82 Recovered Field Binder POV CA Growth Rate

Temperature (°C)	1000/RT (mol/kJ)	Reaction Rate (CA/day)
68	0.3528	0.0079
79	0.3417	0.0172
92	0.3270	0.0411
Activation Energy (kJ/mol)	69.8 kJ/mol	

Table D17. LBB US82 Recovered 1st Layer (0~0.5 in below Seal Coat) Binder POV CA Growth

Temperature (ºC)	Time (Day)	CA (arb. unit)	Limiting Viscosity (rad/s, @60ºC)	DSR Function (MPa/s, 15ºC, 10 rad/s)
68	0	1.209	-	0.000225
	8	1.166	-	0.000299
	18	1.345	-	0.000778
	30	1.409	-	0.001162
79	0	1.209	-	0.000225
	7	1.310	-	0.000650
	14	1.426	-	-
	25	1.584	-	-
92	0	1.209	-	0.000225
	5	1.406	-	0.001224
	12	1.660	-	0.002591
	20	2.022	-	0.005919

Table D18. LBB US82 Recovered 1st Layer (0~0.5 in below Seal Coat) Binder POV CA Growth Rate

Temperature (ºC)	1000/RT (mol/kJ)	Reaction Rate (CA/day)
68	0.3528	0.0067
79	0.3417	0.0151
92	0.3270	0.0403
Activation Energy (kJ/mol)	76.0 kJ/mol	

Table D19. LBB US82 Recovered Seal Coat Binder POV CA Growth

Temperature (°C)	Time (Day)	CA (arb. unit)	Limiting Viscosity (rad/s, @60°C)	DSR Function (MPa/s, 15°C, 10 rad/s)
68	0	1.184	-	0.000059
	8	1.258	-	0.000128
	30	1.404	-	0.000414
79	0	1.184	-	0.000059
	7	1.298	-	0.000195
	14	1.430	-	0.000277
	25	1.638	-	0.000554
92	0	1.184	-	0.000059
	5	1.506	-	0.000548
	12	1.804	-	-
	20	2.114	-	0.002020

Table D20. LBB US82 Recovered Seal Coat Binder POV CA Growth Rate

Temperature (°C)	1000/RT (mol/kJ)	Reaction Rate (CA/day)
68	0.3528	0.0072
79	0.3417	0.0182
92	0.3270	0.0456
Activation Energy (kJ/mol)	78.0 kJ/mol	

Table D21. LFK US69 Recovered Binder POV CA Growth

Tempe-rature (°C)	Time (Day)	CA (arb. unit)	Tempe-rature (°C)	Time (Day)	CA (arb. unit)	Tempe-rature (°C)	Time (Day)	CA (arb. unit)
	0	1.425		0	1.425		0	1.425
60	16	1.497	**80**	8	1.485	**98**	4	1.500
				16	1.519		8	1.830

Table D22. LFK US69 Recovered Binder POV CA Growth Rate

Temperature (°C)	1000/RT (mol/kJ)	Reaction Rate (CA/day)
60	0.3612	0.0045
80	0.3407	0.0059
98	0.3251	0.0506
Activation Energy (kJ/mol)	64.3 kJ/mol	

Table D23. LRD FM649 Recovered Binder POV CA Growth

Tempe-rature (°C)	Time (Day)	CA (arb. unit)	Tempe-rature (°C)	Time (Day)	CA (arb. unit)	Tempe-rature (°C)	Time (Day)	CA (arb. unit)
	0	1.185		0	1.185		0	1.185
60	16	1.220	**80**	8	1.232	**98**	4	1.331
	32	1.217		16	1.346		8	1.515

Table D24. LRD FM649 Recovered Binder POV CA Growth Rate

Temperature (°C)	1000/RT (mol/kJ)	Reaction Rate (CA/day)
60	0.3612	0.0022
80	0.3407	0.0100
98	0.3251	0.0412
Activation Energy (kJ/mol)	80.8 kJ/mol	

Table D25. LRD04 IH35 #3 Recovered Binder POV CA Growth

Tempe-rature (°C)	Time (Day)	CA (arb. unit)	Tempe-rature (°C)	Time (Day)	CA (arb. unit)	Tempe-rature (°C)	Time (Day)	CA (arb. unit)
	8	0.939		8	1.028		4	0.984
60	24	1.009	**80**	16	1.116	**98**	8	1.282
				24	1.206		12	1.489

Table D26. LRD04 IH35 #3 Recovered Binder POV CA Growth Rate

Temperature (°C)	1000/RT (mol/kJ)	Reaction Rate (CA/day)
60	0.3612	0.0043
80	0.3407	0.0111
98	0.3251	0.0631
Activation Energy (kJ/mol)	72.9 kJ/mol	

Table D27. LRD US277 Recovered Field Binder POV CA Growth

Tempe-rature (°C)	Time (Day)	CA (arb. unit)	Tempe-rature (°C)	Time (Day)	CA (arb. unit)	Tempe-rature (°C)	Time (Day)	CA (arb. unit)
	8	1.190		8	1.264		4	1.280
60	24	1.253	**80**	16	1.398	**98**	8	1.546
				24	1.510		12	1.758

(1st Round)

Table D28. LRD US277 Recovered Field Binder POV CA Growth Rate (1st Round)

Temperature (°C)	1000/RT (mol/kJ)	Reaction Rate (CA/day)
60	0.3612	0.0039
80	0.3407	0.0154
98	0.3251	0.0598
Activation Energy (kJ/mol)	75.2 kJ/mol	

Table D29. LRD US277 Recovered Field Binder POV CA Growth (2nd Round)

Temperature (ºC)	Time (Day)	CA (arb. unit)	Limiting Viscosity (rad/s, @60ºC)	DSR Function (MPa/s, 15ºC, 10 rad/s)
68	0	1.165	190300	0.000678
	8	1.201	236000	0.000715
	13	1.260	-	0.000801
	18	1.291	-	0.001402
	24	1.325	-	0.001624
	30	1.331	-	0.001418
	35	1.374	-	0.001728
	40	1.363	-	0.00181
79	0	1.165	190300	0.000678
	7	1.294	268000	0.000821
	10	1.320	391000	0.001688
	14	1.376	-	0.00178
	20	1.475	-	0.002262
	25	1.570	-	0.00295
	30	1.584	-	0.003066
92	0	1.165	190300	0.000678
	5	1.387	-	0.002352
	8	1.475	-	0.002611
	12	1.642	-	0.004033
	17	1.805	-	0.005911
	20	1.944	-	0.005756

Table D30. LRD US277 Recovered Field Binder POV CA Growth Rate (2nd Round)

Temperature (ºC)	1000/RT (mol/kJ)	Reaction Rate (CA/day)
68	0.3528	0.0053
79	0.3417	0.0145
92	0.3270	0.038
Activation Energy (kJ/mol)	83.2 kJ/mol	

Table D31. MnRoad Recovered Binder POV CA Growth

Tempera-ture (ºC)	Time (Day)	CA (arb. unit)	Tempera-ture (ºC)	Time (Day)	CA (arb. unit)	Tempera-ture (ºC)	Time (Day)	CA (arb. unit)
	0	1.243		0	1.243		0	1.243
60	8	1.332	**80**	8	1.447	**98**	4	1.508
	16	1.335		16	1.544		8	1.685
	32	1.403						

Table D32. MnRoad Recovered Binder POV CA Growth Rate

Temperature (ºC)	1000/RT (mol/kJ)	Reaction Rate (CA/day)
60	0.3612	0.0045
80	0.3407	0.0188
98	0.3251	0.0553
Activation Energy (kJ/mol)	69.5 kJ/mol	

Table D33. ODA FM1936 Recovered Binder POV CA Growth

Tempera-ture (°C)	Time (Day)	CA (arb. unit)	Tempera-ture (°C)	Time (Day)	CA (arb. unit)	Tempera-ture (°C)	Time (Day)	CA (arb. unit)
	8	1.092		8	1.118		4	1.239
60	24	1.058	**80**	16	1.287	**98**	8	1.356
				24	1.455		12	1.681

Table D34. ODA FM1936 Recovered Binder POV CA Growth Rate

Temperature (°C)	1000/RT (mol/kJ)	Reaction Rate (CA/day)
60	0.3612	(negtive)
80	0.3407	0.021
98	0.3251	0.0553
Activation Energy (kJ/mol)	47.2 kJ/mol	

Table D35. PHR FM2994 Recovered Binder POV CA Growth

Tempera-ture (°C)	Time (Day)	CA (arb. unit)	Tempera-ture (°C)	Time (Day)	CA (arb. unit)	Tempera-ture (°C)	Time (Day)	CA (arb. unit)
	0	1.336		0	1.336		0	1.336
60	16	1.423	**80**	8	1.459	**98**	4	1.600
	32	1.416		16	1.543		8	1.816

Table D36. PHR FM2994 Recovered Binder POV CA Growth Rate

Temperature (°C)	1000/RT (mol/kJ)	Reaction Rate (CA/day)
60	0.3612	0.0063
80	0.3407	0.0194
98	0.3251	0.0458
Activation Energy (kJ/mol)	55.0 kJ/mol	

Table D37. WAC IH35 Recovered Binder POV CA Growth

Tempera-ture (°C)	Time (Day)	CA (arb. unit)	Tempera-ture (°C)	Time (Day)	CA (arb. unit)	Tempera-ture (°C)	Time (Day)	CA (arb. unit)
	8	1.112		8	1.090		4	1.234
60	24	1.130	**80**	16	1.225	**98**	8	1.406
							12	1.523

Table D38. WAC IH35 Recovered Binder POV CA Growth Rate

Temperature (°C)	1000/RT (mol/kJ)	Reaction Rate (CA/day)
60	0.3612	0.0011
80	0.3407	0.0174
98	0.3251	0.0362
Activation Energy (kJ/mol)	98.7 kJ/mol	

Table D39. WFS US59 Recovered Binder POV CA Growth

Tempera-ture (°C)	Time (Day)	CA (arb. unit)	Tempera-ture (°C)	Time (Day)	CA (arb. unit)	Tempera-ture (°C)	Time (Day)	CA (arb. unit)
	8	1.139		8	1.210		4	1.428
60	24	1.162	**80**	16	1.367	**98**	8	1.506
				24	1.409		12	1.666

Table D40. WFS US59 Recovered Binder POV CA Growth Rate

Temperature (°C)	1000/RT (mol/kJ)	Reaction Rate (CA/day)
60	0.3612	0.0014
80	0.3407	0.0124
98	0.3251	0.0297
Activation Energy (kJ/mol)	85.7 kJ/mol	

Table D41. YKM SH36 Recovered Binder POV CA Growth

Tempera-ture (°C)	Time (Day)	CA (arb. unit)	Tempera-ture (°C)	Time (Day)	CA (arb. unit)	Tempera-ture (°C)	Time (Day)	CA (arb. unit)
	0	1.111		0	1.111		0	1.111
60	8	1.142	**80**	8	1.261	**98**	4	1.395
	32	1.243		16	1.443		8	1.542

Table D42. YKM SH36 Recovered Binder POV CA Growth Rate

Temperature (°C)	1000/RT (mol/kJ)	Reaction Rate (CA/day)
60	0.3612	0.0041
80	0.3407	0.0207
98	0.3251	0.0538
Activation Energy (kJ/mol)	71.7 kJ/mol	